OXFORD BROOKES UNIVERSITY

SCHOOL OF ENGINEERING

Graham Donald McMeeking M.Sc.

DEPOSITION AND CHARACTERISATION OF NICKEL OXIDE BASED COATINGS FOR ADVANCED GLAZING APPLICATIONS

SUBMITTED FOR THE DEGREE OF

DOCTOR OF PHILOSOPHY, MARCH 1997

DECLARATION

The research results submitted in this thesis are the outcome of investigations made by the author. Acknowledgement is given directly in the text or by means of references, wherever work performed by others is utilised.

The material in this thesis has not already been accepted for any degree, and is not being simultaneously submitted in candidature for any other degree.

Signed G. McMeeking

Signed _____

Research Supervisor

PUBLICATIONS AND PATENT LIST

1. Hutchins, M.G. and McMeeking G.D., International Energy Agency Solar Heating and Cooling Programme. Task 10 Solar Energy Materials Research and Development, Subtask C, Optical switching devices, Optical Properties of the Asahi all Solid State Electrochromic Window, 1990.

2 Hutchins, M.G. and McMeeking, G.D., Xinfang, Proc. SPIE **1272** 1990 139.

3 Hutchins, M.G. and McMeeking, G.D., Biosensor Patent no. 90 27 607.2 1990 (European patent no. 91311904.6).

4 Hutchins, M.G. and McMeeking, G.D., Making Electrochromic films Patent No. 90 27 608.0 1990 (European patent no. 91311905.3).

5 Hutchins, M.G. McMeeking, G.D., Xinfeng, H., and Orel, Z., Comparison of Nickel Oxide based Coatings Conf. Proc., Birmingham University, Institute of Metals 1991.

6 Hutchins, M.G., McMeeking, G.D. and Orel Z.C., Optical Materials Technology for Energy Efficiency and Solar Energy Conversion XI: Chromogenics for Smart Windows SPIE **1728** 1992 66.

7 McMeeking, G.D. and Nagai, J., Deposition and characterisation of Nickel Oxide Based Coatings., IUMRS conf. proc., Tokyo, 1993.

8 Crnjak Orel, Z., Hutchins, M.G. and McMeeking, G.D., Solar Energy Materials 30 1993 327

9 Nagai, J. and McMeeking G.D., Electrochromic Glazings for Solar Energy Control, Conference Proceedings, The Fourth International Symposium on New Glass, Tokyo, 1993 111.

10 Nagai, J., McMeeking, G.D., Seike, T. and Noutomi, Y., Glazings Today, December 1994 33.

11 Nagai, J., McMeeking, G.D. and Noutomi, Y., IEA Solar Heating and Cooling Program Task 18, Sub Task B3 Chromogenic Glazings Optical and Electrochemical Properties of OCLI WO_3 Films 1995.

12 Nagai, J., McMeeking, G.D. and Noutomi, Y., IEA Solar Heating and Cooling Program Task 18, Sub Task B3, Chromogenic Glazings, Optical and Electrochemical Properties of a Gentex device 1995.

13 Nagai, J., Seike, T. and McMeeking, G.D., Japanese Patent applied for no.930368 1993.

ABSTRACT

This thesis is a comparative study of nickel oxide based thin films for use as a counter electrode in a variable transmittance electrochromic device. Coatings have been prepared using anodic electrodeposition, colloidal precipitation and radio frequency (r.f.) sputtering. Systematic studies of the effect of deposition process parameters on optical and electrochromic properties of such films have been undertaken. Optimum conditions for the deposition of coatings deposited by colloidal and anodic deposition have been determined. A novel process for the colloidal deposition of electrochromic α-$Ni(OH)_2$ coatings using a simple one dip process is reported. Also the electrochromic properties of coatings anodically deposited from aqueous solutions containing $NiSO_4$ and NH_4OH were improved by the addition of the non-ionic surfactant polyoxyethylene sorbitan monolaurate.

Spectroscopic and electrochemical analytical techniques were used to identify the chemical composition of the coloured and bleached states. It was found using Fourier transform infra-red spectrophotometry (FTIR) that coatings deposited by anodic and colloidal deposition contained β-$Ni(OH)_2$ and α-$Ni(OH)_2$ respectively in the as-deposited and transparent states. For coatings deposited by both techniques β or γ-NiOOH was detected in the coloured state using FTIR. Using Raman spectroscopy, γ-NiOOH was detected in the coloured state for coatings deposited by anodic deposition from solutions containing the additive polyoxyethylene sorbitan monolaurate. β-$Ni(OH)_2$ was also detected in the transparent state of r.f. sputtered coatings that were electrochemically cycled in 1M $KOH_{(aq)}$. Using cyclic voltammetry the oxidation of nickel hydroxide to the oxyhydroxide was detected during colouration for coatings produced using anodic electrodeposition, colloidal precipitation and r.f. sputtering (after cycling sputtered films for 1 hour in 1M $KOH_{(aq)}$). This

information has been compared for films prepared using the different deposition techniques to enable the respective colouration mechanisms to be elucidated.

Prototype electrochromic devices have been constructed and their performances assessed. It can be concluded that nickel oxide based coatings can be used as suitable counter electrodes for hydrated electrochromic devices.

For Sue

For now we see through a glass darkly;
but then face to face; now I know in part;
but then shall I know even as also I am known.

1 Cor. 13:12 (A.V. King James)

ACKNOWLEDGEMENTS

I offer my thanks to the staff and my fellow researchers of the Department of Engineering at Oxford Brookes University and to Dr. Junichi Nagai of Asahi Glass Co. Ltd. Yokohama, Japan, Dr. Zorica Crnjak Orel of the Chemical Institute, Ljubljana, Slovenia and Professor Hu Xingfang of the Institute of Ceramics, Shanghai, China, for advice and help during this project. In particular I would like to offer my gratitude to my supervisor Professor Michael G. Hutchins, for his counsel during the course of this project. His wisdom and patience were a constant source of encouragement during my research.

My gratitude also goes to my family particularly my Grandfather who initiated my interest in science, and also my friends in England and Japan who have been constantly supportive. Finally I would like to thank my wife, Sue, for her unwavering support, love, inspiration, faith and kindness.

LIST OF CONTENTS

CHAPTER 1

INTRODUCTION

ELECTROCHROMIC NICKEL OXIDE FOR

ADVANCED GLAZING APPLICATIONS

CHAPTER 2

ADVANCED GLAZINGS AND

CHROMOGENIC MATERIALS REVIEW

CHAPTER 3

ANODIC DEPOSITION OF NICKEL OXIDE BASED COATINGS

CHAPTER 4

COLLOIDAL PRECIPITATION

OF NICKEL OXIDE BASED MATERIAL

CHAPTER 5

ANALYSES PERFORMED ON R.F. SPUTTERED NICKEL OXIDE COATINGS

CHAPTER 6

ELECTROCHROMIC DEVICES CONTAINING NICKEL OXIDE AND NICKEL HYDROXIDE ELECTRODES

CHAPTER 7

DISCUSSION AND CONCLUSIONS

APPENDIX 1

EXPERIMENTAL TECHNIQUES

FOR THE DEPOSITION AND CHARACTERISATION

OF NICKEL OXIDE AND NICKEL HYDROXIDE COATINGS

LIST OF FIGURES

CHAPTER 1

INTRODUCTION

ELECTROCHROMIC NICKEL OXIDE FOR

ADVANCED GLAZING APPLICATIONS

CHAPTER 2

ADVANCED GLAZINGS AND

CHROMOGENIC MATERIALS REVIEW

CHAPTER 3

ANODIC DEPOSITION OF NICKEL OXIDE BASED COATINGS

CHAPTER 5

ANALYSES PERFORMED ON R.F. SPUTTERED NICKEL OXIDE COATINGS

CHAPTER 6

ELECTROCHROMIC DEVICES CONTAINING NICKEL OXIDE AND NICKEL HYDROXIDE ELECTRODES

APPENDIX 1

EXPERIMENTAL TECHNIQUES DEPOSITION AND CHARACTERISATION OF NICKEL OXIDE BASED COATINGS

LIST OF TABLES

CHAPTER 1

INTRODUCTION

ELECTROCHROMIC NICKEL OXIDE FOR

ADVANCED GLAZING APPLICATIONS

CHAPTER 2

ADVANCED GLAZINGS AND

CHROMOGENIC MATERIALS REVIEW

CHAPTER 5

ANALYSES PERFORMED ON R.F. SPUTTERED NICKEL OXIDE COATINGS

CHAPTER 6

ELECTROCHROMIC DEVICES CONTAINING NICKEL OXIDE AND NICKEL HYDROXIDE ELECTRODES

CHAPTER 7

DISCUSSION AND CONCLUSIONS

APPENDIX 1 EXPERIMENTAL TECHNIQUES DEPOSITION AND CHARACTERISATION OF NICKEL OXIDE BASED COATINGS

LIST OF PLATES

CHAPTER 3

ANODIC DEPOSITION OF NICKEL OXIDE BASED COATINGS

CHAPTER 4

COLLOIDAL PRECIPITATION

OF NICKEL OXIDE BASED MATERIAL

APPENDIX 1
EXPERIMENTAL TECHNIQUES
DEPOSITION AND CHARACTERISATION OF
NICKEL OXIDE BASED COATINGS

GLOSSARY OF TERMS AND ABBREVIATIONS

ABBREVIATIONS:

AM2	Air mass 2 (for a zenith angle of 60° - the angle subtended by the zenith and the line of sight with the sun).
ECW	Electrochromic window
FTIR	Fourier transform infra-red (usually referring to a spectrophotometer).
IBS	Ion backscattering spectrometry
ITO	$Sn:In_2O_3$ Tin doped indium oxide (percentage of Sn by mass is usually 5%).
NIR	Near-infra-red
PVA	Polyvinylalcohol
P.V.D.	Physical vapour deposition (for example sputtering).
Q.C.M.	Quartz crystal microbalance
R.F.	Radio frequency (usually used in connection with sputtering).
S.C.E.	Saturated Calomel electrode
S.E.R.S.	Surface enhanced Raman spectroscopy
TCO	Transparent conductive oxide
UV	Ultraviolet
VIS	Visible
XPS	X-ray photoelectron spectroscopy
XRD	X-ray diffraction

TERMS:

A	Electron affinity, the energy liberated when one mole of an element in the form of gaseous atoms is converted into negative ions, usually given in eV (see eV), or Ampere, a unit of electrical energy equal to the flow of 6×10^{18} electrons s^{-1} or area (m^2).
A_{ssb}	Interfacial area of solid and substrate (m^2)
A_{ssl}	Area of solid/solution interface (m^2)

$A(\lambda)$		Absorbance at wavelength λ
a		Lattice constant usually given in Å (1×10^{-10} m)
C.E.		Colouration efficiency ($cm^2\ C^{-1}$)
C_0		Concentration of species O (mol cm^{-3}).
C_R		Concentration of species R (mol cm^{-3}).
C_0^σ		Concentration of species O at the electrode (if x is the distance from the electrode then in this case x = 0) (mol cm^{-3}).
C_0^∞		Concentration of species O in the bulk of the solution (mol cm^{-3}).
C_R^σ		Concentration of species R at the electrode (if x is the distance from the electrode then in this case x = 0) (mol cm^{-3}).
cm^{-1}		Wavenumber (number of waves per cm ($1/\lambda$))
D	=	Diffusion coefficient ($cm^2\ s^{-1}$)
D_0		Diffusion coefficient of the species O ($cm^2\ s^{-1}$)
D_R		Diffusion coefficient of the species R ($cm^2\ s^{-1}$)
E		Potential versus a reference electrode (V) (see V)
E_e		Equilibrium, or reversible voltage (v) (see V)
E_e^θ		Standard potential (V) (see V)
ΔE_p	=	Peak potential (V) (see V)
E_p^A	=	Peak anodic potential (V) (see V)
E_p^C	=	Peak cathodic potential (V) (see V)
$E_{p/2}$	=	Half peak potential (V) (see V)
$E(\lambda)$		Emittance at wavelength λ
eV		Electron volt, the increase in energy or the work done on an electron when passing through a potential of 1 volt. 1 eV = 1.602×10^{-19} joule.
F		Farad C mol^{-1}.
G_v^s		Free energy per unit volume of solid (J m^{-3}).

G^{sl}_{v} Free energy per unit volume of solution (J m^{-3}).

I Ionisation energy, the work that must be done to remove an electron from an atom in eV (see eV), or, current density (A cm^{-2}).

I_p Peak current density (A cm^{-2}), sometimes superscripted with A and C indicating peak anodic and cathodic processes respectively.

K The SI unit of thermodynamic temperature defined as the fraction 1/273.16 of thermodynamic temperature of the triple point of water.

K_{sp} Solubility product (usually given at 298 K - see K).

k^{θ} Standard rate constant for an electron transfer couple.

l Azimuthal or orbital angular momentum number

M Molar, concentration of 1 mole dm^{-3}.

m Metre, SI unit of length, defined as the length of the path travelled by light during 1/299 792 458 of a second.

mA Milliampere, 1 x 10^{-3} Ampere (see A).

$mAcm^{-2}$ Current density, the current flowing through a conductor per unit cross sectional area (in this case milliampere per centimetre squared).

ml Magnetic orbital quantum number

mm Millimetre 1 x 10^{-3} m

mV Millivolt 1 x 10^{-3} Volt (see V)

mVs^{-1} Millivolts per second.

n Principal quantum number, or, the number of electrons involved overall in a reaction.

nm Nanometre 1 x 10^{-9} m

n_{α} Number of electrons involved before and including the rate determining step.

P Equilibrium gas pressure at fixed adsorbent temperature (Nm^{-2}).

P^t	Vapour pressure of the adsorbate at the temperature of the experiment (Nm-2).
pH	$\log_{10}[1/H^+]$ where H^+ is the hydrogen ion concentration.
R	Gas constant (JK^{-1} mol^{-1})
R_{sc}	Integrated solar reflectance for the coloured state.
R_{sb}	Integrated solar reflectance for the bleached state.
R_{vc}	Integrated visible reflectance for the coloured state.
R_{vb}	Integrated visible reflectance for the bleached state.
$R(\lambda)$	Reflectance at wavelength λ
r	Ionic radius or radius of curvature (m).
r*	Critical radius of nucleus (m).
S	Spreading coefficient
s	Second (measure of time), or the spin number.
Scm^{-1}	Conductivity of solution, where S = siemens = Ω^{-1}.
$S\theta$	Geometric factor associated with activation barrier against nucleation.
T	Temperature (K)
T	Torr, unit of pressure used in the research area of high vacuum. This unit is equivalent to 133.322 pascals.
t	Time (various units)
$T(\lambda)$	Transmittance at wavelength λ
U	A measure of the transfer of thermal energy, units $Wm^{-2}K^{-1}$; or Hubbard U = I - A, where I is the ionisation energy and A is the electron affinity (see ionisation energy and electron affinity).
V	Volt, the difference of potential between two points on a conducting wire carrying a constant current of one ampere when the power dissipated between these two points is one watt.

Vc	Freedricksz transition,the voltage at which liquid crystal molecules align (see V).
V_m	Monolayer capacity (m^3 g^{-1} at standard temperature and pressure)
V_s	Volume of solid, or, volume of the spherical cap (m^3).
V_{sl}	Volume of solution (m^3).
W	Watt, equal to 1 joule per second, or bandwidth.
x	Distance perpendicular from an electrode (cm).

GREEK:

α	Phase of nickel hydroxide
α_c	Cathodic transfer coefficient (dimensionless).
β	Phase of nickel hydroxide or oxyhydroxide
γ	Phase of nickel oxyhydroxide
γ_i	Substrate/film interface free energy (Jm^{-2})
γ_f	Film free surface energy (Jm^{-2})
γ_{LG}	Liquid-gas interfacial tension (Jm^{-2})
γ_{SL}	Solid-liquid interfacial tension (Jm^{-2})
γ_{SG}	Solid-gas interfacial tension (Jm^{-2})
γ_s	Substrate free surface energy (Jm^{-2})
γ_{ssl}	Solid/solution interfacial free energy (or interfacial tension) (Jm^{-2}).
γ_{sbsl}	Substrate/solution interfacial free energy (or interfacial tension) (Jm^{-2}).
γ_{ssb}	Solid/substrate interfacial free energy (or interfacial tension) (Jm^{-2}).
Δ_0	Ligand field splitting parameter
ΔG_r	Excess free energy associated with formation of a sphere of material of radius r ($J\ mol^{-1}$).
ΔG_s	Free energy increase due to spreading (for example a liquid on a surface) ($Jmol^{-1}$).

ΔG_v Change in volume free energy (Jm^{-3}).

ΔG^* Maximum excess free energy associated with the formation of a nucleus of critical radius r* (see r*) ($J\ mol^{-1}$).

ΔG^*_{het} Excess free energy associated with heterogeneous nucleation ($J\ mol^{-1}$).

ΔH_L Heat of liquefaction of second and subsequent layers ($J\ mol^{-1}$).

ΔH_1 Heat of adsorption of the first layer ($J\ mol^{-1}$).

θ Contact angle (usually measured in degrees)

λ Wavelength (nm-see nm)

λ_c Wavelength at which the material becomes infra-red reflecting (nm - see nm).

μm Micron 1×10^{-6} metre

σ_e Electronic conductivity Scm^{-1}

σ_i Ionic conductivity Scm^{-1}

τ_{sb} Integrated solar transmittance for the coloured state.

τ_{sc} Integrated solar transmittance for the coloured state.

τ_{vb} Integrated visible transmittance for the bleached state.

τ_{vc} Integrated visible transmittance for the coloured state.

υ Sweep rate (usually Vs^{-1}), or, equilibrium volume of adsorbed gas per unit mass of absorbent at pressure P (see P).

υ_m Volume of the gas required to cover unit mass of the absorbent with a complete monolayer ($m^3\ g^{-1}$) at standard temperature and pressure).

Ω Sheet resistance (since $\rho_s = \rho y/A = \rho/h$ (see figure 1) and the units of ρ are Ω.cm then the unit of sheet resistance is Ω, however, in the literature $\Omega/\square$ is extensively used).

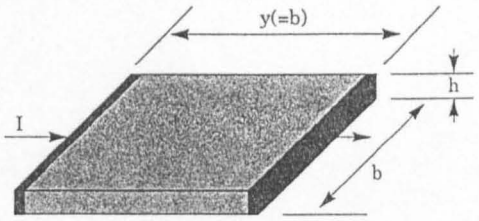

Figure 1 Geometry defining the sheet resistivity of a film of thickness h

OTHER TERMS:

Å Angstrom (1 x 10^{-10} m) (see m)

° Degree C, or, degree with respect to angular displacement

CHAPTER 1

INTRODUCTION

ELECTROCHROMIC NICKEL OXIDE FOR ADVANCED GLAZING APPLICATIONS

CHAPTER 1

INTRODUCTION

ELECTROCHROMIC NICKEL OXIDE FOR ADVANCED GLAZING APPLICATIONS

1.1 ELECTROCHROMISM

The flow of solar radiation into buildings can be dynamically controlled using switchable or 'smart' windows (1.1, 1.2). By altering the optical properties of these systems the solar radiation entering a building can be modulated. This can be achieved in at least two ways:

(i) by the application of an electric field across a window coating as in electrochromic or liquid crystal systems (active control), or

(ii) through the use of thermochromic or photochromic systems which exhibit a change in optical properties when exposed to the solar spectrum (passive control) (1.2).

The concept of the switchable window emerged from the twofold concern for energy efficiency and privacy control (1.3). Although the energy benefits afforded by electrochromic devices are controversial (see Chapter 2 for further discussion), savings in energy may be gained when these devices are used in conjunction with other systems of control (1.4).

Other chromogenic materials such as thermochromic (1.5, 1.6), photochromic (1.7) and liquid crystal-based (1.8) systems, are also suitable for switchable glazings. Thermochromic materials exhibit temperature dependent optical

properties (1.5, 1.6). Photochromic materials show light intensity dependent optical properties (1.7). Liquid crystals materials exhibit field induced alteration of optical properties (1.8). These and other chromogenic materials are discussed in detail in Chapter 2.

During the 1960's, liquid crystal and electrochromic devices competed as systems for display technologies (1.1). Liquid crystal devices were selected for their superior switching speeds and interest in electrochromic materials diminished (1.2). Nevertheless, electrochromic systems have important advantages over liquid crystal devices, particularly for glazing applications (1.2). They possess optical memory (1.5) and have low power requirements (1.6) rendering them more suitable for switchable window systems (1.2).

Electrochromism is defined as the ability of a material to alter its colour when an electric field is applied (1.9). The flow of current through the material results in its' oxidation or reduction. This chemical change produces the observed colouration (1.9). The charge carriers responsible for the flow of current are ions, for example, OH^-, H^+, Li^+, Na^+, K^+. Consequently electrochromism only occurs in devices, i.e. an electrochemical cell (1.9).

1.2 ELECTROCHROMIC DEVICES

Although many electrochromic window (ECW) device configurations are possible, most devices consist of an electrochromic material coated on to a transparent conductor. This conductor is in contact with a liquid or solid electrolyte and a counter electrode completes the cell (see figures 1.1a-1.1c) (1.10-1.14, 1.47, 1.48). The counter electrode is usually an electrochromic material in contact with another transparent (or otherwise) conductor (1.10-1.14). Devices

incorporating this type of structure are known as complementary devices (see figure 1.1b).

An alternative configuration utilises an ion storage layer as the counter electrode instead of the electrochromic layer (see figure 1.1e) (1.10-1.14). Other devices do not employ ion storage layers or electrochromic materials as the counter electrode but function by reversible redox of particular chemical species on conductors such as $Sn:In_2O_3$ (ITO) (1.2).

Lamination is required for ECW devices containing liquid or polymeric electrolytes. (see figures 1.1a, 1.1d and 1.1e). This prevents the leakage of electrolyte material and interaction with the external atmosphere. However, interactions with certain components of the atmosphere are necessary for the functioning of some solid state devices (1.51).

Electrochromic mirrors (1.1d) are already a successful product (for example, that marketed by the company, 'Gentex'). The only difference between this device and an ECW, is that the electrical connection to tungsten trioxide is achieved with an aluminium electrode. The aluminium coating reflects light when the WO_3 is in the transmissive state (1.50).

Essentially, all electrochromic devices are reversible electrochemical cells consisting of electronic conductors coated with electrochromic materials separated by an ion conducting and electron blocking electrolyte. At the electronic conductors, electron transfer occurs. Oxidation and reduction occur in the electrochromic materials.

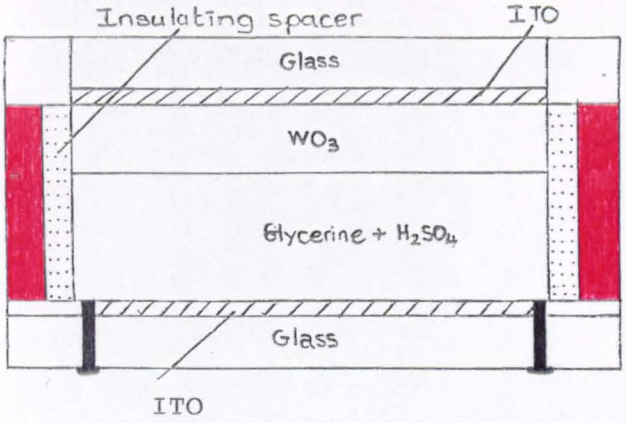

a

POLYAMPS = 2-Acrylamido-2 methyl propane sulphonic acid

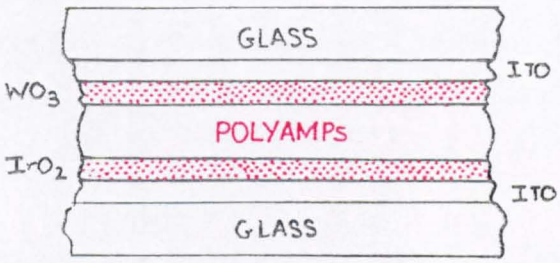

b

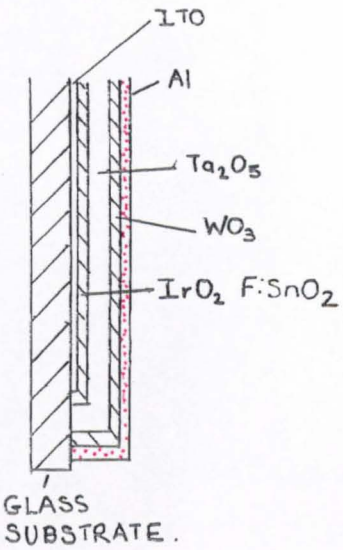

d

PEO = Polyethylene oxide

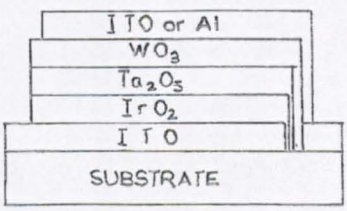

C

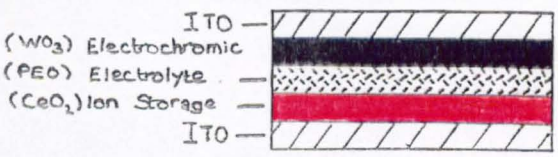

e

Figure 1.1 Electrochromic device structure: (a) ECW containing liquid electrolyte (1.47), (b) ECW laminated device using polymeric electrolyte (1.48), (c) ECW all-solid state device produced by Nikon (1.49), (d) Electrochromic mirror (1.50), (e) ECW device using ion storage layer (1.50).

1.3 ROLE OF THE TRANSPARENT CONDUCTOR

The principle role of a conductor is to act as a blocking electrode to ion movement. It also facilitates electron transport between the electrode and the respective electrochromic media. A metal coating (>400 Å) could be used as the conductor. However, this would render devices reflective in the transmissive state. Although this effect is utilised in electrochromic mirrors (see figure 1.1), it is of no practical use in ECW applications which demands the utilisation of conductors that are transparent in the visible part of the electromagnetic spectrum. However, a thin layer of a metal (about 200 Å) could be used. Thin metal coatings, known as hot heat mirrors, are composed of metals that have high infra-red reflectance, such as Au, Ag, Cu, Al or In (1.39). However, such coatings are impractical for ECW applications because they limit the possibility of solar gain in the winter months.

During the winter months solar gain is desirable for energy efficiency. For this reason semiconductor oxides, such as, tin oxide doped with antimony (1.40), indium oxide (1.41), indium oxide doped with tin (1.42) and tin oxide doped with fluorine (1.39), are used in ECW devices. These semiconductors have high free charge carrier concentrations and wide band gaps so that they transmit light in the range 0.30μm to 1.50 μm (1.39). The optical window of 0.30 to 1.50 μm facilitates the transmission of the solar spectrum through the ECW device. The penetrating solar radiation irradiates the area behind the window. Absorption by objects in the building occurs. This energy is then re-emitted in the thermal infra-red. Some of this radiation would be lost through an uncoated window. However, windows coated with a transparent conductive oxide (TCO) such as ITO are transparent in the visible part of the electromagnetic spectrum, are reflective in the thermal infra-red. Thermal

losses can therefore be minimised by utilising these transparent coatings in ECW systems. During the summer months however, solar gain is undesirable. One of the purposes of the ECW device is therefore to modulate the near-infra-red (NIR) radiation between 0.8 to 1.5 μm to account for seasonal variations in temperature.

For visual effect, the response time of ECW devices should be as fast as possible. The response time of solid state devices can be decreased by using a transparent conductor with low sheet resistance. Generally, the higher the sheet resistance of a transparent conductor the slower the response time of the device (see figure 1.2) (1.43). The response time for a 2 x 2 metre device is dramatically shorter for ITO having a sheet resistance of 1 Ω than it is for ITO with a sheet resistance of 10 Ω (see figure 1.2).

1.4 FUNCTION OF THE ELECTROLYTE

The electrolyte acts as an electron blocking media and as an ion transfer media. The type of electrolyte used is dependent on its' compatibility with the electrochromic media used in the device (1.15). It is important that ion conductors exhibit cyclic stability, high ionic conductivity, ultaviolet stability, ease of deposition, and stability to atmospheric conditions (1.51, 1.57). Electrolytes may be cationic or anionic the selection of which is determined by the colouration mechanism of the electrochromic materials in the device (1.44). Mismatch between the electrolyte and the electrochromic material can result in devices that either do not function at all or exhibit poor durability to cycling and ultraviolet stability.

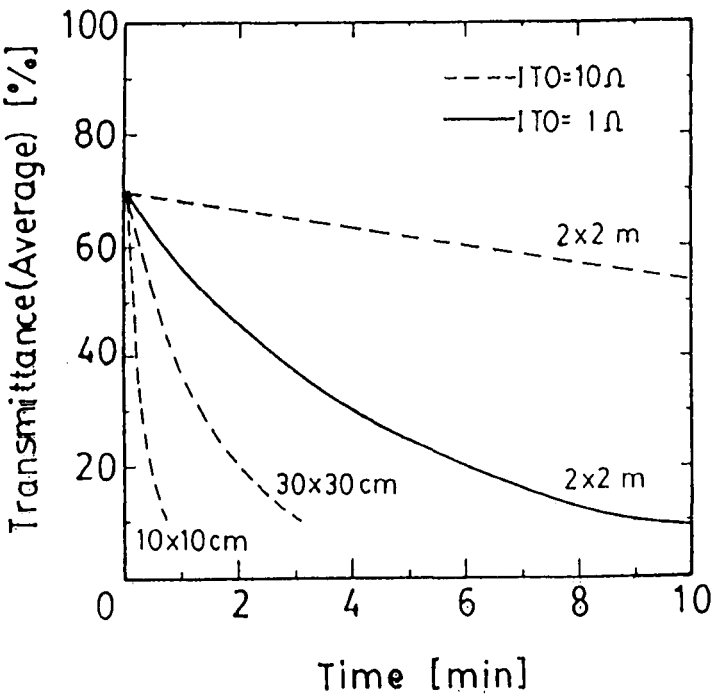

Figure 1.2 Average transmittance % versus colouration time for devices using ITO having sheet resistances of 1Ω and 10 Ω.

1.5 CATHODIC AND ANODIC ELECTROCHROMIC MATERIALS

Electronic materials may be anodic or cathodic compounds. These are substances that colour due to charge (electron) extraction and injection respectively (1.9). Many materials exhibit electrochromism (see table 1.1 (1.9)). They can be solids such as metal oxides (amorphous or crystalline), polymers, or liquids. As previously stated (see section 1.4), knowledge of the mechanism of colouration in electrochromic compounds is important for solid state device design (1.15).

Table 1.1 Crystallinity and colouration type of some electrochromic materials

Material	State	Colouration
Tungsten trioxide	Crystal and amorphous	Cathodic
Molybdenum trioxide	Crystal and amorphous	Cathodic
Vanadium pentoxide	Crystal	Cathodic
Nickel oxide	Amorphous	Anodic
Iridium oxide	Amorphous	Anodic
Polyaniline	Amorphous polymer	Anodic
Prussian blue	Amorphous or solution	Anodic

1.5.1 Mechanism of colouration for the cathodic material, tungsten trioxide

For the cathodic material, tungsten trioxide (bronsted acid), colouration occurs by simultaneous cation and electron insertion to form a bronze (see equation 1.1) Bleaching occurs by the reverse process (1.16).

$$WO_3 + XM^+ + xe^- \rightleftharpoons M_xWO_3 \qquad 1.1$$

where M can be H^+, Li^+, Na^+ or K^+ (1.26)

1.5.2 Mechanisms of colouration for the anodic materials, nickel oxide and nickel hydroxide

There is considerable dispute about the colouration mechanism of nickel oxide based coatings. The nature of the controversy is the chemical identity of the electroactive species present in the bleached and coloured states and the ion(s) necessary for colouration (1.17).

Nickel oxide based coatings are prepared using a variety of techniques that result in variations in the basic structure and density of the films. For example, the coatings may be crystalline, amorphous or mixed (1.17). Total or partial conversion to the hydroxide may occur after cycling in alkaline solutions (1.17, 1.28). Cycling of the material in aprotic solutions containing ions such as lithium may lead to the formation of a nickelate (1.18). Coatings may be sensitive to, or modified by, the analysis technique and the in-situ and ex-situ properties of the coatings may differ significantly (1.17). Finally, surface morphology, density and porosity may influence which ions are desorbed and adsorbed (1.17).

There are at least seven suggestions for the colouration mechanism of nickel oxide based coatings (see equations 1.2-1.8). Some researchers support a hydroxyl reaction first observed in studies on nickel hydroxide battery electrodes (1.19-1.21). In this mechanism, nickel hydroxide is present in the bleached state. However, in some nickel oxide based systems nickel hydroxide is not detected in the bleached state (1.27)

$$Ni(OH)_2 + OH^- \rightleftharpoons NiOOH + H_2O + e^- \qquad 1.2$$

Other researchers claim that the colouration process is due to the reversible transfer of a proton between the electrode and the electrolyte (1.22). However, since the electrolyte normally used with NiO is 1M KOH which has a pH value of 14, this is unlikely (1.17, 1.18, 1.21, 1.30, 1.31, 1.45, 1.46).

$$Ni(OH)_2 \rightleftharpoons NiOOH + H^+ + e^- \qquad 1.3$$

A modification to the reaction given in equation 1.2 is the oxidation of nickel hydroxide beyond the trivalent state to the quadravalent (1.17, 1.23, 1.24).

$$Ni(OH)_2 + 0.33K^+ + 2OH^- \rightleftharpoons 0.33K(NiO_2)_3 + 2H_2O + 1.67\ e^- \qquad 1.4$$

Other research indicates that colouration may occur due to hydroxyl insertion into nickel oxide films with low density (1.25).

$$NiO + OH^- \rightleftharpoons NiOOH + e^- \qquad 1.5$$

In aqueous electrolytes, it is more likely that the nickel oxide represented in equation 1.5 is hydrated (1.17).

$$NiO.H_2O + OH^- \rightleftharpoons NiOOH.H_2O + e^- \qquad 1.6$$

The mechanism is further complicated by the phases of nickel hydroxide and nickel oxyhydroxide (1.58).

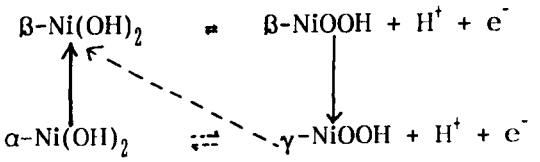

1.7

Finally, certain forms of sputtered NiO may colour by cation extraction (1.18, 1.26, 1.57). This type of nickel oxide is deposited at low powers (100 W) and high pressures 6 x 10^{-2} torr (T) (1.18) (see equation 1.8).

$$M_yNi_{1-x}O \rightleftharpoons M_{y-z}Ni_{1-x}O + zM^+ + ze^- \qquad 1.8$$

where M may be Li^+, Na^+ or K^+.

1.5.2.1 *Analytical techniques used to determine the mechanism of colouration*

In order to identify the mechanism responsible for colouration two approaches have been adopted:

(i) the characterisation of the materials present in the reduced and oxidised forms of nickel oxide based systems (nickel oxide, nickelates, nickel hydroxide and oxyhydroxide or mixtures thereof), and

(ii) the characterisation of the ion responsible for colouration.

Nickel oxide based coatings have been examined using many techniques. The aim of these investigations has been to identify the materials present in the reduced, oxidised and intermediate states. Techniques reported in the research

literature, include, Raman spectroscopy (1.52, 1.53, 1.59-1.63), infra-red spectroscopy (1.17, 1.21, 1.58, 1.60, 1.64), ultraviolet/visible near-infra-red (1.17, 1.18, 1.28, 1.30, 1.52), X-ray diffraction (1.17, 1.54), impedance spectroscopy (1.55, 1.67), cyclic voltammetry (1.17, 1.52, 1.55), XPS (1.17), auger (1.17), ion backscattering (1.17) and ESCA (1.17, 1.18). These analyses are discussed in Chapter 2.

Techniques used to identify the ion responsible for colouration include, nuclear reaction analysis (1.29, 1.60), lithium ion bombardment (1.18), crystal balance (1.27, 1.65, 1.66), impedance (1.68), ion selective membranes (1.17) and aprotic solutions (1.17, 1.26, 1.56) have also been used to identify the ion(s) involved in the colouration process. The various interpretations of the colouration mechanism are discussed in Chapter 2.

1.6 ELECTROCHROMIC NICKEL OXIDE BASED COATINGS

Although the focus of attention in electrochromic materials research has been the cathodic compound tungsten trioxide (1.29 1.69-1.76), it exhibits a blue colouration in electrochromic devices which renders it unsuitable for architectural glazings. For this application a neutral bronze shading is preferred (1.17).

An alternative is the anodic compound iridium oxide which can exhibit a neutral bronze colouration. However, because iridium is a rare metal (the principal source is meteoritic material), the cost is prohibitive. Furthermore, it only exhibits a small degree of colouration (dynamic range) (1.32).

A more suitable alternative is nickel oxide. Electrochromic oxides of nickel can

exhibit a grey/bronze (1.28, 1.30, 1.31, 1.32) or a brown/bronze colouration (1.17). Other reasons for the current interest in nickel oxide are that it exhibits reversible electrochromism, full colouration and bleaching below the oxygen and hydrogen evolution potentials, low photochromism, open circuit memory and large dynamic ranges (1.17). Furthermore, it can be deposited using a variety of techniques including, r.f. sputtering (1.18, 1.33), evaporation (1.34), colloidal precipitation (1.4, 1.21, 1.35, 1.36), solgel (1.37), anodic (1.17, 1.21) and cathodic electrodeposition (1.38), chemical vapour deposition (1.76) and pyrolytic deposition (1.77). Electrochromic nickel oxide is usually referred to in the literature as hydrated nickel oxide. This is partially because nickel oxide usually contains some water, but mainly this refers directly to the hydroxide (1.17). Nickel hydroxide is not the same chemical compound as nickel oxide.

1.7 SUMMARY OF THIS THESIS

Nickel oxide based coatings are currently being considered as an anodic material for all solid state device applications. It is not certain which deposition method will be used to produce NiO coatings for large area device applications. This thesis is a comparative study of nickel oxide based coatings deposited using colloidal and anodic electrodeposition. The electrochromic properties of these coatings are compared with NiO films deposited using sputter deposition reported elsewhere (1.18, 1.33).

The subjects of the literature review (Chapter 2) are advanced glazings and chromogenic materials. Chapter 3 contains the experimental results of anodic electrodeposition of ß-$Ni(OH)_2$ electrodes. Experiments conducted on colloidal precipitation of α-$Ni(OH)_2$ are presented in Chapter 4. The experiments on the

cyclic stability of r.f. sputtered NiO in 1M KOH are discussed in Chapter 5. Details of the electrochromic devices constructed in this study are explained in Chapter 6. The results of this thesis, the conclusions reached and areas for future work are discussed in Chapter 7. Details of the experimental techniques used throughout this study are described in Appendix 1. Patents applications were submitted during the course of this study (1.45, 1.46).

1.8 ACHIEVEMENTS OF THE THESIS

The initial aim of this study was to deposit electrochromic nickel oxide based coatings using the electrochemical technique, anodic electrodeposition (1.17). During this investigation it was found that colloidal precipitation occurred from the electrodeposition solution and that the precipitation process produced coatings that exhibited similar electrochemical and optical properties to coatings that were electrodeposited (1.21). This method of depositing electrochromic coatings from one solution of NH_4OH and $NiSO_4$ has not previously been reported in the literature (1.21, 1.45).

It was established that colloidal precipitation occurred without the application of an electric field. However, coatings that were electrodeposited from solutions that contained the same concentrations of reactants reported in the literature, exhibited poor electrochromic and mechanical properties (1.21).

The addition of detergent improved the mechanical and electrochromic properties of electrodeposited coatings (1.21). This was also not previously reported in the literature for anodically deposited electrochromic coatings. The as-deposited state of coatings produced by colloidal and anodic electrodeposition were analyzed by Fourier transform spectrophotometry. Using

this technique ß-$Ni(OH)_2$ was detected in electrodeposited coatings, whereas for colloidally produced films, α-$Ni(OH)_2$ was identified. In the coloured state ß-NiOOH or γ-NiOOH was detected for anodic coatings deposited from stable solutions (1.21) and colloidally deposited coatings. Using Raman analysis it was confirmed that the phase of the oxyhydroxide was γ-NiOOH for anodically deposited films.

Films produced by colloidal precipitation and anodic electrodeposition were very sensitive to surface contamination. An electrochromic biosensor was conceived from this observation (1.45).

Electrochromic devices were fabricated using polyvinylalcohol (PVA), water and a base as an electrolyte. The device with the fastest response contained NiO as an anode and MnO as a cathode. However devices were also fabricated that only contained NiO, hydrated PVA and an ITO counter electrode.
A number of areas for further work were highlighted by this study:

(i) The ion responsible for colouration of coatings deposited by colloidal, anodic and sputter deposition should be identified

(ii) A quantitative method for determining the durability of coatings produced using these techniques should be developed.

(iii) Electrochemical measurements should be performed in environments other than aqueous.

(iv) Electrochemical measurements and deposition should be performed in inert atmospheres (such as N_2 or Ar).

(v) The temperature of deposition should be controlled using a thermostatically controlled system.

(vi) The use of buffered deposition solutions should be investigated to facilitate the deposition of uniform coatings.

(vii) A Coulomb meter should be used during electrochemical measurements to improve the accuracy of charge measurements.

This research will accelerate the production of an all-solid state ECW devices.

1.9 REFERENCES

1.1 Deb, S.K., Appl. Opt. Suppl. **3** 1969 193.

1.2 Lampert, C.M., and Granqvist, C.G., (1990), in Lampert, C.M., and Granqvist, C.G. (eds.), Large-Area Chromogenics: Materials and Devices for Transmittance Control (1st Edn.). Bellingham, Washington, U.S.A., SPIE Press **IS4** 2.

1.3 Selkowitz, S.E. and Lampert, C.M. (1990), in Lampert, C.M., and Granqvist, C.G. (eds.), Large-Area Chromogenics: Materials and Devices for Transmittance Control (1st Edn.). Bellingham, Washington, U.S.A., SPIE Press **IS4** 22.

1.4 Reilly, S., Daruish, A. and Selkowitz, S., Solar Energy Materials **22** 1991 1.

1.5 Day, J.H., Chem. Rev. **63** 1963 65.

1.6 Day, J.H., Chem. Rev. **68** 1968 649.

1.7 Brown, G.H. (ed.) (1971) Photochromism. New York, Wiley.

1.8 Lampert, C.M. (1990), in Lampert, C.M., and Granqvist, C.G. (eds.), Large-Area Chromogenics: Materials and Devices for Transmittance Control (1st Edn.). Bellingham, Washington, U.S.A., SPIE Press **IS4** 550.

1.9 Haas, T.E. and Goldner, R.B. (1990), in Lampert, C.M., and Granqvist, C.G. (eds.), Large-Area Chromogenics: Materials and Devices for Transmittance Control (1st Edn.). Bellingham, Washington, U.S.A., SPIE Press **IS4** 170.

1.10 Yoshimura, T., Masaki, W., Koike, Y., Kiyota, K. and Tanaka, M., Japanese Journal of Applied Physics 22 1 1983 152.

1.11 Yoshimura, T., Masaki, W., Koike, Y., Kiyota, K. and Tanaka, M., Japanese Journal of Applied Physics 22 1 1983 157.

1.12 Goldner, R.B., Haas, T.E., Seward, G., Wong, K.K., Norton, G., Foley, G., Wei, S., Schulz, S. and Chapman, R., Solid State Ionics 28-30 1988 1715.

1.13 Thomas, G.R. and Owen J.R., Solid State Ionics 53-56 1992 513.

1.14 Mizuhashi, M., et.al. (1990), in Lampert, C.M., and Granqvist, C.G. (eds.), Large-Area Chromogenics: Materials and Devices for Transmittance Control (1st Edn.). Bellingham, Washington, U.S.A., SPIE Press IS4 494.

1.15 Lampert, C.M., Troung, V.V., Nagai, J., Hutchins, M.G. IEA Task X-C, Glazing Materials, Technical Report LBL-29632 1990.

1.16 Rauh, D.R., and Cogan, S.F., Solid State Ionics 28-30 1988 1707.

1.17 Lampert C.M. (1990), in Lampert, C.M., and Granqvist, C.G. (eds.), Large-Area Chromogenics: Materials and Devices for Transmittance Control (1st Edn.). Bellingham, Washington, U.S.A., SPIE Press IS4 414.

1.18 Xingfang, H., Xiaofeng, C. and Hutchins, M.G., Optical Materials Technology for Energy Efficiency and Solar Energy Conversion XI: Chromogenics for Smart Windows SPIE 1728 1992 173.

1.19 Carpenter, M.K., Connel, R.S. and Corrigan, D.A., Solar Energy Materials 6 1987 333.

1.20 Carpenter, M.K., Corrigan, D.A., Journal of Electrochemistry Society **136** 1989 1022.

1.21 Hutchins, M.G., McMeeking G.D., and Orel Z.C., Optical Materials Technology for Energy Efficiency and Solar Energy Conversion XI: Chromogenics for Smart Windows SPIE **1728** 1992 66.

1.22 Pennisi, A., Lampert, C.M., Proc. SPIE **1016** 1988 131.

1.23 Desilvestro, J., Corrigan, D.A. and Weaver, M.J., Journal of Physical Chemistry **90** 1986 6408.

1.24 Corrigan, D.A. and Knight, S.L., Journal of Electrochemistry Society **135** 1989 885.

1.25 Delichere, P., Joiret, A., Hugot-Le Goff Proc. SPIE **165** 1988 1016.

1.26 Passerini, S. and Scrosati, B., Solid State Ionics **53-56** 1992 520.

1.27 Nagai, J., Optical Materials Technology for Energy Efficiency and Solar Energy Conversion XI: Chromogenics for Smart Windows, SPIE **1728** 1992 194.

1.28 Conell, R.S., Corrigan, D.A. and Powell, B.R., Solar Energy Materials and Solar Cells **25** 1992 301.

1.29 Lampert, C.M., Solar Energy Materials **11** 1984 1.

1.30 Hutchins, M.G and McMeeking, G.D., Xinfang, H., Proc. SPIE 1990 1272.

1.31 Hutchins, M.G. and Xingfang H., (unpublished paper) 1989.

1.32 Cogan, S.F. and Rauh, D.R. (1990), in Lampert, C.M., and Granqvist, C.G. (eds.), Large-Area Chromogenics: Materials and Devices for Transmittance Control (1st Edn.). Bellingham, Washington, U.S.A., SPIE Press **IS4** 482.

1.33 Svensson, J.S.E.M. and Granqvist, C.G., Solar Energy Materials **16** 1987 19.

1.34 Lynam, N.R. and Habibi, H.R., Materials Technology for Energy Efficiency and Solar Energy Conversion. SPIE VII 1016 1988 63.

1.35 Folquer, M.E., Vilche, J.R. and Arvia. A.J., Journal of Electrochemical Society **127** 1980 2634.

1.36 Macagno, V.A., Vilche, J.R. and Arvia A.J., Journal of Electrochemical Society **129** 1982 301.

1.37 Lynam, N.R., Moser, F.H., Bryant, P.B., Optical Materials Technology for Energy Efficiency and Solar Energy Conversion SPIE VI 823 1987 130.

1.38 Carpenter, M.K., Conell, R.S., Corrigan, D.A., Solar Energy Materials **16** 1987 333.

1.39 Lampert, C.M., Solar Energy Materials 6 1981 1.

1.40 Mulla, I., Soni, Rao, V. and Sinha, A., Journal of Materials Science, **21** 1986 1280.

1.41 Nath, P. and Bunshah, R., Thin Solid Films, **69** 1980 63.

1.42 Fan, J. and Bachner, F., Journal of Electrochemical Society, **122** 1975 1719.

1.43 Nagai, J., Towards Advanced Glazings Based on Electrochromics, Japanese Electrochemical Society 2E10 1991 112.

1.44 Troung, V., et.al. (1990), in Lampert, C.M., and Granqvist, C.G. (eds.), Large-Area Chromogenics: Materials and Devices for Transmittance Control (1st Edn.). Bellingham, Washington, U.S.A., SPIE Press IS4 386.

1.45 Hutchins, M.G. and McMeeking, G.D., Making Electrochromic films Patent No. 90 27 608.0 1990 (European patent no. 91311905.3).

1.46 Hutchins, M.G. and McMeeking, G.D., Biosensor Patent no. 90 27 607.2 1990 (European patent no. 91311904.6).

1.47 Deb, S.K., Materials and Optics for Solar Energy Conversion and Advanced Lighting Technology, SPIE **692** 1986 19.

1.48 Cogan, S.F., Plante, T.D., McFadden, R.S. and Rauh. D.R., Optical Materials Technology for Energy Efficiency and Solar Energy Conversion SPIE VI **823** 1987 106.

1.49 Saito, T., Ushio, Y.,Yamada, M. and Niwa, T., Solid State Ionics **40/41** 1990 499.

1.50 Lynam, N.R. and Agrawal, A. (1990), in Lampert, C.M., and Granqvist, C.G. (eds.), Large-Area Chromogenics: Materials and Devices for Transmittance Control (1st Edn.). Bellingham, Washington, U.S.A., SPIE Press IS4 46.

1.51 Bauche, F.G.K., and Duffy, J., Chemistry in Britain **July 1985** 643.

1.52 Desilvestro, J., Corrigan, D.A. and Weaver M.J., Journal of Physical Chemistry **90** 1986 6408.

1.53 Johnston, C. and Graves, P.R., Applied Spectroscopy **44** 1 1990 105.

1.54 McEwen, R.S. Journal of Physical Chemistry **75** 12 1971 1782.

1.55 Gorenstein, A., et.al. (1990), in Lampert, C.M., and Granqvist, C.G. (eds.), Large-Area Chromogenics: Materials and Devices for Transmittance Control (1st Edn.). Bellingham, Washington, U.S.A., SPIE Press IS4 272.

1.56 Decker, F., Passerini, S., Pileggi R. and Scrossati B., Electrochemica Acta **37** 6 1992 1033.

1.57 Ganson, G. and Hartman, R., Solid State Electrolytes for Sensors and Electrochemistry, Conf. proc. (in press) Sicily, Italy, July 1992.

1.58 Oliva, P., Leonardi, J., and Laurent, J.F., Delmas, C., and Braconnier, J.J., Figlarz, M. and Fievert, F., de Guibert, A., Journal of Power Sources **8** 1982 229.

1.59 Cordoba-Torresi, S.I., Hugot-Le-Goff, A. and Joiret, S., Journal of Electrochemical Society **138** 6 1991 1554.

1.60 Melendres, C.A. and Pankuch, M., Journal of Electroanalytical Chemistry **333** 1992 103.

1.61 Delichere, P., Joiret, S., Hugot-le-Goff, A., Bange, K., Hetz, B., Journal of Electrochemical Society **135** 7 1988 1856.

1.62 Bockris, J.O.M., Reddy, A.K.N. and Rao, B., Journal of Electrochemical Society **113** 1966 1133.

1.63 Hugot-Le-Goff, A., Joiret, S. and Cordoba de Torresi, S., Proc., Electrochemical Society **90-2** 1990 70.

1.64 Nazri, G., Corrigan, D.A. and Maheswari, S.P., Langmuir 5 1 1989 17.

1.65 Hugot-le-Goff, A., Journal of Electrochemistry **138** 1991 1548.

1.66 Faria, I.C., Torresi, R.M. and Gorenstein, A., Optical Materials Technology for Energy Efficiency and Solar Energy Conversion XI: Chromogenics for Smart Windows, SPIE **1728** 1992 54.

1.67 Fantini, M. and Gorenstein, A., Solar Energy Materials **16** 1987 487.

1.68 Matupally, S., Strienz, C.C. and Weidner, J.W., J. Electrochem. Soc. **142** 5 1995.

1.69 Vuillemin, B. and Bohnke, O., Solid State Ionics **68** 1994 257.

1.70 Badilescu, S., Ashrit, P.V., Minh-Ha, N., Bader, G. and Girouard, F.E., Thin Solid Films **250** 1994 47.

1.71 Ho, K.C., Rukavina, T.G. and Greenberg, C.B., J. Electrochem. Soc. **141** 8 1994 2061.

1.72 Inaba, H., Iwaku, M., Nakase, K., Yasukawa, H., Seo, I., Oyama, N., Electrochimica Acta **40** 2 1995 227.

1.73 Tassi, E.L. and De Paoli, M.A., Electrochimica Acta **39** 16 1994 2481.

1.74 Maruyama, T. and Kanagawa, T., J. Electrochem. Soc. **141** 9 1994 2435.

1.75 Shen, P.K., Chen, K.Y. and Tseung, C.C., J. Electrochem. Soc., 141 7 1994 1758.

1.76 Arakaki, J., Reyes, R., Horn, M. and Estrada, W., Solar Energy Materials and Solar Cells **37** 1995 33.

1.77 Maruyama, T. and Arai, S., Solar Energy Materials and Solar Cells **30** 1993 257

CHAPTER 2

ADVANCED GLAZINGS AND CHROMOGENIC MATERIALS REVIEW

CHAPTER 2

ADVANCED GLAZINGS AND CHROMOGENIC MATERIALS REVIEW

2.1 INTRODUCTION

Over the last two decades the energy crisis has deepened. In response, governments world-wide have established energy saving policies to restrict the waste of energy. Energy saving strategies involving heating, air conditioning and lighting systems are now routine in industry and the home environment.

However, even if energy inefficiency caused by human wastage could be reduced to a minimum, energy losses would still occur due to the poor thermal efficiency of buildings. Approximately 50% of the energy in the UK is used in commercial and residential buildings (2.1). About 70% of this energy is used in space and water heating (2.2). Due to the poor thermal efficiency of buildings a considerable portion of this energy is wasted (see figure 2.1).

2.2 ENERGY EFFICIENCY

It is possible to considerably reduce heat losses (hence reducing expenditure), by adopting energy saving strategies. Energy efficiency in buildings can be achieved through active and passive solar collection, and thermal insulation.

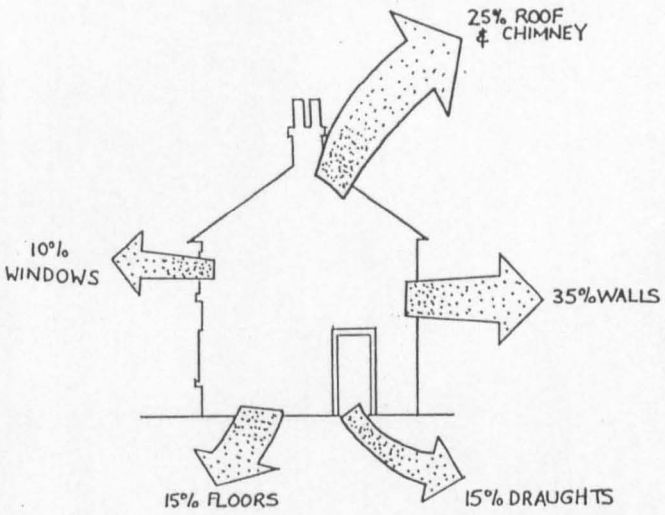

Figure 2.1 Thermal losses of 'between-the-wars' building.

2.2.1 Active solar energy collection

A way of reducing costs is to actively collect solar energy (2.4). This involves the use of mechanical and electrical equipment to collect and distribute thermal energy throughout buildings.

2.2.2 Passive solar energy collection

The 'passive' approach involves the use of conventional building elements for solar energy collection, heat storage and heat distribution (2.5). The processes of heat transfer occur naturally by convection, conduction and radiation. It is also possible for a building to have a distinct energy advantage by simply orientating the building in the correct direction. In the northern hemisphere buildings with a south facing aspect have energy benefits over buildings with other orientations (2.6).

2.2.3 Insulation

Insulating materials can be used to reduce radiative, convective and conductive heat losses (2.7). Insulators can be used to lag areas containing or transporting heated water (except radiators) and to insulate lofts and cavity walls. Draught excluders around windows and doors prevent loss by convection.

2.3 THERMAL LOSSES THROUGH GLAZINGS

Thermal losses through single glazed windows account for 10% of the total heat lost from buildings (see figure 2.1). The thermal insulation of a window can be improved by using double glazing. 'U' values can be reduced from about 5.6 $Wm^{-2}K^{-1}$ to 3.0 $Wm^{-2}K^{-1}$. This can result in a net gain in heat in all but the coldest winter months of December and January (2.8).

Heavy curtains, blinds and other insulating shutters can be used to reduce the 'U' value by decreasing heat losses to 2 $Wm^{-2}K^{-1}$ (2.9). It is also possible to reduce heat losses without totally blocking visible radiation from entering the building (which is a source of passive solar heating). This can be achieved by gas-filling the double glazing with a greenhouse gas, or by the use of triple glazing or heat mirror coatings. The use of low E coatings (heat mirrors) alone reduces the 'U' value of single glazing to 4.2 $Wm^{-2}K^{-1}$. There is, however, an accompanying reduction of 15% transmittance, but this is compensated for by the improved 'U' value (2.9). Double glazed units are now standard issue in new buildings (see table 2.1 for 'U' values).

Table 2.1 Performance of coated glass

Unit Type	Uncoated 'U' value $Wm^{-2}K^{-1}$	Coated 'U' value $Wm^{-2}K^{-1}$	Uncoated Light Transmittance	Coated Light Transmittance
Single glazing	5.6	4.2	88%	70-75%
Double glazing	3.0	2.0 * 1.6	80%	62-68%

* The 'U' value for a double glazed unit with a gas-filled cavity.

A double glazed unit with an air space of 12 mm has a 'U' value is 3 $Wm^{-2}K^{-1}$. The deposition of a heat mirror on the internal surface of the glass (to avoid weathering of the heat mirror), reduces the heat losses to 2 $Wm^{-2}k^{-1}$. Introduction of krypton or carbon dioxide into the air gap in the double glazing further decreases the 'U' value to 1.6 $Wm^{-2}K^{-1}$ (see table 2.1 (2.9)).

2.3.1 Transparent insulation materials

There are several media that exhibit transparency and good insulating properties. These are monolithic and granular aerogels (2.10), geometric media (2.11) and evacuated systems (2.12). Unfortunately, some of these systems exhibit angular optical dependence.

2.3.1.1 *Monolithic and granular aerogels*

Aerogels are insulating materials that can be used as glazings or to obtain solar gain when placed next to walls. They consist of micron sized capillaries or grains usually in glass (2.10). A major drawback of these systems is that they exhibit angular optical scattering. Consequently, optical transparency is impaired. Another problem with aerogels is that materials currently under investigation change colour due to water adsorption. This could be overcome by using appropriate sealing compounds but this would add to the price of the finished product.

2.3.1.2 *Geometric media*

These systems usually consist of fine capillaries fabricated from transparent plastic tubes (2.11). A honeycomb structure is formed by welding these tubes together. The purpose of this arrangement is to guide light, this occurs because the tubes have a higher refractive index than the air. The tubes also prevent air turbulence and consequently, available solar energy can be directed towards an aperture or surface and losses due to convective air currents can be reduced.

Geometric media can be positioned in front of selective solar absorbers. Undesirable solar gain in the summer can be reduced by simply placing a blind in front of geometric media. Radiation is no longer incident on the absorber when the blind is closed. In the near future switchable glazings may replace the conventional shutter type system.

2.3.1.3 *Evacuated glazings*

These systems consist of dewar type arrangements minus the mirror surface, i.e. an evacuated gap sandwiched between two glass substrates. The spacing gap usually consists of solder glass (2.12). Large area evacuated glazings may be difficult to manufacture and the vacuum in the gap separating the panes of glass may be hard to guarantee for a specified lifetime.

2.4 WINDOW DESIGN

Although the thermal properties of windows can be tailored, individual windows cannot be manufactured to be appropriate in all seasons. This is particularly important in temperate climates, for example, in Japan (winter 0 - summer 37°C). In the winter it is necessary to have solar gain by transmitting from the visible to the near infra-red and reflecting thermal wavelength radiation back into the building. In the summer months, however, it is necessary to reflect all radiation away from the building to the lower limit of the visible electromagnetic spectrum (800 nm). This cannot be achieved with a static heat mirror coating in a double glazed system.

An attractive solution to this problem is a heat mirror that could be adjusted dynamically. This could be achieved mechanically by using hot heat mirror inserts in the summer (although this would be impractical for large area glazings). Transparent venetian shutters coated with hot heat mirrors could be incorporated into double glazed windows (coated with cold heat mirrors). These devices would however, be prone to the failures inherent in mechanical devices. Currently external shutters are employed to reduce the incident solar intensity. Unfortunately, architects are reluctant to install such devices

because of the possibility of legal action if a component of the shutter should fall off, damaging property or injuring passers-by. The simplest shading system is, of course, curtains but these do not offer the possibility of 'grey scale' dynamic control. Furthermore, since they are usually situated inside buildings they are not as thermally efficient as external shading devices.

A more desirable system would be a glazing that could be switched between transmissive and non-transmissive states by the application of an electric field or otherwise, i.e. a 'smart' window. Smart windows contain spectrally selective materials to control solar radiation.

2.5 SPECTRALLY SELECTIVE MATERIALS

There are at least six types of spectrally selective materials: solar absorbers (2.13), angular selective coatings (2.14), light transport systems (2.15) and holographic media (2.16), heat mirrors (2.17) and switchable coatings (2.18). These materials have selective optical properties that affect the solar spectrum. Consequently, it is necessary to investigate the nature of the solar spectrum in detail before examining the various spectrally selective materials. The plot shown in figure (2.2) is a plot of the solar spectral distribution for air mass 2 compared with the emissive spectra for a blackbody at several different temperatures (2.19). A blackbody is a system that absorbs all radiation that is incident upon it. It is not only a perfect absorber, it is also a perfect emitter. At a certain temperature a black body will absorb all the radiation incident upon it while also emitting the maximum thermal radiant energy at each frequency for a body at that temperature. Therefore, a blackbody that is at a fixed temperature radiates a characteristic spectrum. This is the radiancy distribution.

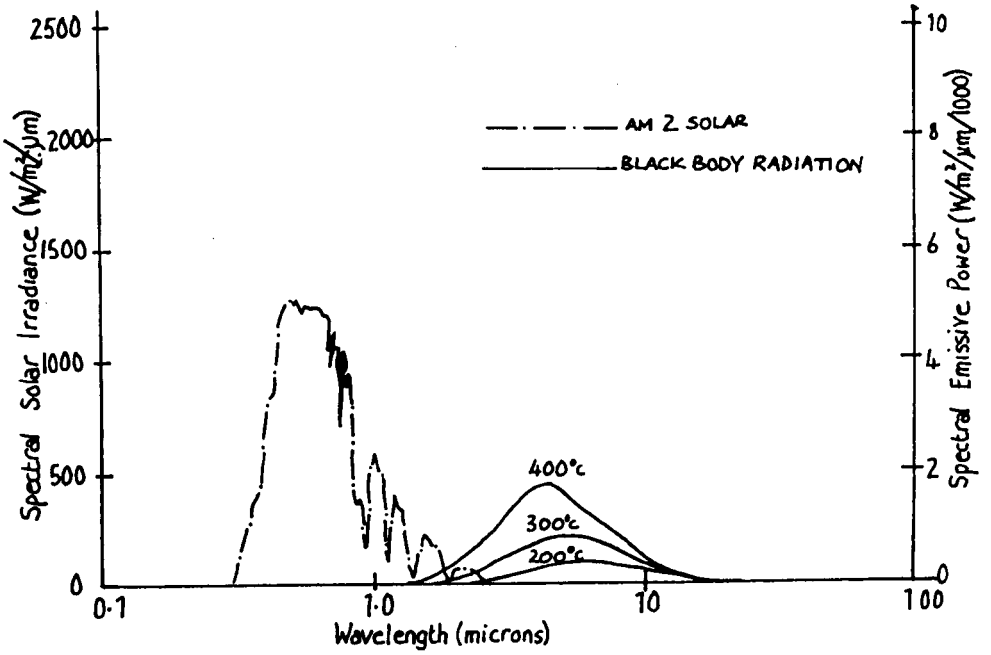

Figure 2.2 AM2 solar distribution and blackbody radiation versus wavelength.

The sun is a blackbody radiator with an effective temperature of 5800 K. Most of the solar radiation is in the ultraviolet (UV), visible (VIS) and near-infrared (NIR). In the atmosphere, absorption and scattering of this radiation occurs due to air molecules, water, and dust, and more recently atmospheric pollutants. Because of this absorption the terrestrial solar spectrum is confined to the range 0.29 μm to 2.50 μm.

2.5.1 Solar absorbers

Due to the energy crisis that commenced in the early 1970's, research on absorbers has concentrated on the application of solar collectors for conversion of solar radiation into electrical power. However, absorbers can be used in conjunction with more conventional systems in space heating (2.20).

Mass wall collectors utilise selective absorbers (2.21). Selective absorbers have high solar absorbtance in the 0.30 μm - 3.00 μm region but a low infra-red emittance (high infra-red reflectance) in the 3.00 μm - 100.00 μm region (see figure 2.3). The transition λ_c wavelength at which the material becomes infra-red reflecting depends on the operating temperature of the coating. At higher temperatures the wavelength maximum of the blackbody spectrum shifts to shorter wavelengths (Wien's displacement law).

Mass wall collectors usually consist of a single diffusing glazing that is in front of a wall. Sandwiched between the wall and the glazing is an absorbing foil (2.22). Most selective absorbers consist of low emissivity (highly reflective in the infra-red) substrates coated with selectively absorbing or transmitting films. These coatings can be deposited using a variety of techniques, such as chemical vapour deposition, electrodeposition, chemical oxidation, vacuum evaporation and r.f. sputtering.

Examples of selective absorbers are electrochemically oxidised nickel-plated coatings, black chrome on steel, or copper oxide on copper. Several companies now manufacture these coatings under a variety of trade names including, Skysorb, Cusorb, Sunstrip and Maxorb. There are also commercially available solar absorbing paints such as Solariselect.

Thermal efficiencies of walls painted with matt black paint and walls covered with strips of self adhesive Maxorb foil have been measured (2.22). The efficiencies were calculated by determining the net energy capture of both systems.

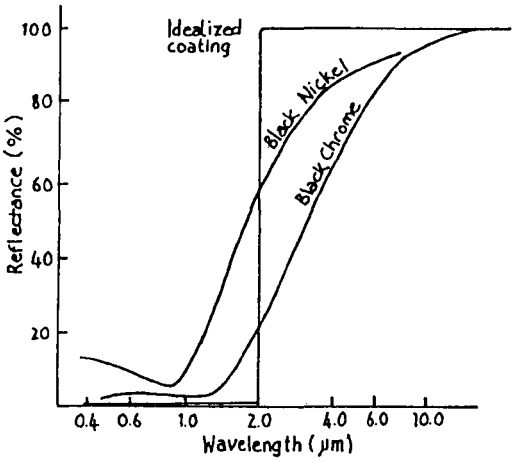

Figure 2.3 Reflectance versus wavelength for black nickel and black chrome and idealized coating.

In winter conditions (January 1984) with low cloud cover (bright) the efficiencies were 29.9% and 19.3% for selective and matt black coatings on walls, respectively. The corresponding efficiencies during overcast weather in February were 14.6% and 8.8% respectively. These results indicate that Maxorb greatly enhanced the net energy capture of the wall both in bright and overcast conditions and was more efficient than materials such as matt black paint. At night reradiation is reduced due to the low emissivity of the selective coatings (see figure 2.3 for reflectance curves of black nickel and chrome and an idealized coating). However, it is beyond the scope of this thesis to present a complete review of selective absorbers (2.23-2.26).

2.5.2 Angular selective transmittance coatings

This type of coating can consist of a columnar structured film (2.14). The columnar structure in this case is not perpendicular to the substrate material, instead it is inclined at a certain angle. This gives rise to angular dependent light transmission. For the control of solar energy the angular transmittance

is dependent on the zenith of the sun. This effect may be used to control solar throughput due to seasonal and daily variations in the position of the sun.

2.5.3 Light transport and holographic media

Light can be guided by a variety of means. Perhaps the most familiar light guides are optical fibres (2.15). Other systems such as holographic gratings can also be used (2.16). These systems may be used for directing sunlight away from expensive antique articles or to guide light to areas that would normally be inaccessible to direct sunlight. Major problems associated with stability of holographic grating are water absorption (dichromated gelatin), ultaviolet degradation and temperature changes.

2.5.4 Heat mirror coatings

Heat mirror coatings are already a commercially successful product, manufactured by companies such as Asahi Glass (Japan). They can be produced by a variety of techniques such as sputtering, evaporation or pyrolytic deposition. Heat mirrors may be 'hot' or 'cold' the use of which is dependent on the climate in the area of application.

2.5.4.1 *Hot heat mirrors*

These coatings are used in countries with hot climates. This type of mirror reflects all solar radiation with wavelengths longer than 0.70 μm, typically up to 100μm (2.17). This still means that the window is transparent in the visible portion of the electromagnetic spectrum 0.40 μm - 0.70 μm (see figure 2.4).

This type of coating reduces air conditioning costs by limiting the solar throughput into the building area behind the window.

2.5.4.2 *Cold heat mirrors*

Although hot heat mirrors are used in countries with tropical climates they are not applicable in temperate climates. This is because they reflect the NIR preventing solar gain in the winter. For this application a coating is required that transmits a larger proportion of the NIR (see figure 2.5). These coatings maximise the solar throughput into the dwelling whilst reflecting the thermal infra-red back into the dwelling thereby reducing heating costs (2.17).

2.5.4.3 *Composition of heat mirror coatings*

The optical properties of heat mirrors can be tailored by materials selection. Hot heat mirrors consist of metals that have high infra-red reflectance, such as Au, Ag, Cu, Al or In (2.17). Other systems use multilayer coatings such as TiO_2-Au-TiO_2 (2.27) and Al_2O_3-Cu-Al_2O_3 (2.28). Cold heat mirrors for passive solar gain consist of semiconductor oxides such as tin oxide doped with antimony (2.29), indium oxide (2.30) indium oxide doped with tin (2.31) and tin oxide doped with fluorine (2.17). As mentioned in section 1.3, these semiconductors have wide band gaps (3.75eV) and high free charge carrier concentrations. Unfortunately, it is beyond the scope of this thesis to present a complete review of the research that has been performed on these materials (2.32-2.34).

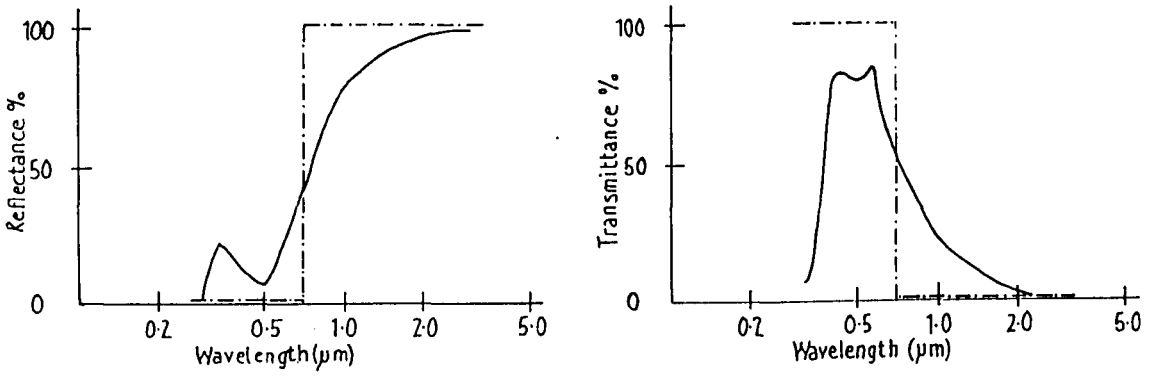

Figure 2.4 Reflectance and transmittance versus wavelength of a hot heat mirror coating.

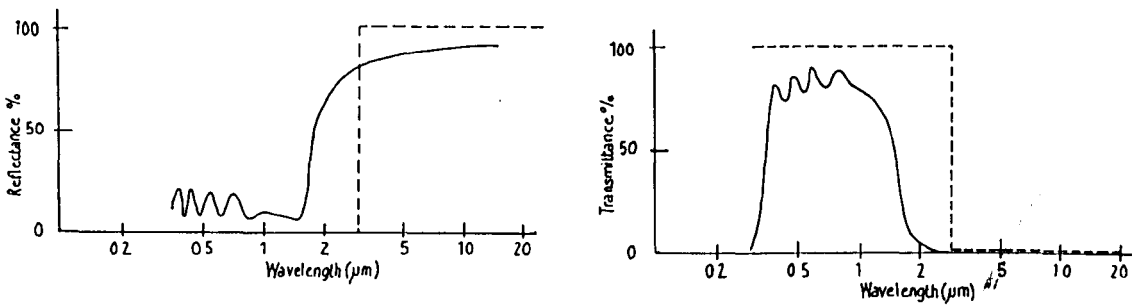

Figure 2.5 Reflectance and transmittance versus wavelength for a cold heat mirror coating.

2.5.5 Switchable coatings

Perhaps the most promising area of research in solar energy control is that of switchable glazings (2.18, 2.35-2.39, 2.136). This is because most devices discussed so far do not exhibit the type of dynamic control possessed by switchable glazings. The only systems currently available for this purpose are mechanical shutters such as blinds and curtains. For such devices to operate at their maximum efficiency they have to be situated outside windows.

Consequently, switchable windows are now being considered as highly attractive options for the control of solar radiation through windows particularly in cooling dominated climates (2.18). However, the energy benefits of some types of smart glazings are controversial. This is because devices that exhibit colouration such as electrochromic windows (ECW) absorb radiation (2.18, 2.41). Absorbed radiation is reradiated at thermal wavelengths. For ECW devices alone, it will be difficult to obtain cooling benefits in the summer months. However, ECW devices will be used in combination with heat mirrors to remove unwanted thermal radiation from the device (2.40, 2.41). The classes of materials that are now under consideration are thermochromics (2.42), photochromics (2.43), liquid crystals (2.44) and electrochromics (2.45). Thermochromic and photochromic materials are passive systems. Devices that contain liquid crystal or electrochromic materials are active devices requiring the application of an electric field.

2.6 CHROMOGENIC MATERIALS

Chromogenic materials are used to control the transport of electromagnetic radiation. There are four main classes of chromogenic materials: photochromic, thermochromic, electrochromic and liquid crystal based systems.

2.6.1 Photochromic materials

Photochromic systems exhibit a reversible change in their optical properties as a function of light intensity. The phenomenon of photochromism was discovered by the scientific community at the beginning of the last century. However the change in colour of dyed fabrics and pigments upon exposure to light has been known to artists for many centuries. Many materials, both organic and inorganic, exhibit photochromism (2.46). Photochromism in organic materials is caused by homolytic and heterolytic cleavage, cis-trans isomerisation and tautomerisation. A disadvantage of organic materials is the build up of fatigue products during colour bleach cycles and the stability to ultraviolet radiation. For these reasons the focus of research has been directed towards inorganic photochromic glasses (2.47, 2.48). These materials exhibit high resistance to fatigue during the colour/bleach cycling process. The property of photochromism is used in ophthalmic glasses (2.49). Other applications that are now being researched are holographic television displays (2.50), optical switches (2.51) waveguides (2.52) and smart window applications (2.18).

2.6.2 Thermochromic materials

The study of thermochromics dates from the latter half of the last century. Thermochromic coatings show a reversible change in their optical properties as a function of ambient temperature. The effect of thermochromism can be caused by several mechanisms, most of which are due to equilibria between different molecular species or isomers. Examples of these phenomena are cis-trans isomerism and crystal phase transition (such as in polymeric liquid crystals). Thermochromism is known in organic (2.53) and inorganic materials

(2.54). The focus of attention in this area of research has been on oxides that exhibit a semiconducting to metallic transition at certain critical temperatures (2.55). The materials that have been at the focus of attention in this area since 1959 are the oxides of vanadium (2.56). However other materials are now being evaluated such as polymeric liquid crystals (2.57), cloud gels (2.58) and inorganic fibre/liquid composites (2.59) that can exhibit thermochromism via the Christiansen effect (2.60).

2.6.3 Electrochromic materials

Electrochromic compounds exhibit a reversible change in their optical properties as a function of an applied electric field. The mechanism of this change is the insertion of small ions. The process can be reversed by subsequently removing these ions from the electrochromic material. An advantage of these types of materials is the open circuit memory they exhibit once electrically switched to a particular optical density. This has energy saving benefits since the electric field only has to be applied when a change in optical state is required. Colour changes due to the insertion of sodium ions into tungsten bronzes were reported in 1951 (2.61). Electrochromics were originally researched as candidate materials for display technology. However, the slow switching speeds and poor cyclic durability of these materials led to liquid crystals being used instead. Recently, however, the potential usefulness of electrochromic materials has been realised (2.62). There is scope for further research in this area due to the many organic and inorganic compounds that exhibit electrochromism (2.63). A variety of electrolytes, inorganic as well as organic, can be used in electrochromic devices (2.63).

There are many applications for electrochromic materials (2.63). These include

rewritable media (2.64), biosensors (2.64), gas sensors (2.64), displays (2.62), rear view mirrors and smart window technology (2.65).

2.6.4 Liquid crystal based systems

Liquid crystal based devices show reversible optical changes as a function of applied voltage. The optical properties of a liquid crystal can be altered by applying an electric field via conductive substrates which are transparent in smart window applications. The change in optical properties occurs because of the birefringent nature of liquid crystal molecules (2.66). When the liquid crystal molecules reorientate due to a change in the electric field intensity the refractive index of the media changes abruptly (typical switching speeds vary from 1 second to 1 x 10^{-3} s). This change in optical properties is known as the Freedricksz transition (2.67) and occurs at a critical voltage Vc (2.68). Unfortunately most liquid crystal (nematics and cholesterics) systems do not exhibit open circuit memory, so when the electric field is removed the optical properties of the system return to that of the unpowered state (2.69). However, recently ferroelectric smectic c liquid crystal systems have been developed that show open circuit memory (2.69). This type of liquid crystal is now being researched for applications such as LCD television screens (2.69).

Several liquid crystal based systems have been developed. One system contains a mixture of dichroic dye molecules with liquid crystal molecules (2.70). The dye molecules acquire the same orientation as the liquid crystal molecules due to mechanical forces. This is known as the guest host effect. Optical modulation is achieved by applying an electric field. This effectively rotates the plane of the dye molecule parallel to the molecular director so that it is parallel with the applied electric field. Another system involves

dispersing a liquid crystal such as a nematic in a medium such as a polymer. The liquid crystal molecules occupy microcavities within the polymer. When an electric field is applied the liquid crystal molecules align with respect to the field. The system is designed such that the refractive index of the aligned molecules perpendicular to the substrate is equal to that of the polymer. This arrangement allows light to be transmitted through the medium in a specular manner. In the unpowered state the refractive index of the liquid crystal molecular axis is different to the polymer in the direction of the incoming wavefront and consequently light is scattered. The variable specular optical transmittance ('grey scale') that can be obtained with this device is due to the different sizes of cavities within the system. Consequently, each cavity has its own critical switching voltage, Vc. As the voltage is gradually increased all the liquid crystal molecules align. This is known as the Christiansen effect (2.60).

Recently devices have been constructed that include dye molecules dispersed with liquid crystal molecules in a polymer. These not only scatter light but can also be used as switchable absorbers. Clearly the next stage of development will be to include smectic c liquid crystal molecules with a dye within a polymer (2.25-2.29). This system would exhibit optical bistability, open circuit memory and modulation of near infra-red radiation.

Although the applications of liquid crystal technology are enormous, perhaps the most important is their use in birefringent displays, phase gratings and switchable lenses, dyed fluorescent or dichroic guest host displays, chiral temperature stage colour devices, nonlinear optics, high resolution laser storage, new erasable rewriteable materials for projection masks, copiers, memories, data storage and smart windows (2.57, 2.65).

2.6.5 Alternative chromogenic materials and effects

Many other chromogenic effects could be utilised to control solar radiation. Perhaps the most familiar are crystals, such as copper sulphate, that alter their colour with respect to water content. Upon hydration the material exhibits an intense blue colour (in the solid state). However, in the dehydrated form the material is white. This occurs because of the loss of aqua ligands. The type and number of ligand substitution dictates the colour of compounds. Reversibility of this effect is dictated by the lability of the complex used. Difficulties with this system may be those of inserting ligands into the material and reversible extraction. Another potentially very useful chromogenic effect is that of barochromism, observed in materials such as samarium sulphide (2.71). The change in optical properties is caused by changes in pressure. Another possibility would be to use magnetic field dependent optical properties.

Electrochromic and liquid crystal materials exhibit changes in optical properties with respect to an applied electric field. There are other possibilities for modulating the optical properties of a material by the application of an electric field. It may be possible to use reversible electroplating (2.72). The major advantage of such a coating would be that it could be used as a variable reflector. Another possibility is the Kerr or Pockel's effect (2.73). The Kerr effect is the field induced double refraction observed in some gases and liquids. The Pockel's effect is seen in noncentrosymmetric piezoelectric media. Both effects can be used to modulate polarised light when used with crossed polars. Another related property is the magneto optical modulation known as the Faraday effect (2.73). The Faraday effect is the rotation of the plane of polarised light under the application of a magnetic field.

Unfortunately, it would be difficult if not impractical to use any of these effects in large area devices (2.65). This is because all of the aforementioned effects would require sophisticated operating systems would be very expensive to construct or require high operating voltages. However it may be possible to incorporate some of these effects into other devices. For example liquid crystals are sensitive to pressure and exhibit changes in optical properties with respect to a magnetic field.

2.7 DEVICE REQUIREMENTS

Optical modulators that are based on electrochromic materials or liquid crystals require transparent conductors so that the optical properties of these materials can be adjusted. The transparent conductive materials can be indium tin oxide (2.74) or a thin layer of a noble metal such as gold or silver (2.75). It is also possible to use grid wire structures as transparent conductors (2.75). Electrochromic devices also require transparent ion conductors. For multilayer devices it is necessary to employ anti-reflection coatings (2.76). This is because at each coating in a multilayer some light will be reflected and some absorbed hence the total transmittance is reduced.

2.8 APPLICATIONS OF CHROMOGENIC MATERIALS

Materials that alter their optical properties reversibly as a function of temperature, electric field, magnetic field or light intensity can be used for a variety of applications. If they exhibit field induced and temperature dependent optical properties they become even more useful. Examples of this type of behaviour are liquid crystals and electrochromics. Most liquid crystals show a change in optical properties as a function of applied magnetic field,

electric field and temperature. The major application investigated in this thesis is electrochromic smart glazings.

2.8.1 Smart windows

2.8.1.1 *Characteristic features*

Large area chromogenic coatings on glass may be used to control solar transmittance (0.3 μm - 3 μm) through windows. Smart windows can be used for architectural, automotive, display and aerospace applications.

Most chromogenic materials are variable absorbers. Unfortunately, materials that absorb radiation also reradiate radiation. This follows from the law of the conservation of energy and can be represented by equation 2.1.

$$A(\lambda) = E(\lambda) \tag{2.1}$$

$$A(\lambda) + R(\lambda) + T(\lambda) = 1 \tag{2.2}$$

where,

$A(\lambda)$ = Absorbance at wavelength λ

$R(\lambda)$ = Reflectance at wavelength λ

$T(\lambda)$ = Transmittance at wavelength λ

$E(\lambda)$ = Emittance at wavelength λ

However, some chromogenic materials, such as electrochromic tungsten trioxide and thermochromic vanadium dioxide, can exhibit variable reflectance in the infra-red (3 μm - 100 μm), and consequently variable thermal emittances (see equation 2.2). A change in the visible optical properties of smart windows renders them useful for privacy control. For the device to be effective this must occur over the range 0.4 μm - 0.8 μm.

Most chromogenic materials are intensely coloured in the coloured state. Tungsten trioxide is profoundly blue in the reduced state although this colour can vary with respect to stoichiometry, morphology, additives, etc. Coatings or devices that exhibit intense colouration would lead to a change in the colour balance of areas located behind windows. Therefore, a material that is grey in the coloured state would be most desirable for glazing applications. This is possible with thermochromic vanadium dioxide (2.56) and electrochromic nickel oxide based coatings (2.104, 2.113, 2.114, 2.131). However, even though high optical densities can be achieved with the desired colouration properties they are not suitable for privacy control because there is a degree of transparency in the coloured state. For some applications (such as bathrooms etc.) a material exhibiting the Christiansen effect may be suitable (2.60). It is very difficult to see through such a material in the unpowered state because of light scattering.

For chromogenic materials such as liquid crystals and electrochromics the application of an electric field is required to produce a change in optical properties. This involves the use of energy. However, smart window technology may lead to a reduction of cooling and heating costs (in cooling dominated climates). The energy savings gained could be gauged by the power required to switch the device, and energy used for space lighting behind the window, offset against the savings gained by reduction in air conditioning cooling costs (summer months). The net energy saved would also be affected by the heat reradiated through the window due to absorption according to equation 2.1. However, smart windows that are now being researched will initially be used in conjunction with heat mirror coatings (separate from the ECW device) to reflect thermal radiation out of the building (2.41).

Although the majority of chromogenic materials can be used to modulate the solar spectrum, some only have limited application because they do not completely satisfy consumer requirements. The modulation range that is desirable for the control of the solar spectrum is 0.3 - 2.5 μm. Only liquid crystal, thermochromics and electrochromics satisfy this criteria. A major advantage of liquid crystal and electrochromic systems is the ability to dynamically control transmittance by altering the intensity of the applied electric field. Therefore these systems can also be used for privacy control. It may also be feasible to switch thermochromic materials using an electrical heater. Another important requirement is that devices should display reflectance modulation. Currently the only systems that display large reflectance modulations are thermochromics. Reflectance modulation is also possible with electrochromic devices but this is usually only of the order of 20%.

Other selection criteria are based on safety and voltage regulations that vary from country to country. Liquid crystal devices are scattering in the off state and usually require a relatively high switching voltage (>50 V). Therefore the failed state would be opaque. This would be a disadvantage during power cuts. Electrochromic devices usually operate at relatively lower voltages (-1 - + 2 V). During power cuts simple short circuit would render devices transparent.

A device based on electrochromic materials is currently the most attractive option for smart window applications because they have the advantage of large dynamic ranges, reflectance modulation (albeit small), open circuit memory, low voltage requirements and the ability to modulate the solar spectrum in the range 0.3 - 2.5μm.

2.9 ELECTROCHROMIC MATERIALS

2.9.1 Electronic generation of colour

There are two limiting cases for the generation of colour in electrochromic materials (2.77). In the first case the addition or removal of electrons leads to the creation of what are classically known as a colour centres. These behave as localised chromophores and extend over a few atoms or molecules. This type of chemical process occurs in certain organic dyes and metal complex ions such as W^{6+} to W^{5+}. Finally electrons can be removed or added to a crystalline or extended amorphous band structure. These of course are only the limiting cases and in reality possible intermediate cases may involve intervalence transfer, small polarons and large polaron models. Another type of intermediate may be that of the initial state being localized but the final state delocalized over a band structure.

2.9.2 Intercalation of ions

Intercalation reactions are solid state chemical reactions in which a chemical species, usually an ion, penetrates a host material. This chemical species then becomes a guest within the host structure. The intercalation of ions within a structure can lead to structural stresses within the host material, particularly if a change in lattice parameter occurs due to the chemical species reacting with the host material. This can lead to delamination or fracturing of the material (2.77). Therefore, the ideal host material should have a large internal free volume, exhibit minimal bond formation and breaking and the guest species should be a small ion. Tungsten trioxide satisfies these criteria. For this reason the focus of attention in the area of electrochromic materials has been WO_3 (2.36, 2.62, 2.77, 2.79).

2.10 ELECTROCHROMISM OF CONDUCTING POLYMERS

There has been considerable interest in the last few decades in conducting polymers (2.80). Some organic polymers exhibit conductivities greater than copper. The most widely researched conducting polymers are polyacetylene (2.81), polypyrolle (2.82), polythiophene (2.83) and polyaniline (2.84). Most polymers can be easily shaped and formed (some are thermoplastic) and are therefore very attractive for industrial applications.

However, conducting polymers, such as, polypyrolle and polyacetylene, are not stable to oxidation (from the air) or pollutants such as SO_2 and O_3 (sulphur dioxide and ozone). Furthermore photochemical chain scission of polymer chains and other photochemical reactions can occur in ultraviolet light. Several techniques have emerged to solve these problems. Oxidation can be reduced by using lamination, addition of stabilisers or by copolymerization (polypyrolle with polyethylene). Stability to uultraviolet light can be improved by the addition of stabilisers (2.85).

Some conducting polymers exhibit electrochromism (see table 2.2). This is because the doping of polymers leads to a geometrically relaxed state (2.86). This is a localized effect over a few monomer units. The result is a new electronic structure. The valence and conduction bands split to form new levels within the band gap. This can produce two states: polaron and bipolaron. In the polaron model three new absorption bands occur whereas in the bipolaron model, there are two new levels (2.86). These transitions occur from the valence band to the various proposed levels within the bandgap. It is these levels that are ultimately responsible for the optical absorption.

Semiconducting materials are usually manufactured by doping of materials such as silicon with phosphorous. Initially it was thought that the same process occurred in polyacetylene, where iodine is added to increase the conductivity of the material. It was soon realised that the process was that of oxidation/reduction (2.86). Thus doping and undoping of materials can occur by electrochemical oxidation and reduction. Because oxidation/reduction processes can occur in conducting polymers they are potentially useful electrochromic materials.

Table 2.2 Bandgap, colouration and conductivity of electrochromic polymers (2.51)

Polymer	Bandgap Eg (eV)	Colours	Conductivity (Scm^{-1})
Polyaniline	3.5	Green in oxidised state transparent in neutral state	1-100
Polypyrolle	3.2	Brown in oxidised state yellow in neutral state	1-100
Polythiophene	2.2	Blue in oxidised state yellow in neutral state	1-100

2.10.1 Electrochromism of polyaniline

Polyaniline is an anodic electrochromic material. Colouration occurs due to proton extraction (2.86). This leads to the delocalisation of charge across the molecular chain. The degree of protonation of the chain decreases with respect to increasing positive potential until the structure consists of quinodiimine and aromatic species.

2.11 TUNGSTEN TRIOXIDE

The electrochromic behaviour of tungsten trioxide was first identified by Deb (2.78). The nature of the electronic colouration of tungsten trioxide is dependent on the degree of crystallinity. In amorphous tungsten trioxide the colour centre is localized over only a few atoms due to the reduction of W^{6+} to W^{5+} however, in crystalline material, delocalization of electrons occurs. The evidence for this is the high infra-red reflectance of crystalline material in the coloured state. Rapid switching is characteristic in amorphous material whereas slow switching occurs in crystalline material suggesting different applications for amorphous and crystalline materials. Amorphous tungsten trioxide is suitable for display technology, whereas crystalline material is more suited to advanced glazing applications because of the high reflectivity in the coloured state (2.77). As previously discussed, reflectance modulation is preferred to absorption modulation because of the reradiation of heat.

2.11.1 Electronic structure

One model used to predict the behaviour of tungsten bronzes assumes that the material is a solid solution of M_xWO_3 (where M = Li, Na, K) in WO_3 (2.77). Using

this model it is predicted that tungsten trioxide has filled valence bands involving tungsten sigma orbitals (6s, 6p and two 5d sigma orbitals) and oxygen sigma orbitals (2s and 2po). The remaining three 5dπ orbitals on the tungsten and 2pπ orbitals on oxygen form a conduction band that is unpopulated in WO_3. However, this band accepts the donated electrons when M_x is inserted, as $M_x^+ + xe^-$ (where x is an integer). The states arising from the ns orbitals associated with M are much higher than the conduction d-pπ conduction band. Clearly, for small values of x the bronzes exhibit semiconducting properties. However, for higher values of x the bronzes become more metallic in behaviour and can be best understood by applying the free electron model proposed by Drude (2.77).

2.11.2 Thin films of WO_3

It is possible to modulate the transmittance of electromagnetic radiation through WO_3 by the injection and extraction of cations. There are two modes by which the transmittance can be modulated: absorption and reflectance. Reflectance and absorption modulation is achieved in crystalline and amorphous materials, respectively (2.77, 2.79). The first alternative is undesirable because it leads to energy being absorbed by the window and consequently reradiated. Reflectance modulation is more desirable because unwanted radiation can be reflected away from the building (2.79).

2.12 NICKEL OXIDE

2.12.1 Chemical properties of nickel oxide

Nickel ($3d^8 4s^2$) exhibits two oxidation states, +2 and +3. In the first transition

series the +3 state becomes more unstable with respect to increasing atomic number (2.123). For nickel only the +2 state is important in aqueous solution. The only compound of any importance in the +3 state is nickel oxyhydroxide (2.123). Although the colour of stoichiometric bulk nickel oxide is usually given as green, other colours ranging from green to metallic are reported (2.53, 2.124). These differences may be due either to impurities or non-stoichiometry.

Nickel hydroxide, referred to in the literature as hydrous nickel oxide also exhibits electrochromism (2.91). This material can be made chemically by reacting a Ni^{2+} salt with an alkaline metal hydroxide solution (2.123). Nickel hydroxide has alpha and beta phases: α-nickel hydroxide has a turbostatic structure that contains hydrogen bonded water; ß-nickel hydroxide contains non-hydrogen bonded O-H. Conversion of α- and ß-nickel hydroxide to NiO occurs at 150 °C and 200 °C respectively (2.94). Transformations between alpha and beta phases can occur hydrothermally or in alkaline solutions (2.104). However, conversion of bulk NiO to $Ni(OH)_2$ is extremely difficult and does not occur even after boiling in water. However, electrochemical conversion of NiO thin films (deposited by PVD processes) with defects to ß-nickel hydroxide is reported by some researchers (2.104, 2.118). Nickel oxide and nickel hydroxide are two different chemical species.

2.12.2 Crystal structures of nickel oxide and nickel hydroxide

The crystal structure of nickel oxide is similar to that of sodium chloride (NaCl). It has been shown that at ordinary temperatures (298k) the structure of nickel oxide is slightly distorted from the ideal cubic NaCl structure (2.87). The ratio of ionic sizes in NaCl is, $r(Na^+)/r(Cl^-) = 0.53$. For nickel oxide the

ratio is smaller, $r(Ni^{2+})/r(O^{2-})$ = 0.49. Evidently, nickel oxide can gain stability by squeezing slightly inwards along the three-fold axis. The resultant rhombohedral angle becomes α=60°4.2'. The structure of nickel hydroxide is similar to that of cadmium iodide (2.92).

2.12.3 The electronic structure of nickel oxide

According to the band theory of solids, as Ni^{2+} ions are brought together, the 3d orbitals overlap to form a 3d band capable of holding 10 electrons (2.53). However, only 8 electrons are available. Therefore, this band can only be partially filled. So nickel oxide should be a good conductor of electricity. However, the reverse is true: pure stoichiometric nickel oxide is an excellent insulator. Band theory cannot be used to predict the electrical behaviour of nickel oxide but six other models have been proposed.

2.12.3.1 *The antiferromagnetic model*

Nickel oxide is an antiferromagnetic material (2.87, 2.89). An electron moving through this structure cannot progress from one site to the next without transporting its spin. Therefore, it would be prevented from moving by the antiferromagnetic superstructure. Using this model, it is possible to predict that the 3d band would be split into two sub bands each of which would hold electrons of a particular spin. However, when nickel oxide is heated above the Neel temperature it does not become a better conductor, as predicted by this model.

2.12.3.2 *Crystal and ligand field model*

Each Ni^{2+} ion is surrounded octahedrally by six O^{2-} ions. The field of the ligands splits the levels into a lower set of three (d_{xy}, d_{yz}, d_{xz}) and an upper

set of two (d_{z^2}, $d_{x^2-y^2}$). The three lower orbitals are completely filled with six electrons, there are still two left and these do not fill the upper set. When energy bands are split by the crystal field, the upper one is only partly filled in nickel oxide. This model also predicts that nickel oxide should be a good conductor (2.89).

2.12.3.3 *Hubbard model*

Another explanation for the break down of band theory when applied to materials such as NiO, is that electrons become localised due to mutual repulsion (2.156, 2.157). In the Hubbard model it is assumed that the most important effects originate from repulsion between electrons in the same atom.

According to band theory, an array of atoms that possess a single valence s orbital should give rise to a band of crystal orbitals each delocalised throughout the array. However, if the overlap between orbitals is very small, the ground state consists of one electron delocalised on each atom. This is because of the extra repulsion that arises if an electron is transferred from one atom to another. The energy required to move one electron from an atom in this array is simply the ionisation energy, I. However, the atom accepting this ionised electron will have a particular electron affinity, 'A'. Therefore, the electron affinity must be subtracted from the ionisation energy I, yielding the energy required to move an electron from one atom to another. This value is known as the 'Hubbard U' (see equation 2.3).

$$U = I - A \qquad 2.3$$

The 'Hubbard U' can be interpreted as the repulsion energy between two electrons on the same atom. If the overlap between orbitals of different atoms is small, the effect of electron repulsion is to make the half filled band insulating. The ionisation energy 'I' (required to remove an electron from an atom) and electron affinity 'A' (due to the addition of an electron to a half filled orbital) can be depicted as lower and upper energy levels respectively

(see figure 2.6). The gap 'U' separating these two energy levels is known as the Mott-Hubbard splitting (as in equation 2.3). The lower and upper levels are each occupied by one electron per atom. These levels are also known as sub bands (2.156, 2.157). As the interatomic overlap increases, the breadth of each of these sub bands increases. Eventually the band width 'W' is equal to the Mott-Hubbard splitting 'U' (see figure 2.6). Beyond this point there is no energy gap and the array initially considered essentially becomes metallic. Therefore, it can be deduced that band theory can be successfully applied if $W > U$.

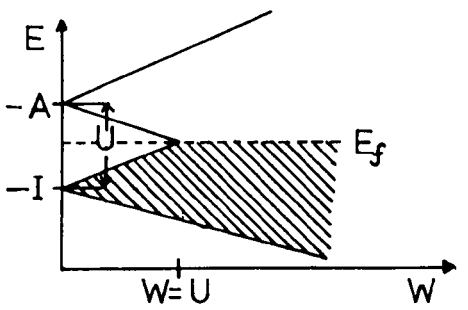

Figure 2.6 Hubbard sub-bands as a function of bandwidth.

2.12.3.4 *The Mott model*

The Mott model has been used to predict semiconductor to metallic type behaviour in materials such as VO_2 (2.55). The insulating behaviour of nickel oxide can be predicted using Mott theory. In this model, the lattice is considered to consist of a cubic array of one-electron atoms of lattice constant 'a'. Mott modelled the free carrier concentration as the lattice constant was varied. This was confirmed experimentally by subjecting materials to hydrostatic pressure. Mott argued that for large values of 'a' the array is an insulator. This occurs because transporting an electron to another site that

has opposite spin requires activation energy to overcome coulombic repulsion. Therefore electrons remain localized to their respective atomic sites and the system remains an insulator (2.89, 2.90). However, for very small values of 'a', neighbouring orbitals overlap and this causes delocalised structures and metallic type behaviour.

2.12.3.5 *d-d transition model*

The d-d model can also be used to interpret the insulating behaviour of NiO. However, recently it has been proposed that the insulating behaviour of nickel oxide is because NiO is an ordinary band insulator, the optical bandgap is due to $3d^8$ to $3d^9L$ transition (2.137).

2.12.3.6 *Comparison of the electronic properties of nickel oxide and titanium monoxide*

Another way to interpret the electronic behaviour of NiO is to compare the electrical properties of NiO and titanium monoxide. In this comparison it is considered that the cause of the very low conductivity ($1 \times 10^{14}\ \Omega^{-1}\ cm^{-1}$) of NiO is because of the lack of overlap between the 'd' orbitals of Ni atoms (2.158). The t_{2g} (d_{xy}, d_{xz}, d_{yz}) levels are fully occupied in Ni^{2+} species, therefore these electrons are not delocalised. However, the e_g (d_{z^2} and $d_{x^2-y^2}$) levels are singly occupied in Ni^{2+}, but unfortunately these orbitals point directly to the oxide ions in the lattice thus restricting metal-metal e_g orbital overlap. Because of the intervening oxide ions, the e_g orbitals are unable to overlap. Thus the e_g orbitals remain localised on individual Ni^{2+} atoms (see figure 2.7).

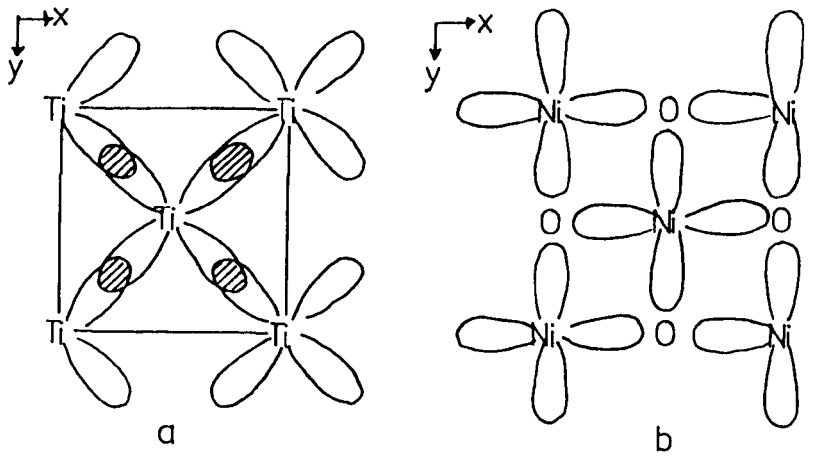

Figure 2.7 (a) TiO structure parallel to a unit cell face excluding the oxide ions. Overlap of d_{xy} (and d_{xz}, d_{yz}) leads to a t_{2g} band. (b) Structure of NiO showing the $d_{x^2-y^2}$ (and d_{z^2}) pointing directly toward the oxide ions and therefore unable to form an e_g band.

Titanium monoxide has a conductivity approaching that of a metal ($1 \times 10^3\ \Omega^{-1}\ cm^{-1}$) because the 'd' orbitals of the metal atoms overlap. In this case the t_{2g} (d_{xy}, d_{xz}, d_{yz}) orbitals are only partially filled, therefore, such orbitals can participate in bonding (see figure 2.7).

In electrochromic materials research insulating nickel oxide is not used. This is because it is necessary to have a certain degree of electron mobility in

order to inject and extract charge. For this reason nickel oxide with incorporated defects is used. This can be produced by using physical vapour deposition such as electron beam evaporation (2.118), or r.f. sputter deposition (2.104, 2.100, 2.113, 2.114).

One of the causes of defects in nickel oxide is nickel metal ion vacancies. In order for nickel oxide to remain stable when it contains vacancies it is necessary for other nickel ions in the structure to increase their oxidation state from 2+ to 3+. This means that the bulk material itself is semiconducting, 'p' type where the majority carriers are holes. This semiconducting nature facilitates the transfer of electrons throughout the structure (via the movement of holes) during the application of an electric field.

The electrical conductivity due to defects in NiO plays an important role in the colouration mechanism. During anion injection or cation extraction it is necessary to remove electrons from nickel oxide or nickel hydroxide to a conductor (TCO or otherwise). Nickel oxide and nickel hydroxide are both 'p' type semiconductors.

2.12.4 Colouration mechanism(s) of nickel oxide and nickel hydroxide coatings

The controversies regarding the colouration mechanism were previously discussed in Chapter 1. The contentious issues are the chemical identity of the bleached and coloured states and the ion(s) responsible for colouration. Analyses have been performed to ascertain the chemical species present in the coloured and bleached states. These investigations have been conducted on NiO produced using different deposition techniques. Other experiments have been executed to identify the ion that causes electrochromism in NiO based coatings.

This is not only of academic interest but has crucial implications on device design.

Classification of the analytical techniques used to identify the mechanism of colouration of nickel oxide based coatings is difficult. This is because most of the analytical methods have been used to prove more than one mechanism. Other problems are that, analyses have been performed on coatings produced using different deposition techniques and conditions, electrochemical experiments have been performed in various electrolytes and different post-deposition treatments have been applied prior to analysis. Whilst some researchers agree on the ion responsible for colouration, they disagree about the chemical identity of the coloured and bleached states. However, three main mechanisms of colouration are reported in the literature. These are, electrochromism due to metal cation (2.104, 2.112, 2.124, 2.126, 2.127), proton (2.110) and hydroxide ion (2.111, 2.125, 2.129, 2.130) insertion. Cation insertion can be further reduced to cation insertion in hydrated (2.124) and anhydrous electrolytes (2.115, 2.116).

2.12.4.1 *Electrochromism of nickel oxide based coatings by cation insertion*

There are two mechanisms that involve cation insertion into nickel oxide based coatings (see equations 2.4 and 2.5).

BLEACHED COLOURED

$$Ni(OH)_2 + 0.33M^+ + 2OH^- \rightleftharpoons 0.33M(NiO_2)_3 + 2H_2O + 1.67\ e^- \qquad 2.4$$

$$M_yNi_{1-x}O \rightleftharpoons M_{y-z}Ni_{1-x}O + zM^+\ ze^- \qquad 2.5$$

where, M can be Li^+, Na^+ or K^+.

Some researchers support injection of M^+ (see equation 2.4) during the anodization of electrochemically deposited nickel hydroxide coatings (2.104, 2.126, 2.127). Quartz crystal microbalance has been employed to add credence to this claim (2.112, 2.124). The argument here is that greater changes in mass occur upon anodization of NiO based coatings in electrolytes containing cations of higher atomic masses than lower atomic masses (2.124). However, other researchers (using Q.C.M.) have reported that OH^- injection occurs during the anodic cycle and that the injection of this ion is responsible for the observed change in mass (2.111).

A possible source of error arising in the argument of cation insertion during the anodic cycle is the assumption that water is desorbed from the coating during colouration (2.112, 2.125). This has not been proved experimentally. However, desorption of water is implied in equation 2.10. In the case of water being retained within the coating (perhaps necessary for self-bleaching) the mechanism portrayed in equation 2.6 may be more accurate.

BLEACHED COLOURED

$$Ni(OH)_2 + OH^- \rightleftharpoons NiOOH.H_2O + e^- \qquad 2.6$$

Other researchers support cation insertion during the cathodic cycle (2.113-2.116). The theory in this case, is that the oxidation state of Ni^{3+} is reduced to that of Ni^{2+} by the insertion of cations (Li^+, Na^+, K^+). During this reduction process the coating becomes transparent. Upon colouration (oxidation for NiO), metal cations such as Li^+ are ejected.

For sputtered NiO coatings, it has been reported that bleaching can occur by lithium ion injection (see equation 2.4) from a lithium gun (2.113). However, it is also known that oxidised sputtered NiO coatings bleach when heated (2.89, 2.113). Bombardment of coatings with ions can lead to an increase in substrate temperature. The temperature of the substrate was not reported in the literature. Furthermore, it is not clear from the literature if coatings were previously cycled in 1M KOH (or LiOH) prior to bombardment with Li+ (2.113). Infra-red analyses of sputtered coatings reported in the literature did not reveal the presence of bonded or non-bonded O-H (2.114). However, these measurements were performed using a low globar voltage and number of scans. Also it is difficult to detect water (bonded or non-bonded) in coatings thinner than 700 A (using a low globar voltage and number of scans).

This notwithstanding, correlation was obtained between the amount of lithium ions injected and changes in optical density. SIMS analysis also confirmed the presence of lithium in coatings. The concentration was greater in the bleached state (2.113). This appears to be evidence for lithium ion bleaching of coatings.

Bleaching by lithium ion insertion using electrochemical methods has been reported in the literature (2.111, 2.116). However, the concentration of water in the electrolyte was not reported (2.115, 2.116). Nor were these studies

supported by infra-red spectrophotometric investigations of the bleached and coloured states. Analysis may have confirmed the absence of O-H within the coating thus adding further credence to the M^+ argument for sputtered coatings in anhydrous electrolytes (2.115, 2.116).

If the organic electrolytes used in some studies (2.113, 2.115, 2.116) contain no water, then initial bleaching may occur by lithium ion insertion. If lithium ion insertion occurs then there may be two environments - hydrated and anhydrous (2.125). In the hydrated environment, nickel oxide based coatings exhibit electrochromism due to hydroxide or hydrogen ion insertion and extraction. In the anhydrous environment, NiO may exhibit electrochromic activity due to cation insertion and extraction (2.113, 2.115, 2.116). Since, however, the actual water concentrations in the anhydrous electrolytes are currently unknown, this argument is difficult to substantiate (2.113, 2.115, 2.116).

Studies on nickel oxide electrodes in anhydrous electrolytes, has confirmed that Li+ can be included within NiO coatings. Lithium ion intercalation improves the cyclic stability of NiO and ß-$Ni(OH)_2$ coatings and increases the oxygen overvoltage by impeding the formation of O_2. The improved durability of such materials may be due to the ability of lithium to retain water (2.108). A disadvantage of lithium ion injection is that some forms of nickel hydroxide (α-$Ni(OH)_2$) are poisoned by lithium (2.94).

2.12.4.2 *Electrochromism of nickel oxide based coatings by proton insertion*

In this case colouration of electrochemically deposited nickel hydroxide occurs by proton extraction (see equation 2.7).

BLEACHED **COLOURED**

$$Ni(OH)_2 \rightleftharpoons NiOOH + H^+ + e^- \qquad 2.7$$

Nuclear reaction analysis has been used to measure the amount of hydrogen present in NiO based coatings in the bleached and coloured states (2.110, 2.125). This was achieved by bombarding coatings with 7 MeV ^{15}N ions. Nuclear reactions within the coatings produce ^{12}C (see equation 2.8).

$$^{15}N + {}^{1}H \rightarrow {}^{12}C^* + {}^{4}He \qquad 2.8$$

Some researchers claim to have detected more hydrogen in the bleached state than in the coloured state (2.110), others claim that there is no difference (2.117). However, even if there is less hydrogen in the coloured state this does not necessarily imply that the coating colours by hydrogen ion extraction. If water is desorbed during the oxidation (by OH^-) of nickel hydroxide then the same result would be observed. Furthermore, water desorption or absorption may have occurred during the experiment (2.93). Other experimental evidence that is cited for proton insertion is cyclic voltammetry (2.103-2.106, 2.108, 2.109). However, some researchers claim that cyclic voltammetry can be used to prove OH^- insertion (2.96, 2.107).

2.12.4.3 *Electrochromism of nickel oxide based coatings by hydroxide ion insertion*

Insertion of hydroxide ions into evaporated nickel oxide based coatings is reported in the literature (2.111). Essentially there are two mechanisms involving colouration by OH^- insertion, the oxidation of NiO to NiOOH (2.111, 2.129, 2.125) and the oxidation of electrochemically deposited $Ni(OH)_2$ to NiOOH by hydroxide ion insertion (see equations 2.9, 2.10) (2.98, 2.118, 2.130).

BLEACHED **COLOURED**

$$NiO + OH^- \rightleftharpoons NiOOH + e^- \qquad 2.9$$

$$Ni(OH)_2 + OH^- \rightleftharpoons NiOOH + H_2O + e^- \qquad 2.10$$

Raman analysis has been used extensively to analyze nickel oxide based coatings in order to identify the colouration mechanism (2.92, 2.93, 2.125, 2.126). However, the precise chemical identity of the coloured and bleached states are controversial. There are at least two interpretations:

(i) Bleached : NiO, Coloured : NiOOH (2.125, 2.126, 2.129).

(ii) Bleached : unassigned state, Coloured : γ-NiOOH (2.92).

Some researchers claim that ß-nickel hydroxide is present in the bleached state (2.92, 2.94-2.96, 2.98). Finally, some researchers assert that γ-NiOOH is irreversible (2.94) whereas others report that it is reversible (2.92).

It is claimed by some researchers that Raman spectroscopy may not be suitable for analyzing materials with low crystallinity (2.95). This is an issue because nickel oxide coatings in the as-deposited state usually exhibit low degrees of crystallinity. It has also been reported that Raman spectroscopy is not suitable for analyzing O-H stretches in weak Raman diffusers such as $Ni(OH)_2$. However, other researchers believe that this technique is suitable for coatings with very low structural order (2.125). It has also been reported that surface enhanced Raman spectroscopy (S.E.R.S) can be used to detect the presence of ß-$Ni(OH)_2$ in NiO electrodes deposited by anodic oxidation of nickel (2.128). Other researchers report that ß-$Ni(OH)_2$ is not detected in the bleached state (2.129).

Infra-red analysis of most nickel oxide based coatings deposited, using a variety of techniques has revealed the presence of α- or ß-nickel hydroxide in the transparent state (2.92, 2.94-2.96, 2.98). For the coloured state ß- or γ-nickel oxyhydroxide has been identified (2.96). Some researchers have identified the presence of water in coatings of nickel oxide using in situ FTIR (2.96, 2.97). A characteristic feature of the infra-red spectrum of α-nickel hydroxide is a broad O-H stretch centred around 3400 cm^{-1} (2.96). For ß-$Ni(OH)_2$ the stretch is much sharper and centred at around 3647 cm^{-1} (2.96, 2,98, 2.118, 2.128). Other absorbance bands reported in the literature for ß-$Ni(OH)_2$ are the in-plane δ OH deformation (540 cm^{-1}) and out-of plane γ OH deformation (350 cm^{-1}) and finally the υ Ni-O stretching vibration (450 cm^{-1}). For α-$Ni(OH)_2$ these bands are shifted to longer wavenumbers (2.96).

The phases of the oxyhydroxide cannot be identified using infra-red techniques. However, a nickel-oxygen stretch at around 580 cm^{-1} is attributed by some researchers to the Ni-O stretch of ß- and γ-nickel oxyhydroxide

(2.96). In order to distinguish between the phases of NiOOH it is necessary to use Raman spectroscopy (2.92). Although some researchers claim this technique is not suitable for discriminating between the phases of NiOOH (2.125).
Another issue is the composition depth profile of nickel oxide coatings. Nickel oxide coatings have been analyzed using angular spectrophometric FTIR. Using this technique some researchers have reported a layered structure of α- and ß-$Ni(OH)_2$ for the bleached state (2.96).

The penetration depth of an electromagnetic wave through a multilayer coating can be altered by adjusting the angle of incidence of the impinging EM wave. When such a wave enters a material that has two layers of different refractive indices, it is totally internally reflected at a critical angle. When this occurs an evanescent wave is set up which decays exponentially with respect to path length in the reflecting phase. Thus, by varying the angle of incidence it is possible to analyze different depths of a coating of nickel oxide. The characteristic broad stretch centred at 3400 cm^{-1} of α-$Ni(OH)_2$ can be resolved in the spectra obtained at smaller angles of incidence. In the Ni-O stretch region the same pattern was observed. The phase detected near the surface of the conductor was predominantly α-$Ni(OH)_2$, whereas mainly ß-$Ni(OH)_2$ was detected at the surface (at high angles of incidence) adjacent to the electrolyte (2.96).

Quartz crystal microbalance (Q.C.M) analysis has been performed on nickel oxide based coatings (2.112, 2.124). An increase in mass with respect to charge extracted is observed for evaporated NiO coatings in organic solvents (2.112). This change in mass is ascribed to the injection of hydroxide ions (when the nickel oxide is anodic). Other researchers also report a gain in mass of NiO when anodised in solutions of alkaline bases. In this case, the change in mass is ascribed to cation insertion into NiO. This involves the injection of positively charged ions into an anode by ion exchange (2.124).

Researchers who claim to have observed an increase in mass during anodic cycles have also observed a simultaneous change in the infra-red properties of such coatings. This change indicates that there is an increase in the free hydroxide stretch during colouration (2.112). This is the clearest evidence so far for hydroxide ion injection from organic electrolytes (containing water) into an evaporated coating of NiO.

Further evidence for OH^- injection into NiO was obtained using radiochemical techniques. Hydroxide ions containing ^{18}O were inserted into NiO. After colouration radioactively labelled ^{18}O was detected in the NiO (2.130).

2.12.5 Other analyses of nickel oxide based coatings

2.12.5.1 *X-ray diffraction*

X-ray diffraction (XRD) has been performed on coatings of nickel oxide produced by sputtering and NiOOH has been detected in the coloured state (2.99). The major problem associated with analyzing nickel oxide based coatings is that nickel oxide and nickel hydroxide are usually deposited in the amorphous form (2.100). Although the degree of crystallinity of as deposited nickel oxide can be improved by heating, the annealing temperatures used lead to decomposition of nickel hydroxide as shown in equation 2.11 (2.99, 2.101, 2.102). Thus, although nickel oxide has been detected in the bleached state of nickel oxide based coatings it may not be the electroactive species (2.100).

$$(\alpha,\beta)\ Ni(OH)_2 \quad \text{Heat}(\alpha 150°C,\ \beta\ 200°C) \rightleftharpoons NiO + H_2O \qquad 2.11$$

Therefore, annealing of nickel oxide coatings prior to XRD analyses is not a satisfactory technique for elucidating the identity of the as-deposited material or electroactive species.

2.12.5.2 *Impedance spectroscopy*

This technique is becoming increasingly popular in electrochromic materials research. Nickel oxide has been analyzed using this technique. The conclusions of most studies are that the coloured state is a better conductor than the bleached state (2.103), the colouration process is diffusion controlled (2.105) and the rate of diffusion changes with respect to colouration (2.103). The internal diffusion coefficient of protons has been reported for nickel hydroxide coatings (2.138). The proton diffusion coefficient for the fully bleached state was 6.4×10^{-11} cm^2 s^{-1}, whereas for the fully coloured state it was 3.4×10^{-8} cm^2 s^{-1}. This implies that NiOOH facilitates the conduction of protons.

2.12.5.3 *Cyclic voltammetry*

Cyclic voltammetry is another technique that has been used by researchers to analyze nickel oxide based coatings (2.96, 2.103-2.109). Anodic, cathodic and oxygen evolution peaks are reported in most papers on nickel oxide based coatings in which cyclic voltammetry was used (2.96, 2.97, 2.103-2.109). The voltages (relative to S.C.E.) at which the anodic and cathodic peaks occur are 420 mV and 250 mV respectively (2.96). Most researchers use cycling rates of $< = 10$ mVs^{-1} to analyze nickel oxide based coatings (2.103-2.108). At these cycling rates nickel oxide based coatings exhibit reversible colouration and bleaching (2.106). Both anodic and cathodic peaks are observed. However, in

most cases (for nickel oxide based coatings) if this cycling rate is exceeded then colouration and bleaching are not observed. Some researchers report that nickel oxide based coatings exhibit faradaic upto 150 mVs^{-1} (2.97). However, other researchers report that the Faradaic anodic peak is missing at scanning rates faster than 10 mVs^{-1} (2.106). This may be because mass transport of hydroxide ions (or hydrogen ions) is dominant over electron transport. In other words the diffusion rate of hydroxide or hydrogen ions into or out of nickel oxide, is not fast enough to offset a faster scanning rate.

The maximum scanning rate possible, may be a function of porosity. The absence of a discussion about the electrochemical reversibility of nickel oxide at different scanning rates in the literature, is probably due to the prevailing belief that is often quoted, that nickel oxide based electrodes are reversible (2.97). Although most nickel oxide based coatings do not exhibit classical reversibility at cycling rates faster that 10 mVs^{-1} (particularly electrochemically and chemically deposited coatings), this does not imply that nickel oxide based coatings exhibit irreversible electrochromism, rather it may imply that the colouration process is diffusion controlled (2.103). If the magnitude of dv/dt (where v is voltage and t is time) is too high then hydroxide ions (or hydrogen ions) will not have time to penetrate (or desorb from) the coating.

2.12.5.4 *X-ray photoelectron spectroscopy (XPS)*

This technique has been used to evaluate the oxidation state of nickel within electrochemically deposited nickel oxide based coatings in the bleached state. The volume concentration of oxygen was measured within the coatings. Most

studies have confirmed the presence of nickel oxide and double oxygen 1s peaks have been observed in some samples. A possible interpretation of this data is the presence of hydroxyl groups. Experiments have also been performed on cycled coatings (1M KOH). Different peaks were found in these experiments. The interpretation of this data was that the peaks corresponded to the chemical species Ni_2O_3 and $Ni(OH)_2$ (2.97).

2.12.5.5 *Auger spectroscopy*

Auger spectroscopy has also confirmed the presence of nickel oxide in electrochemically deposited material. Using this technique some researchers claim to have detected a surface overlayer comprising of highly oxidised nickel. Underneath this layer it is also claimed that nickel hydroxide has been detected. However, it is difficult to prove these claims since this technique only reveals information about elemental composition. Furthermore, there is no evidence for the presence of water or hydrogen in any of the spectra in the literature (2.97).

2.12.5.6 *Ion backscattering spectrometry (IBS)*

The analysis of nickel oxide based samples using IBS only revealed the presence of nickel oxide in electrochemically produced material (2.97). This technique is usually used to perform elemental analysis and is unsuitable for determining molecular structure.

2.12.5.7 *Optical properties of nickel oxide based coatings*

Some nickel oxide based coatings exhibit a brown/bronze colour upon colouration that some researchers believe is suitable for advanced glazing applications such as smart windows (2.97). Other researchers report that a neutral colouration is preferable. This is possible to achieve with nickel oxide based coatings (2.104, 2.112, 2.113). Typical optical spectra of a nickel oxide based coating prepared by anodic electrodeposition, in the bleached and coloured states are shown in figure 2.8. This nickel oxide system exhibits a brown/bronze colour upon colouration (2.97). Examples of nickel oxide based systems that exhibit a neutral grey upon colouration (2.104, 2.112, 2.113, 2.130) (see figures 2.9, 2.10). These types of nickel oxide based coatings can be deposited by sputtering (2.104, 2.112, 2.113) and evaporation (2.131).

The optical properties of NiO oxide based coatings are very sensitive to deposition conditions (2.114). Furthermore, films deposited using different techniques exhibit very different optical characteristics. When coatings deposited by anodic electrodeposition are oxidised they exhibit a brown/bronze colouration (see figure 2.8). This is because in the visible part of the spectrum the transmittance is not uniform, i.e. there is non-uniform absorbance across the visible part of the electromagnetic spectrum (see figure 2.8).

Coatings deposited by sputtering exhibit uniform absorbance across the visible part of the electromagnetic spectrum and therefore the colour of the coating is grey (see figure 2.9) (2.104, 2.113, 2.114). This type of spectrum is characteristic of NiO deposited at low powers (100 W) and high pressures (6 x 10^{-2} T) by sputtering (deposition rate > 0.1 As^{-1}). Other researchers have

produced coatings by electron beam evaporation that exhibit grey colouration (see figure 2.10).

2.12.6 Summary of analyses performed to determine the colouration mechanism(s) of nickel oxide and nickel hydroxide electrodes

Analyses have been performed on nickel oxide based coatings produced by a variety of deposition techniques. The density of NiO_x and $Ni(OH)_2$ is dependent on deposition technique. It is likely that at least one of the reasons why different colouration mechanisms have been reported is due to the different densities of as-deposited coatings. Other properties of coatings that will differ are chemical composition and hence point of zero charge, surface morphology, and porosity (2.97). Coatings with the highest density are produced by sputter coating whereas those deposited using colloidal precipitation are the least dense. It is also evident that coatings deposited by simple chemical or electrochemical methods will be composed of hydroxides of nickel (2.98) or non-stoichiometric oxides of nickel (2.125). Coatings of nickel oxide deposited by PVD (physical vapour deposition) contain defects which are chemically active and must play an important role in the electrochromism of nickel oxide coatings (2.93).

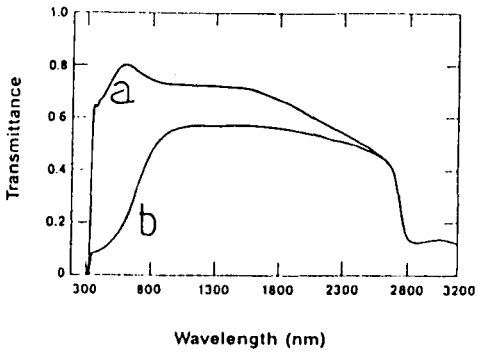

Figure 2.8 Anodically deposited nickel oxide based material: (a) in the bleached state, and (b) in the coloured state.

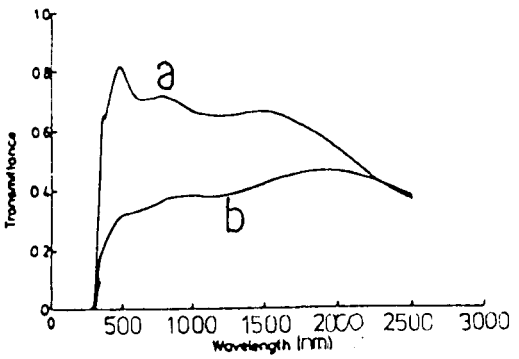

Figure 2.9 R.f. sputter deposited nickel oxide based coating: (a) in the bleached state, and (b) in the coloured state.

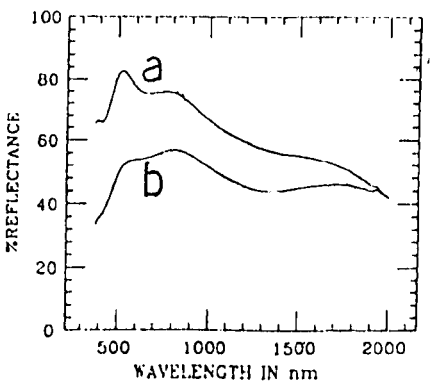

Figure 2.10 Evaporated nickel oxide coating: (a) in the bleached state, and (b) in the coloured state.

It has been reported that some forms of sputtered NiO may bleach by lithium ion bombardment (2.113). However, nickel oxide based coatings are sensitive to heating and further research is necessary to confirm the substrate temperature during lithium ion bombardment (2.114). Other researchers have reported electrochemical bleaching due to lithium ion injection (2.115, 2.116). However, as previously mentioned the water concentrations in the anhydrous electrolytes used in these studies are not quoted (2.113, 2.115, 2.116). It is difficult to substantiate the claim that only lithium ions are involved in the electrochromic process without precise knowledge of the concentration of water.

This notwithstanding, good correlation was obtained between the amount of lithium ions injected and changes in optical density for both lithium bombardment and electrochemical injection (2.113). Also SIMS analysis revealed that the concentration of lithium ions was higher for the bleached state than the coloured state in coatings that were bombarded (2.113) and electrochemically switched (2.115, 2.116).

Some researchers claim that cations are absorbed during colouration and that insertion of cations with higher atomic masses causes a greater change in mass (as measured using Q.C.M.) during the anodic cycle than those of lower atomic masses (2.124, 2.125). However, other researchers claim to have detected OH^- during colouration using Q.C.M. supported by infra-red studies (in organic electrolytes containing water) (2.111).

It has been reported that nickel hydroxide can be oxidised by the loss of a hydrogen ion to the electrolyte. This is based on the NRA analysis performed by Svensson et. al.(2.110). Unfortunately, NRA analyses performed by other

researchers have shown no change in the hydrogen content of coatings in the bleached and coloured states (2.117). Other evidence for colouration due to hydrogen ion extraction is cyclic voltammetry (2.103-2.106, 2.108, 2.109). However, some researchers use cyclic voltammetry as supportive evidence for the oxidation of nickel oxide based coatings by hydroxide ion injection (2.96, 2.107).

Finally, some researchers support oxidation due to hydroxide ion injection (2.98, 2.111, 2.118, 2.125, 2.129, 2.130). The major proof for this is Q.C.M. (2.111) Raman (2.125, 2.129) infra-red studies (2.96, 2.98, 2.118) and radiochemical analysis using ^{18}O (2.130). However, researchers disagree about the chemical composition of the bleached state and the phases of material present in the coloured state. As previously mentioned some researchers using Raman have identified NiO (2.125, 2.129) in the bleached state whereas others using infra-red (2.98) and S.E.R.S (2.128) have found ß-$Ni(OH)_2$. The phase of the coloured state is also controversial. Some researchers claim that it is ß-NiOOH (2.94), whereas others that it is γ-NiOOH (2.92). Hydroxide ion injection has been identified in aqueous and organic environments for nickel oxide deposited using P.V.D processes (2.111) and anodic deposition (2.125, 2.129). Furthermore, conversion of NiO to ß-$Ni(OH)_2$ in alkaline electrolytes has been reported in the literature for both sputtered (2.104) and evaporated coatings (2.118). The electrochromic properties of such coatings are enhanced by the formation of ß-$Ni(OH)_2$ within the coating (2.104). Other researchers report that $Ni(OH)_2$ is not the electroactive species present in NiO coatings (2.125, 2.129).

It is not possible to report a global mechanism for the electrochromism of NiO based coatings at this stage. This is because researchers have clearly analyzed chemically and physically different as-deposited nickel oxide based

coatings. However, some conclusions can be drawn with regard to what may be observed for certain types of coatings and their electrochemical behaviour in aqueous and organic electrolytes.

Chemically or electrochemically deposited coatings from solutions where α- or β-$Ni(OH)_2$ is precipitated, will be composed of, or contain, α- or β-$Ni(OH)_2$ (2.98). Q.C.M nuclear analyses have not yet been reported on coatings deposited from $NiSO_4$ and NH_4OH. For this reason it cannot be stated emphatically that these types of coatings undergo colouration due to hydroxide ion injection. However, NiOOH has been identified in the coloured state of coatings deposited by anodic electrodeposition from solutions containing $NiSO_4$ and NH_4OH (2.98). Unfortunately researchers disagree about the phase of this chemical species. Some researchers have reported that it is γ-NiOOH (2.92) whereas others claim it is β-NiOOH (2.94).

NiO coatings deposited by P.V.D processes generally contain defects (2.93). After the first few electrochemical cycles in aqueous environments nickel oxide may be oxidised to nickel oxyhydroxide by either hydroxide ion injection (2.118) or proton extraction (2.104). Some researchers claim that repetitive cycling of NiO coatings in 1M KOH leads to the formation of β-$Ni(OH)_2$ in sputtered (2.104) and evaporated coatings (2.118). Whereas, other researchers deny that this process occurs (2.125).

Another possibility is the bleaching of nickel oxide (deposited by P.V.D) by cation injection in anhydrous electrolytes (2.115, 2.116). Lithium ion bleaching can also be achieved using a lithium gun (2.113). This may imply that in anhydrous environments NiO bleaches by cation insertion (2.115, 2.116). However in organic electrolytes containing traces of water, nickel oxide may undergo electrochromism by hydroxide or hydrogen ion injection (2.125).

2.13 ELECTRODEPOSITION OF NICKEL OXIDE BASED COATINGS

2.13.1 Anodic and cathodic deposition

Two techniques have been used to electrodeposit nickel oxide based coatings: cathodic (2.107) and anodic (2.132) deposition. The terms anodic and cathodic refer to the polarity of the substrate electrode when the deposition of nickel oxide based systems occur. Nickel oxide based films have been electrodeposited by anodic and cathodic deposition from electrolytes with different compositions.

2.13.1.1 *Electrolytes for anodic deposition*

The electrolytes reported in the literature for the anodic deposition of nickel oxide based electrodes are:

(i) 0.100 M $NiSO_4$. $6H_2O$ and 0.100 M NH_4OH (2.132),

(ii) 0.100 M $NiSO_4$. $6H_2O$, 0.100 M $C_2H_5NaO_2$ and 0.001 M KOH (2.105),

(iii) 7.000 M H_2SO_4, anodic oxidation of nickel (2.133),

(iv) 0.450 M $Ni(NO_3)_2$. $6H_2O$ and 1.750 M NaOH (1.132).

(v) 0.005 M $NiCl_2$ and 0.005 $K_3Fe(CN)_6$ and 0.500 M KCl followed by substrate immersion in 1 M KOH (1.106).

Although electrochromic nickel oxide based coatings can be anodically deposited from all these solutions, not all of these electrolytes can be used to deposit films that are homogeneous and mechanically stable. The optical uniformity of samples produced from electrolytes (ii), (iii) and (v) is very

poor, rendering these electrolytes unsuitable for the fabrication of hydrated layers in electrochromic devices. Electrolyte (i) has been used by several researchers and produces uniform, reversible and mechanically stable films (2.132). Electrolyte (ii) can also be used to produce reversible and mechanically stable electrochromic films, however there is less uniformity in the electrodeposit (2.105). The electrolyte in (iv) can be used to produce uniform films but the electrolyte is not as stable as the electrolyte in (i) (2.132). Anodic deposition of nickel oxide based material (2.132, 2.98) was used in this study using electrolyte (i) (2.132).

2.13.1.2 *Electrolytes for cathodic deposition*

The electrolyte used in the literature for cathodic electrochemical deposition is:

(v) 0.01 M $Ni(NO_3)_2$ (unbuffered) (1.107).

Essentially, this technique involves the cathodization of an indium tin oxide coated glass substrate in a nickel nitrate solution (v). The critical parameters of this method are the current density and the concentration of ions in the electrolyte. The current density quoted in the literature is 0.04 mA cm^{-2} (1.125). If this current density or the concentrations in (iv) and (v) are exceeded then a non-uniform film is the result. It is also necessary to clean the films in 5 M KOH by applying an electric field to the indium tin oxide film. The field is periodically reversed whilst the film is in contact with a KOH solution. Films produced from this electrolyte by cathodization do not exhibit good long term reversibility (2.125).

2.13.2 Summary of electrochemical deposition methods

Film uniformity and durability to electrochemical cycling is important in most electrochromic devices such as smart window technology where the anticipated minimum number of electrochemical cycles is 1×10^5. Nickel oxide based coatings deposited from electrolytes (ii), (iii), (iv), (v) are not suitable for electrochromic device application. This is because films produced from these solutions are either non-uniform ((ii), (iii)), or not stable to electrochemical cycling ((iv), (v)). Some researchers claim that using electrolyte (i) the above criteria can be met (2.132), although this is disputed elsewhere (2.98, 2.125). However, the mode of electrodeposition chosen for this study was anodic deposition using electrolyte (i), 0.1 M $NiSO_4$. $6H_2O$ and 0.1 M NH_4OH (2.132).

2.13.3 Mechanism of Electrodeposition

2.13.3.1 *Anodic deposition from nickel sulphate and ammonium hydroxide*

According to the literature, anodic deposition of nickel hydroxide from a solution containing 0.1 M $NiSO_4$ and 0.1 M NH_4OH proceeds by the deposition of the metal followed by the anodic oxidation of the metal to nickel hydroxide or nickel oxide (2.132). However, other researchers have reported that electrochromic coatings can be produced from such solutions without an applied electric field (2.98)

The mechanism of deposition for anodization using 0.1 M $NiSO_4.6H_2O$ and 0.1 M NH_4OH may involve electrophoresis (2.133). At lower concentrations of NH_4OH with respect to $NiSO_4$, a mixture of anodization (in this case the oxidation of a metallic surface) and electrophoresis may occur. The mechanism for electroless deposition is colloidal precipitation (2.98). This is simple precipitation from a solution onto a substrate followed by film growth due to added material. Electrophoresis is the movement of a charged surface plus attached material (i.e. dissolved or suspended material) relative to stationary liquid by an applied electric field. On arrival at the electrode, deposition can occur. Electrophoresis is used in biology to separate proteins that have charges. Such species exhibit different degrees of migration when subjected to an applied field (2.134).

Colloidal precipitation can occur from lyophobic sols (solvent-hating sols) that are unstable. The definition of lyophobic sols is controversial (2.135). Strictly speaking the term is a misnomer since it implies that colloid particles do not have an affinity for water. This cannot be the case. If it were so it would be impossible to form a dispersion in the first place. However, most of the properties of nickel hydroxide colloids are similar to those ascribed to the term 'lyophobic sol'. The unstable nature of this solution is graphically portrayed in plates 3.1 and 3.2. This is due in part, to the low solubility of nickel hydroxide and because of the concentration of the electrolyte. The concentration of the electrolyte is usually increased if precipitation is desired. Precipitation can be reduced by decreasing the concentration of the electrolyte. However, the deposition rate is lowered in colloidal and anodic deposition.

2.13.3.2 *Anodic oxidation of nickel in sulphuric acid*

The mechanism for the formation of nickel oxide in this process is the oxidation of nickel. This can be achieved by anodizing nickel in an acidic oxidising agent (2.133).

2.13.3.3 *Cathodic deposition from nickel nitrate*

Precipitation of nickel hydroxide onto an electrode surface occurs in response to the rise in pH (see equations 2.12, 2.13) which accompanies the electrochemical reduction of the nitrate ion (2.107)

$$NO_3^- + 7\ H_2O + 8e- \rightleftharpoons NH_4^+ + 10\ OH^- \qquad 2.12$$

$$10\ OH^- + 5\ Ni^{2+} \rightleftharpoons 5\ Ni(OH)_2 \qquad 2.13$$

2.13.4 Coprecipitation of metal ions

The coprecipitation of metal ions has been reported for cathodic precipitation of nickel oxide based electrodes from nickel nitrate solutions. Various metal ion species have been added to deposition electrolytes such as Cd^{2+}, Ce^{3+}, Pb^{2+}, Co^{2+}, Y^{3+}, Fe^{3+}. The incorporation of Y^{3+}, Ce^{3+} and La^{3+} lead to considerable improvement in the degradation of the electrochromic response of nickel oxide based coatings. The reasons for this improvement are not clear (2.119). It is significant that all the ions that improve the electrochromic response are in the oxidation state of 3+. This may lead to an increase in the amount of water included in the coating (2.108, 2.119). It is also likely that the electrochromic

response is improved by the inclusion of ions that create a mixed oxidation state hydroxide or oxide. The mixed oxidation state may improve the electrochromic properties of the coating by facilitating electron transfer and/or the trapping of hydroxide ions at defect sites (2.93).

2.14 ULTRAVIOLET-VISIBLE SPECTRA OF TRANSITION METAL COMPLEXES

The electronic excitation of transition metal complexes usually occurs in the ultraviolet to visible part of the spectrum 10,000 - 50,000 cm^{-1} (1μm - 0.2μm). Electromagnetic radiation of this range of the spectrum may be absorbed for a variety of reasons. These can be classified as follows:

(i) Ligand spectra

(ii) Counter ion spectra

(iii) Charge transfer spectra

(iv) Ligand field spectra

2.14.1 Ligand spectra

Many ligands such as water exhibit absorption bands that are normally observed in the ultraviolet. These absorption bands also appear in the spectra of complexes that incorporate such ligands, but they are shifted from their original positions (2.139).

2.14.2 Counter ion spectra

In order to preserve charge neutrality a complex ion must be associated with a counter ion. The absorption spectra of the counter ion must be known in order to interpret the spectra for the entire system (2.139).

2.14.3 Charge transfer spectra

When a transition occurs between metal and ligand orbitals, a charge transfer spectra is observed. Some complex ions such as MnO_4^- exhibit intense absorption in the visible part of the electromagnetic spectrum because of charge transfer (2.139). In the case of MnO_4^- this process occurs by ligand to metal charge transfer (by reduction of the metal).

2.14.4 Ligand field spectra

This type of spectra originate from transitions between the 'd' orbitals of a metal species that have been split from their original degenerate state due to the ligand field effect (2.139).

In this study the causes of ligand field spectra are reviewed. Excellent reviews of ligand, counter ion and charge transfer spectra can be found elsewhere (2.139).

2.14.5 Ligand field spectra (terms and Russel-Saunders states)

Various processes can give rise to the spectra of transition metal complexes. The models discussed so far are usually applied to complexes in which only single electron transfer occurs. Such models can be used to explain the spectra of d^1 complexes such as $[Ti(H_2O_6)]^{3+}$, but when more than one 'd' electron (such as in Ni^{2+}) is present the interactions between the quantum numbers of the individual 'd' electrons must also be considered (2.140).

Four, one-electron quantum numbers can be assigned to an electron in an ion. These are designated n (the principal quantum number), l (the azimuthal or orbital angular momentum quantum number), m_l (the magnetic orbital quantum number), and s (the spin quantum number). In a d^2 ion the interactions that can occur between electrons are of three types:

(i) Spin-spin coupling

(ii) Orbit-orbit coupling

(iii) Spin-orbit coupling

In comparison to the other coupling mechanisms, in spin-orbit coupling only the coupling between the spin and orbit of individual electrons is considered. This is because the coupling between the spin of one electron and the orbital momentum of another is so small that it is ignored. According to the Russel-Saunders scheme (2.140) it is assumed that:
spin-spin coupling > orbit-orbit coupling > spin-orbit coupling

This rule can be applied to elements of the first transition series and including Zn, thereafter a phenomena known as jj coupling must be applied (2.140). However, since the transition metal species considered in this study is Ni, jj coupling will not be considered further.

2.14.5.1 *Spin-spin coupling*

For a system of electrons, the resultant spin quantum can be determined from equation 2.14 (2.140):

$$S = (s_1 + s_2),(s_1 + s_2 - 1),.....(s_1 - s_2) \qquad 2.14$$

where, $s = \pm 1/2$ and S is the total spin quantum number.

2.14.5.2 *Orbit-orbit coupling*

The orbital angular momentum of two electrons can be represented by l_1 and l_2 (see equation 2.15). The total orbital angular momentum number can be determined by adding l_1 and l_2 vectorially (2.141):

$$L = (l_1 + l_2),(l_1 + l_2 - 1),...(l_1 - l_2) \qquad 2.15$$

In the same manner that l defines an orbital (i.e. for an s orbital, l = 0), L defines a quantum number or energy for a system of electrons. Using this scheme the following term letters can be derived (2.141):

L	0	1	2	3	4	5	6
Term letter	S	P	D	F	G	H	I

2.14.5.3 *Spin-orbit coupling*

By coupling the resultant spin and orbital momenta of a system of electrons, the total orbital angular momentum number J can be determined (see equation 2.16)

$$J = (L + S),(L + S - 1),....(L - S) \qquad 2.16$$

where, the terms L and S are those previously described (see equations 2.14 and 2.15). Whilst terms of different L values have appreciably disparate energies, for given values of L and S several levels may reside closely together. The number of these levels is known as the multiplicity (see equation 2.17).

$$\text{Multiplicity} = 2S + 1 \qquad 2.17$$

where, S was previously described in equation 2.14. The terms singlet, doublet and triplet arise when the multiplicity is 1, 2 and 3 respectively (2.142).

All of this information can be summarised in one symbol known as the term symbol (see equation 2.18).

$$\text{Term symbol} = {}^{(2S+1)}L_j \qquad 2.18$$

In the case of d^8, the values for L are 4, 3, 2, 1 and 0 (using equation 2.15). These values yield the terms letters G, F, D, P and S and multiplicities of 1 and 3 (using equation 2.17). However, not all of these terms are allowed because they are in contravention of the Pauli exclusion principle (2.142). For d^8 (and d^2) the allowed terms are ^3F, ^3P, ^1G, ^1D, ^1S. The lowest energy term is

determined by applying Hund's rules. The following general canon can be applied (2.142):

(i) The most stable state is the one possessing the maximum multiplicity.

(ii) If a group of terms has the same multiplicity the one with the largest value of L has the lowest energy.

2.14.6 Racah parameters B and C

The energy separation between the various terms previously described can be expressed in terms of two electron repulsion parameters known as the Racah parameters B and C (2.143). In the first transition series only the d electrons are considered. Therefore, the energy differences between states of disparate multiplicities are given by multiples of B and C. Ions of the first transition series have a C/B ratio of approximately 4, $B \approx 1000\ cm^{-1}$. These parameters are determined experimentally from the spectra of complex ions (2.144).

2.14.7 Selection rules for d-d transitions

2.14.7.1 *Spin-forbidden transitions*

Transitions in which there is a change in the number of unpaired electron spins are known as spin-forbidden (2.145-2.149). Therefore, for optical absorption to occur $\Delta S=0$. It can be deduced that transitions are forbidden when $\Delta S \neq 0$.

2.14.7.2 *Orbitally-forbidden (Laporte rule) transitions*

The transition of electrons between states of the same parity are forbidden by the Laporte selection rule (2.145-2.149). This means that d-d and p-p electron transitions in the same quantum shell are forbidden but s-p and p-d electron redistribution are allowed. If this rule and the spin-forbidden selection rule were strictly applied then transition metal complex ions would not exhibit strong absorption. In fact, when both of these rules apply as in the case of Mn^{2+} (d^5) the absorption intensity is very weak.

The five d orbitals of a given shell are degenerate in a free atom. However, in a d metal complex, if a deviation of the spherical environment of the ion occurs then these orbitals are no longer degenerate, electrons can absorb energy and transitions can occur between energy levels (see figure 2.11). In this case, the restriction of the Laporte rule no longer applies because if a deviation of the spherical environment occurs then the complex is no longer centrosymmetric. Deviation from symmetry may occur due to the asymmetric vibration of ligands. An electron transition that is 'allowed' by the vibration of a molecule is known as a vibronic transition. In solids such as NiO, asymmetric vibration of ligands occurs due to phonon (lattice vibration) interactions with the spherical environment surrounding Ni^{2+}. This can lead to d-d electron transitions in solids.

For an octahedral complex (such as $[Ni(H_2O)_6]^{2+}$) the five d orbitals of the central atom are split into two sets, a triply degenerate set known as t_{2g} and a doubly degenerate set labelled e_g. The three t_{2g} orbitals lie below the e_g orbitals. The separation in energy between these orbitals is known as the

ligand-field splitting parameter (Δ_0 - for octahedral symmetry). Because the separation is not large, transitions can occur between these two sets of orbitals, typically in the visible part of the electromagnetic spectrum. Finally, spin-forbidden transitions can be relaxed somewhat by spin-orbit coupling.

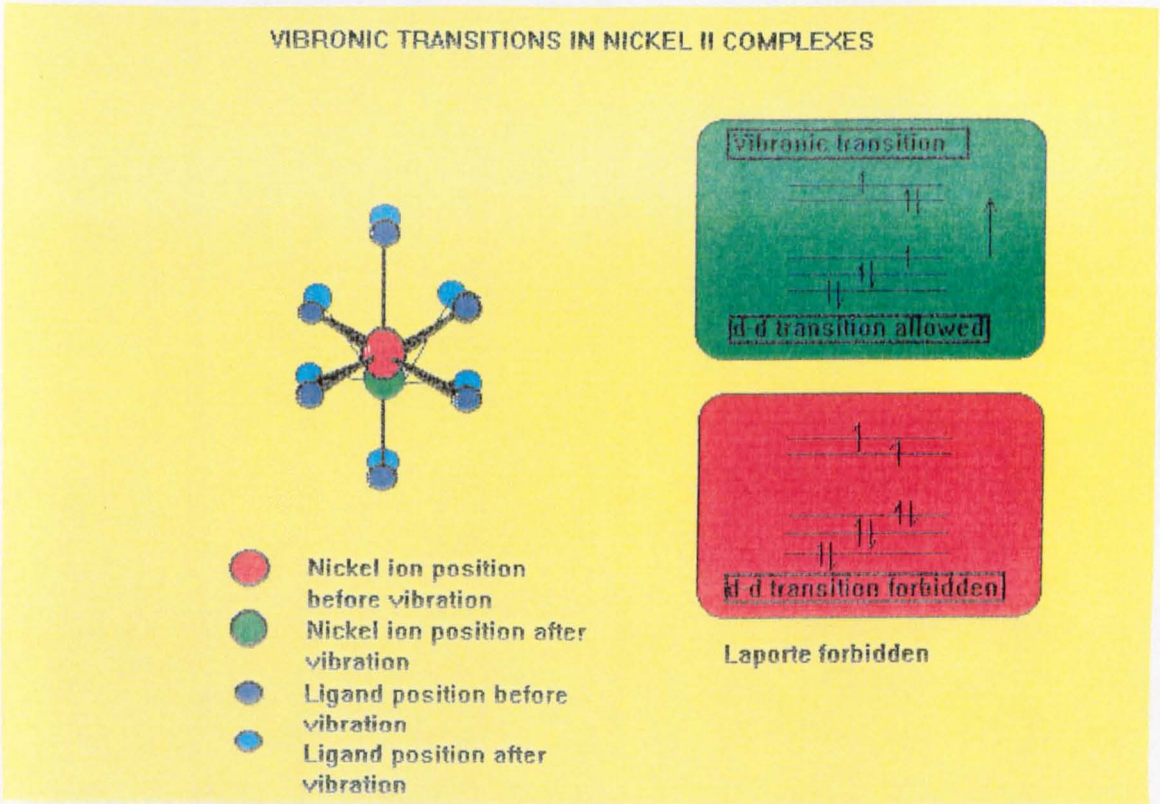

Figure 2.11 Vibronic transitions in nickel II complexes.

2.14.8 Effect of ligand fields on the absorption spectra of complex metal ions

The orbit-orbit coupling terms described are for free ions and define the total orbital angular momentum number. In order to interpret the absorption spectra of complex metal ions, it is necessary to consider the effect of weak and strong ligand fields on these ions. In a weak field environment, it is assumed that the crystal field perturbation is small compared to the inter-electronic repulsion forces but larger than the spin-orbit coupling forces. In this case the orbit-orbit coupling terms arising from the free ion are derived first and then the effect of the crystal field on these terms is considered. In a strong field environment, electron pairing may occur. In this case the effect of the inter-electronic repulsions is less than that of the crystal field. For the purposes of this study only the effect of a weak field environment is considered. In such an environment the terms arising in octahedral and tetrahedral fields can be derived (see table 2.1) (2.150).

2.14.8.1 *Spectra of d^8 ions*

The ground state of the d^8 ion configuration is ^3F, the higher energy terms are ^3P, ^1G, ^1D and ^1S (see equation 2.18). In an octahedral field these terms are split to give those shown in table 2.3 (2.151). Spin-allowed transitions can occur between terms derived from ^3F and ^3P. Three transitions occur from the ground term ($^3A_{2g}$). These transitions are observed in hexa-aquonickel (II) and hexa-aminenickel (II) complexes (see table 2.4 and figure 2.12 for hexa-aquo nickel II (2.152)).

Table 2.3 Terms arising due to weak field ligands in octahedral and tetrahedral environments

Free-ion term	Terms arising in cubic fields
S	A_1
P	T_1
D	$E + T_2$
F	$A_2 + T_1 + T_2$
G	$A_1 + E + T_1 + T_2$

Key: A = singlet state

E = doublet state

T = Triplet

Subscript 1 = symmetrical w.r.t C_2 axis rotation (that is perpendicular to the principal axis).

Subscript 2 = not symmetrical w.r.t C_2 axis rotation (that is perpendicular to the principal axis).

Table 2.4 Electronic spectra of hexa-aquonickel (II) and hexa-aminenickel (II) complexes.

Complex	$^3A_{2g} \Rightarrow {}^3T_{2g}$ cm^{-1}	$^3A_{2g} \Rightarrow {}^3T_{1g}$ cm^{-1}	$^3A_{2g} \Rightarrow {}^3T_{1g}$ cm^{-1}
$[Ni(H_2O)_6]^{2+}$	8500	13,800	25,300
$[Ni(NH_3)_6]^{2+}$	10,750	17,500	28,200

Key: g = gerade

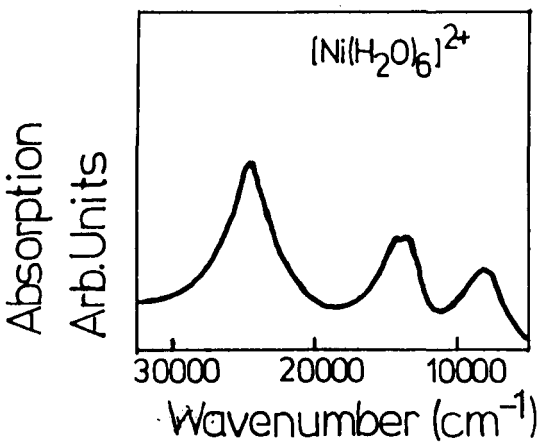

Figure 2.12 Electronic spectra of $(Ni(H_2O)_6)^{2+}$ (d^8).

Ligand field spectra are exhibited by solids that possess localised 'd' electrons (2.153-2.155). These are usually similar to those exhibited by isolated complex ions in solution. Relevant to this study is the similarity between the spectrum of $[Ni(H_2O)_6]^{2+}$ and that of NiO (see figure 2.13).

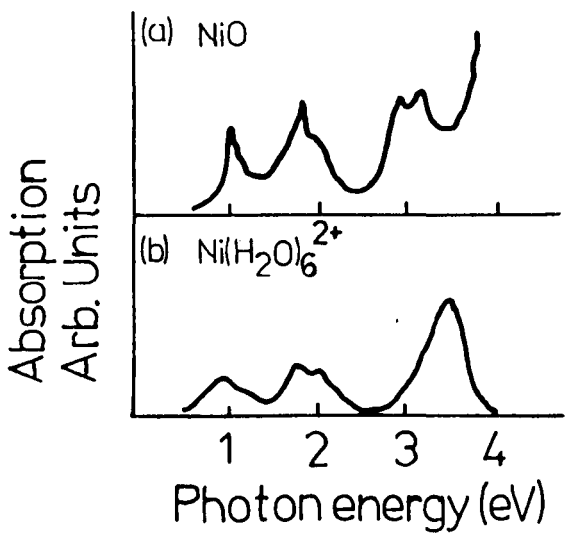

Figure 2.13 Optical absorption of (a) NiO
and (b) $[Ni(H_2O)_6]^{2+}$.

2.15 FACTORS AFFECTING THIN FILM GROWTH

The major processes involved in the deposition of thin films are:

(i) Surface wetting

(ii) Nucleation

(iii) Crystal growth

(iv) Mode of crystal growth

The formation of precipitates in solutions involves two distinct processes (2.159). These are nucleation and crystal growth. It is the relative rates of these processes that determines the particle sizes of precipitates in solution.

The driving force for nucleation and crystal growth is supersaturation (2.159). This is achieved when the solubility product (K_{sp}) of the precipitating material is exceeded (in the case of $Ni(OH)_2$ K_{sp} is 2×10^{-15} at 298 K) (2.160). The initial rate of nucleation is dependent on the degree of supersaturation before phase separation occurs. The rate of crystal growth is dependent on the following factors:

(i) The amount of available material.

(ii) The viscosity of the medium. This affects the rate of diffusion of material necessary for the propagation of crystal growth.

(iii) The ease with which additional material can be incorporated into the crystal lattice of the particle.

(iv) Adsorption of impurities on the particle surface. These act as growth inhibitors (habit modification).

(v) Solution temperature.

A distinction can also be made between two types of nucleation in solutions, these are homogeneous and heterogenous (2.161-2.163). Homogeneous nucleation occurs in the solution, whereas heterogenous nucleation usually occurs on surfaces such mould walls or particles of dirt.

2.15.1 Homogeneous nucleation

When molecules cluster together to form a small solid sphere from a solution of free energy G_1, the free energy of this system changes to G_2 (see equation 2.19).

$$G_2 = V_S G^S_V + V_{Sl} G^{Sl}_V + A_{Ssl}\gamma_{Ssl} \qquad 2.19.$$

where, V_S = Volume of solid

V_{Sl}= Volume of solution

G^S_V= Free energy per unit volume of solid

G^{Sl}_V= Free energy per unit volume of solution

A_{Ssl}= Area of solid/solution interface

γ_{Ssl} = Solid/solution interfacial free energy

The formation of a solid results in a change in free energy (see equation 2.20)

$$\Delta G = -V_S \Delta G_V + A_{Ssl}\gamma_{Ssl} \qquad 2.20.$$

also, $$\Delta G_V = G^{Sl}_V - G^S_V \qquad 2.21.$$

where, γ_{ssl} = solid/solution interfacial free energy

ΔG_v = Change in volume free energy

The excess free energy ΔG_r (see equation 2.22) associated with the formation of a solid particle can be minimised by the correct choice of particle shape. If γ_{ssl} (see equation 2.20) is isotropic then this shape is that of a sphere of radius r.

$$\Delta G_r = -\frac{4}{3}\pi r^3 \Delta G_v + 4\pi r^2 \gamma_{ssl} \qquad 2.22$$

From equation 2.22 and figure 2.14 it can be seen that the interfacial free energy increase is proportional to r^2, whereas the increase in volume free energy is proportional to r^3. Therefore, the creation of small particles of a solid always leads to an increase in free energy. For a given degree of supersaturation (σ) there is a certain critical radius r* that is associated with a maximum excess free energy. If $r < r^*$ the system can lower it's free energy by dissolution of the solid. However, if $r > r^*$ the free energy of the system decreases as the solid grows (see figure 2.14). By differentiating equation 2.22 the critical radius for nucleation r* and the maximum excess free energy (ΔG^*) associated with a nucleus of radius r* can be found (see equations 2.23 and 2.24).

$$r^* = \frac{2\gamma_{ssl}}{\Delta G_v} \qquad 2.23$$

$$\Delta G^* = \frac{16\pi\gamma_{ssl}^3}{3(\Delta G_v)^2} \qquad 2.24$$

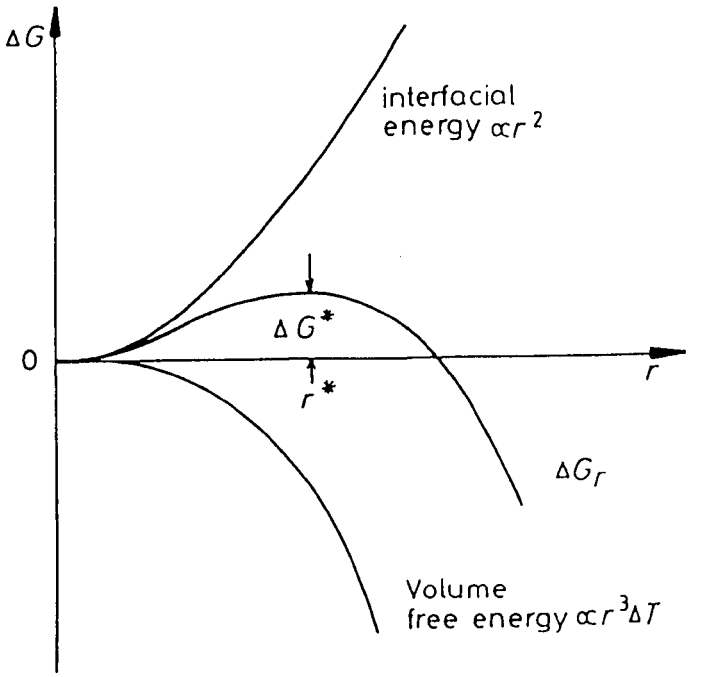

Figure 2.14 The free energy change associated with homogeneous nucleation of a sphere of radius r.

From equations 2.23 and 2.24 it can be shown that by decreasing the interfacial energy term γ_{ssl}, the excess energy ΔG^* can be reduced. This can be achieved if nucleation occurs on a surface (heterogeneous nucleation).

2.15.2 Heterogeneous nucleation

The total interfacial free energy can be minimised if the as-formed nucleus (or embryo) has the shape of a spherical cap with a wetting angle θ given by the condition that the interfacial tensions γ_{sbsl}, γ_{ssb} and γ_{ssl} balance in the plane of the surface where nucleation occurs (see equation 2.25 and figure 2.15).

$$\gamma_{sbsl}=\gamma_{ssb}\gamma_{ssl}\cos\theta \qquad 2.25$$

where, γ_{sbsl} = Substrate/solution interfacial tension

γ_{ssb} = Solid/substrate interfacial tension

γ_{ssl} = Solid/solution interfacial tension

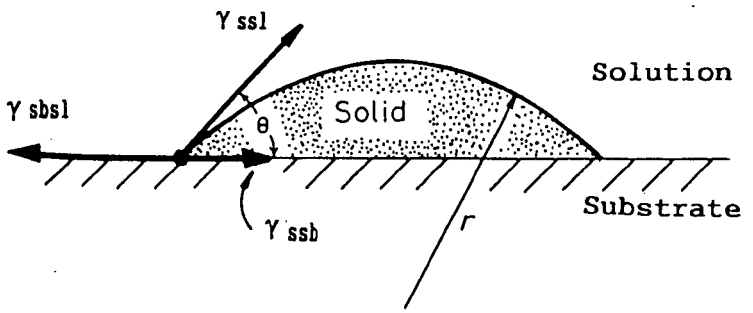

Figure 2.15 Heterogeneous nucleation of a spherical cap on a substrate surface.

The formation of such an embryo is associated with an excess free energy ΔG_{het} (see equation 2.26).

$$\Delta G_{het} = -V_s\Delta G_v + A_{ssl}\gamma_{ssl} + A_{ssb}\gamma_{ssb} - A_{ssb}\gamma_{sbsl} \qquad 2.26$$

where,

V_s = Volume of the spherical cap

A_{ssl} = Interfacial area of solid /solution interface

A_{ssb} = Interfacial area of solid and substrate

γ_{ssl} = Interfacial free energy of solid /solution interface

γ_{ssb} = Interfacial free energy of solid/ substrate interface

γ_{sbsl} = Interfacial free energy of substrate/ solution interface.

The major difference between equations 2.20 and equation 2.26 is that there are now three interfacial free energy terms to consider. The first two terms $A_{ssl}\gamma_{ssl}$ and $A_{ssb}\gamma_{ssb}$ are positive and arise from interfaces created during the nucleation process.

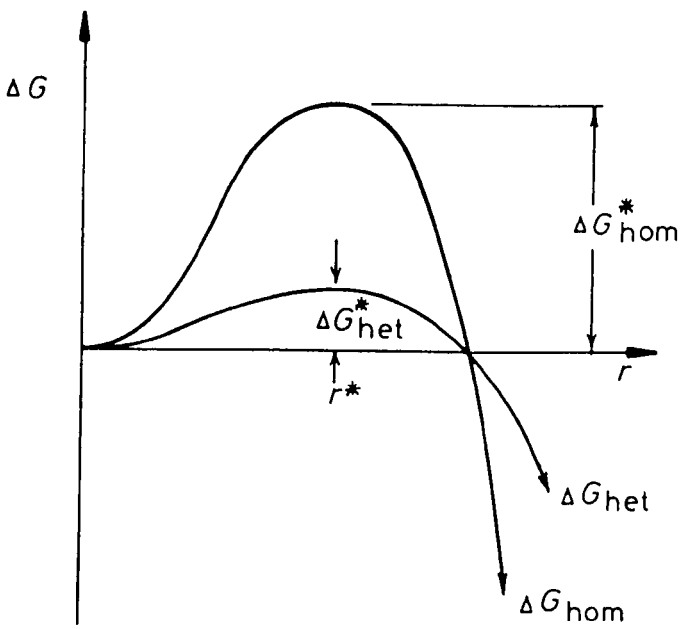

Figure 2.16 The free energy change associated with homogeneous and heterogenous nucleation of a sphere of radius r.

However, the third term arises from the destruction of the substrate/liquid interface, this results in a negative energy contribution. Therefore, the excess free energy ΔG^*_{het} becomes more negative if the interfacial free energy between substrate and solution increases. It can also be shown that:

$$\Delta G_{het} = -\{\frac{4}{3}\pi r^3 \Delta G_v + 4\pi r^2 \gamma_{sl}\} S\theta \qquad 2.27$$

where, $S\theta$, also known as the geometric factor is:

$$S\theta = (2+\cos\theta)(1-\cos\theta)^2 \qquad 2.28$$

By differentiating equation 2.27 it can be shown that:

$$r^* = \frac{2\gamma_{sl}}{\Delta G_v} \qquad 2.29$$

and,

$$\Delta G^* = \frac{16\pi\gamma_{sl}^3 S\theta}{3\Delta G_v^2} \qquad 2.30$$

Now, since $S\theta <= 1$, the activation barrier against heterogeneous nucleation (ΔG^*_{het}) is smaller than ΔG^*_{hom} by $S\theta$.

2.15.3 Surface wetting

In the previous analysis it was assumed that substrates are perfectly clean i.e. no adsorbed contaminants such as grease or gases. Contaminants trapped between nuclei and substrates raise the values of γ_{ssl}, and ΔG_{het} and ultimately decrease the rate of nucleation. Contamination can be reduced by cleaning the surface of substrates with surfactants, heating under ultra high vacuum (1×10^{-10} T) and ultraviolet treatment. These procedures can improve the wetting of surfaces (2.164).

2.15.4 Contact angles and wetting

A surface becomes wetted when one fluid is displaced by another on the surface of a substrate. The following treatment is restricted to wetting in which a gas is displaced by a liquid at the surface of a solid. Three types of wetting can be identified (2.165):

(i) Spreading wetting

(ii) Adhesional wetting

(iii) Immersional wetting

2.15.4.1 *Spreading wetting*

This phenomena occurs when a liquid already in contact with a solid spreads so as to increase the solid-liquid and liquid-glass interfacial areas. The spreading coefficient (S) can be determined from equations 2.31 and 2.32.

$$S = \frac{\Delta G_s}{A} \qquad 2.31$$

where, ΔG_s is the free energy increase due to spreading and A is the interfacial area between the solid and the liquid.

$$S = \gamma_{SG} - (\gamma_{SL} + \gamma_{LG}) \qquad 2.32$$

When S is positive or zero, the liquid spreads spontaneously over the surface of the solid. However, when S is negative, the liquid remains as a drop having a particular contact angle θ (see figure 2.17).

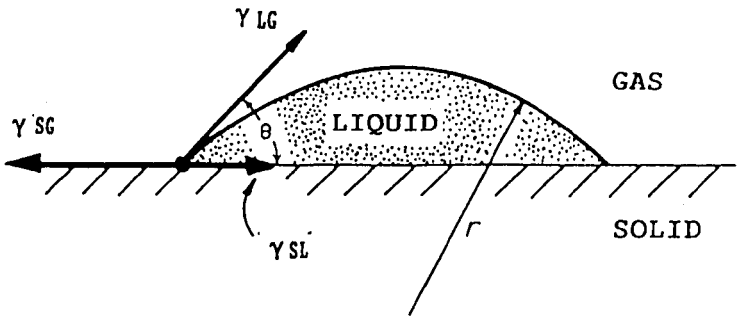

γ_{LG} = Liquid-gas interfacial tension

γ_{SL} = Solid-liquid interfacial tension

γ_{SG} = Solid-gas interfacial tension

Figure 2.17 Contact angle between solid-liquid-gas interface.

2.15.4.2 *Adhesional wetting*

Wetting of this type occurs when a liquid, not originally in contact with a solid, makes contact and adheres to it. A difference between this type of wetting and spreading wetting is that the liquid gas interfacial area decreases. The work of adhesion, that is, the work required to separate a unit area of the solid liquid interface is given by the Dupre equation (2.166) and:

$$W_a = -\frac{\Delta G_a}{A} \qquad 2.33$$

$$W_a = \gamma_{SG} + \gamma_{LG} - \gamma_{SL} \qquad 2.34$$

combining equation 2.34 with Young's equation (2.196) the following equation is obtained:

$$W_a=\gamma_{LG}(1+\cos\theta) \qquad 2.35$$

When the contact angle is zero, $\cos\theta = 1$ and $W_a = 2\gamma_{LG}$. Therefore, zero contact angle occurs when the forces between the solid and liquid are equal or greater than those between liquid and liquid. A finite contact angle results when the liquid adheres less to the solid than itself.

2.15.4.3 *Immersional wetting*

In immersional wetting a solid completely immersed in a liquid. Therefore, the interfacial area of contact between solid and liquid remains constant. The free energy of immersion for a solid in a liquid is given by the following equation,

$$-\Delta G_i=\gamma_{SG}-\gamma_{SL} \qquad 2.36$$

and,

$$-\Delta G_i=\gamma_{LG}\cos\theta \qquad 2.37$$

If $\gamma_{SG} > \gamma_{SL}$, then $\theta < 90°$ and spontaneous immersional wetting occurs. However, if $\gamma_{SG} < \gamma_{SL}$ then $\theta > 90°$, work must be performed to immerse the solid in a liquid.

2.15.5 Complete wetting of a surface

In terms of liquid/solid contact complete wetting occurs when a liquid spreads so as to completely cover the surface of a solid (2.167). Incomplete wetting occurs when a contact angle forms between a solid and a liquid. Therefore a condition for complete wetting is that the contact angle between a liquid and a solid should be zero. As previously mentioned it is also important that there should be no contaminants on the surface of the solid.

2.15.6 Growth of a pure solid

The mode of solid (or film) propagation is dependent on the nature of the surface state of the solid (2.168). There are basically two types of solid surface states:

(i) Atomically flat
(ii) Atomically rough

Atomically rough surfaces propagate by a continuous growth process, while flat interfaces migrate by a lateral growth process.

2.15.6.1 *Continuous growth*

This process occurs on solids that have atomically rough surfaces (see figure 2.18). The interface at the solid liquid interface is disordered and atoms arriving at random positions on the solid surface do not significantly disrupt the equilibrium configuration at the interface.

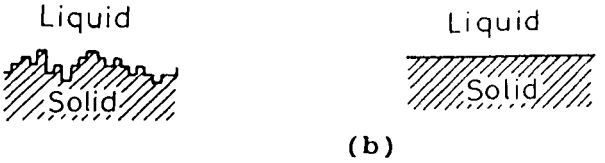

(a) (b)

Figure 2.18 (a) Atomically rough, and (b) smooth surfaces in contact with liquids.

2.15.6.2 *Lateral growth*

The propagation method for atomically flat surfaces is that of lateral growth (2.169). In the case of a molecule leaving the liquid to attach to the solid surface it can readily be seen that the interfacial energy will increase. Therefore the probability is low that this molecule will remain on the surface. It is more probable that it will return to the liquid. However, for molecules that attach to ledges, the interfacial energy is lower and there is no change in the interfacial energy for those molecules that attach to ledges that have jogs (see figure 2.19).

2.15.7 Non-equilibrium features at the film growth interface

Ledges and jogs are non-equilibrium features of the interface so growth is dependent on the supply of ledges and jogs. There are three ways that such features can be supplied:

(i) repeated surface nucleation
(ii) by spiral growth
(iii) from twin boundaries

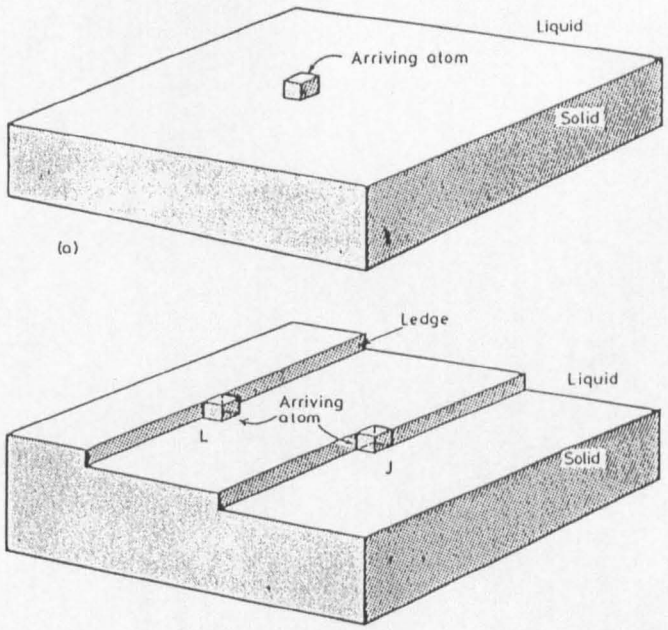

Figure 2.19 Atomically smooth solid liquid interfaces with molecules represented by cubes: (a) addition of a single molecule to a smooth surface, (b) addition to a ledge and, (c) addition to a jog on a ledge.

2.15.7.1 *Surface nucleation*

Previously it was shown that a molecule that attaches to a smooth atomic surface would be unstable and return to the solution. However, if a number of molecules come together they form a disk shaped layer as shown in figure 2.20. It is possible for this arrangement to become stable and continue to grow (2.170).

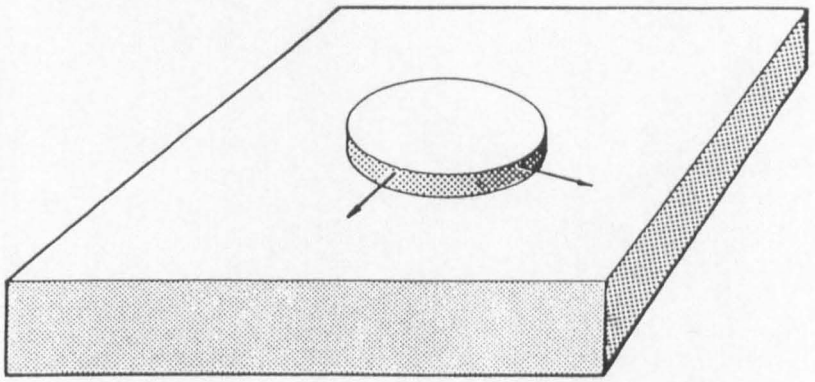

Figure 2.20 Ledge creation via surface nucleation.

Once this disk has nucleated, growth proceeds very rapidly. However, when the disk has grown and covers the entire surface nucleation must occur on the newly formed surface before further growth can occur.

2.15.7.2 *Spiral growth*

If a solid contains dislocations then the problem of creating new interfacial steps is avoided. In this treatment the presence of a screw dislocation will be considered (see figure 2.21).

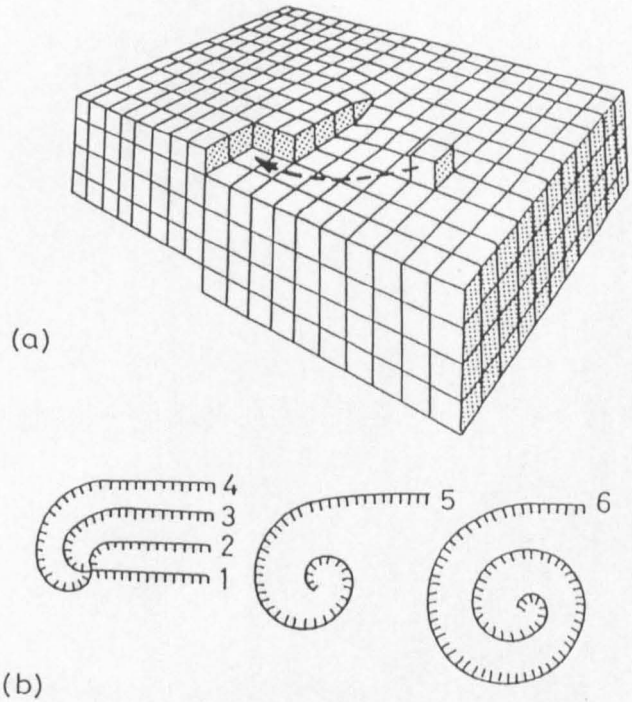

Figure 2.21 (a) A screw dislocation terminating in the solid liquid interface and, (b) propagation of growth due to the addition of material to the spiral.

The addition of molecules to the ledge causes the ledge to rotate about the point where the dislocation emerges, therefore the ledge never runs out of interface. If molecules add at an equal rate at all points on the step the angular velocity of the step, initially is the greatest nearer the core of the dislocation (2.171). Therefore, as growth proceeds the ledge develops into a spiral as shown in figure 2.21 (b).

2.15.7.3 *Growth from twin intersections*

Another permanent source of steps can be generated by the presence of twin boundaries. During crystal growth of materials that exhibit faceting, it is normal to obtain more than one crystal. A twin occurs when two crystals form. In the case of a twin, the interfacial facets intersect at the grain boundary between the two crystals. This can act as a permanent source of new steps in a similar manner to that of the spiral growth mechanism (2.171).

2.15.8 Deposition of uniform thin films from colloidal hydrosols

In order to achieve uniform thin film deposition from colloidal hydrosols it is necessary to control the following parameters:

(i) pH
(ii) Degree of supersaturation
(iii) Surface roughness of substrates
(iv) Contact angle
(v) Mode of growth

2.15.8.1 *Effect of pH*

The wetting properties of colloidal hydrosols on surfaces such as polythene (a hydrophobic material) are affected by pH of the colloidal hydrosol (2.172). These surfaces can be coated with uniform hydrated oxides at certain pH values (i.e. when the colloidal hydrosol is wetting).

2.15.8.2 *Degree of supersaturation*

A certain amount of supersaturation is vital for nucleation and crystal growth propagation. However, if the degree of supersaturation is too high, coarse filterable precipitates are formed that can lead to the deposition of non-uniform coatings (2.173). Therefore, to control film uniformity, the degree of supersaturation must also be controlled.

2.15.8.3 *Surface roughness*

Film uniformity is also affected by the substrate surface roughness. If the substrate material is very rough, when nucleation and film growth proceeds the defects on the surface are propagated as the film grows. Therefore, the surface of the coating generally is a replica of the substrate surface (2.174).

2.15.8.4 *Contact angle*

The wetting of a surface can be determined from the contact angle. The major factors affecting the wetting angle are surface contaminants, surface roughness and method of film preparation. Insufficient non-uniform surface wetting can affect the rate of nucleation and lead to non-uniform film growth (2.175).

2.15.8.5 *Cleanliness of the substrate*

This can be improved by scrubbing the surface of the substrate with nonionic or ionic surfactants. During this process the surface of substrates should be copiously flushed with deionised water. Once the substrate has been rinsed

thoroughly in deionised water it can then be dried in an inert atmosphere such as N_2 at 0% relative humidity. Further improvements in surface cleanliness can be achieved by exposure to ultraviolet light and ozone followed by heating the substrate at an appropriate temperature under ultra high vacuum (1×10^{-10} Torr) (2.176).

2.15.8.6 *Effect of surface roughness on contact angle*

If the contact angle between a liquid and a substrate is < 90°, the liquid will penetrate the surface of the solid and fill up most of the pores and hollows at the surface of the solid, thus forming a plane surface that is part solid and part liquid. In this case the contact angle θ decreases. If, however, the contact angle θ is> 90°, then the liquid does not penetrate the pores and hollows at the surface of the solid. In this case the liquid can be regarded as resting on part solid and part air. Under these circumstances because the adhesional forces between the liquid and the entrapped air are weak the contact angle increases (2.177).

2.15.8.7 *Effect of substrate deposition conditions on contact angle*

The substrate preparation method can affect the contact angle, if the substrate materials that have crystallised in contact with water usually have lower contact angles than those that have been prepared in air. This is because the surface of substrates crystallised in an atmosphere containing water may have water molecules trapped at the surface of the substrate. In

this case the entrapment of traces of water in the surface layers serves to lower the contact angle (2.177).

2.15.9 Modes of growth

A film spreads across or uniformly wets a surface when

$$\gamma_f + \gamma_i < \gamma_s \qquad 2.38$$

γ_f = Film free surface energy

γ_i = Substrate/film interface free energy

γ_s = Substrate free surface energy

When film spreading occurs, the total free surface energy is lower for the wetted surface (hence the importance of cleaning) than the bare surface alone. This leads to smooth uniform growth, atomic layer by atomic layer. This is sometimes referred to as the Frank-Van der Merwe growth mode (see figure 2.22 (a)). In order for this mode of growth to occur the bonding between the film and substrate must be strong enough to reduce γ_i in equation 2.38. If the bonding between the film and substrate is weak then,

$$\gamma_i = \gamma_s + \gamma_f \qquad 2.39$$

and no spreading occurs. Instead 3D island formation occurs. This type of growth is known as Volmer-Weber (see figure 2.22 (b)). Another mode of growth involves the deposition of a few uniform layers as in the Frank-Van der Merwe mechanism, however after the deposition of the first few uniform layers the growth mechanism resorts to that of 3D island formation, this type

of film growth is known as Stranski-Krastanov (figure 2.22 (c)). Three dimensional growth of coatings is usually undesirable because it leads to rough non-uniform coatings (2.178).

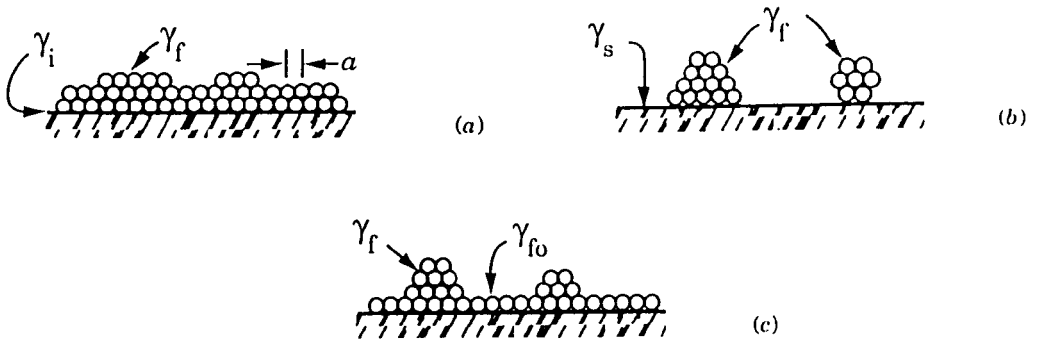

Figure 2.22 Modes of film growth: (a) Frank-Van der Merwe, (b) Volmer-Weber and, (c) Stranski-Krastanov.

2.16 INFRA-RED REFLECTANCE MEASUREMENTS OF NICKEL OXIDE BASED COATINGS

2.16.1 Selection rules for the spectroscopy of $Ni(OH)_2$

For the purposes of this analysis the infra-red spectrum of ß-$Ni(OH)_2$ will be considered. In order to analyze the spectrum of ß-$Ni(OH)_2$ coatings it is necessary to establish the structural relationship between ß-$Ni(OH)_2$, the basic nickel hydroxide phase, and the spectroscopic unit cell. Within a single layer of the ß-$Ni(OH)_2$ structure the symmetry operations combine to yield a space group of D_{3d}^3 (2.92). The structure of ß-$Ni(OH)_2$ is similar to that of CdI_2 , where the Cd^{2+} ion can be replaced by Ni^{2+} and the I^- ion by hydroxyl ions. A unit cell of $Ni(OH)_2$ contains metal ions that are bonded to the hydroxyl ions of the same layer. These are also in contact with hydroxyl ions in adjacent layers. Therefore each hydroxyl ion forms three bonds to a nickel ion of its own layer and is in contact with three hydroxyl ions in an adjacent layer. This unit cell has the factor group of C_{3v} (see figure 2.23).

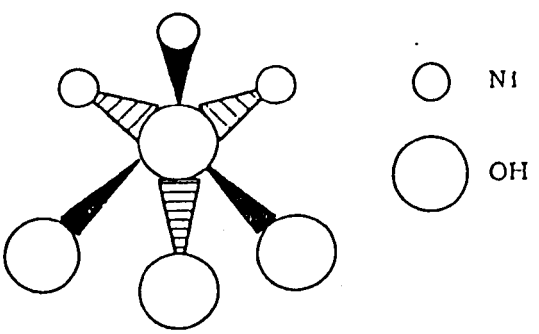

Figure 2.23 Unit cell of nickel hydroxide.

The hydroxyl ions in this unit cell are not directly bonded to hydroxyl ions in adjacent layers. The infra-red spectrum of ß-$Ni(OH)_2$ has a sharp band at 3630 cm^{-1} that is indicative of free O-H stretches. Therefore, it can be concluded that there is no significant hydrogen bonding in the structure. The unit cell for ß-$Ni(OH)_2$ can therefore be reduced to that shown in figure 2.24

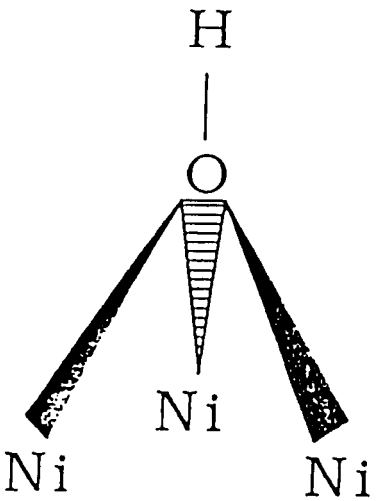

Figure 2.24 Unit cell for ß-$Ni(OH)_2$

This system also has the C_{3v} factor group. The vibration modes of ß-$Ni(OH)_2$ can be predicted from a knowledge of the symmetry elements of this unit cell (see figure 2.24). The symmetry elements of this cell are described in the character table 2.5.

Table 2.5 Symmetry elements of the ß-$Ni(OH)_2$ cell

C_{3v}	E	$2C_3$	$3\sigma_v$		
A_1	1	1	1	Z	x^2+y^2, z^2
A_2	1	1	-1	R_z	
A_3	2	-1	0	(x,y)	(R_x,R_y) (x^2-y^2,xy) (xz,yz)

Yielding the reducible representations, X^R

C_{3v}	E	$2C_3$	$3\sigma_v$
X_RAll	15	0	3
X_RTRANS	3	0	1
X_RROT	3	0	-1

$$\Gamma_{ALL} = 4A_1 + A2 + 5E \quad 2.40$$

$$\Gamma_{ROT} = A2 + E \quad 2.41$$

$$\Gamma_{TRANS} = A1 + E \quad 2.42$$

However;

$$\Gamma_{ALL} = \Gamma_{VIB} + \Gamma_{ROT} + \Gamma_{TRANS} \quad 2.43$$

$$\Rightarrow \Gamma_{VIB} = 3A_1 + 3E \quad 2.44$$

It can therefore be deduced that there are six infra-red and Raman active modes of vibration for $Ni(OH)_2$ that can be predicted for ß-$Ni(OH)_2$ that are not all mutually exclusive (see table 2.6). These bands are reported in the literature (2.92).

Table 2.6 Mode assignments of Raman and Infra-red bands of ß-$Ni(OH)_2$

Frequency cm^{-1}	Activity	Symmetry Type	Assignments
3630	Infra-red	A_1	Asymmetric υ_{OH}
3580	Infra-red Raman	A_1	Symmetric υ_{OH}
553	Infra-red	E	Deformation δ_{OH}
450	Infra-red Raman	A_1	υ_{NiO}
350	Infra-red	E	OH libration
318	Raman	E	Ni-OH lattice

2.16.1.1 *Surface selection rule for reflectance measurements*

In a reflectance measurement the electric field that oscillates normal to a metal (or TCO for infra-red reflectance) surface is considerably larger than the field oscillating parallel to the surface which is negligible. Therefore, it can be deduced that the electric field that is normal to the surface can interact with surface species that have vibrating dipoles normal to the surface (of a metal or TCO), giving rise to absorption bands, whereas an electric field oscillating parallel to the surface produces absorption bands of negligible intensity. This is one of the two effects that constitutes the surface selection rule.

A vibrating dipole of surface species is accompanied by an image dipole within

a metal (or TCO). The surface selection rule is also derived from the image dipole. A dipole vibrating normal to the surface gives rise to an image dipole that is parallel to the dipole of the surface species, whereas the dipole vibrating parallel to the metal surface generates an image that is antiparallel. The surface selection rule is often used to determine the orientation of species on metal surfaces (2.179)

2.17 CYCLIC VOLTAMMETRY

This is an electrochemical analytical technique that is based on the analysis of current-voltage curves. First of all a working electrode is polarized with a triangular voltage. If the applied potential is negative then reduction can occur. The working electrode then passes through an intermediate range, the voltage becomes positive and the electrode is reoxidised. Therefore, for a quasi-reversible reaction both reduction and oxidation peaks occur (the full nature of reversible systems is discussed in section 2.17.1). If the reaction is completely irreversible then only one peak occurs (although in some cases this may be due to a fast following chemical reaction). The position of the peak potentials of cathodic and anodic peaks as functions of the rate of change of voltage reveals information about the reversibility of a particular system, and details concerning the mechanism of specific electrochemical process (2.180)

2.17.1 Reversible systems

In order to predict what a reversible voltammogram should be like it is necessary to consider a simple reversible chemical process such as that depicted in equation 2.45 where O and R are electroactive species (2.181).

$$O + ne^- \rightleftharpoons R$$

In equation 2.45 it is assumed that only O is originally present in solution. If a very slow scanning rate is applied to the system depicted in equation 2.45, the voltammogram will be similar to that shown in figure 2.25 (a steady state response). However, as the scanning rate is raised, the height of the peaks increases. In order to explain this phenomena it is necessary to consider the shape of the concentration profiles of O as a function of applied potential.

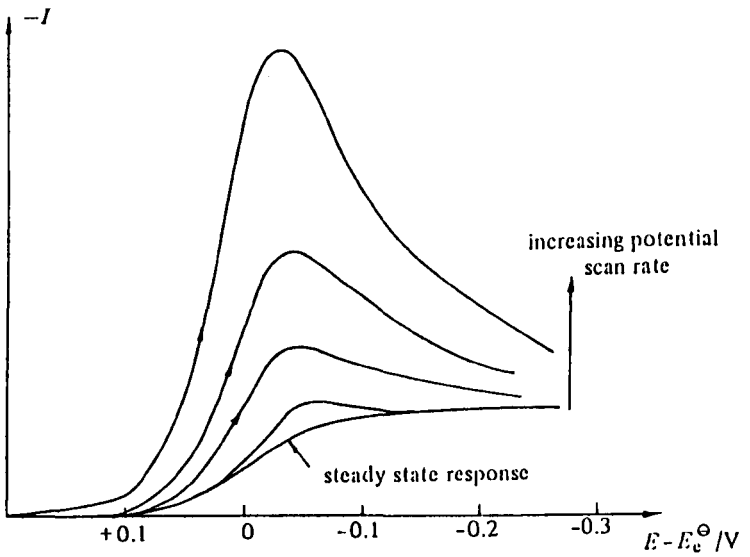

Figure 2.25 A series of linear sweep voltammograms for the reduction of the species O using several different scan rates.

Under steady state conditions the concentrations of species at a certain distance from the electrode are maintained uniform by natural convection.

This, notwithstanding, within the region next to the electrode (Nernst diffusion layer) the concentration gradients are linear. For a reversible reaction the ratio of C_0^0/C_R^0 is given by the Nernst equation (see equation 2.46).

$$E_e = E_e^{\Theta} + \frac{RT}{nF} Log_e \frac{C_O^o}{C_R^o} \qquad 2.46$$

where,

E_e = Equilibrium, or reversible voltage (V)

E_e^{θ} = Standard Potential (V)

R = Gas constant (JK^{-1} mol^{-1})

T = Temperature (K)

n = Number of electrons involved in overall reaction

F = Farad ($C\ mol^{-1}$)

C_0^0 = Concentration of species O at the electrode (if x is the distance from the electrode then in this case x = 0)

C_R^0 = Concentration of species R at the electrode (if x is the distance from the electrode then in this case x = 0)

Therefore as the potential is made more negative the concentration of the reactant at the surface of the electrode decreases. If the sweep rate is increased, the diffusion layer does not have the time to relax to its equilibrium state. The surface concentration of O decreases from the bulk value (in order to satisfy the Nernst equation) as soon as the potential at which O is reduced is achieved, a current can flow in an external circuit that is proportional to the value of the concentration gradient at the electrode

surface. However, at the same time the electrode potential is continuing to change, the surface concentration of O is further reduced until it reaches zero. When $(C_O)_{x=0}$ reaches zero the concentration gradient starts to decrease due to relaxation. Hence the current flowing must also decrease. Overall this behaviour leads to a peak shaped current response. It can also be shown that the concentration gradients at the surface of electrodes and the current flowing in the external circuit will increase with sweep rates as a result of the shorter time scale of the experiment (less relaxation).

At slow sweep rates the current should trace the forward curve when the electric field is reversed. However, this is not the case for faster sweep rates. In this case there is a sufficient concentration of R present near the electrode surface and in fact R continues to form until the potential reaches E_e^θ. As the potential approaches E_e^θ, the R present near the electrode starts to be reoxidised back to O (in order to satisfy the Nernst equation). Therefore, a reverse current flows. As the electrode potential changes, R eventually reaches 0. Using the same arguments that were employed for the forward cycle it can also be shown that a current peak will occur on the reverse cycle.

To be completely rigorous it is necessary to solve Ficks' second law for O and R in order to determine the exact form of the cyclic voltammogram.

$$\frac{\delta C_O}{\delta t} = D_O \frac{\delta^2 C_O}{\delta x^2} \qquad 2.47$$

$$\frac{\delta C_R}{\delta t} = D_R \frac{\delta^2 C_R}{\delta x^2} \qquad 2.48$$

D_R = Diffusion coefficient of the species R

D_0 = Diffusion coefficient of the species O

O is initially present and assuming that $D_0 = D_R = D$, the initial boundary conditions are:

$t = 0$	$x > 0$	$C_0 = C_0^*$ and $C_R = 0$
$t > 0$	$x > \infty$	$C_0 = C_0^*$ and $C_R = 0$
$t > 0$	$x = 0$	

$$D\frac{\delta C_O}{\delta x} + D\frac{\delta C_R}{\delta x} = 0$$

$$\left(\frac{C_O}{C_R}\right)_{x=0} = \exp\left\{\frac{nF}{RT}\left(E - Ee^{\Theta}\right)\right\}$$

$$-I = nFD\left(\frac{\delta C_O}{\delta x}\right)_{x=0}$$

Using a sweep rate of υ

$0 < t < \lambda \quad E = E_1 - \upsilon t$

$t > \lambda \quad E = E_1 - 2\upsilon\lambda + \upsilon t$

where E_1 is the initial potential and λ the time at which the sweep rate is reversed.

t = time (s)

x = distance perpendicular from the electrode (cm).

E = Potential versus a reference electrode (V)

It can also be shown that the peak current (I_p);

$$I_p = -0.4463nF\left(\frac{nf}{RT}\right)^{\frac{1}{2}} C_O^{\infty} D^{\frac{1}{2}} \upsilon^{\frac{1}{2}} \qquad 2.49$$

where,

D = Diffusion coefficient ($cm^2\ s^{-1}$)

C_0^{∞} = Concentration of species O in the bulk of solution (mol cm^{-3})

I_p = Peak current density (A cm^{-2})

This is known as the Randles - Sevcik equation. At 298 K, this reduces to:

$$I_p = -(2.69x10^5) n^{\frac{3}{2}} C_O^{\infty} D^{\frac{1}{2}} \upsilon^{\frac{1}{2}} \qquad 2.50$$

where, I_p is the peak current density (A cm^{-2}) D is in $cm^2 s^{-1}$ υ is in Vs^{-1} and C_0^* is in mol cm^{-3}. It can be deduced from equation 2.50, that the peak current is proportional to the concentration of electroactive species and to the square roots of the sweep rate and diffusion coefficient.

There are several tests that can be performed to asses if an electrochemical system is reversible.

1 $\Delta E_p = E_p^A - E_p^C = 59/n$ mV

2 $| E_p - E_{p/2} | = 59/n$ mV

3 $| I_p^A / I_p^C | = 1$

4 $I_p \propto \upsilon^{1/2}$

5 E_p independent of υ

6 At potentials beyond E_p, $I^{-2} \propto t$

where,

ΔE_p = Peak potential (V)

$E_{p/2}$ = Half peak potential (V)

E_p^A = Peak anodic potential (V)

E_p^C = Peak cathodic potential (V)

I = Current density (A cm^{-2})

2.17.2 Irreversible systems

In the case of reversible electrochemical systems, the rate of electron transfer is faster than that of mass transport (2.182). In this case, Nernst equilibrium is always maintained at the surface of the electrode. However, when the rate of electron transport is deficient such that surface equilibrium is not maintained, then the shape of the cyclogram changes. At low potential sweep rates the rate of electron transfer is greater than that of mass transfer. In this case a reversible cyclic voltammogram is recorded. As the sweep rate is increased, the rate of mass transport increases and becomes comparable to the rate of electron of electron transfer. Perhaps the most noticeable effect of this is the increase in peak separation.

Irreversible cyclic voltammograms can be described mathematically in the same manner as reversible cyclic voltammograms:

$$E_p^c = K - \frac{2.3RT}{2\alpha_c n_\alpha F}\log\upsilon \qquad 2.51$$

where,

$$K = Ee^{\ominus} - \frac{RT}{\alpha_c n_\alpha F}\left(0.78 - \frac{2.30}{2.00}\log\left(\frac{\alpha_c n_\alpha FD}{k^{\ominus 2}RT}\right)\right) \qquad 2.52$$

where,

α_c = Cathodic transfer coefficient (dimensionless).

n_α = Number of electrons involved before and including the rate determining step.

k^θ = Standard rate constant for an electron transfer couple.

It can be shown that for an irreversible system, Ep^C shifts by $30/\alpha_c n_\alpha$ mV for each decade change in υ at 298 K. This peak shifts in a negative direction as υ increases. The shape factor $|E_p - E_{p/2}|$ is also different for an irreversible system and is given by:

$$|E_p - E_{p/2}| = \frac{48}{\alpha_c n_\alpha} \qquad 2.53$$

where, the units are mV at 298 K.

Perhaps the most obvious difference between irreversible and reversible cyclic voltammograms is the absence of a reverse peak in the former case. However, in some cases this could be due to a fast following chemical reaction. Therefore, other diagnostic tests must be performed to ascertain if the cyclic voltammogram is irreversible.

For totally irreversible systems at 298 K:

1 No reverse peak

2 $I_p^C \propto \upsilon^{1/2}$

3 E_p^C shifts $30/\alpha_c n_a$ mV for each decade increase in υ

4 $| E_p - E_{p/2} | = 48/\alpha_c n_a$ mV.

It is also possible for a system that is reversible at lower scanning rates to change from reversible to quasi-reversible and finally irreversible behaviour simply from a plot of I_p as a function of $\upsilon^{1/2}$.

Diagnostic tests for quasi reversible systems:

1 $| I_p |$ increases with $\upsilon^{1/2}$ but is not proportional.

2 $| I_p^A / I_p^C | = 1$ provided $\alpha_C = \alpha_A = 0.5$

3 ΔE_p is greater than 59/n mV and increases with increasing υ

4 E_p^C shifts negatively with increasing υ

2.18 SPECIATION IN SOLUTION

In an aqueous solution, metal ions are surrounded by a solvation sheath of coordinated water molecules (2.183). When a different ligand (such as NH_3) reacts with a metal ion, stepwise replacement of the coordinated water molecules by these ligands occurs (see equation 2.54). If the equilibrium lies to the right then a complex is formed (of course a complex was already present on the left hand side of equation 2.54).

$$[M(H_2O)_n] + L \rightarrow [M(H_2O)_{n-1}\ L] + H_2O \qquad 2.54$$

The stepwise replacement of water by other ligands is usually represented in a more convenient manner (see equation 2.55).

$$M + L \rightarrow ML \qquad 2.55$$

An equilibrium constant can be ascribed to this equation (see equation 2.56)

$$K_1 = \frac{[ML]}{[M]\ [L]} \qquad 2.56$$

For further stepwise replacement of other water molecules by ligands the following equations can be written (see equations 2.57 -2.60):

$$M + L \rightleftharpoons ML \qquad 2.57$$

$$ML + L \rightleftharpoons ML_2 \qquad 2.58$$

$$ML_2 + L \rightleftharpoons ML_3 \qquad 2.59$$

$$ML_3 + L \rightleftharpoons ML_4 \qquad 2.60$$

For complexes such as $[Ni(H_2O)_6]^{2+}$, this stepwise replacement may continue until all six water molecules have been replaced by other ligands. In a solution containing $NiSO_4$ and NH_3 (NH_3 ionizes to form NH_4OH, $K_b = 1.8 \times 10^{-5}$), the actual speciation in solution will be strongly dependent on pH and the concentration of ions in solution particularly the concentration of NH_3. Similar behaviour is also observed for solutions containing $[Cu(H_2O)_6]^{2+}$ and NH_3 (2.184). A graphic example of speciation in a solution containing $[Cu(H_2O)_6]^{2+}$ and NH_3 is shown in figure 2.26 (2.184). As the ammonia concentration increases, the proportion of copper in the various complex ions increases to a maximum and then decreases. It is also evident that certain complex ions predominate within a given ammonia concentration range and that the ranges of each complex overlap. Only at very high and very low concentrations of ammonia is a single species present.

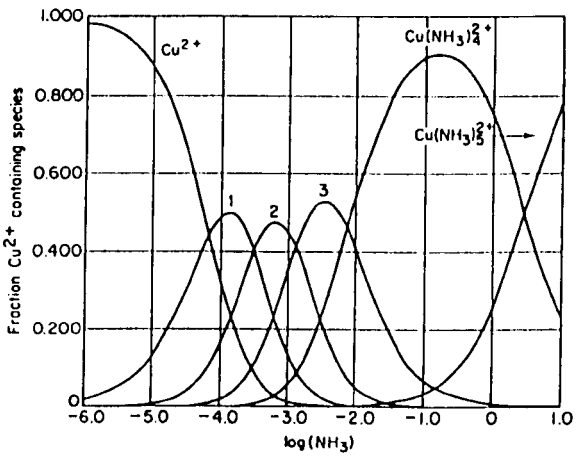

Figure 2.26 Complex ions present in aqueous solutions containing various proportions of Cu^{2+} and NH_3. The number of NH_3 ligands in the complex ion is indicated in the three centre curves.

For further stepwise replacement of water molecules by ligands the following equations can be written (see equations 2.61-2.63):

$$K_2 = \frac{[ML_2]}{[ML]\ [L]} \qquad 2.61$$

$$K_3 = \frac{[ML_3]}{[ML_2]\ [L]} \qquad 2.62$$

$$K_4 = \frac{[ML_4]}{[ML_3]\ [L]} \qquad 2.63$$

Further equations can be derived for complexes such as $[Ni(H_2O)_6]^{2+}$.

The magnitude of the equilibrium constants K_1 - K_4 for equations 2.60-2.61 usually decreases in the order $K_1 > K_2 > K_3 > K_4 > K_n$. These equilibrium constants are also known as formation or stability constants. For a particular reaction the overall stability constant (ß) may be used (see equation 2.64 and table 2.7)

$$\beta_4 = \frac{[ML_4]}{[M]\ [L_4]} \qquad 2.64$$

where, β_4 is also given by equation 2.65

$$\beta_4 = K_1 K_2 K_3 K_4 \qquad 2.65$$

The stability constants for various complexes are shown in table 2.7 (2.185)

Table 2.7 Stepwise and overall stability constants

M	L	$\log K_1$	$\log K_2$	$\log K_3$	$\log K_4$	$\log K_5$	$\log K_6$	$\log \beta$
Cu^{2+}	NH_3	4.17	3.53	2.88	2.05			12.6
Ni^{2+}	NH_3	2.80	2.24	1.73	1.19	0.75	0.03	8.7
Ag^{+}	NH_3	3.14	3.82					7.0
Hg^{2+}	CN^{-}	18.00	16.70	3.83	2.98			41.5
Hg^{2+}	I^{-}	12.87	10.95	3.67	2.37			29.9
Cu^{2+}	en	10.55	9.05					19.6
Ni^{2+}	en	7.45	6.23	4.34				18.0

2.18.1 Effect of electrodeposition deposition on the metal ion ligand sheath

The electrocrystallisation of materials involves several distinct processes some of which were previously discussed in 2.15 (2.186). These are:

1 Diffusion of ions in solution to the surface of the electrode.

2 Electron transfer

3 Formation of ad-atoms due to partial or complete loss of solvation sheath (ligands).

4 Ad-atom surface diffusion.

5 Ad-atom aggregation leading to the formation of critical nuclei on smooth surfaces.

6 Ad-atom incorporation at lattice sites.

7 Evolution of crystallographic and morphological attributes of deposits.

These processes are shown in figure 2.27 (2.187)

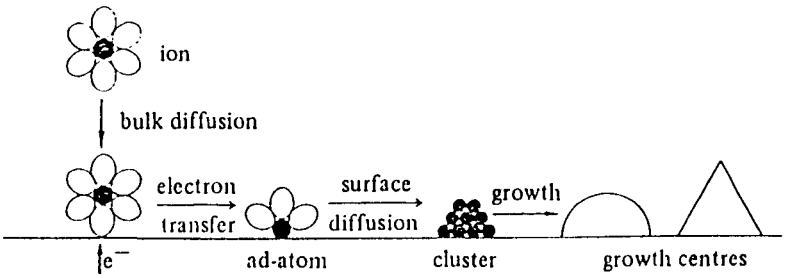

Figure 2.27 Processes involved in the electrocrystallisation of a metal on a substrate.

Of relevance to this study is the possibility of inclusion of ligands (such as NH_3) within electrocrystallised coatings. In the ideal case, all of the ligands should be removed from the metal ion immediately after the formation of an ad-atom on the surface of a substrate or growing film. Unfortunately in some cases this does not occur and the ad-atom retains a partial solvation sheath. This can occur when charge transfer is not complete and a neutral atom is not produced (2.188). In this case, at least part of the solvation sphere remains (see figure 2.28). However, after surface migration has occurred to a suitable lattice site, further loss of the solvation sheath occurs making this type of ad-atom indistinguishable from others. It is likely that the same phenomena occurs in colloidal precipitation of materials such as $Ni(OH)_2$ since essentially Ni^{2+} is reduced by OH^-. It is conceivable, particularly during the deposition of hydroxides and oxides that some solvent inclusion occurs in the same manner

that gas entrapment occurs during physical vapour deposition techniques (in the case of this study NH_3, H_2O and polyoxyethylene sorbitan monolaurate) (2.189).

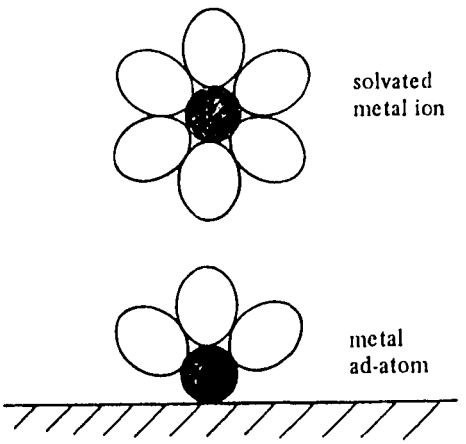

Figure 2.28 Formation of an ad-atom due to the reduction of a solvated metal ion in solution. Some ad-atoms retain a partial solvation sheath.

2.18.2 Equilibrium constant

At equilibrium, the product of the concentrations of the products divided by the product of the concentration of the reactants is equal to a constant. This constant is known as the equilibrium constant. The numerical value of the equilibrium constant is affected by state variables such as temperature and pressure (2.190). In this study the most important state variable was temperature since thin films were mainly deposited from solutions.

2.19 ROLE OF BUFFERS IN SOLUTIONS

A buffer can be defined as an aqueous solution in which the pH changes only slightly when small quantities of a strong acid or base are added (2.191). A Buffer usually contains a weak acid and a salt of that acid or alternatively a weak base plus a salt of that base. These solutions have the ability to react with both strong and acids and strong bases. For example if a small quantity of hydrochloric acid is added to a solution containing acetic acid and sodium acetate, the acetate ions (that are basic) react with the hydrogen ions to form more hydrogen acetate molecules (see equation 2.66). During the course of this reaction the pH does not change appreciably (2.192).

$$H^{+} + C_2H_3O_2^{-} \rightarrow HC_2H_3O_2 \qquad 2.66$$

Alternatively, if hydrogen ions are removed by the addition of a base such as sodium hydroxide (forming water) the molecular hydrogen acetate ionizes to form more hydrogen ions (see equation 2.67)

$$HC_2H_5O_2 \rightarrow H+ C_2H_3O_2^{-} \qquad 2.67$$

2.20 MEASUREMENT OF SURFACE AREA

The theory proposed by Braunauer, Emmet and Teller known as the BET theory is a modification of Langmuir treatment (2.193). It differs from the Langmuir treatment in that it allows multilayer physical adsorption. BET theory can be represented by equation 2.68. This equation is usually applied to non - porous adsorbents.

$$\frac{P}{\upsilon(P^*-P)} = \frac{1}{\upsilon_m C} + \frac{C-1}{\upsilon_m C}\frac{P}{P^*} \qquad 2.68$$

where,

P	=	Equilibrium gas pressure at fixed adsorbent temperature.
P^*	=	Vapour pressure of the adsorbate at the temperature of the experiment.
υ	=	Equilibrium volume of adsorbed gas per unit mass of absorbent at pressure P.
υ_m	=	Volume of the gas required to cover unit mass of the absorbent with a complete monolayer.
C	≈	$\exp[(\Delta H_l - \Delta H_1)/RT]$
ΔH_l	=	Heat of liquefaction of second and subsequent layers.
ΔH_1	=	Heat of adsorption of the first layer.

Of particular importance is the monolayer capacity, V_m, since it can be used for calculating the surface area of an adsorbent if the effective area occupied by each adsorbate molecule is known. This equation can be modified for porous adsorbents (electrochromic materials are usually porous). If the adsorption is limited to n molecular layers (where n is also related to the pore size), the equation becomes:

$$V = \frac{V_m c x}{(1-x)} \cdot \frac{1-(n-1)x^n + nx^{(n+1)}}{1+(c-1)x - cx^{(n+1)}} \qquad 2.69$$

where, x is P/P^* (2.194)

2.21 MASS TRANSPORT IN ELECTROLYTES

In electrochemical systems there generally three modes of mass transport these are:

(i) Diffusion

(ii) Migration

(iii) Convection

2.21.1 Diffusion

Diffusion is the movement of a species such as an ion down a concentration gradient. This occurs whenever there is a chemical change at a surface (such as an electrode surface). In the case of an electrochemical reaction, an electrode converts a certain species (O) to a product (R). Close to the electrode there is a boundary layer (up to 10^{-2} thick). Inside this layer the concentrations of O and R are a function of distance from the electrode surface. Since O in this case is being converted to R, the concentration of O is lower in this boundary layer than it is in the bulk, the opposite is true for R. Therefore, O diffuses towards the electrode, whereas R diffuses away from it (2.195).

2.21.2 Migration

This form of mass transport occurs due to the movement of charged species in a potential gradient (2.195). The movement of charged species in an electrolyte is the mechanism for how charge passes through the electrolyte. When a potential difference is applied to an electrolyte (via electrodes) the passage of current through the external circuit must be balanced by the passage of ions in solution (movement of cations to the cathode and anions to the anode). However, this may not necessarily be the most important form of mass transport since the forces causing migration are electrostatic. Therefore, the charge can be carried by any ionic species in solution (this is a problem particularly if there is a large concentration of inert electrolyte in solution).

2.21.3 Convection

Mass transport can also occur by convection. Convection in solutions is usually caused by the movement of species by mechanical forces. This form of mass transport can be eliminated, at least on a short time scale (<10 seconds) by carrying out electrolysis in a thermostatically controlled bath in the absence of stirring or agitation. For industrial applications the electrolyte is agitated or flowed through the cell. These are forms of forced convection that have a large influence on current density (2.195).

2.22 ELECTROCHROMIC DEVICES

Solid state device structure was discussed in Chapter 1. Many combinations of electrochromic materials and ion storage layers are possible. To summarise there are many possible electrochromic device configurations, the majority of which are derived from 5 basic systems:

(i) S/TCO/Anodic EC/Metal oxide electrolyte/cathodic EC/TCO

(ii) S/TCO/Cathodic EC/Metal oxide electrolyte/Ion storage/EC/TCO

(iii) S/TCO/Anodic EC/Liquid electrolyte/cathodic EC/TCO/S

(iv) S/TCO/Anodic EC/Polymeric electrolyte/cathodic EC/TCO/S

(v) S/Al/Anodic EC/Metal oxide electrolyte/cathodic EC/TCO/S

where, S = substrate, TCO = Transparent conductor, Al = Aluminium

The choice of device structure is dependent on application. For example, structures (i) and (ii) are suitable for architectural applications (where high cyclic and ultraviolet durability are required), whereas, device structures (iii) and (iv) may be selected if cheap highly transparent and non-coloured ultraviolet filters can be fabricated. The system depicted in (v) is suitable for rear view mirrors as a switchable anti-dazzle device.

An important aspect of solid state device design is the selection of a suitable electrolytes. This is because WO_3 dissolves in basic electrolytes and NiO_x dissolves in acidic media (2.120). Another problem associated with selecting a suitable electrolyte is the physical form of the electrolyte. A liquid electrolyte would be ideal because of the high mobility of ions. However such electrolytes would be unsuitable for large area applications due to the hydrostatic

pressure that liquids exert (2.121). A problem that would be experienced with liquid electrolytes particularly aqueous ones would be gaseous evolution during the electrochemical processes of oxidation and reduction (hydrogen and oxygen during cathodic and anodic processes respectively).

For large area applications and where good ultraviolet stability is required, research has focused on solid state inorganic electrolytes such as $Ta_2O_5.H_2O$, $LiNbO_3$ and polymeric electrolytes such as polyethylene oxide and polypropylene oxide doped with alkali salts such as $LiCF_3SO_3$ (2.122). These materials contain the necessary ion(s) to colour and bleach both cathodic and anodic electrochromic materials. It is beyond the scope of this thesis to present all of the metal oxides currently under investigation.

The choice of electrolyte is dependent on a number of factors. Perhaps the most important are:

(i) ion(s) necessary for colouring the electrochromic media (2.120).
(ii) stability to ultraviolet radiation.
(iii) stability to changes in atmospheric conditions (2.122).

As well as selecting suitable ions for colouration it is necessary to minimise the mechanical damage that these ions cause to electrochromic materials under the application of an electric field (2.77, 2.103). This can be achieved for some electrochromic materials such as WO_3 by using electrolytes that contain small ions such as Li+ (2.77). Most ceramic materials exhibit good stability to ultraviolet radiation, however materials such as polymers generally do not (2.122).

The following characteristics are important for all solid state electrolytes (2.120, 2.122) that are used in electrochromic devices:

(i) High ion conductivity preferably higher than 10^{-7} Scm^{-1} (2.122) at room temperature. Ideally for fast switching speeds the ionic conductivity should be higher than 10^{-4} Scm^{-1} (2.120, 2.122).

(ii) The transference number should be as close to unity as possible i.e.

$$t_i = \sigma_i / \sigma \qquad 2.70$$
$$= 1$$

where, $\sigma = \sigma_e + \sigma_i$ is the total conductivity and σ_e is the electronic conductivity and σ_i is the ionic conductivity.

(iii) From (ii) it can be deduced that the electrical resistivity of the electrolyte should be high (i.e. greater than 10^{12} Ω cm at room temperature).

(iv) The ion conductor should be chemically compatible with all electrochromic materials used in the device (2.120).

(v) Electrolytes should be easy to fabricate, have high mechanical strength and optical transmittance properties (i.e. they should not be coloured).

A large number of conducting solids exhibit transport properties for cations such as H^+, Li^+, Na^+ and Ag^+ (2.120). Anions can also be the conducting species. For electrolytes that contain ions such as, F^-, Cl^-, Br^-, I^- and OH^-, only F^- containing electrolytes exhibit high conductivity at room temperature. This is in part due to the high electronegativity of fluorine and consequently a small ion radius, therefore the mobility of ions is high. However, it is inconceivable

that any material would be electrochemically durable to the injection or extraction of F^-.

A major problem associated with the manufacture of electrochromic windows is production costs. Currently the costs associated with making a five layer device may be prohibitive for most companies, particularly if a further step of lamination is required. The production process would probably involve the PVD deposition of a transparent conductor followed by the deposition of electrochromic material, electrolyte, counterelectrode and another transparent conductor. Alternatively electrolytes could be spin coated on to an electrochromic material. The device could then be assembled by simply placing the substrate with electrochromic material and electrolyte in contact with a suitable counter electrode.

2.23 REFERENCES

2.1 Burberry, P. (1978), Building for Energy Conservation. New York, The Architectural Press Ltd, Halsted Press Division, John Wiley & Sons.

2.2 Flood, M. (1983), Solar Prospects: The Potential for Renewable Energy. London, Wildwood House.

2.3 Double Glazing and Double Windows. Building Research Digest, 140 1972.

2.4 Jesch, L.F., Solar Energy Today UK-ISES 1981 45.

2.5 Trombe, F., Robert, J.F., Cabanat, M. and Sesolis, B., Passive Collection of Solar Energy in Buildings, Conf. proc. C19, UK ISES, 1979 4.

2.6 Jesch, L.F., Solar Energy Today UK-ISES 1981 23

2.7 Platzer, W.J., Solar Energy Materials 16 1987 275

2.8 Double Glazing and Double Windows. Building Research Digest, 140. April 1972.

2.9 Turrent, D., Doggart, J. and Ferraro, R., Passive Solar Housing in the UK. A Report to the Energy Technology Support Unit, Harwell. March 1980.

2.10 Nordgaard, A. and Beckman, W.A., Solar Energy **49** 5 1992 387.

2.11 Platzer, W.J., Solar Energy **49** 5 1992 359.

2.12 Collins, R.E., Fischer-Cripps, A.C. and Tung, J.Z., **49** 5 1992 333.

2.13 Seraphin, B.O., Solar Energy Conversion, Oxford, Pergammon Press 1979 287.

2.14 Smith, G.B., Ditchburn R.J., Martin P.J. and Netterfield R.P., Solar Energy Materials and Solar Cells **25** 1992 149.

2.15 McCluney, R., Solar Energy Materials **21** 1990 191.

2.16 Smith, H.M., Topics in Applied Physics, **20**, Springer-Verlag, Berlin, 1977.

2.17 Lampert, C.M., Solar Energy Materials **6** 1981 1.

2.18 Lampert, C.M. and Granqvist, C.G. (1990), in Lampert, C.M., and Granqvist, C.G. (eds.), Large-Area Chromogenics: Materials and Devices for Transmittance Control (1st Edn.). Bellingham, Washington, U.S.A., SPIE Press **IS4** 2.

2.19 Duffie, J.A. and Beckman, W.A. (1974) Solar Energy Thermal Processes. New York, John Wiley and Sons.

2.20 Gillet, W.B. and Hutchins, M.G., Heating Water by the Sun. UK-ISES 1981.

2.21 Clarke, D. (1988), Solar Optical Materials. Oxford, Pergammon Press, 83.

2.22 Littler, J. and Watson, M. Coatings for Energy Efficiency and Solar Applications. Conf. Proc. **C38** UK ISES, 1984 71.

2.23 Niklasson, G.A. and Granqvist, C.G., Journal of Materials Science, **18** 1983 3475.

2.24 Meinel, A.B. and Meinel, M.P. (1976), Applied Solar Energy: An Introduction. Pennsylvania, Addison-Wesley.

2.25 Seraphin, B.O. Solar Energy Conversion: Solid State Physics Aspects, Topics in Applied Physics. Springer Berlin, Heidelberg, **31** 1979 5.

2.26 Bogaerts, W.F. and Lampert, C.M. Journal of Materials Science, **18** 1983 2847.

2.27 Granqvist, C.G., Applied Optics, **20** 1981 2606.

2.28 Angadi, M.A. and Nallamshetty, K., Solar Energy Materials, 17 1988 137.

2.29 Mulla, I., Soni, Rao, V. and Sinha, A., Journal of Materials Science, 21 1986 1280.

2.30 Nath, P. and Bunshah, R., Thin Solid Films, 69 1980 63.

2.31 Fan, J. and Bachner, F., Journal of Electrochemical Society, 122 1975 1719.

2.32 Hamberg, I. and Granqvist, C.G., Journal of Applied Physics, 60 1986 123.

2.33 Berning, P.M., Applied Optics, 22 1983 4127.

2.34 Chopra, K.L., Major, S. and Pandya, K., Thin Solid Films, 102 1983 1.

2.35 Zhang, H.T., Subramanian, P., Fussa-Rydel, O., Bebel, J.C. and Hupp, J.T., Solar Energy Materials and Solar Cells 25 1992 315.

2.36 Deb, K., Solar Energy Materials and Solar Cells, 25 1992 327.

2.37 Lampert, C.M., Solar Energy Materials, 11 1984 1.

2.38 Lampert, C.M., SPIE., **324** 1982 1.

2.39 Jorgenson, G.V. and Lee, J.C., SPIE., **562** 1985 1.

2.40 McMeeking, G.D., to Hutchins, M.G., Private communication, Nov 91.

2.41 Reilly, S., Daruish, A. and Selkowitz, S., Solar Energy Materials **22** 1991 1.

2.42 Jorgenson, G.V. and Lee, J.C. (1990), in Lampert, C.M., and Granqvist, C.G. (eds.), Large-Area Chromogenics: Materials and Devices for Transmittance Control (1st Edn.). Bellingham, Washington, U.S.A., SPIE Press **IS4** 142.

2.43 Hoffman, H.J. (1990), in Lampert, C.M., and Granqvist, C.G. (eds.), Large-Area Chromogenics: Materials and Devices for Transmittance Control (1st Edn.). Bellingham, Washington, U.S.A., SPIE Press **IS4** 86.

2.44 Lampert, C.M. (1990), in Lampert, C.M., and Granqvist, C.G. (eds.), Large-Area Chromogenics: Materials and Devices for Transmittance Control (1st Edn.). Bellingham, Washington, U.S.A., SPIE Press **IS4** 550.

2.45 Lynam, A.R. and Agrawal A. (1990), in Lampert, C.M., and Granqvist, C.G. (eds.), Large-Area Chromogenics: Materials and Devices for Transmittance Control (1st Edn.). Bellingham, Washington, U.S.A., SPIE Press IS4 46.

2.46 Brown, G.H. (ed) (1971), Photochromism. New York, Wiley.

2.47 Brown, G.H. (ed) (1971), Photochromism. New York, Wiley 667.

2.48 Araujo, R.J., Contemporary Physics **21** 1980 77.

2.49 Araujo, R.J., Journal of Non-Crystalline Solids **47** 1982 69.

2.50 Hilsum, C. and Raynes, B. (eds.). Phil. Trans. R. Soc. London, **A309** 1983 213.

2.51 Shibaev, V.P. and Plate, N.A., Advances in Polymer Science, Springer-Verlag, Berlin **60/61** 1984 173.

2.52 Ringsdorf, H. and Zentel, R., Macromol.Chem.,**180** 1979 803.

2.53 Day, J.H., Chem. Rev. **63** 1963 65.

2.54 Day, J.H., Chem. Rev. **68** 1968 649.

2.55 Adler, D., Rev. Mod. Phys. **40** 1968 714.

2.56 Morin, F.J., Phys. Rev. Lett. **3** 1959 34.

2.57 Coles, H.J. and Simon, R. (1985), Polymeric Liquid Crystals (1st edn.) New York and London, Plenum 351.

2.58 Boy, E.and Meinhardt, S.,in Proc.2nd Int. Workshop on Transparent Insulation Materials in Solar Energy Conversion for Buildings and Other Applications (Freiburg, Germany,24-25 March, 1988).

2.59 Andersson, A.M.,Niklasson, G.A. and Granqvist, C.G., Appl. Opt. **26** 1987 2164.

2.60 Christiansen, C., Ann.Phys.Chem. **23** 1984 298.

2.61 Brim, E.O., Brantley, J.H., Lorenz, J.H. and Jellinck, M.H., Journal of American Chemical Society **73** 1951 5427.

2.62 Deb, S.K., Appl. Opt. Suppl. **3** 1969 193.

2.63 Lampert, C.M., Solar Energy Materials **11** 1984 1.

2.64 Hutchins, M.G. and McMeeking, G.D., Biosensor Patent no. 90 27 607.2 1990 (European patent no. 91311904.6).

2.65 Selkowitz (1990), in Lampert, C.M., and Granqvist, C.G. (eds.), Large-Area Chromogenics: Materials and Devices for Transmittance Control (1st Edn.). Bellingham, Washington, U.S.A., SPIE Press IS4 22.

2.66 Coles, H.J., Fine Chemicals for the electronics Industry, RSC 60 1986 97.

2.67 Reintzer, F., Montash Chem., 9 1888 421.

2.68 Basturk, N. and Grupp, J. (1990), in Lampert, C.M., and Granqvist, C.G. (eds.), Large-Area Chromogenics: Materials and Devices for Transmittance Control (1st Edn.). Bellingham, Washington, U.S.A., SPIE Press IS4 557.

2.69 Blinc, R., Clark, N.A., Goodby, J., Rikin, S.A. and Yoshino K., Ferroelectrics, 58/59 1984.

2.70 Heilmeier, G.H. and Zanoni, L.A. Appl. Phys. lett. 13 1968 91.

2.71 Hickey, C.F. and Gibson, U.J., J. Appl. Phys. 62 1987 3912.

2.72 Camilibel, I., Singh, S., Stocker, H.J., Van Uitert, L.G. and Zydzik, G.J., Appl. Phys. Lett. 33 1978 793.

2.73 Hartfield, E. and Thomson, B.J. (1978), Handbook of Optics., New York, Mcgraw-Hill, 17.

2.74 Smith, G.B., Niklasson, G.A., Svensson, J.S.E.M. and Granqvist, C.G., J. Appl. Phys. 59 1986 571.

2.75 Hamberg, I. and Granqvist, C.G., J. Appl. Phys. 60 1986 R 123.

2.76 Harding, G.L., Hamberg, I. and Granqvist, C.G., Solar Energy Materials, 12 1985 187.

2.77 Haas, T.E. and Goldner, R.B. (1990), in Lampert, C.M., and Granqvist, C.G. (eds.), Large-Area Chromogenics: Materials and Devices for Transmittance Control (1st Edn.). Bellingham, Washington, U.S.A., SPIE Press IS4 170.

2.78 Deb, S.K., Applied Optics, Supplemental 3 1969 801.

2.79 Goldner, R.B. and Rauh, D.R., Proc. SPIE 428 1983 38.

2.80 Yang, S.C. and Durand, R.R., U.S. Patent 4586792 1984; U.S. Patent 1986.

2.81 Shirakawa, H., Louis, E.J., McDiarmid, A.G., Chiang C.K. and Heeger, A.J. Journal of Chemical Society Chemistry Communication 1977 578.

2.82 Diaz, A.F., Kanazawa, K.K. and Gardin, G.P., Journal of Chemistry Society, Chemistry Communication 1979 635.

2.83 Chen, J., Heeger, A.J. and Wudl, F., Solid State Communcations **58** 1986 251.

2.84 Diaz, A.F. and Logan, J.A., Journal of Electroanalytical Chemistry **111** 1980 111.

2.85 Yang, S.C. (1990), in Lampert, C.M., and Granqvist, C.G. (eds.), Large-Area Chromogenics: Materials and Devices for Transmittance Control (1st Edn.). Bellingham, Washington, U.S.A., SPIE Press **IS4** 335.

2.86 Inganas, O. (1990), in Lampert, C.M., and Granqvist, C.G. (eds.), Large-Area Chromogenics: Materials and Devices for Transmittance Control (1st Edn.). Bellingham, Washington, U.S.A., SPIE Press **IS4** 328.

2.87 Van Vlack, L.H. (1985), Elements of Materials Science and Engineering (5th edn.). Reading, Massachusetts, Addison-Wesley, 345.

2.88 Miedzinska, K.M.E., Hollebone, B.R. and Cook, C.G., Journal of Physics and Chemical Solids **49** 11 1988 1355.

2.89 Rao, C.N.R., and Gopalakrishnan, J. (1986), New Directions in Solid State Chemistry (1st edn.). Cambridge Solid State Science Series, Cambridge, Cambridge University Press, 267.

2.90 Mott, N.F. (1974) Metal-Insulator Transitions. London, Taylor & Francis Ltd and New York, Harper & Row Publishers Inc./Barnes & Noble Import Division.

2.91 Kober, F.P. Journal of Electrochemical Society: Electrochemical Science **114** 3 1967 215.

2.92 Johnston, C., and Graves, P.R., Applied Spectroscopy **44** 1 1990 105.

2.93 Falaras, P., et.al. (1990), in Lampert, C.M., and Granqvist, C.G. (eds.), Large-Area Chromogenics: Materials and Devices for Transmittance Control (1st Edn.). Bellingham, Washington, U.S.A., SPIE Press **IS4** 447.

2.94 Oliva, P., et.al. Journal of Power Sources, **8** 1982 229.

2.95 Graves, P.R. to McMeeking, G.D., private communication, September 1991.

2.96 Nazri, G., Corrigan, D.A., and Maheswari, S.P., Langmuir 5 1 1989 17.

2.97 Lampert, C.M. (1990), in Lampert, C.M., and Granqvist, C.G. (eds.), Large-Area Chromogenics: Materials and Devices for Transmittance Control (1st Edn.). Bellingham, Washington, U.S.A., SPIE Press IS4 414.

2.98 Hutchins, M.G., McMeeking, G.D. and Orel Z.C., Optical Materials Technology for Energy Efficiency and Solar Energy Conversion XI: Chromogenics for Smart Windows 1728 1992 66.

2.99 Yamada, S., Yoshioka, T., Miyashita, M., Urabe, K., and Kitao, M., Proc. SPIE 1016 1988.

2.100 Chu, N.Y.C. (1990), in Lampert, C.M., and Granqvist, C.G. (eds.), Large-Area Chromogenics: Materials and Devices for Transmittance Control (1st Edn.). Bellingham, Washington, U.S.A., SPIE Press IS4 285.

2.101 Tewari, P.H. and Campbell, A.B., Journal of Colloid and Interface Science 55 3 1976 531.

2.102 Cronan, C.L., Micale, F.J., Topic, M., Leidheisser, H., Zettlemoyer, A.C. and Popovic, S., 55 3 1976 531.

2.103 Gorenstein, A., et.al. (1990), in Lampert, C.M., and Granqvist, C.G. (eds.), Large-Area Chromogenics: Materials and Devices for Transmittance Control (1st Edn.). Bellingham, Washington, U.S.A., SPIE Press IS4 272.

2.104 Conell, R.S., Corrigan, D.A. and Powell, B.R., Solar Energy Materials and Solar Cells 25 1992 301.

2.105 Fantini, M. and Gorenstein, A., Solar Energy Materials 16 1987 487.

2.106 Joseph, J, Gomathi, H. and Rao, G.P., Solar Energy Materials 23 1991 1.

2.107 Carpenter, M.K., Conell, R.S. and Corrigan, D.A., Solar Energy Materials 16 1987 333.

2.108 Lampert, C.M., Ma, Y.P., Pennisi, A. and Simone, F., Electrical and Optical Properties of Electrochromic Devices Utilizing Solid Polymer Electrolytes, Department of Energy Report No. DE-AC03-76SF00098 1990.

2.109 Desilvestro, J., Corrigan, D.A. and Weaver M.J., Journal of Physical Chemistry **90** 1986 6408.

2.110 Svensson, J.S.E.M. and Granqvist, C.G., Solar Energy Materials **16** 1987 19.

2.111 Nagai, J., Optical Materials Technology for Energy Efficiency and Solar Energy Conversion XI: Chromogenics for Smart Windows **1728** 1992 194.

2.112 Hugot-le-Goff, A., Journal of Electrochemistry Society, 138 1991 1548.

2.113 Xingfang, H. and Xiaofeng, C., Hutchins, M.G., SPIE., Optical Materials Technology for Energy Efficiency and Solar Energy Conversion XI: Chromogenics for Smart Windows **1728** 1992 173.

2.114 Hutchins, M.G., McMeeking, G.D. and Xinfang, SPIE, 1990 1272.

2.115 Decker, F., Passerini, S., Pileggi R., and Scrossati B., Electrochemica Acta **37** 6 1992 1033.

2.116 Passerini, S., and Scrosati, B., Solid State Ionics **53-56** 1992 520.

2.117 Bange, K., Baucke, F., and Metz, B., Proc. SPIE 1016, (in press).

2.118 Lynam, N.R. and Habibi, H.R., Optical Materials Technology for Energy Efficiency and Solar Energy Conversion VII SPIE **1016** 1988 63.

2.119 Corrigan, D.A. and Carpenter, M.K. (1990), in Lampert, C.M., and Granqvist, C.G. (eds.), Large-Area Chromogenics: Materials and Devices for Transmittance Control (1st Edn.). Bellingham, Washington, U.S.A., SPIE Press **IS4** 298.

2.120 Lampert, C.M., Troung, V.V., Nagai, J., Hutchins, M.G. IEA TASK X-C, Glazing Materials, Technical Report LBL-29632 1990.

2.121 Nagai, J., et.al. (1990), in Lampert, C.M., and Granqvist, C.G. (eds.), Large-Area Chromogenics: Materials and Devices for Transmittance Control (1st Edn.). Bellingham, Washington, U.S.A., SPIE Press **IS4** 368.

2.122 Truong V., et.al. (1990), in Lampert, C.M., and Granqvist, C.G. (eds.), Large-Area Chromogenics: Materials and Devices for Transmittance Control (1st Edn.). Bellingham, Washington, U.S.A., SPIE Press **IS4** 386.

2.123 Nicholls, D. (1974), Complexes and First-Row Transition Elements (1st edn.). London, MacMillan, 194.

2.124 Faria, I.C., Torresi, R.M. and Gorenstein, A., Optical Materials Technology for Energy Efficiency and Solar Energy Conversion XI: Chromogenics for Smart Windows, SPIE **1728** 1992 54.

2.125 Corodoba, S.I., Hugot-Le-Goff, A. and Joiret, S., Journal of Electrochemical Society **138** 6 1991 1554.

2.126 Corrigan, D.A. and Knight, S.L., Journal of Electrochemical Society **136** 1989 613.

2.127 Desilvestro, J., Corrigan, D.A. and Weaver, M.J., Journal of Electrochemical Society **135** 1988 885.

2.128 Melendres, C.A. and Pankuch, M., Journal of Electroanalylitcal Chemistry **333** 1992 103.

2.129 Delichere, P., Joiret, S., Hugot-le-Goff, A., Bange, K. and Hetz, B., Journal of Electrochemical Society **135** 7 1988 1856.

2.130 Feuillade, G. and Jacoud, R., J. Electrochim. Acta, **16** 1971 833.

2.131 Seike, T. and Nagai, J., Solar Energy Materials 22 1991 107.

2.132 Lampert, C.M., Omstead, T.R. and Yu, P.C., Solar Energy Materials **14** 1986 161.

2.133 Delichere, P., Joiret S. and Hugot-le Goff, A., Optical Materials Technology for Energy Efficiency and Solar Energy Conversion VII **1016** 1988 165.

2.134 Shaw, J., (1980) Introduction to Colloid and Surface Chemistry (3rd edn.). London, Butterworths, 148.

2.135 Shaw, J., (1980) Introduction to Colloid and Surface Chemistry (3rd edn.). London, Butterworths, 5.

2.136 Nagai, J., McMeeking, G.D., Seike, T., Noutomi, Y., Glazings Today December 1994 33.

2.137 Sawatzky, G.A. and Allen, J.W., Phys. Rev. Lett. 53 1984 2339.

2.138 Matupally, S., Strienz, C.C. and Weidner, J.W., J. Electrochem. Soc. **142** 5 1995 1401.

2.139 Nicholls, D., (1974), Complexes and First-Row Transition Elements (1st edn.). London and Basingstoke, The Macmillan Press Ltd., 73.

2.140 Nicholls, D., (1974), Complexes and First-Row Transition Elements (1st edn.). London and Basingstoke, The Macmillan Press Ltd., 77.

2.141 Nicholls, D., (1974), Complexes and First-Row Transition Elements (1st edn.). London and Basingstoke, The Macmillan Press Ltd., 78.

2.142 Nicholls, D., (1974), Complexes and First-Row Transition Elements (1st edn.). London and Basingstoke, The Macmillan Press Ltd., 79.

2.143 Nicholls, D., (1974), Complexes and First-Row Transition Elements (1st edn.). London and Basingstoke, The Macmillan Press Ltd., 80.

2.144 Nicholls, D., (1974), Complexes and First-Row Transition Elements (1st edn.). London and Basingstoke, The Macmillan Press Ltd., 81.

2.145 Atkins, P.W., (1994), Physical Chemistry (5th edn.). Oxford, Melbourne and Tokyo, Oxford University Press, 596.

2.146 Herzberg, G., (1945), Atomic Spectra and Atomic Structure (2nd edn.). New York, Dover Publications, 157.

2.147 Miessler, G.L. and Tarr, D.A., (1991) Inorganic Chemistry. London, New Jersey and Tokyo, Prentice-Hall International Edn., 318.

2.148 Hollas, J.M., (1993), Modern Spectroscopy (2nd Edn.). Chichester, New York, Brisbane, Toronto and Singapore, John Wiley & Sons, 209.

2.149 Sharpe, A.G., (1992), Inorganic Chemistry (3rd Edn.). Singapore, Longman Scientific & Technical, 479.

2.150 Nicholls, D., (1974), Complexes and First-Row Transition Elements (1st edn.). London and Basingstoke, The Macmillan Press Ltd., 81.

2.151 Nicholls, D., (1974), Complexes and First-Row Transition Elements (1st edn.). London and Basingstoke, The Macmillan Press Ltd., 84.

2.152 Nicholls, D., (1974), Complexes and First-Row Transition Elements (1st edn.). London and Basingstoke, The Macmillan Press Ltd., 94.

2.153 Nicholls, D., (1974), Complexes and First-Row Transition Elements (1st edn.). London and Basingstoke, The Macmillan Press Ltd., 91.

2.154 Cox, P.A., (1987), The Electronic Structure and Chemsitry of Solids (1st edn.). Oxford, Oxford University Press., 151.

2.155 Cox, P.A., (1995), Transition Metal Oxides an Introduction to Their Electronic Structure and Properties (1st edn.). Oxford, Oxford Univeristy Press., 135.

2.156 Cox, P.A., (1987), The Electronic Structure and Chemistry of Solids (1st edn.). Oxford, Oxford University Press., 134.

2.157 Cox, P.A., (1995), Transition Metal Oxides an Introduction to Their Electronic Structure and Properties (1st edn.). Oxford, Oxford University Press., 82.

2.158 West, A.R., (1984) Basic Solid Sate Chemistry (Rev. ed. of: Solid State Chemistry and its Applications). Chichester, New York, Brisbane, Toronto and Singapore, John Wiley & Sons., 117.

2.159 Shaw, J., (1980) Introduction to Colloid and Surface Science (3rd Edn.) London, Butterworths, 10

2.160 Keennan, C.W., Kleinfelter, D.C. and Wood, J.H., (1980) General College Chemistry (6th Edn.) San Francisco, Harper & Row, 510.

2.161 Porter, D.A. and Easterling, K.E., (1981) Phase Transformations in Metals and Alloys (1st Edn.) Berkshire, Van Nostrand Reinhold, 186.

2.162 Ohring, M., (1992) The Materials Science of Thin Films (1st Edn.) San Diego, Academic Press Inc., 199.

2.163 Smith, L.D., (1995) Thin-Film Deposition; Principles and Practice (1st Edn.) New York, Mcgraw Hill Inc., 93.

2.164 Smith, L.D., (1995) Thin-Film Deposition; Principles and Practice (1st Edn.) New York, Mcgraw Hill Inc.,197.

2.165 Shaw, J., (1980) Introduction to Colloid and Surface Science (3rd Edn.) London, Butterworths, 127.

2.166 Shaw, J., (1980) Introduction to Colloid and Surface Science (3rd Edn.) London, Butterworths, 87.

2.167 Jakubke, H.D. and Jeschkeit, H., (Eds.) (1994) Concise Encyclopedia Chemistry (1st Edn.) New York, De Gruyter, 1173.

2.168 Porter, D.A. and Easterling, K.E., (1981) Phase Transformations in Metals and Alloys (1st Edn.) Berkshire, Van Nostrand Reinhold, 173.

2.169 Porter, D.A. and Easterling, K.E., (1981) Phase Transformations in Metals and Alloys (1st Edn.) Berkshire, Van Nostrand Reinhold, 199.

2.170 Porter, D.A. and Easterling, K.E., (1981) Phase Transformations in Metals and Alloys (1st Edn.) Berkshire, Van Nostrand Reinhold, 200.

2.171 Porter, D.A. and Easterling, K.E., (1981) Phase Transformations in Metals and Alloys (1st Edn.) Berkshire, Van Nostrand Reinhold, 202.

2.172 Kenney, J.T., Townsend, W.P., and Emerson, J.A., Journal of Colloid and Interface Science, **42** 3 1973 589.

2.173 Shaw, J., (1980) Introduction to Colloid and Surface Science (3rd Edn.) London, Butterworths, 11.

2.174 Smith, L.D., (1995) Thin-Film Deposition; Principles and Practice (1st Edn.) New York, Mcgraw Hill Inc., 166.

2.175 Hirth, J.P. and Pound, G.M., (1963) Condensation and Evaporation: Nucleation and Growth Processes. Oxford, Pergammon Press.

2.176 Smith, L.D., (1995) Thin-Film Deposition; Principles and Practice (1st Edn.) New York, Mcgraw Hill Inc., 198.

2.177 Shaw, J., (1980) Introduction to Colloid and Surface Science (3rd Edn.) London, Butterworths, 134.

2.178 Smith, L.D., (1995) Thin-Film Deposition; Principles and Practice (1st Edn.) New York, Mcgraw Hill Inc., 144.

2.179 Suetaka, W., (1995) Surface Infra-red and Raman Spectroscopy: Methods and Applications (1st Edn.) New York, Plenum, 16.

2.180 Jakubke, H.D. and Jeschkeit, H., (Eds.) (1994) Concise Encyclopedia Chemistry (1st Edn.) New York, De Gruyter, 292.

2.181 Greef, R., Peat, R., Peter, L.M., Pletcher, D., and Robinson, J., (1990) Instrumental Methods in Electrochemistry (2nd Edn.) New York, Ellis Horwood, 180.

2.182 Greef, R., Peat, R., Peter, L.M., Pletcher, D., and Robinson, J., (1990) Instrumental Methods in Electrochemistry (2nd Edn.) New York, Ellis Horwood, 185.

2.183 Nicholls, D., (1974), Complexes and First-Row Transition Elements (1st edn.). London and Basingstoke, The Macmillan Press Ltd., 28.

2.184 Jagowski, J.J., (1973) Modern Inorganic Chemistry, New York, Marcel Dekker, 652.

2.185 Nicholls, D., (1974), Complexes and First-Row Transition Elements (1st edn.). London and Basingstoke, The Macmillan Press Ltd., 30.

2.186 Greef, R., Peat, R., Peter, L.M., Pletcher, D., and Robinson, J., (1990) Instrumental Methods in Electrochemistry (2nd Edn.) New York, Ellis Horwood, 283.

2.187 Greef, R., Peat, R., Peter, L.M., Pletcher, D., and Robinson, J., (1990) Instrumental Methods in Electrochemistry (2nd Edn.) New York, Ellis Horwood, 284.

2.188 Greef, R., Peat, R., Peter, L.M., Pletcher, D., and Robinson, J., (1990) Instrumental Methods in Electrochemistry (2nd Edn.) New York, Ellis Horwood, 292.

2.189 Ohring, M., (1992) The Materials Science of Thin Films (1st Edn.) San Diego, Academic Press Inc., 96

2.190 Jakubke, H.D. and Jeschkeit, H., (Eds.) (1994) Concise Encyclopedia Chemistry (1st Edn.) New York, De Gruyter, 623.

2.191 Jakubke, H.D. and Jeschkeit, H., (Eds.) (1994) Concise Encyclopedia Chemistry (1st Edn.) New York, De Gruyter, 151.

2.192 Keennan, C.W., Kleinfelter, D.C. and Wood, J.H., (1980) General College Chemistry (6th Edn.) San Francisco, Harper & Row, 494.

2.193 Brunauer, S., Emmett, P.H., and Teller, E., J. Am. Chem. Soc., $_{60}$ 1938 309.

2.194 Brunauer, S., Deming, L.S., Deming, W.S. and Teller, E., J. Am. Chem. Soc., **62** 1940 1723.

2.195 Greef, R., Peat, R., Peter, L.M., Pletcher, D., and Robinson, J., (1990) Instrumental Methods in Electrochemistry (2nd Edn.) New York, Ellis Horwood, 26.

2.196 Shaw, J., (1980) Introduction to Colloid and Surface Science (3rd Edn.) London, Butterworths, 128.

CHAPTER 3

ANODIC DEPOSITION OF NICKEL OXIDE BASED COATINGS

CHAPTER 3

ANODIC DEPOSITION OF NICKEL OXIDE BASED COATINGS

3.1 DEPOSITION FROM STABLE AND UNSTABLE SOLUTIONS

3.1.1 Deposition from unstable solutions

Initially, as reported in the literature (3.1), nickel oxide based coatings were deposited from unstable electrolytes containing 0.100 M $NiSO_4$ and 0.100 M NH_4OH. The term, 'unstable solution' is used to describe solutions from which voluminous precipitation of $Ni(OH)_2$ occurs. This is defined in equation 3.1 and portrayed in plates 3.1 - 3.2. The precipitation of material in an electroplating solution may be undesirable because precipitates may be included in the as-deposited film. The inclusion of large precipitates can lead to coatings possessing poor mechanical properties such as durability and adhesion (3.2).

$$NiSO_4 + 2NH_4OH \rightleftharpoons Ni(OH)_2 + (NH_4)_2SO_4 \qquad 3.1$$

Coatings produced from unstable solutions had poor electrochromic properties such as poor reversibility and low dynamic ranges and displayed inadequate uniformity and adhesion (3.1). As solutions aged coatings that were deposited at various intervals during the solution ageing interval showed progressively poorer electrochromic properties. A systematic study in which solution concentrations, ageing and deposition times were the variables, was conducted in order to improve the electrochromic properties of coatings.

3.1.2 Deposition from stable solutions

A stable solution was prepared by the addition of a solution stabiliser (such as a detergent) to an unstable solution. The term 'stable solution' refers to a solution that has a reasonable shelf life before voluminous precipitation occurs (3.3). The shelf life of coating solutions is important for industrial applications because aged solutions produce different coatings to those that are freshly prepared. A familiar example is the settling of pigment particles from paint oils. Coatings prepared from freshly prepared paint differ substantially from paint that has been allowed to settle and has not been stirred prior to coating.

Most of the deposition solutions used in this study were colloids. These are thermodynamically unstable. Precipitation eventually occurs even with the addition of solution stabilisers in such solutions (3.4). However, it was only necessary that the period of solution stability exceed the deposition time required to produce coatings with good electrochromic properties. In this study solutions were stabilised for 24 hours without voluminous precipitation occurring. Films with identical optical properties were produced after the solution had aged for several hours (3.20). For unstable systems this could only be accomplished by simultaneously immersing more than one substrate into a solution that contained 0.100 M $NiSO_4$ and 0.100M NH_4OH (3.1).

Coatings produced from stable solutions had good electrochromic properties such as good reversibility and large dynamic ranges, and displayed superior uniformity and adhesion when compared with films deposited from unstable solutions. A systematic study in which deposition time, solution ageing and concentrations were the variables, was conducted in order to improve the electrochromic properties of the coatings.

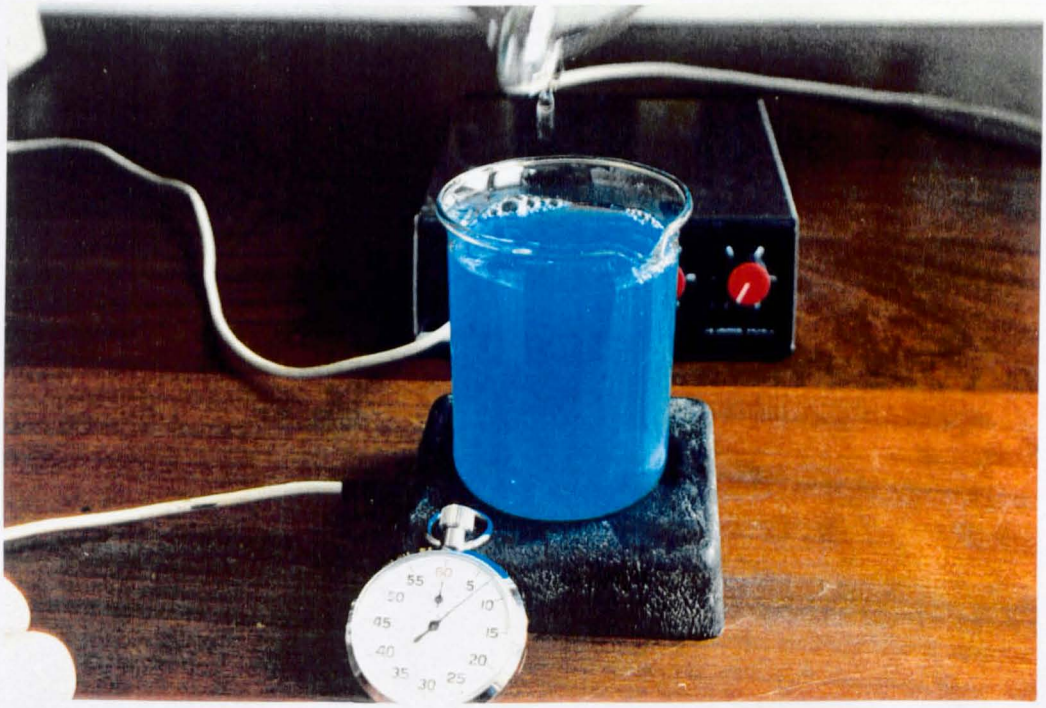

Plate 3.1 Solution originally containing 0.100 M NH_4OH and 0.100 M $NiSO_4$ after 7 seconds.

Plate 3.2 Solution originally containing 0.100 M NH_4OH and 0.100 M $NiSO_4$ after 60 minutes.

3.2 EXPERIMENTAL

3.2.1 Summary of experimental

This section describing experimental procedures is divided into two parts, the deposition of nickel oxide based coatings from unstable and stable solutions. In these sections systematic studies are described in which the variables were:

(i) Solution concentration
   . *$NiSO_4$ and NH_4OH for unstable solutions*
   . *$NiSO_4$, NH_4OH and stabilising agent for stable solutions*

(ii) Solution ageing

(iii) Deposition time

3.2.2 Anodic electrodeposition of nickel oxide based coatings

Initially, nickel oxide based coatings were deposited anodically using the same deposition parameters and electrolyte described in the literature (3.1). The electroplating solution used was 0.100 M nickel sulphate and 0.100 M ammonium hydroxide. Coatings produced using this method exhibited very poor electrochromic properties, such as residual colouration after bleaching and non-uniform colouration. As the study progressed, the concentrations of $NiSO_4$ and NH_4OH were altered and solutions stabilisers were added to the deposition solution to improve the mechanical and electrochromic properties of the coatings. The volume of the electrochemical working solutions used in this study was 250 cm^3. All solutions were magnetically stirred for 4 minutes prior

to deposition. A scanning potentiostat (Princeton Applied Research Model 362) was used to electrodeposit anodically the coatings. Platinum and saturated (KCl) calomel electrodes were used as the counter and reference electrodes respectively. The deposition substrates were either fluorine or indium doped tin oxide coated glass (sheet resistance of 40 Ω). Substrate cleaning was very important. Initially substrates were cleaned ultrasonically in a bath containing 10% Decon 90 for 20 minutes followed by rinsing with distilled water and drying in a N_2 jet. It was later found that a vast improvement in coating adhesion could be achieved by wetting the surface with a film of water prior to deposition.

Nickel hydroxide based films were deposited by cycling between +1500 mV and - 500 mV at $20mVs^{-1}$. Various thicknesses of nickel oxide based material were deposited by cycling for different periods of time. Post deposition treatment consisted of washing with distilled water followed by drying in a nitrogen jet. Prior to colouration the films were bleached at a negative potential of - 500 mV in 1 M potassium hydroxide for two minutes. Solar and visible optical properties were measured at -500 mV and +750 mV corresponding to the bleached and coloured states, respectively. These potentials were applied for two minutes. The working area of electrochromic films that was used was 50 X 50 mm^2. The charge extracted was measured using a chart recorder connected to the current monitor of the scanning potentiostat. Solar and visible optical properties of the films were measured using a Beckman ultraviolet/visible/near-infra-red spectrophotometer. The infra-red reflectance of the films was measured for the range 2500nm to 25000nm at different applied voltages using a Bruker IFS25 Fourier transform infra-red spectrophotometer. To confirm the chemical identity of the bleached and coloured states, Raman, cyclic voltammetry and X-ray diffraction analyses were performed on selected films.

3.2.2.1 *Solution mixing method*

The solution volume used throughout this study was 250 cm^3. Separate solutions of $NiSO_4$ and NH_4OH were prepared. The required concentration of $NiSO_4$ was dissolved in 50 cm^3 of distilled water and the appropriate concentration of NH_4OH was made up to 200 cm^3 with distilled water (see plates 3.3 and 3.4). When solution stabilisers (such as the detergent polyoxyethylene sorbitan monolaurate) were used, they were added to the solution containing NH_4OH. The mixture was then stirred using a magnetic stirrer to ensure thorough mixing of NH_4OH with the detergent. The solution containing NH_4OH (and when appropriate, the detergent polyoxyethylene sorbitan monolaurate) was then poured into the solution containing $NiSO_4$ such that the total solution volume was 250 cm^3. This was then magnetically stirred as described in 3.2.2. The solution ageing time commenced when the first drop of the NH_4OH solution made contact with the $NiSO_4$ solution.

Plate 3.3 From left to right: solutions of $NiSO_4$, NH_4OH + polyoxyethylene sorbitan monolaurate.

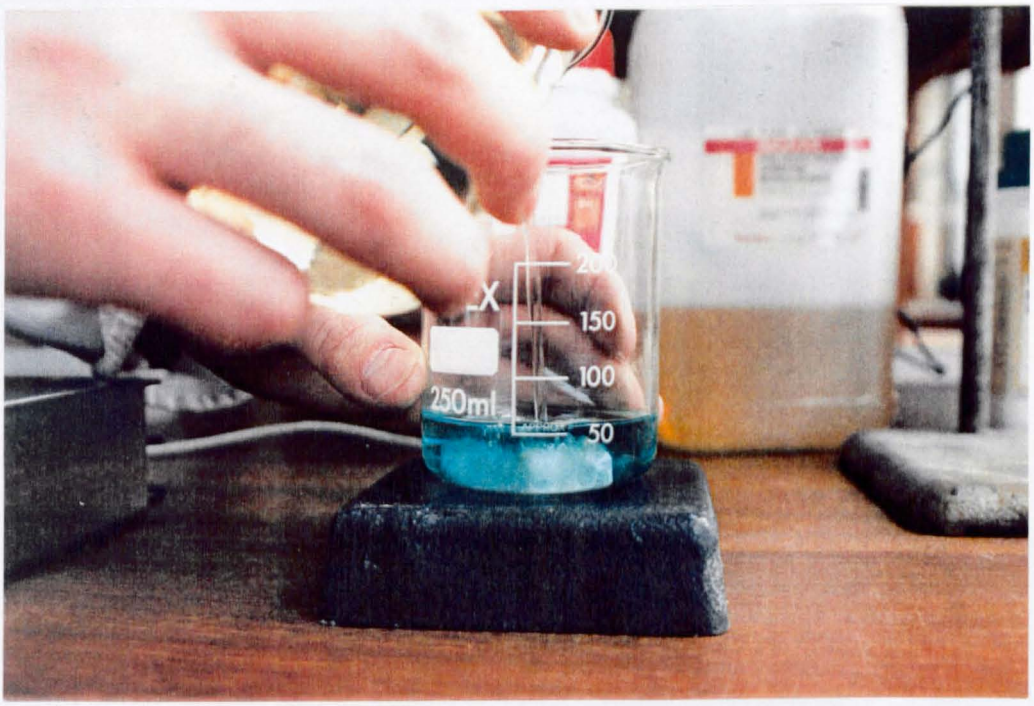

Plate 3.4 Mixing of $NiSO_4$ solution with NH_4OH and polyoxyethylene sorbitan monolaurate solution.

3.2.2.2 *Reproducibility of experimental data for coatings deposited by anodic and deposition*

Five types of analysis were performed on coatings that were deposited in this study. These were:

(i) Ultraviolet-visible-near-infra-red spectroscopy

(ii) Fourier transform spectroscopy

(iii) Raman spectroscopy

(iv) Cyclic Voltammetry

(v) X-ray diffraction

In this study the major technique used to analyze coatings was ultraviolet-visible-near-infra-red spectroscopy (Beckman spectrophotometer 3470). The error incurred in performing measurements using this technique for all coatings deposited during this study was ± 1%. After depositing many coatings using identical deposition conditions and post deposition treatments, it was found that the reproducibility of data points was good. This is illustrated in figure 3.1 where the error incurred during the measurements was within ± 1%. However, the reproducibility of all the measurements in this study was not determined. It is recognised that measurement errors occurred during the course of experiments, therefore the best curve or straight line has been drawn between data points. These curves and straight lines are only drawn as a visual aid to the eye.

At the end of this experimental, ten identical coatings were anodically deposited using the optimised conditions found for stabilised solutions (see section 3.2.6.4 and 3.2.6.5) the dynamic range was 81.6 ± 0.5% to 22.8 ± 0.7% (solar transmittance). These errors are smaller than those incurred in using the ultraviolet-visible-near-infra-red spectrophotometer (± 1%).

The reproducibility of Fourier transform spectrophotometry and Raman spectroscopy for all the coatings produced in this study was good. Essentially the same bands and peak heights were found for the as-deposited, bleached and coloured states, for coatings produced using identical deposition parameters . Cyclic voltammogram reproducibility was also good, oxidation and reduction peaks were located in same positions (at the appropriate scanning rates) for coatings produced using identical deposition conditions. Unfortunately, no X-ray diffraction peaks could be found for any of the samples deposited using the deposition techniques utilised in this study, therefore, it is inappropriate to discuss the errors involved in this measurement.

3.2.3 Experimental for deposition of nickel oxide based material from unstable solutions

3.2.3.1 *Solar and visible optical properties as a function of equimolar concentration of $NiSO_4$ and NH_4OH*

Films were anodically deposited on to ITO coated glass substrates from solutions that contained a range of equimolar amounts of nickel sulphate and ammonium hydroxide. The deposition voltages and cycling rates were those stated in 3.2.2 and remained constant throughout the experiment. The concentration range was 0.024 M to 0.800 M for the equimolar study. The scan rate was 20 mVs^{-1}, the deposition voltages were +1.500 V and -0.500 V and the deposition time was 30 minutes. The coatings with the best electrochromic and mechanical properties were deposited from solutions containing 0.024 M $NiSO_4$ and 0.024 M NH_4OH. Following the results of this experiment, another study was planned where the variable was deposition time. The deposition solution contained 0.024 M $NiSO_4$ and 0.024 M NH_4OH. The aim was to determine if the thickness of the coating affected the bleaching properties of the coating.

3.2.3.2 *Solar and visible optical properties as a function of NH_4OH concentration*

The concentration of nickel sulphate was kept constant (0.100 M) whilst the concentration of ammonium hydroxide was varied between 0.048 M up to 0.480 M. The scan rate was 20 mVs^{-1}, the deposition voltages were +1.500 V and -0.500 V and the deposition time was 30 minutes.

3.2.3.3 *Solar and visible optical properties as a function of $NiSO_4$ concentration*

The concentration range for nickel sulphate was 0.024 M to 0.800 M and a concentration of 0.100 M ammonium hydroxide was used. The scan rate was 20 mV s^{-1} and the deposition voltages were +1.500 V and -0.500 V and the deposition time was 30 minutes.

3.2.3.4 *Solar and visible optical properties as a function of deposition time from solutions containing 0.024 M $NiSO_4$ and 0.024 NH_4OH.*

In this experiment the deposition time was altered for equimolar concentrations (0.024 M) of nickel sulphate and ammonium hydroxide. The scan rate was 20 mVs^{-1}, the deposition voltages were +1.500 V and -0.500 V and the deposition time was 30 minutes.

3.2.4 Results for deposition from unstable solutions

3.2.4.1 *Equimolar concentrations of nickel sulphate and ammonium hydroxide.*

Coatings were deposited from solutions containing equimolar ratios of nickel sulphate and ammonium hydroxide in the range 0.024 M to 0.800 M. The deposition time was 30 minutes. The curves shown in figure 3.1 have several important features. There is a minima in the coloured solar transmittance (τ_{sc}) curve for films that were anodically deposited from solutions containing 0.100 M (equimolar concentrations) of nickel sulphate and ammonium hydroxide.

There was, however, a minima in the bleached solar transmittance (τ_{sb}) curve for anodically deposited films that coincided with the minima in the coloured solar transmittance curve. The films with the best electrochromic properties were anodically deposited from solutions that contained 0.024 M of nickel sulphate and 0.024 M ammonium hydroxide. The solar transmittance of the coloured (τ_{sc}) and bleached (τ_{sb}) states were 0.30 and 0.70 respectively. Solution stability was not observed over the range of concentrations used.

A further experiment was conducted where the concentration of $NiSO_4$ and NH_4OH was 0.100 M. In this experiment deposition time was adjusted. However, it was not possible to produce coatings that had good dynamic ranges by simply adjusting the deposition period (see figure 3.2), but this experiment clearly revealed that the bleaching properties of the coatings were related to the deposition time, and hence thickness.

Of particular interest are the minima in the coloured transmittance curves that occur in the same concentration range for material deposited by colloidal and anodic deposition. However, the bleached solar transmittance of coatings deposited by colloidal deposition were constant over this concentration range whereas those deposited by anodic deposition exhibited minima in the same range as the coloured transmittance curves for both anodic and colloidal coatings (see figure 3.1). The reduction in the dynamic range at this point for anodic coatings (despite the low coloured τ_{sc}) may be due to a difference in structure or diffusion channel dimensions. Unfortunately, these coatings were amorphous so it was not possible to detect this change.

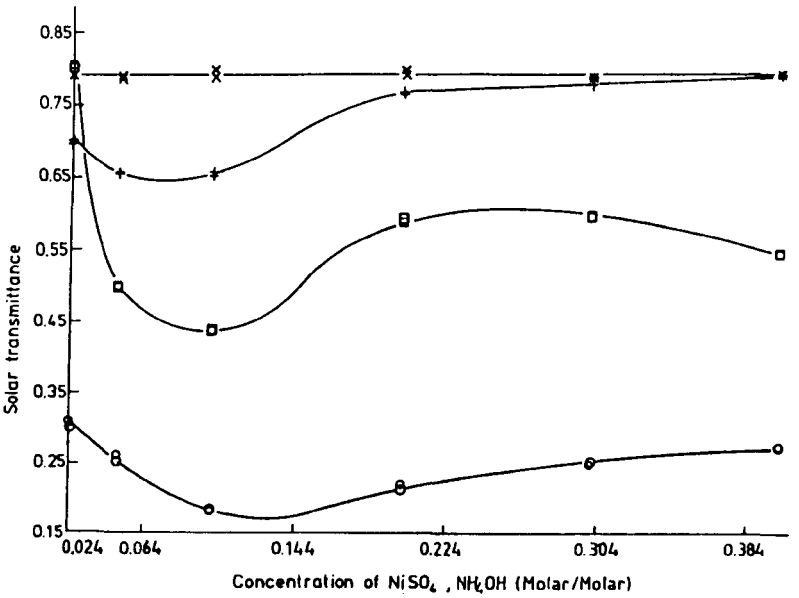

Figure 3.1 The dependence of the solar transmittance of the bleached and coloured states as a function of equimolar concentrations of nickel sulphate and ammonium hydroxide, for anodised and colloidally precipitated films (anodic coating, τ_s bleached = □; τ_s coloured = ○: colloidal coating, τ_s bleached = x; τ_s coloured = +). These curves and lines are only a visual aid to the eye.

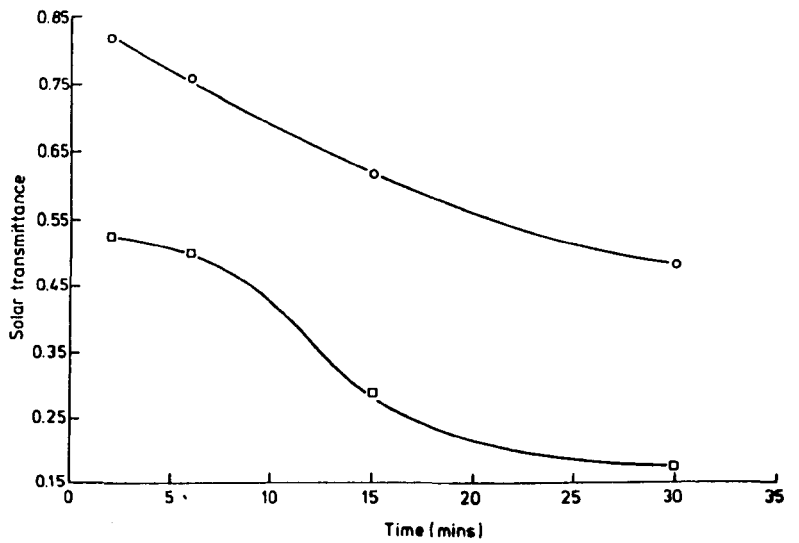

Figure 3.2 Solar transmittance of the bleached and coloured states as a function of deposition time. The concentration of nickel sulphate was 0.100 M and the ammonium hydroxide concentration was 0.100 M (τ_s bleached = ○; τ_s coloured = □). These curves are only a visual aid to the eye.

3.2.4.2 *Influence of ammonium hydroxide concentration*

In the next series of depositions, films were produced by anodic deposition from solutions where the nickel sulphate concentration was constant at 0.1 M and the concentration of ammonium hydroxide varied between 0.048 M to 0.480 M. The deposition time was 30 minutes. As the ammonium hydroxide concentration was increased from 0.048 M to 0.480 M, the bleached solar transmittance for anodic deposition decreased and reached a lower value at 0.290 M ammonium hydroxide (see figure 3.3). The value of the bleached solar transmittance was 0.18.

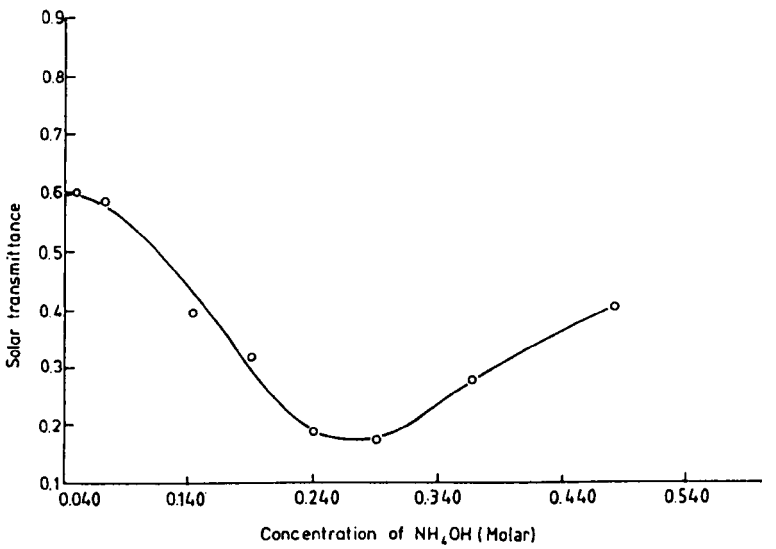

Figure 3.3 The dependence of solar transmittance for the bleached state on the concentration of ammonium hydroxide. The concentration of nickel sulphate was 0.100 M (t_s bleached = 0). These curves are only a visual aid to the eye.

3.2.4.3 *Influence of nickel sulphate concentration*

Films were anodically deposited from solutions containing 0.100 M ammonium hydroxide, whilst the nickel sulphate concentration was varied in the range 0.100 M to 0.800 M. As the nickel sulphate concentration increased, the coloured solar transmittance increased (see figure 3.4). The bleached solar transmittance increased slightly for the same concentration range. It was observed that at 0.320 M nickel sulphate, precipitation stopped. However, films deposited from solutions that containing higher concentrations of nickel sulphate were not mechanically stable to electrochemical oxidation and reduction.

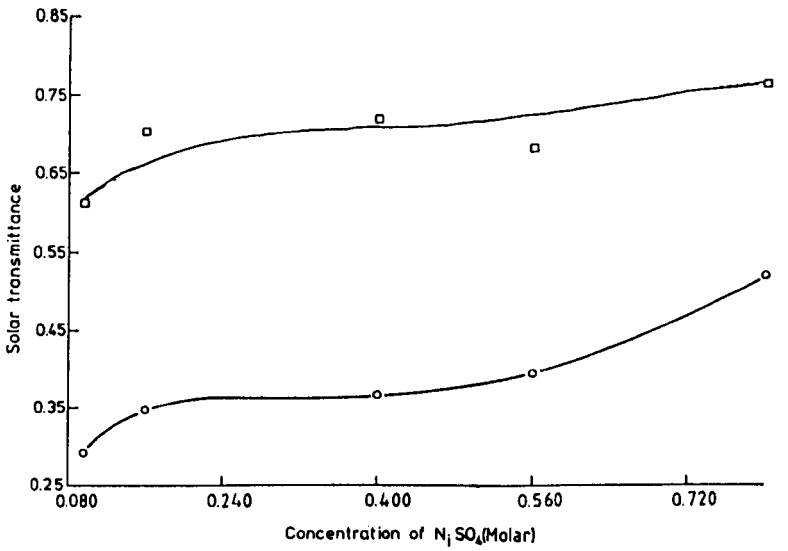

Figure 3.4 Solar transmittance of the bleached state as a function of nickel sulphate concentration. The concentration of ammonium hydroxide was constant at 0.100 M (t_s bleached = □; t_s coloured = ○). These curves are only a visual aid to the eye.

3.2.4.4 *Influence of deposition time*

The influence of deposition time for anodically deposited films was investigated by producing films from solutions containing 0.024 M nickel sulphate and ammonium hydroxide. The deposition time was varied. Films were deposited from electrolytes containing equimolar concentrations of nickel sulphate and ammonium hydroxide (0.024 M). The deposition time was varied between 5 and 40 minutes. As the deposition time increased, the solar transmittance decreased for the coloured and bleached states (see figure 3.5). After 40 minutes the solar transmittance of the coloured state was 0.26. Unfortunately, the solar transmittance of the bleached state was lower than 0.70. Films produced using these deposition parameters were not homogeneous.

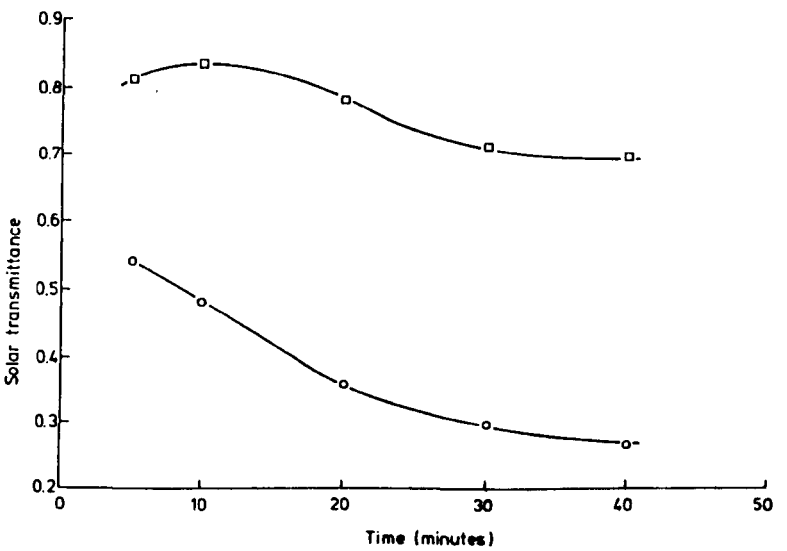

Figure 3.5 The influence of deposition time on the solar transmittance of the bleached and coloured states. Equimolar concentrations of nickel sulphate and ammonium hydroxide, 0.024 M were used (τ_s bleached = □; τ_s coloured = ○). These curves and lines are only a visual aid to the eye.

In the coloured state the films had a mottled appearance and in the bleached state, areas of the film retained some residual colouration. It was observed during the deposition process that agglomerates of precipitate formed on the surface of the substrate as deposition was occurring. These precipitates may have interfered with mass transport to the conductive substrate, thus leading to non uniformities in the film.

3.2.4.5 *Summary of results for coatings deposited from unstable solutions*

The best coatings deposited from unstable solutions exhibited solar transmittances of 0.30 and 0.70 in the coloured and bleached states respectively. The solution concentrations were 0.024 M $NiSO_4$ and 0.024 NH_4OH. Although this dynamic range is comparable with literature values (3.1), the optical homogeneity of the bleached and coloured states was poor even in the best films. The adhesion of films deposited from unstable solutions was also poor. Typically most coatings failed the 'Sellotape' test. The durability of coatings to repetitive cycling between the bleached and coloured states (- 500 mV - +750 mV at 20 mVs^{-1}) in 1M KOH was not satisfactory. Usually, films started to disintegrate after the tenth cycle and some coatings after only one cycle.

3.2.5 Experimental for deposition from stable solutions

3.2.5.1 *Solar and visible optical properties as a function of detergent concentration*

Films were anodically deposited on to ITO coated glass substrates from solutions that contained 0.024 M $NiSO_4$ and 0.024 M NH_4OH for the range of 5 - 40% detergent (poly oxyethylene sorbitan monolaurate). The scan rate was 20 mVs^{-1} and the deposition voltages were +1.500 V and -0.500 V and the

deposition time was 30 minutes. The coloured solar transmittances of these coatings were very high (>0.60). The experiment was repeated for different concentrations of ammonium hydroxide for the range 0.024 M to 0.072 M of ammonium hydroxide.

3.2.5.2 *Solar and visible optical properties as a function of NH_4OH concentration*

In the previous experiment, it was found that by increasing the concentration of NH_4OH in the deposition solution, coatings with superior electrochromic properties were produced. The concentration of nickel sulphate was kept constant at 0.024 M whilst the concentration of ammonium hydroxide was varied between 0.024 M and 0.480 M. The scan rate was 20 mVs^{-1}, deposition voltages were +1.500 V and -0.500 V. The deposition time was 30 minutes. The lowest solar transmittance of 0.22 was observed for coatings deposited at a concentration of 0.100 M of NH_4OH.

3.2.5.3 *Solar and visible optical properties as a function of deposition time*

Nickel oxide based coatings were deposited as a function of deposition time for the range 10 to 60 minutes from solutions containing 0.024 M of $NiSO_4$, 0.072 M NH_4OH and 40% detergent by volume. The scan rate was 20 mVs^{-1} and the deposition voltages were +1.500 V and -0.500 V. This experiment was repeated using 0.1 M ammonium hydroxide. It was found that films with greater dynamic ranges could be produced from these solutions, 0.22 and 0.82 in the coloured and bleached states respectively.

3.2.5.4 *Deposition from stable solutions*

There appeared to be a relationship between the stability of the deposition solution and the mechanical and electrochromic properties of coatings. It was therefore decided to add solution stabilisers to electrolytes containing nickel sulphate and ammonium hydroxide. Initially, various solution stabilisers were used. These included anionic and cationic detergents, gelatin, polyvinylalcohol and polyethyleneglycol. However these materials either enhanced precipitation, produced films with poor adhesion or chelated the nickel from the solution to such an extent that it was difficult to achieve deposition at all. The most successful stabilising agent was gelatin. However, it was difficult to remove gelatin from the coating after the deposition had taken place. This was because the concentrations of gelatin required to stabilise the solution were so high that the solution gelled and solidified during deposition. Coatings were deposited at higher temperatures (80 °C - where the solution of gelatin and water was a liquid) from solutions that contained gelatin but these were less uniform than those deposited at lower temperatures (25 °C). Loss of uniformity was due to the formation of agglomerates (enhanced precipitation) that was enhanced by the increase in Brownian motion conferred by the higher temperatures of the solutions. A major disadvantage of using gelatin is that the chemical nature of gelatin is poorly understood and therefore, the composition of the material can vary considerably from batch to batch. So, even if the other problems associated with gelatin could be overcome it may be difficult to obtain reproducible results.

Eventually a suitable solution stabiliser was identified. This was selected from a class of materials known as non-ionic detergents. The non-ionic detergent used was polyoxyethylene sorbitan monolaurate. This was chosen because it

did not interfere with the ions in the solution as an ionic detergent may have done. Also this detergent did not chelate the nickel ions too strongly (it was not possible to electroplate from solutions that contained detergents with phosphate stabilisers). Films with superior electrochromic and mechanical properties were made from solutions that contained >10% by volume of polyoxyethylene sorbitan monolaurate. Whilst the adhesion was not as good as sputtered films, the uniformity and optical homogeneity in the coloured state was of comparable quality.

The most important features of coatings deposited from stable solutions was the lack of residual colouration in the bleached state and the anti-reflection properties of the films. The combination of these factors raised the value for the bleached solar transmittance from 0.70 (as deposited from unstable solutions) to 0.82, whilst the coloured solar transmittance was 0.22. Coatings were deposited from solutions containing different concentrations of nickel sulphate, ammonium hydroxide and detergent, and using different deposition and solution ageing times. It was found that the ideal concentrations of $NiSO_4$, NH_4OH and polyoxyethylene sorbitan monolaurate were 0.024 M, 0.100 M and 40% (by volume) respectively. The maximum deposition time used was 2 hours. The scan rate and deposition potentials were the same as those indicated in the experimental. An ageing study was also performed on a solution containing detergent. It was found that coatings with identical properties could be deposited from the same solution even after the solution had aged for several hours. This was difficult to achieve from unstable solutions (this could only be accomplished if more than one substrate was introduced into the deposition solution at the same time).

3.2.6 Results for deposition from stable solutions

3.2.6.1 *Deposition from stable solutions*

The major problem associated with film deposition from unstable solutions was the formation of large agglomerates that ruined the visual appearance of the bleached and the coloured states of the films. As the deposition time increased the value of the bleached state deteriorated (see figure 3.2 and 3.5). Ideally an electrochromic film should exhibit a dynamic range of 0.20 - 0.80 in the coloured and bleached states respectively. This could not be achieved using the deposition parameters mentioned in section 3.2.3. The problem of agglomeration was solved by using a stabilising agent. The stabilising agent used was the non-ionic detergent, polyoxyethylene sorbitan monolaurate (3.6). This was chosen because the addition of various concentrations of cationic and anionic detergents to unstable solutions containing nickel sulphate and ammonium hydroxide enhanced precipitation. In theory the addition of a cationic detergent should have led to colloid stability due to the adsorption of anions onto the surface of the colloid particles (3.7) and to particles acquiring a higher negative charge and hence, greater mutual electrostatic repulsion (3.8). In turn, enhanced mutual repulsion reduces the tendency of individual particles to coalesce to produce larger particles. In the event, the addition of cationic detergents (such as cetyl trimethyl ammonium bromide and cetyltridecyl ammonium hydroxide) led to voluminous precipitation (enhanced precipitation) for a range of concentrations (1 - 40 %). It was also noticed that the deposition rate decreased as the concentration of detergent (for anionic and cationic detergents) increased. The addition of ionic detergents may have caused the precipitate to gel (3.9). This usually decreases the deposition rate. The interaction of detergents with colloids and substrates is

very complex. It has been shown that some detergent's enhance the deposition rate and uniformity whereas other detergents lower the deposition rate whilst improving uniformity (3.2).

The concentration of nickel sulphate used in stable solutions (containing detergents) was 0.024 M. This concentration of nickel sulphate was selected because in previous experiments solutions that contained this concentration produced the films with the largest dynamic range and the highest value for the bleached solar transmittance (figure 3.1). The curves in figure 3.6 indicated that the coloured solar transmittance had an average value of 0.70 for equimolar concentrations of nickel sulphate and ammonium hydroxide (0.024 M).

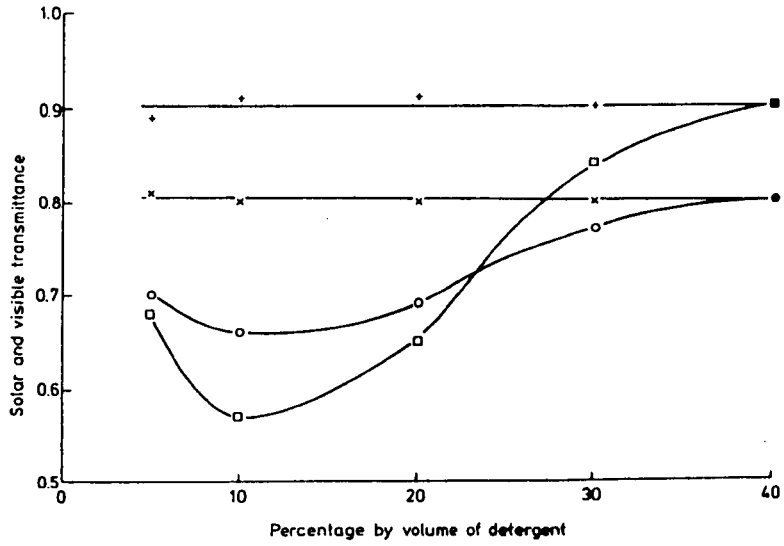

Figure 3.6 Solar and visible transmittance of the bleached and coloured states as a function of added detergent. Equimolar concentrations of nickel sulphate and ammonium hydroxide, 0.024 M were used (τ_s bleached = x; τ_s coloured = O; , τ_v bleached = +; τ_v coloured = □) These curves and lines are only a visual aid to the eye.

Therefore, the concentration of ammonium hydroxide was increased. According to the results (see figures 3.7 and figure 3.8), the concentration of ammonium hydroxide had to be higher to produce films with good coloured electrochromic properties. Correspondingly, it was necessary to use more than 20% of detergent to produce homogeneous films with high bleached solar transmittances.

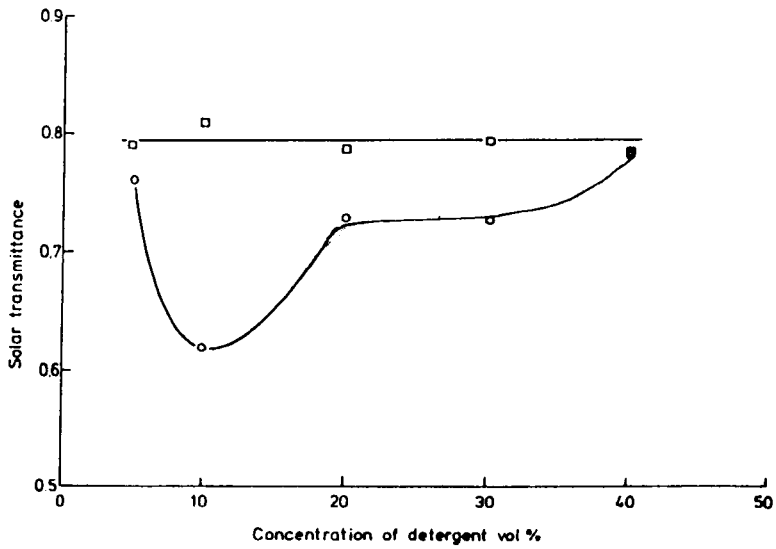

Figure 3.7 The dependence of solar transmittance for the bleached and coloured states on the concentration of detergent. The concentration of nickel sulphate was 0.024 M, the concentration of ammonium hydroxide was 0.048 M, and the deposition time was 30 minutes (t_s bleached = □; t_s coloured = ○). These curves and lines are only a visual aid to the eye.

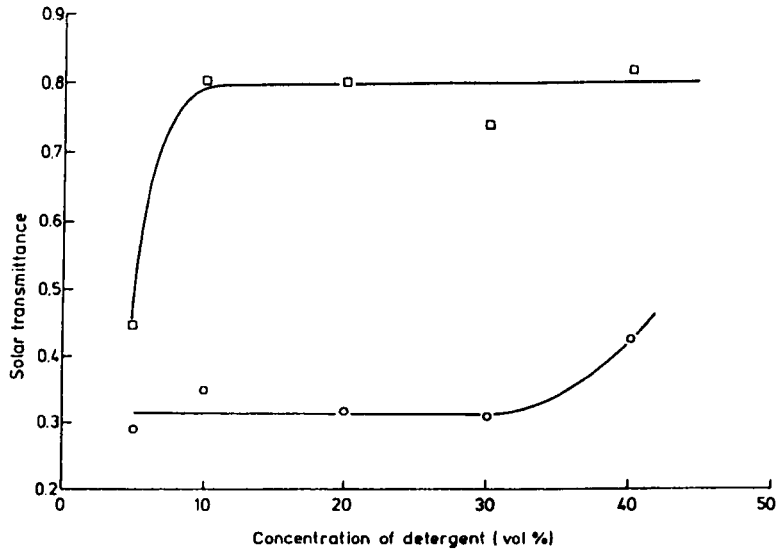

Figure 3.8 Solar transmittance of the bleached and coloured states versus the concentration of detergent. The concentration of nickel sulphate was 0.024 M, the concentration of ammonium hydroxide was 0.044 M, and the deposition time was 30 minutes (t_s bleached = □; t_s coloured = ○). These curves are only a visual aid to the eye.

3.2.6.2 *Influence of ammonium hydroxide concentration*

Films were deposited from solutions where the ammonium hydroxide concentration was varied between 0.048 M and 0.144 M. The nickel sulphate concentration was constant at 0.100 M. The deposition time was 30 minutes. As the ammonium hydroxide concentration was increased, the coloured solar transmittance values decreased until a minimum value was reached at 0.100 M ammonium hydroxide (see figure 3.9). The bleached curve goes through a maxima at this point. As the ammonium hydroxide concentration increased the coloured solar transmittance decreased. The same trend was observed for films that were deposited for 60 minutes (see figure 3.10).

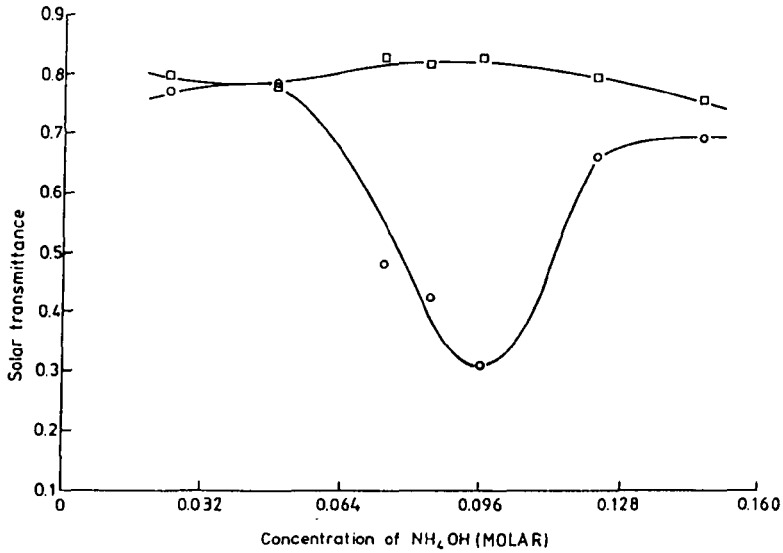

Figure 3.9 The influence of ammonium hydroxide concentration on the solar transmittance of the bleached and coloured states. The concentration of nickel sulphate was 0.024 M, the detergent concentration was constant at 40%, and the deposition time was 30 minutes (t_s bleached = □; t_s coloured = ○). These curves are only a visual aid to the eye.

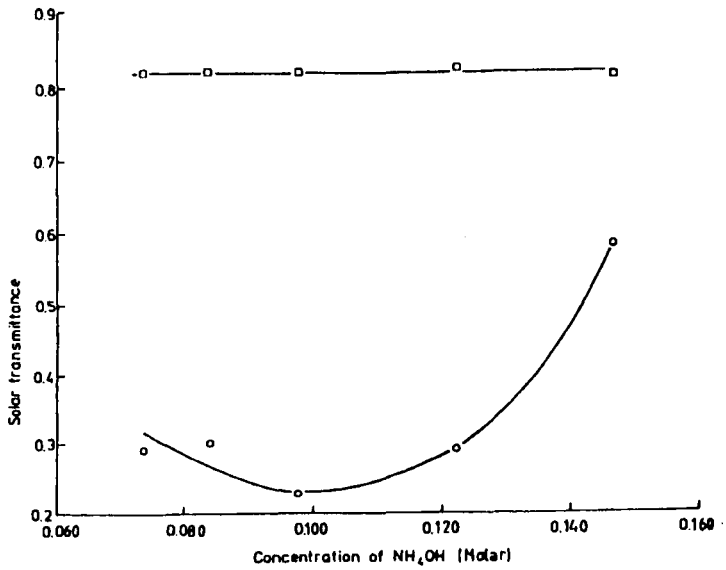

Figure 3.10 The dependence of solar transmittance of the bleached and coloured states on ammonium hydroxide concentration. The concentration of nickel sulphate was 0.024 M, the detergent concentration was constant at 40%, and the deposition time was 60 minutes. The scan rate was 20 mVs^{-1} (t_s bleached = □; t_s coloured = ○). These curves and lines are only a visual aid to the eye.

3.2.6.3 *Influence of detergent concentration*

The next series of films were deposited by anodic deposition from stable solutions (3.11). The solution stabiliser used was the non-ionogenic detergent polyoxyethylene sorbitan monolaurate (Sigma Chemicals). Films were deposited from solutions containing different concentrations of detergent (from 5 - 40 % by volume) and 0.024 M of nickel sulphate and 0.072 M ammonium hydroxide. The addition of the non-ionic detergent improved the solar transmittance of the bleached state to 0.80 for most concentrations of detergent whilst the solar transmittance of the coloured state was approximately 0.30 (figure 3.11).

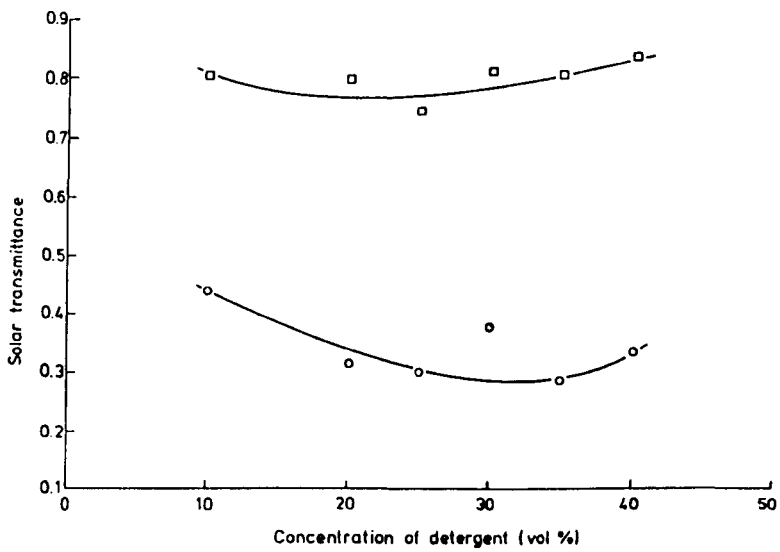

Figure 3.11 Solar transmittance of the bleached and coloured states versus detergent concentration. The concentration of nickel sulphate was 0.024 M, the ammonium hydroxide concentration was 0.072 M, and the deposition time was 60 minutes. The scan rate was 20 mVs^{-1} (t_s bleached = □; t_s coloured = ○). These curves are only a visual aid to the eye.

3.2.6.4 *Influence of deposition time*

For constant concentration of nickel sulphate (0.024 M), ammonium hydroxide (0.072 M) and detergent (40%), the deposition time was varied (10 - 60 minutes). The curves in figure 3.12 show that the bleached state remained constant at 0.80 (within experimental error +/- 1%), whilst the coloured solar transmittance became progressively lower (0.22 at 60 minutes deposition time). It was not possible to produce reversible electrochromic films from solutions containing 0.024 M of nickel sulphate and 0.072 M of ammonium hydroxide without using detergent (see figure 3.13).

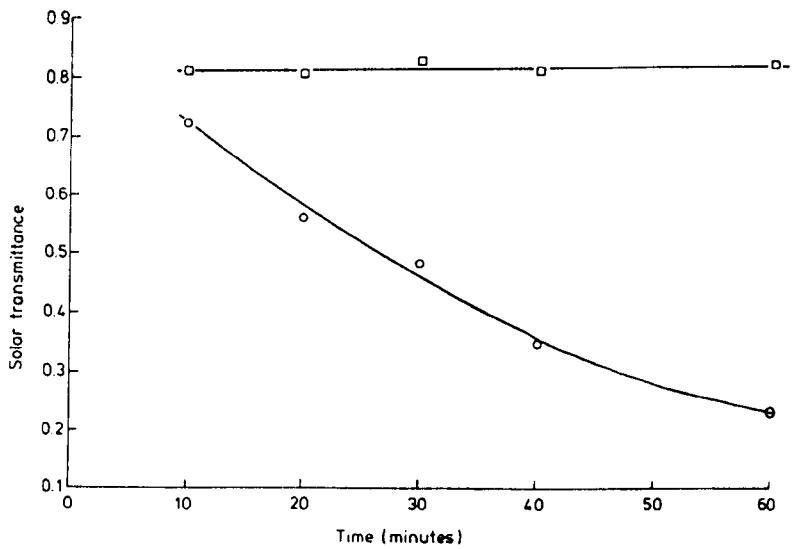

Figure 3.12 Solar transmittance of the bleached and coloured states as a function of deposition time. The concentration of nickel sulphate was 0.024 M, the concentration of ammonium hydroxide was 0.072 M, and the detergent concentration was constant at 40%. The scan rate was 20 mVs^{-1} (t_s bleached = □; t_s coloured = ○). These curves and lines are only a visual aid to the eye.

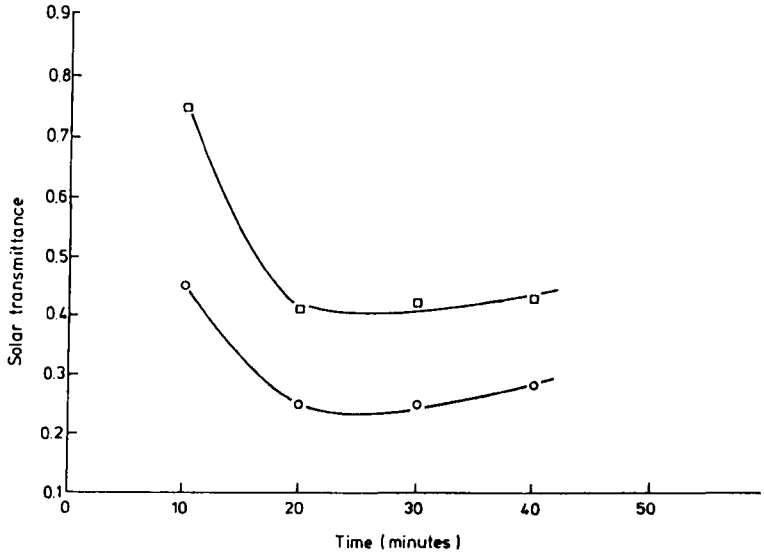

Figure 3.13 The influence of deposition time on the solar transmittance of the bleached and coloured states. The concentration of nickel sulphate was 0.024 M and the concentration of ammonium hydroxide was 0.072 M. The scan rate was 20 mVs^{-1} (τ_s bleached = □; τ_s coloured = ○). These curves are only a visual aid to the eye.

3.2.6.5 *Coatings deposited from stable solutions*

The electrochromic properties of the films were improved by the addition of detergent. The transmittance spectra for the range 300 nm to 2500 nm for the best film produced from stable solutions are presented in figure 3.14. The solar transmittance in coloured state was 0.22, with a correspondingly very high solar transmittance of 0.82 in the bleached state. The films were homogeneous in the bleached and coloured states and bleached instantaneously without any residual colouration. For all films produced from stable solutions anti-reflection properties were observed (see figure 3.15). The shelf life of stable solutions was superior to that of unstable solutions (see figures 3.23 - 3.24).

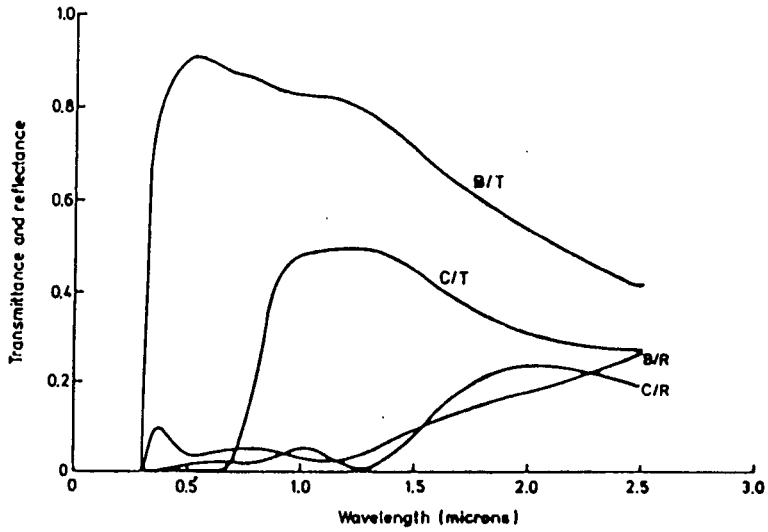

Figure 3.14 Solar transmittance and reflectance of the bleached and coloured states substrate as a function of wavelength. The concentration of nickel sulphate was 0.024 M and the concentration of ammonium hydroxide was 0.072 M (B/T = bleached transmittance, C/T = coloured transmittance; C/R = coloured reflectance B/R = bleached reflectance).

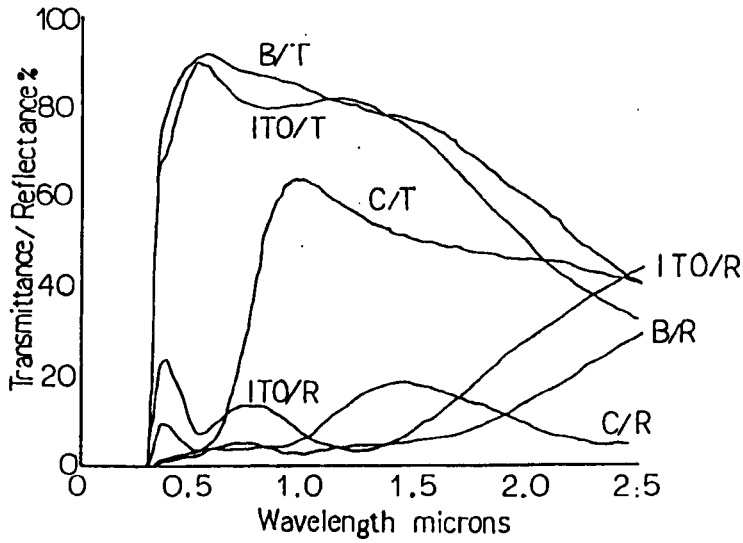

Figure 3.15 Solar transmittance and reflectance for the bleached and coloured states and ITO-coated glass substrate as a function of wavelength. The concentration of nickel sulphate was 0.024 M and the concentration of ammonium hydroxide was 0.072 M (B/T = bleached transmittance, C/T = coloured transmittance; C/R = coloured reflectance B/R = bleached reflectance ITO/T = ITO transmittance).

3.3 ANALYSIS OF NICKEL OXIDE BASED FILMS

3.3.1 Fourier transform infra-red spectrophotometry

Fourier transform infra-red spectrophotometry was used to characterise coatings deposited from stable and unstable solutions in the range of 4000 cm^{-1} - 400 cm^{-1}. In the O-H stretch region, spectra of coatings deposited from both stable and unstable solutions show a sharp hydroxy band at 3647 cm^{-1} and a broad band at around 3360 cm^{-1} (3.10, 3.11), (see figure 3.16). Spectra obtained from films deposited using different deposition times show an increasing peak height at 3647 cm^{-1} with respect to increasing deposition time (film thickness). This implied that this hydroxy stretch was not only due to surface hydroxy groups but also hydroxy groups within the film. Furthermore, as coatings were progressively coloured, the hydroxy stretch at 3647 cm^{-1} became smaller until at + 500 mV it disappeared (see figure 3.17). As the stretch at 3647 cm^{-1} decreased, a stretch at 564 cm^{-1} appeared. The influence of film thickness in the range 400 A to 2400 A for the coloured state is shown in figure 3.18. As the coating thickness increased the infra-red reflectance decreased. By comparison to standard spectra, ß-nickel hydroxide has a sharp band at 3630 cm^{-1} and the broad band at 3400 cm^{-1} is characteristic of α-nickel hydroxide in transmittance (3.10). The broad 3400 cm^{-1} band observed in α-nickel hydroxide is indicative of hydrogen bonded water in the film structure (3.21). The sharp band at 3647 cm^{-1} is similar to that reported elsewhere (3.10-3.12). The deposition of a very thick film from a stable solution led to the identification of a band in the coloured state at 564 cm^{-1}. Also a broad band was observed in the -OH region (see figure 3.19). The infra-red peak around 564 cm-1 is characteristic of both γ- and ß-nickel oxyhydroxide (3.10).

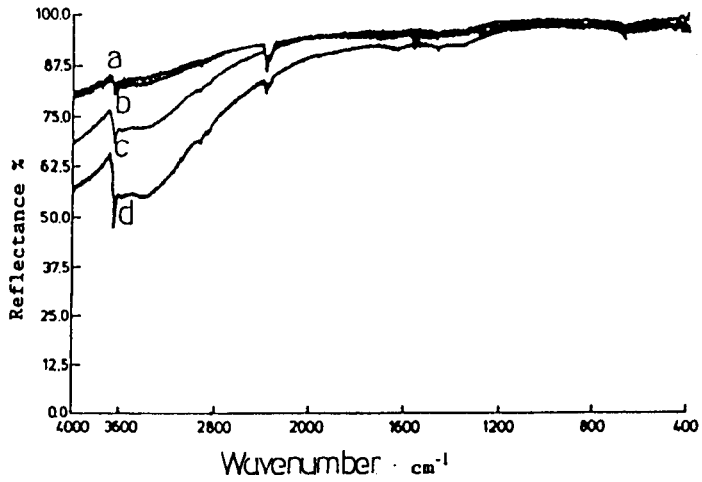

Figure 3.16 The dependence of infra-red reflectance on deposition time for the bleached state. The deposition time for samples was: (a) 20 mins; (b) 30 mins; (c) 40 mins; and (d) 60 mins. The concentration of nickel sulphate was 0.024 M, the concentration of ammonium hydroxide was 0.072 M and the detergent concentration was constant at 40%.

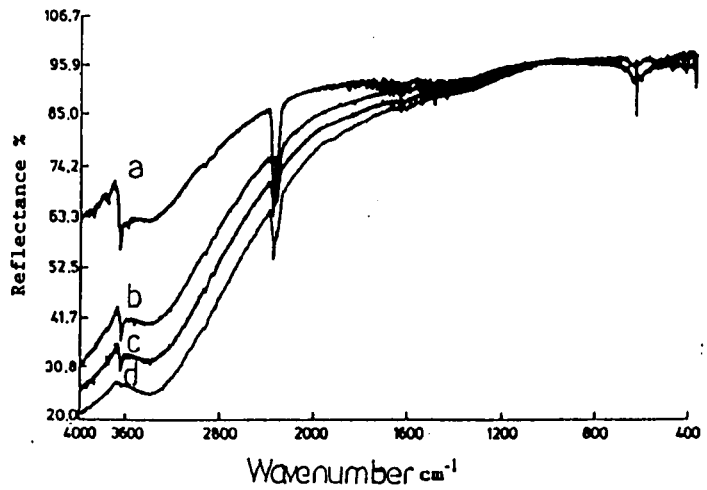

Figure 3.17 Infra-red reflectance versus applied voltage. The applied voltages were: (a) - 500 mV; (b) + 420 mV; (c) + 440 mV; (d) + 500 mV. The concentration of nickel sulphate was 0.024 M, the concentration of ammonium hydroxide was 0.072 M and the detergent concentration was constant at 40%.

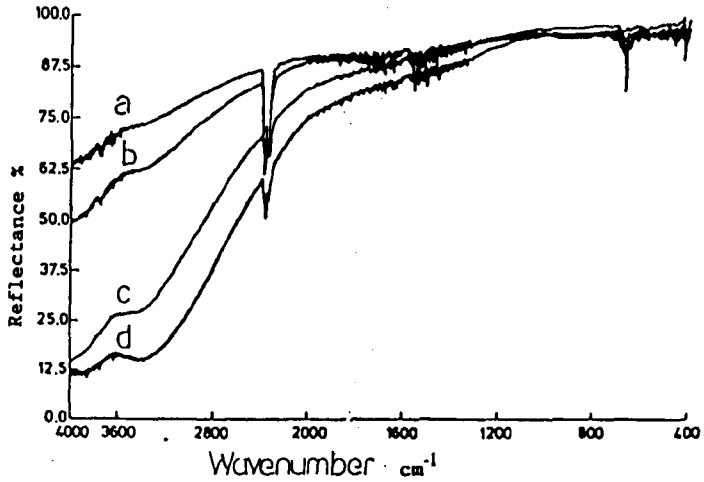

Figure 3.18 Infra-red reflectance as a function of deposition time for the coloured state. The deposition time for samples was: (a) 20 mins; (b) 30 mins; (c) 40 mins; and, (d) 60 mins. The concentration of nickel sulphate was 0.024 M, the concentration of ammonium hydroxide was 0.072 M and the detergent concentration was constant at 40%.

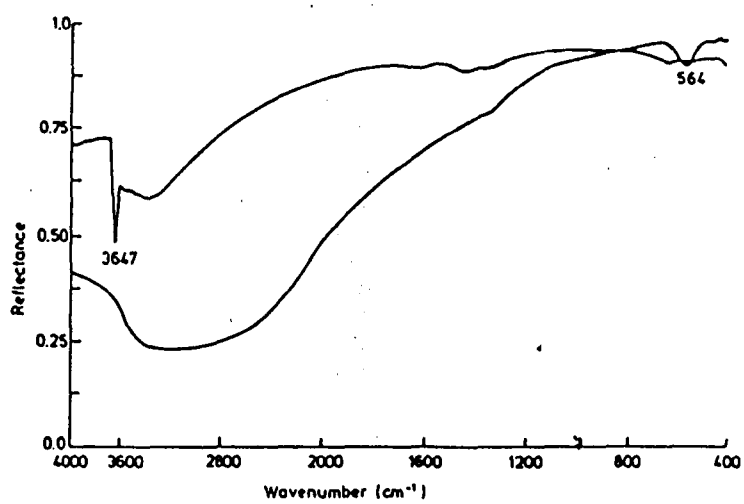

Figure 3.19 Infra-red reflectance: (a) bleached state; and, (b) coloured state as a function of wavelength. The concentration of nickel sulphate was 0.024 M, the concentration of ammonium hydroxide was 0.096 M.

3.3.2 Cyclic voltammetry

Films that were deposited from stable solutions were analyzed using cyclic voltammetry (films deposited from non stable solutions were not mechanically stable to cycling for more than a few cycles). Voltages were measured relative to the saturated calomel electrode. The oxygen evolution, colouration (anodic) and bleaching (cathodic) peaks can be observed in the cyclogram (figure 3.20) (3.12, 3.13). The maxima of the anodic peak occurs at +420 mV that is the same potential at which the hydroxy stretch starts to disappear in the spectral data (see figure 3.17). It was also noticed that as the scanning rate was increased the anodic peak became smaller until at 10 mVs^{-1} the colouration anodic peak was no longer present (see figure 3.20).

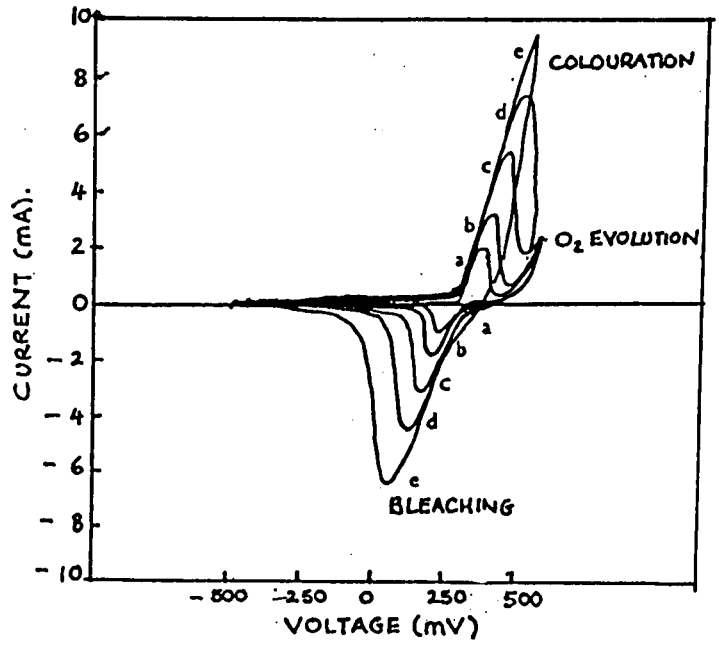

Figure 3.20 Electrocyclogram of anodised film specified as d in figure 3.16: (a)-1 mVs^{-1}; (b)-2 mVs^{-1}; (c)-5 mVs^{-1}; (d)-10 mVs^{-1}; and, (e)-20 mVs^{-1}.

3.3.3 Raman spectroscopy

Raman spectroscopy was used to analyze coatings that were anodically deposited from stable and non stable solutions. Spectra were obtained for the bleached (-500 mV) and coloured (+750 mV) states. No peaks were found that corresponded to α- or β-nickel hydroxide. However, for coatings that were deposited from stable solutions, peaks were detected at 545 cm^{-1} and 489 cm^{-1} (see figure 3.22), that correspond to γ-nickel oxyhydroxide, in the coloured state. This was surprising because, according to the literature, this phase is irreversible and cannot be electrochemically reduced back to the bleached state (3.10). As has been previously indicated in this study, the most reversible electrodeposited coatings were produced from stable solutions. The ability to reduce electrochemically γ-nickel oxyhydroxide has also been reported by other researchers (3.10). Furthermore coatings of β-nickel oxyhydroxide deposited by the oxidation of alkaline nickel (II) solutions with chlorine, bromine and persulphate ions, are irreversible (cannot be electrochemically reduced) (3.16). The lack of evidence of β-$Ni(OH)_2$ in the bleached state may have been because these coatings were amorphous. However, for the bleached state of the coating measured using infra-red spectroscopy the stretch at 3647 cm^{-1} was clearly identified (see figure 3.19).

3.3.4 X-ray diffraction

Analysis was performed on coatings deposited from stable and unstable solutions for the concentration ranges in this study. Unfortunately, none of the coatings deposited in this study exhibited XRD peaks (see figures 3.21). This implies that anodically deposited coatings from both stable and unstable solutions were amorphous. Furthermore, films that were annealed at 200 and

300°C also exhibited no peaks other than those corresponding to the ITO underlayer. However, had peaks been found, they would have been those of nickel oxide rather than ß-nickel hydroxide. This is because ß-nickel hydroxide decomposes to nickel oxide and water at 200°C (18), and is thermodynamically unstable at room temperature, 25°C (19).

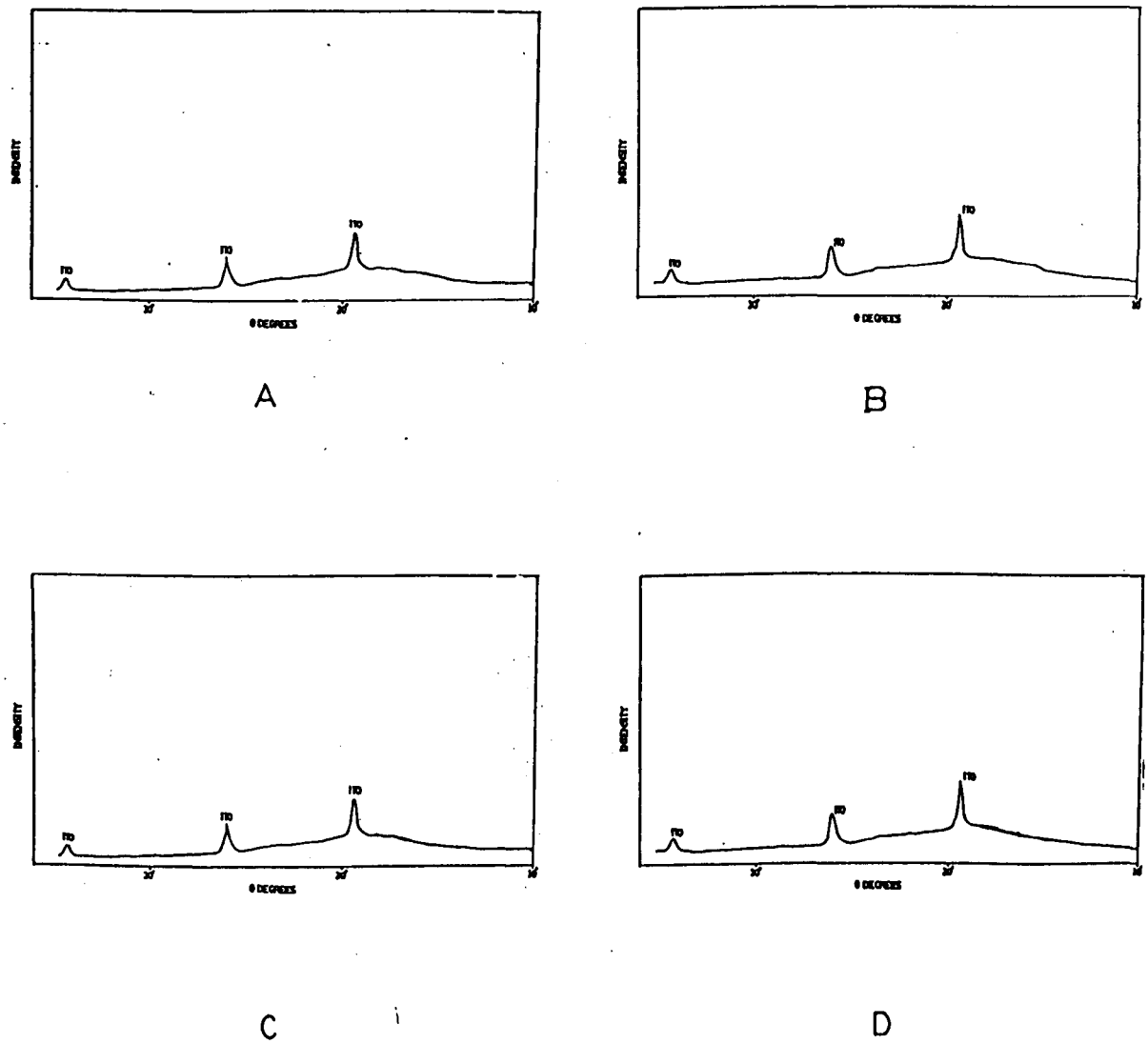

3.21 X-ray diffraction of coatings deposited from stable solutions: (a) in the coloured state; (b) in the bleached state; (c) from unstable solutions in the coloured state; and, (d) from unstable solutions in the bleached state.

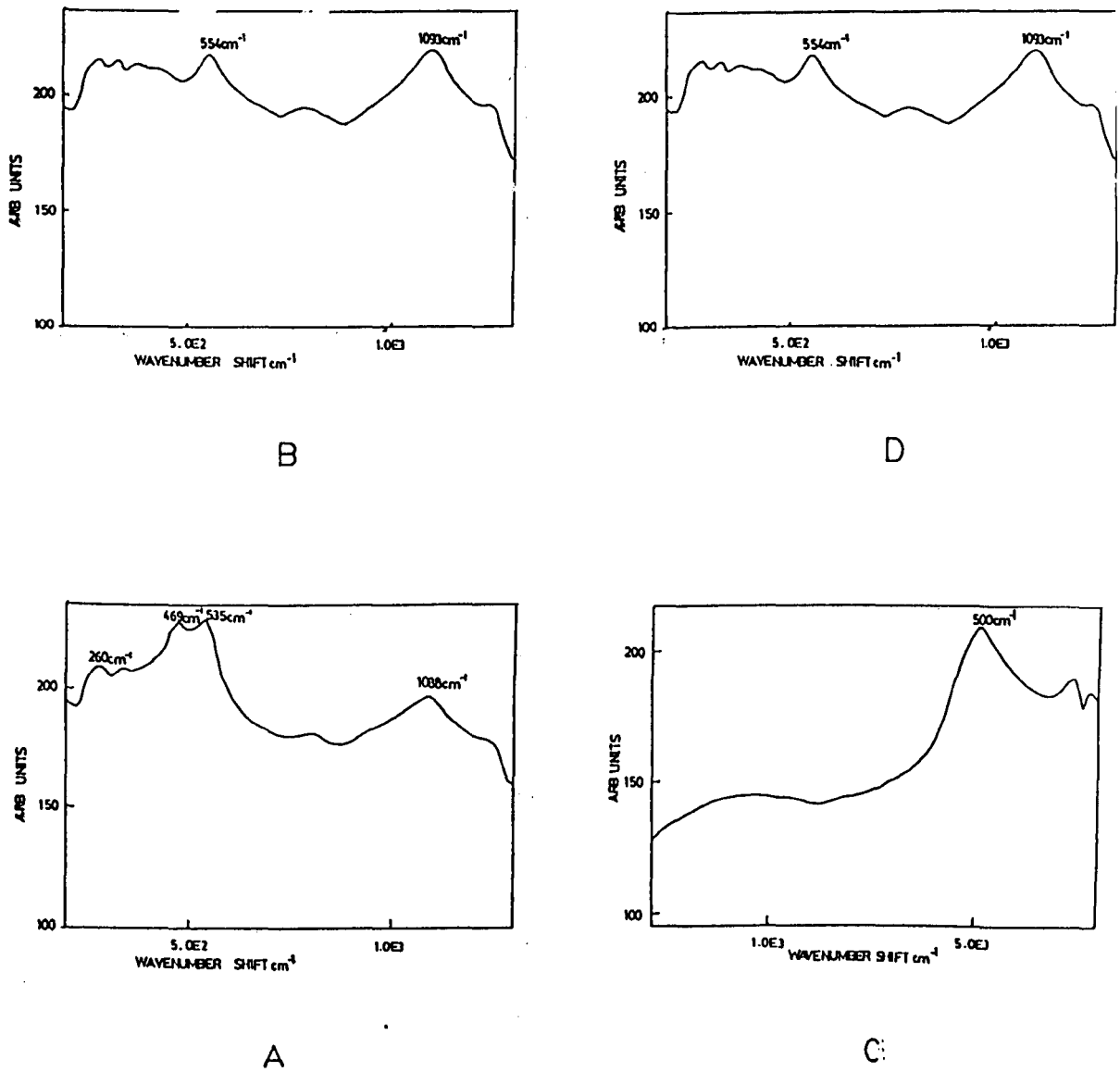

Figure 3.22 Raman spectra of hydrated coatings deposited: (a) from stable solutions in the coloured state; (b) from stable solutions in the bleached state; (c) from unstable solutions in the coloured (c) and state; and, (d) from unstable solutions in the bleached states.

3.3.5 Colouration efficiency

The method of calculation chosen in this study was that of the optical density of $1cm^2$ of coating divided by the charge injected through this area (see equation 3.3).

$$OD = \log \frac{\tau Bleached}{\tau Coloured} \qquad 3.2$$

$$C.E. = \frac{\Delta OD}{Q} \qquad 3.3$$

There was very little difference in the colouration efficiency of coatings deposited from stable and optimised unstable solutions. The solar colouration efficiency (τ_s) for coatings deposited from stable solutions was 29 cm^2 C^{-1} whereas for films deposited from unstable solutions (optimised) it was 25 cm^2 C^{-1}. The visible colouration efficiency was also not significantly different for coatings deposited from stable and optimised unstable solutions. Coatings deposited from solutions containing the same concentrations as used in the literature had colouration efficiencies of 14 cm^2 C^{-1}. This was due to the low value of solar transmittance for the bleached state.

3.4 SUMMARY OF ANODIC DEPOSITION AND CHARACTERISATION OF NICKEL OXIDE BASED COATINGS

Coatings of nickel oxide based material produced using a deposition solution reported in the literature, exhibited poor electrochromic and mechanical properties (3.1, 3.5). Voluminous precipitation of nickel hydroxide material occurs from this solution (3.5). By adjusting the solution concentration, the electrochromic and mechanical properties of coatings were improved. The optimised concentrations for unstable solutions were 0.024 M of $NiSO_4$ and 0.024M NH_4OH. Unfortunately, these coatings exhibited residual colouration and poor mechanical properties. The solar transmittances for the bleached and coloured states were 0.30 and 0.70 respectively.

The key problem identified in the first stage of the experimental was the voluminous precipitation of nickel hydroxide. This obviously had an effect on the electrochromic properties of the as-deposited coatings. For this reason, an experiment was conducted where no electric field was applied to the TCO. Colloidal precipitation occurred on to the TCO (and everything else in contact with the solution). It was found that these coatings were electrochromic. At this stage it was apparent that some precipitation was necessary to produce electrochromic coatings. However, it was also reasoned that if the precipitation could be controlled then coatings with different, perhaps superior properties, could be fabricated. Precipitation was controlled by using the non-ionogenic detergent polyoxyethylene sorbitan monolaurate, although the use of a buffer may have the same effect. The optimised solar transmittances in the bleached and coloured states were 0.82 to 0.22 respectively. These coatings were deposited from solutions that contained 0.024 M of $NiSO_4$ and 0.072 M of NH_4OH.

Using FTIR spectrophotometry, ß-nickel hydroxide was detected in the bleached state of all coatings deposited by anodic deposition. In the coloured

state, the NiO stretch of NiOOH was observed. Using Raman analysis, γ-NiOOH was detected in the coloured state of coatings produced from stable solutions. XRD of anodically deposited coatings did not reveal the presence of (α,β)-nickel hydroxide or nickel oxide in the bleached state. Finally, (β,γ)-nickel oxyhydroxide was not detected in the coloured state.

The colouration efficiency of optimised coatings deposited from stable solutions was 29 $cm^2\ C^{-1}$. For optimised coatings deposited from unstable solutions the value was 25 $cm^2\ C^{-1}$. These values are superior to the colouration efficiency of 14 $cm^2\ C^{-1}$ obtained for coatings produced from solutions reported in the literature (3.1).

Finally, the shelf life of stabilised solutions was longer than that of unstable solutions (see figures 3.23 and 3.24). The maximum precipitation free time achieved was 24 hours. Solutions with greater stabilities can be prepared but the deposition time to produce coatings with large dynamic ranges increases.

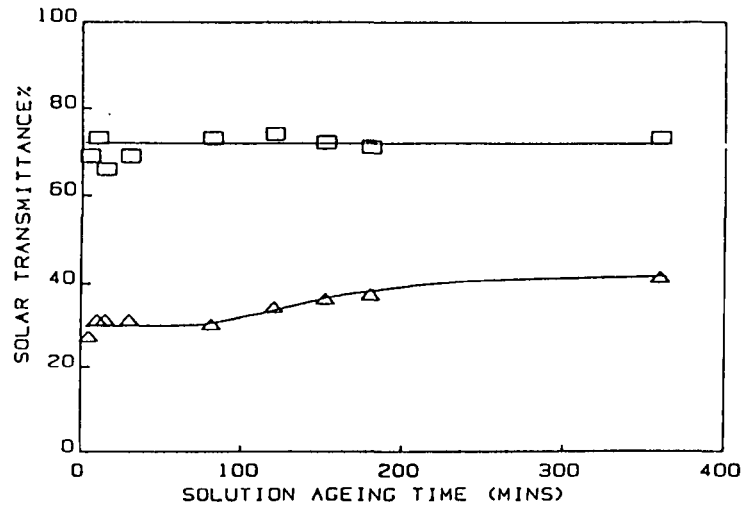

Figure 3.23 The influence of solution ageing time on the solar optical properties of the bleached and coloured states (voltages -500 mV and +750 mV). Deposition solution concentrations were 0.1 M of $NiSO_4$ and NH_4OH. The deposition time was 15 minutes and the scan rate was 20 mVs^{-1}. Electric field was applied prior to substrate immersion (τ_s bleached = □; τ_s coloured = Δ). These curves and lines are only a visual aid to the eye.

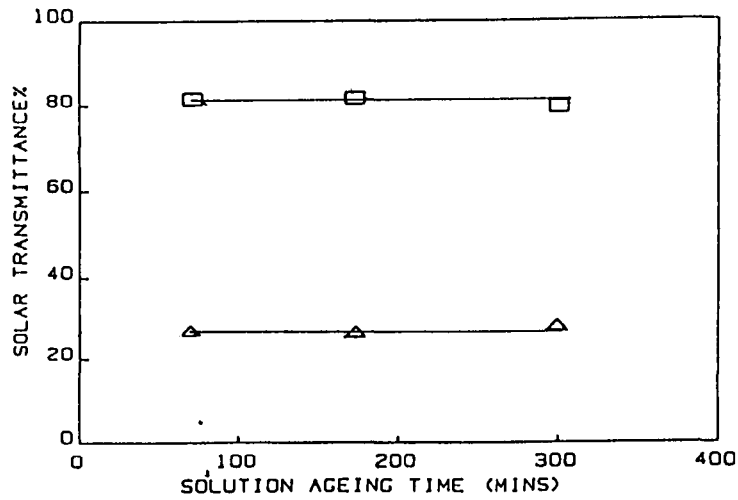

Figure 3.24 Solar optical properties of coatings deposited using a 60 minute deposition time from stabilised solution as a function of time. Deposition solution containing 0.016 M of $NiSO_4$, 0.073 M of NH_4OH and 40% polyoxyethylene sorbitan monolaurate (τ_s bleached = □; τ_s coloured = Δ). Line drawn as a visual aid to the eye only.

3.5 REFERENCES

3.1 Lampert, C.M., Omstead, T.R. and Yu, P.C., Solar Energy Materials 14 1986 161.

3.2 Marshall, J.K. and Kitchener, J.A., J. Colloid and Interface Sci. 22 1966 569.

3.3 Shaw, J., (1980) Introduction to Colloid and Surface Chemistry (3rd edn.). London, Butterworths, 199.

3.4 Shaw, J., (1980) Introduction to Colloid and Surface Chemistry (3rd edn.). London, Butterworths, 183.

3.5 Hutchins, M.G., McMeeking, G.D. and Orel, Z., Optical Materials Technology for Energy Efficiency and Solar Energy Conversion XI: Chromogenics for Smart Windows SPIE **1728** 1992 66.

3.6 Bagchi, P., Journal of Colloid and Interface Science, **47** 1974 86.

3.7 Moriyama, N., Journal of Colloid and Interface Science, 52 1975 303.

3.8 Shaw, J., (1980) Introduction to Colloid and Surface Chemistry (3rd edn.). London, Butterworths, 207.

3.9 Shaw, J., (1980) Introduction to Colloid and Surface Chemistry (3rd edn.). London, Butterworths, 11.

3.10 Johnston, C., Graves, P.R., Applied Spectroscopy, **44** 1990 105.

3.11 Delichere, P., Joiret, S. and Hugot-le Goff, A., Optical Materials Technology for Energy Efficiency and Solar Energy Conversion SPIE VII 1016 1988 165.

3.12 Desilvestro, J., Dennis, A. and Weaver, M.J., Journal of Physical Chemistry 90 1986 6408.

3.13 Nazri, G., Corrigan, D.A. and Maheswari, Langmuir 3 1987 17.

3.14 Lampert, C.M. (1990), in Lampert, C.M., and Granqvist, C.G. (eds.), Large-Area Chromogenics: Materials and Devices for Transmittance Control (1st Edn.). Bellingham, Washington, U.S.A., SPIE Press IS4 414.

3.15 Moriyama, N., Journal of Colloid and Interface Science 50 1975 80.

3.16 Nicholls D. (1974), Complexes and First - Row Transition Elements (3rd ed.). London, MacMillan, 194.

3.17 Graves, P.R., Harwell Research Laboratory Oxfordshire, private communication 1992.

3.18 Cronan, C.L., Micale, F.J., Topic, M., Leidheiser, H., Zettlemoyer, A.C. and Popovic, S., Journal of Colloid and Interface Science 55 1976 546.

3.19 Tewari, P.H., and Campbell, A.B., Journal of Colloid and Interface Science 55 1976 531.

3.20 Hutchins, M.G. and McMeeking, G.D., Making Electrochromic films Patent No. 90 27 608.0 1990 (European patent no. 91311905.3).

3.21 Kober, F.P., J. Electrochem. Soc., 114 1967 215.

CHAPTER 4

COLLOIDAL PRECIPITATION OF NICKEL OXIDE BASED MATERIAL

CHAPTER 4

COLLOIDAL PRECIPITATION OF NICKEL OXIDE BASED MATERIAL

4.1 INTRODUCTION

The fabrication of multilayer electrochromic devices is costly, therefore, low cost routes for the manufacture of such systems have become the focus of attention in electrochromic research (4.1). A one-dip process for producing nickel hydroxide coatings would be cost-effective. Several techniques have been reported that can be used to deposit nickel oxide or materials that can be converted to nickel oxide by the application of heat (to burn off organic materials) followed by electrochemical cycling to convert the as-deposited material to nickel hydroxide are reported in the literature (4.2-4.4). The deposition of nickel hydroxide by colloidal precipitation using a one-step process from a solution containing $NiSO_4$ and NH_4OH is discussed in this study.

This study was carried out in order:

(i) to establish whether the deposition of nickel oxide based material occurred without a potential difference applied across the substrate and counter electrode,

(ii) to determine the effect of colloidal precipitation on anodic electrodeposition, and

(iii) to identify the mechanism of electrodeposition.

4.2 EXPERIMENTAL

Films of nickel oxide based material were deposited on to indium doped tin oxide substrates from unstable solutions containing nickel sulphate and ammonium hydroxide. Substrates were cleaned for 15 minutes in 10% by volume of Decon (alkaline, nonionic and anionic surfactant) in an ultrasonic bath. The substrates were then washed thoroughly with distilled water and dried at 25°C. The solution volume was 250 cm^3. All solutions were stirred for 5 minutes before deposition. The temperature during deposition varied between 18°C to 25°C. It was found that variations of temperature within this range did not critically affect film properties. Deposition was achieved by simple immersion of the indium tin oxide coated substrates into deposition solutions as shown in plate 4.1.

First of all films were deposited from rapidly precipitating solutions containing 0.050 M nickel sulphate and 0.100 M ammonium hydroxide. These concentrations were chosen according to the ratios indicated in equation 4.1.

$$NiSO_4 + 2NH_4OH \rightharpoonup Ni(OH)_2 + (NH_4)_2SO_4 \qquad 4.1$$

The deposition time selected was 15 minutes. Coatings of nickel oxide based material were produced by increasing the deposition time. However, these coatings were mechanically unstable to electrochemical cycling.

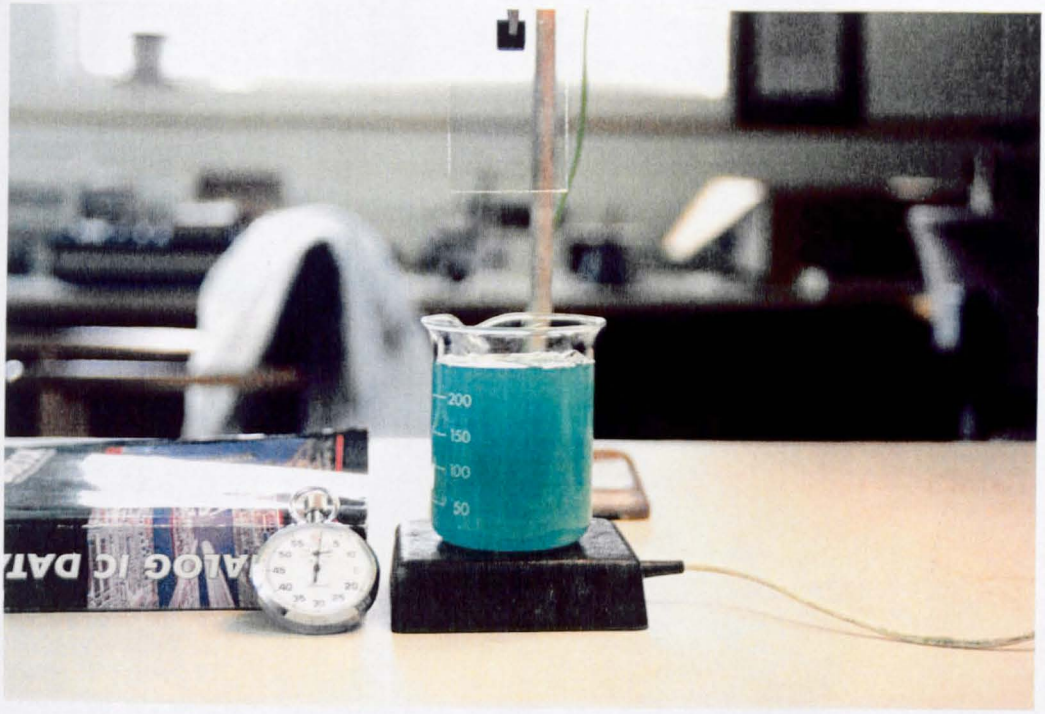

Plate 4.1 Technique for deposition by colloidal precipitation from unstable solutions.

Plate 4.2 Beaker previously containing deposition solution oxidised using sodium hypochlorite (45 seconds).

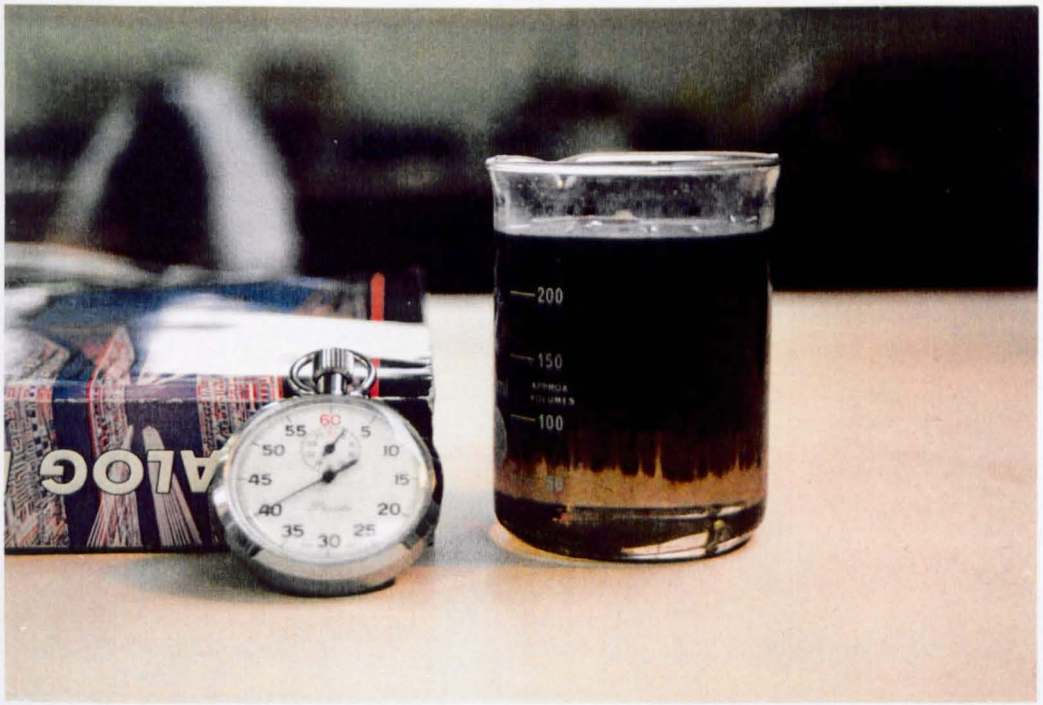

Plate 4.3 Beaker previously containing deposition solution oxidised using a sodium hypochlorite solution after 2 minutes 40 seconds.

Films were deposited from aged solutions for constant deposition times and for different deposition times from identical solutions aged for 5 minutes. The precipitate from the solution was analyzed using Fourier transform infra-red spectrophotometry to establish whether the chemical identity of the precipitate was the same as the coatings.

This was followed by an experiment in which equimolar concentrations of nickel sulphate and ammonium hydroxide were used to deposit nickel oxide based films for the range 0.024 M to 0.400 M. This experiment was carried out in order to compare the optical results from this study with those obtained in the anodic electrodeposition study. A further experiment was performed to find the concentration of ammonium hydroxide at which the maximum deposition rate occurred. In this experiment the concentration of nickel sulphate was

kept constant whilst the ammonium hydroxide concentration was varied in the range 0.024 M to 0.400 M.

4.3 RESULTS FOR COLLOIDALLY PRECIPITATED FILMS

4.3.1 The effect of various deposition parameters on the electrochromic properties of nickel oxide based coatings

4.3.1.1 *Influence of solution ageing time*

The ageing of solutions containing 0.050 M $NiSO_4$ and 0.100 M NH_4OH caused a decrease in optical density as shown in figure 4.1. It can also be shown that, as the solution ages, the anti-reflection properties of the coating reduce for the bleached state (figure 4.2). Therefore, in order to produce films of similar electrochromic properties it is necessary to deposit films from solutions containing the same concentrations of $NiSO_4$ and NH_4OH and aged for identical periods of time. Alternatively, several substrates could be dipped into one solution. The thickest film (1000 A) was deposited from a solution containing 0.100 M $NiSO_4$ and 0.100 NH_4OH aged for 5 minutes (the deposition time was 15 minutes). The solar transmittance values for the coloured and bleached states were 0.43 and 0.77 respectively. Films deposited for 15 minutes exhibited excellent adhesion (films did not detach from the surface of the substrate during a 'Sellotape' test) and were mechanically stable to electrochemical cycling (< 500 cycles).

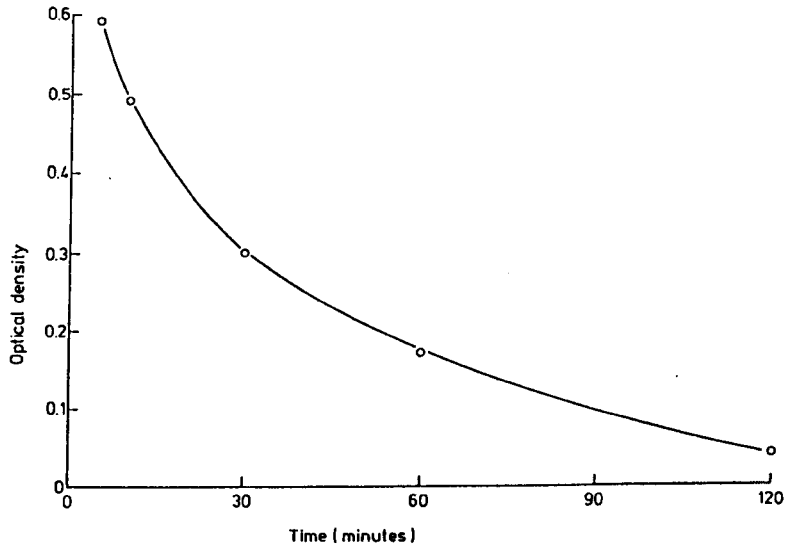

Figure 4.1 The influence of solution ageing on optical density for coatings deposited from solutions containing 0.050 M $NiSO_4$ and 0.100 M NH_4OH. The deposition time was 15 minutes. This curve is only drawn as a visual aid to the eye.

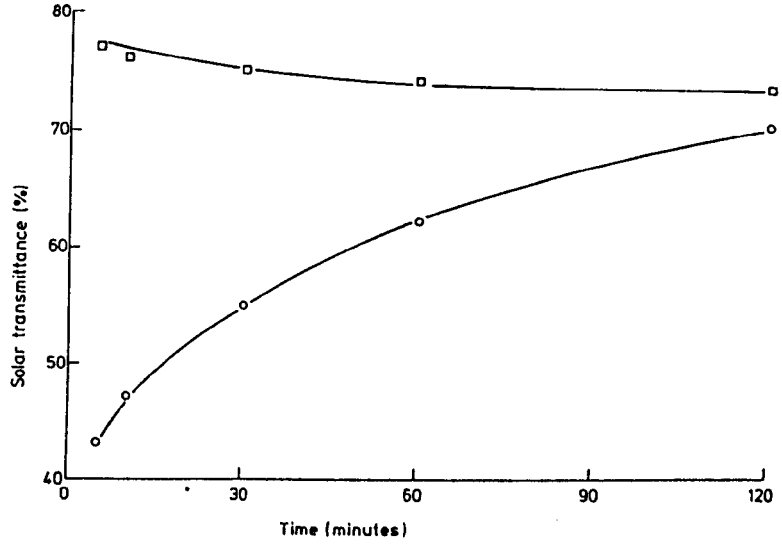

Figure 4.2 Solar transmittance for the bleached and coloured states as a function of solution ageing for films deposited from solutions containing 0.050 M $NiSO_4$ and 0.100 M NH_4OH. The deposition time was 15 minutes (τ_s bleached = □; τ_s coloured = ○). These curves are only drawn as an aid to the eye.

4.3.1.2 *Influence of deposition time*

As the deposition time increased, the coloured solar transmittance of the coatings decreased (see figure 4.3). Coating thickness was increased by extending the deposition time. This improved the solar transmittance value for the coloured state. However, the transmittance of the bleached state also decreased. This was also found for electroplated films deposited from unstable solutions. The mechanical stability of these coatings to electrochemical cycling also degenerated with respect to coating thickness. Deterioration of the mechanical properties and optical homogeneity of the films occurred after the deposition time of 15 minutes. However, films that were deposited for 120 minutes exhibited solar transmittances of 0.22 and 0.68 in the coloured and bleached states respectively. This was significantly larger than the dynamic range found for films anodically deposited from unstable solutions (see Chapter 3) although the mechanical stability of these coatings to electrochemical cycling was poor.

4.3.1.3 *Influence of equimolar concentrations of $NiSO_4$ and NH_4OH.*

The optimum concentration range for equimolar concentrations was 0.100 M nickel sulphate and ammonium hydroxide (see figure 4.4). For the coloured state the solar transmittance was 0.65 and 0.80 for the bleached state. The deposition time was 30 minutes for each sample. Since the degree of flocculation increased with respect to the increasing pH of the solution (apart from high pH when the precipitate dissolves), a further experiment was carried out to determine the effect of the pH of deposition solutions on the electrochromic properties of nickel oxide based coatings.

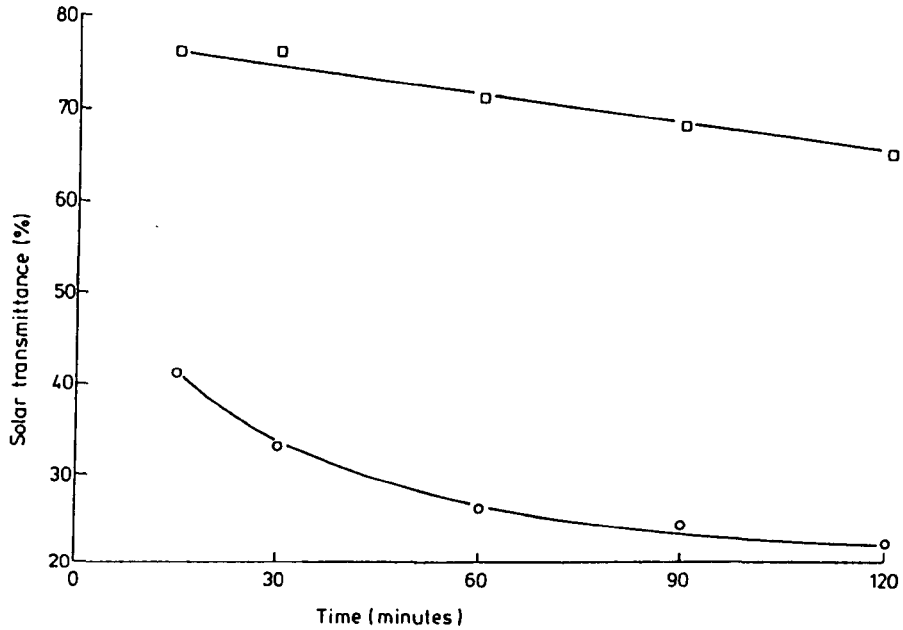

Figure 4.3 The influence of deposition time on the solar transmittance of the bleached and coloured states. Coatings were deposited from solutions containing 0.050 M $NiSO_4$ and 0.100 M NH_4OH. The deposition time was 15 minutes (τ_s bleached = □; τ_s coloured = ○). These curves and lines are only drawn as an aid to the eye.

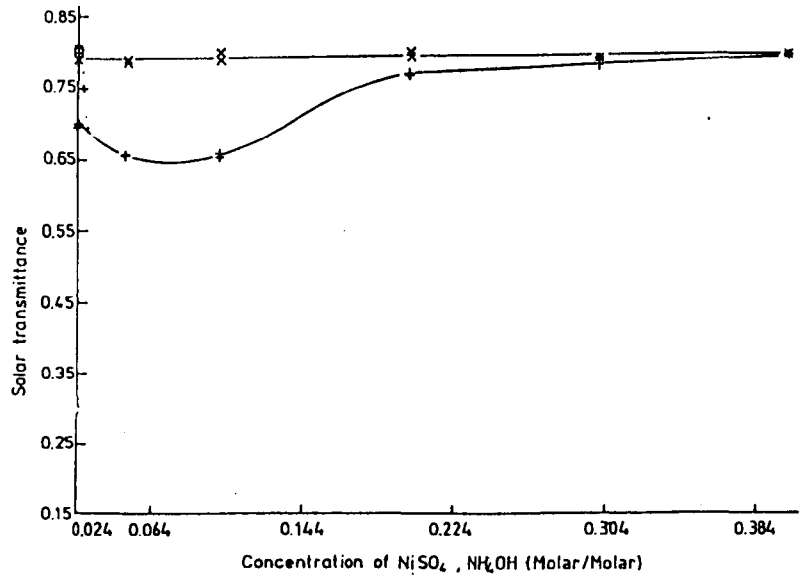

Figure 4.4 Solar transmittance values for the bleached and coloured states as a function of equimolar concentrations from solutions containing $NiSO_4$ and NH_4OH. The deposition time was 15 minutes (τ_s bleached = □; τ_s coloured = ○).These curves and lines are only drawn as an aid to the eye.

4.3.1.4 *Influence of the concentration of ammonium hydroxide*

The coloured solar transmittance of films decreased with increasing pH until a minima was reached at pH 9 (the concentration of NH_4OH was 0.192 M) as shown in figure 4.5. The solar transmittance of the coloured and bleached states was 0.48 and 0.82 respectively (see figure 4.6). This result was not entirely unexpected since to obtain the maximum yield of $Ni(OH)_2$ from reacting Ni^{2+} with OH^- according to equation 4.2, it would be necessary to react 1 mole of Ni^{2+} with 2 moles of OH^-. The pH of the solution is also important because $Ni(OH)_2$ is soluble in solutions of low and high pH. In concentrated ammonia, $Ni(OH)_2$ dissolves due to the formation of amine complexes.

$$Ni^{2}+ + 2OH^- \rightleftharpoons Ni(OH)_2 \qquad 4.2$$

4.3.1.5 *Influence of detergent concentration*

The addition of polyoxyethylene sorbitan monolaurate to solutions containing 0.050 M $NiSO_4$ and 0.100 M NH_4OH reduced the dynamic range of coatings (see figure 4.7). It was also observed that the uniformity and adhesion of coatings improved as the detergent concentration increased to 10%.

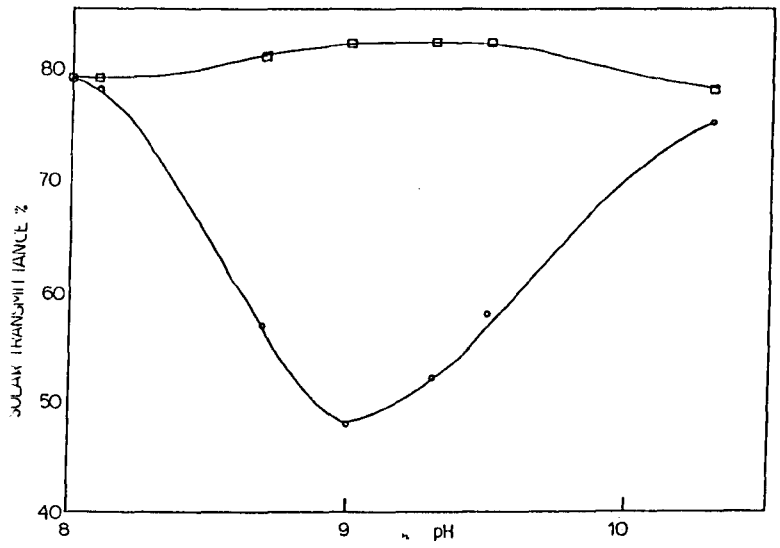

Figure 4.5 The influence of pH on the solar transmittance of the bleached and coloured states. Coatings were deposited from solutions containing 0.100 M $NiSO_4$. The concentration of NH_4OH was varied. The deposition time was 15 minutes (τ_s bleached = □; τ_s coloured = ○). These curves are only drawn as an aid to the eye.

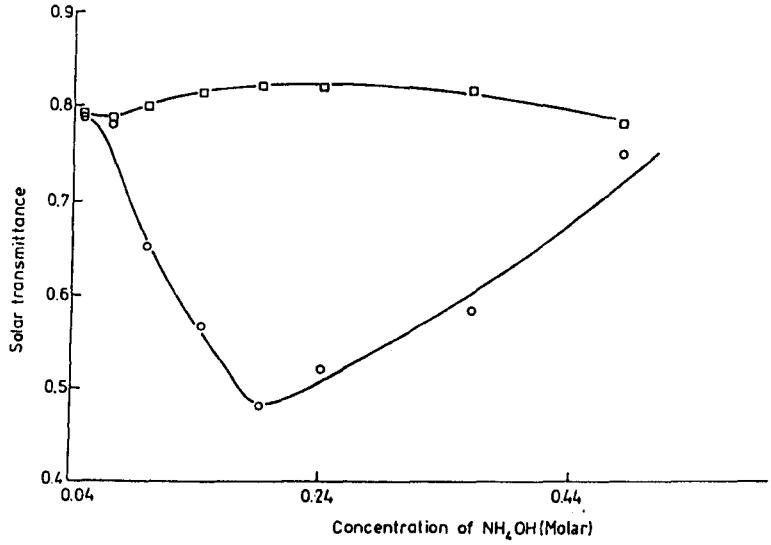

Figure 4.6 Solar transmittance for the bleached and coloured states as a function of NH_4OH concentration from solutions containing 0.100 M of $NiSO_4$. The deposition time was 15 minutes (τ_s bleached = □; τ_s coloured = ○). These curves are only drawn as an aid to the eye.

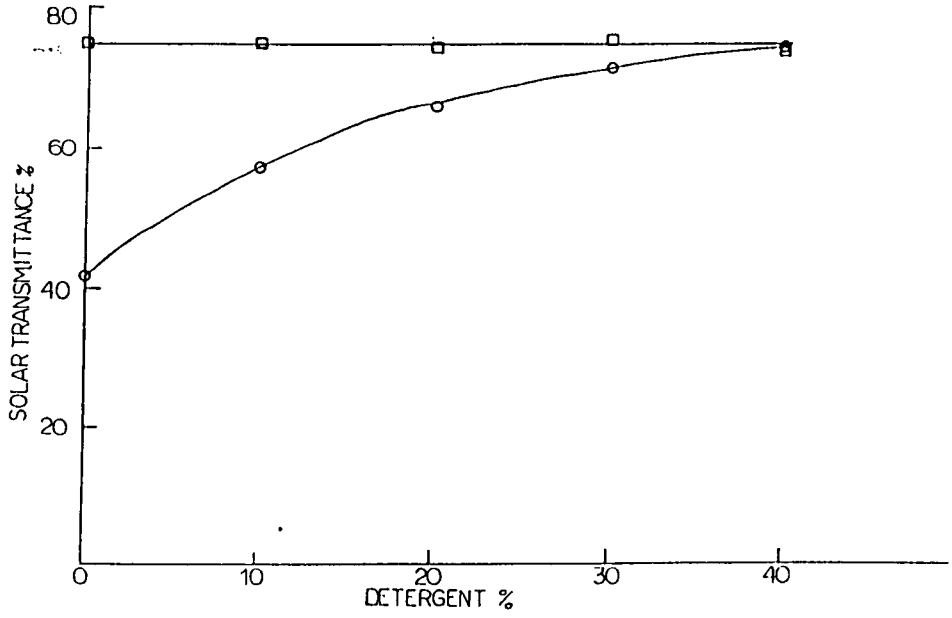

Figure 4.7 The effect of detergent concentration on the solar transmittance of the bleached and coloured states of coatings deposited from solutions containing 0.050 M of $NiSO_4$ and 0.100 M of NH_4OH. The deposition time was 15 minutes. These curves and lines are only drawn as an aid to the eye.

4.3.2 Analyses performed on colloidally deposited coatings

4.3.2.1 *Fourier transform infra-red spectrophotometry*

Fourier transform infra-red spectrophotometry was used to characterise colloidally deposited coatings in the range of 4000 cm^{-1} - 400 cm^{-1}. In the O-H stretch region, a broad band at around 3400 cm^{-1} was detected similar to that reported elsewhere (4.8). This implies that the coatings were composed of α-$Ni(OH)_2$. Therefore, the colloidally deposited material is a different phase of $Ni(OH)_2$ compared to that deposited by anodic deposition (compare figures 3.19 and 4.8).

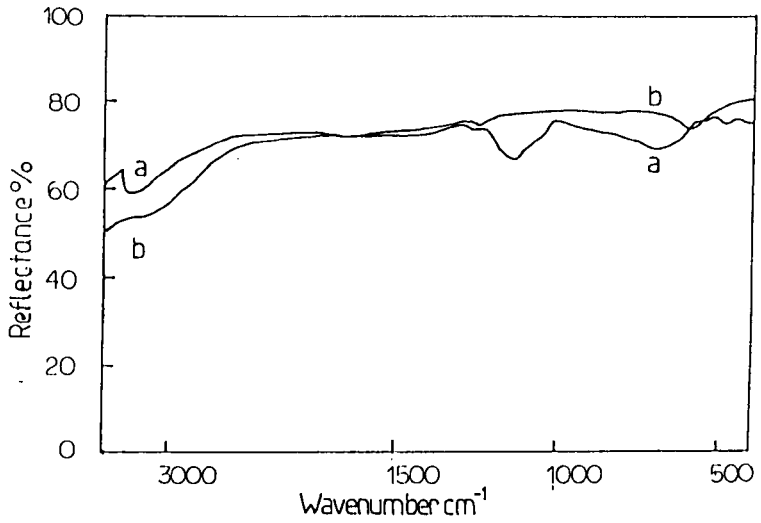

Figure 4.8 FTIR of a colloidally deposited coating: (a) in the bleached state; and, (b) in the coloured state. Coating thickness = 1400 A.

4.3.2.2 *Raman spectroscopy*

None of the phases of nickel hydroxide or nickel oxyhydroxide were detected in colloidally deposited coatings produced from stable or unstable solutions. However ß- or α-nickel hydroxide was detected in the bleached state for a crystallite on the surface of a nickel hydroxide coating deposited from a unstable solution. Peaks were located at 239, 452, 557 and 981 cm^{-1} (see figure 4.10). These peaks were not present for crystallites in the coloured state. The characteristic peaks of ß-nickel hydroxide occur at 318, 449 and 3580 cm^{-1}, whereas, for α-nickel hydroxide the peaks are 317, 451, 710, 988, 1045, 3581 and 3688 cm^{-1} (3.14). Unless the peak at 981 cm-1 corresponds to included sulphate (nitrate inclusion has been reported elsewhere (3.14)) within the precipitate, it is likely that the crystallites on the surface are composed of α-nickel hydroxide. However, α-$Ni(OH)_2$ was detected in colloidally produced coatings by FTIR spectroscopy.

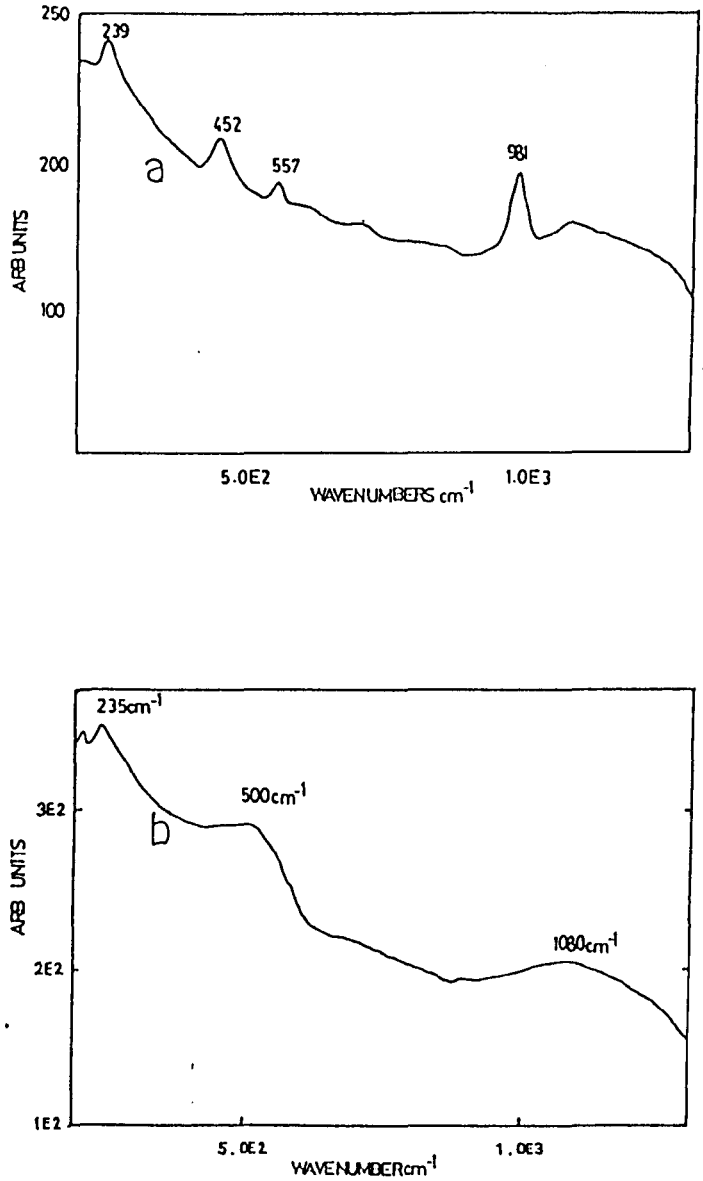

Figure 4.9 Raman spectroscopy of nickel hydroxide coatings produced by colloidal deposition: (a) in the bleached state; and, (b) in the coloured state.

4.3.2.3 *Colouration efficiency*

Coatings deposited from unstable solutions exhibited a colouration efficiency of 29 cm^2 C^{-1}. This is similar to that exhibited by coatings deposited by anodic electrodeposition and is reported in the literature for nickel oxide based coatings deposited using a variety of techniques (4.17).

4.3.2.4 *X-ray diffraction*

Films produced by colloidal deposition did not exhibit any discernable degree of crystallinity. Coatings were also produced using concentrated $Ni(NO_3)_2$ and NH_4OH. There were no discernable peaks in the X-ray spectra.

4.3.2.5 *Cyclic voltammetry*

Cyclic voltammetry of nickel hydroxide coatings deposited by colloidal precipitation was not significantly different to that of coatings deposited by anodic electrodeposition (the anodic colouration peak occured at +0.420V). This confirms that coatings deposited by colloidal deposition were similar to those deposited by anodic electrodeposition (see figure 4.10).

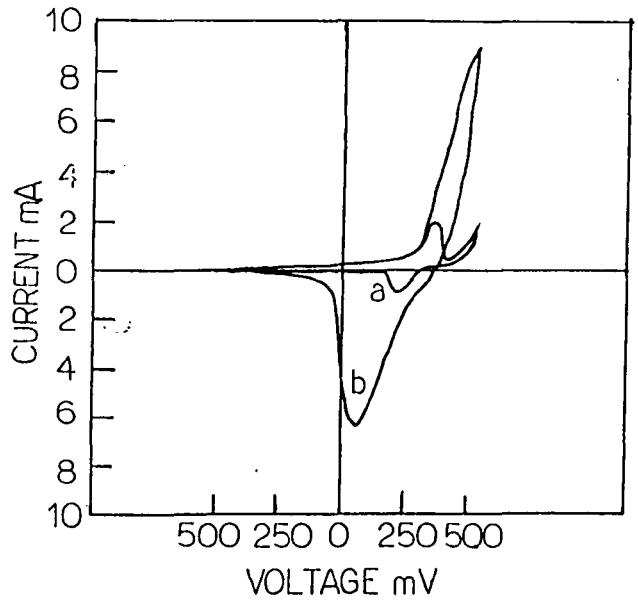

Figure 4.10 Cyclic voltammetry of a coating produced by colloidal deposition: (a) 1 mVs^{-1}; (b) 20 mVs^{-1}.

4.4 SUMMARY OF COLLOIDAL PRECIPITATION STUDY

The rate of precipitation of nickel hydroxide from solutions containing 0.100 M nickel sulphate and 0.100 M ammonium hydroxide (4.5), indicates that film growth occurs in the absence of an applied electric field (see plates 3.1, 3.2). In this study, experiments were conducted that established that colloidal precipitation occurs on to conductive substrates in the absence of an applied electric field when solutions containing 0.100 M $NiSO_4$ and 0.100 M NH_4OH are aged (4.5). Coatings were produced as a function of solution ageing time. Solution ageing time commenced when the first drop of ammonium hydroxide solution made contact with the nickel sulphate solution.

This study demonstrated that coatings of nickel hydroxide could be produced from solutions containing 0.100 M $NiSO_4$ and 0.100 M NH_4OH without the application of an electric field (4.18). Therefore, it is likely that colloidal precipitation interfered with anodic deposition (see Chapter 3). This study confirmed that coatings of nickel hydroxide can be deposited by applying a positive potential to the substrate. Using this technique the deposition rate was higher than that for colloidal precipitation. Deposition did not occur when a negative potential was applied. This may indicate that the colloidal particles in such solutions are negatively charged. It was concluded that the mode of film deposition from solutions containing 0.100 M $NiSO_4$ and 0.100 M NH_4OH was partially caused by electrophoresis when the substrate was anodised.

The most uniform and mechanically stable coatings deposited by colloidal deposition from unstable solutions exhibited a solar transmittance range of 0.41 - 0.76 for the coloured and bleached states respectively. It was not possible to deposit films with larger dynamic ranges that were mechanically stable from unstable solutions (using the concentration ranges, and reagents used in this study). However, coatings deposited from solutions containing detergents exhibited solar transmittances of 0.30 and 0.70 in the coloured and bleached states respectively (4.19).

Coatings produced from solutions containing 0.100 M nickel sulphate and 0.100 M ammonium hydroxide were analyzed using a Fourier transform spectrophotometer. A hydrogen bonded O-H stretch was found at around 3400 cm^{-1} corresponding to α-$Ni(OH)_2$. This indicates that anodic and colloidally deposited coatings were similar in that they both contained $Ni(OH)_2$ albeit of a different phase.

Essentially, the difference between α-$Ni(OH)_2$ and β-$Ni(OH)_2$ is the bonding of OH in $Ni(OH)_2$ films. α-$Ni(OH)_2$ has a turbostratic structure where parallel equidistant layers of nickel hydroxide are separated by layers of water molecules. The OH species of nickel hydroxide can hydrogen bond to interplanar water molecules. β-$Ni(OH)_2$ has a brucite structure where OH can only bond to nickel atoms (4.7).

For the coloured state a peak was detected at 564 cm-1. This was also observed for anodically deposited coatings and is further evidence that anodic and colloidal coatings were very similar.

The ultraviolet/visible/near-infra-red spectra of material deposited by colloidal precipitation was very similar to that deposited by anodic electrodeposition in both the coloured and bleached states (see figure 4.12).

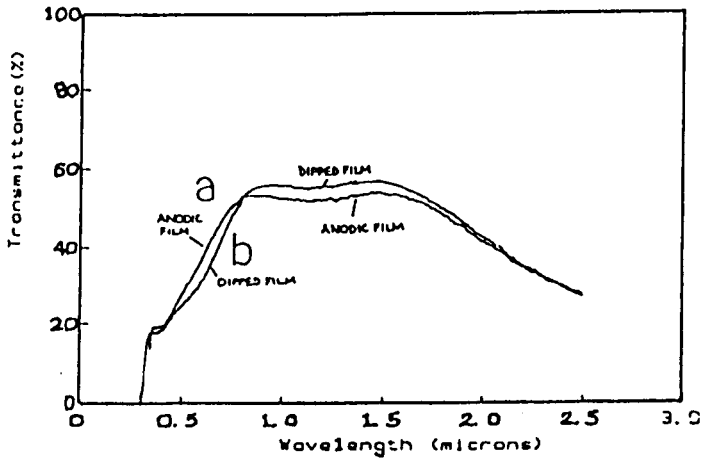

Figure 4.11 Comparison of the spectra of coatings produced in the coloured state (+750 mV for 2 minutes): (a) by anodic deposition; and, (b) by colloidal deposition (coating thickness = 1000 Å).

Raman spectroscopy revealed the presence of α- or β-$Ni(OH)_2$ in the bleached state for microcrystals on the surface of coatings. No phases of $Ni(OH)_2$ were detected in the coating itself. No phases of nickel oxyhydroxide were detected for the coloured state either in the coating or microcrystals on the surface.

X-ray diffraction studies of as-deposited and annealed coatings did not reveal the presence of any phases of nickel hydroxide. Coatings were also electrochemically oxidised to the coloured state. None of the phases of nickel oxyhydroxide were detected.

4.5 REFERENCES

4.1 Nair, P.K., Nair M.T.S., Fernandez, A., Ocampo, M., Journal of Applied Physics 22 1989 829.

4.2 Macagno, V.A., Vilche, J.R., Arvia, A.J., Journal of Electrochemical Technology 127 1980 2636.

4.3 Macagno, V.A., Vilche, J.R., Arvia, A.J., Journal of Electrochemical Technology 129 1980 301.

4.4 Lynam, L.R., Moser, F.H., Hichwa, B.P., Optical Materials Technology for Energy Efficiency and Solar Energy Conversion SPIE VI, 823 1987 130.

4.5 Lampert, C.M. (1990), in Lampert, C.M., and Granqvist, C.G. (eds.), Large-Area Chromogenics: Materials and Devices for Transmittance Control (1st Edn.). Bellingham, Washington, U.S.A., SPIE Press IS4 414.

4.6 Desilvestro, J., Corigan, D.A., Weaver, M.J., Journal of Physical Chemistry 90 1986 6408

4.7 Johnston, C., Graves, P.R., Applied Spectroscopy 44 1990 105.

4.8 Nazri, G., Corrigan, D.A., Maheswari, S.P., Langmuir 3 1987 17.

4.9 Yu, P.C., Lampert, C.M., Optical Materials Technology for Energy Efficiency and Solar Energy Conversion VI SPIE 823 1987 113.

4.10 Allen, T. (1968) Particle Size Measurement, London, Chapman and Hall.

4.11 Beyer, G.L. (1971), Physical Methods of Chemistry, London, Wiley. 125.

4.12 Jelinek, Z.K. (1974), Particle Size Analysis, London, Horwood.

4.13 Tewari, P.H., Campbell, A.B, Journal of Colloid and Interface Science 55 1976 531.

4.14 Kenney, J.T., Townsend, W.P., Emerson, J.A., Journal of Colloid and Interface Science **42** 1974 589.

4.15 Marshall, J.K., Kitchener, J.A., Journal of Colloid and Interface Science **23** 1966 342.

4.16 Shaw, J., (1980) Introduction to Colloid and Surface Chemistry (3rd edn.). London, Butterworths, 163.

4.17 Seike, T., and Nagai, J., Solar Energy Materials **22** 1991 107.

4.18 Hutchins, M.G., McMeeking, G.D., Orel, Z., Optical Materials Technology for Energy Efficiency and Solar Energy Conversion XI: Chromogenics for Smart Windows **1728** 1992 66.

4.19 Hutchins, M.G. and McMeeking, G.D., Making Electrochromic films Patent No. 90 27 608.0 1990 (European patent no. 91311905.3).

CHAPTER 5

ANALYSES PERFORMED ON R.F. SPUTTERED NICKEL OXIDE COATINGS

CHAPTER 5

ANALYSES PERFORMED ON R.F. SPUTTERED NICKEL OXIDE COATINGS

5.1 INTRODUCTION

Radio frequency (r.f.) sputtered NiO coatings (deposited at 6 x 10^{-2} T and 100 W) exhibit different electrochromic properties to coatings deposited using chemical and electrochemical methods (5.1). Specifically, the oxidised state is stable to the atmosphere, the coloured state is grey, and in the as-deposited state (prior to cycling in 1M KOH) there is no evidence for hydrogen bonded or free O-H (5.2). However, after cycling in 1M KOH it was found that there were many similarities between r.f. sputtered coatings and electrochemically prepared nickel hydroxide electrodes.

Generally nickel oxide and nickel oxhydroxide coatings bleach when heated (5.2, 5.3). This is due to loss of oxygen from NiO_x (where $x > 1$). This leads to a reduction in the concentration of Ni^{3+} in the NiO matrix (5.3). It has been reported that NiO deposited by a variety of physical vapour deposition (P.V.D.) processes can be transformed to ß-$Ni(OH)_2$ when electrochemically cycled in 1 M KOH (5.4, 5.5). This transformation is usually accompanied by a simultaneous improvement in the electrochemical and electrochromic response (5.4). Furthermore, changes in the colour of the oxidised state of sputtered NiO (neutral to coloured), are clearly evident in the visible spectra presented by some researchers (5.2, 5.4).

5.2 EXPERIMENTAL

5.2.1 Cycling of r.f. sputtered NiO coatings in 1M KOH

Coatings of 'grey' nickel oxide, previously deposited at Oxford Brookes University, were analyzed using ultraviolet/visible/near-infra-red spectrophotometry, cyclic voltammetry, FTIR spectroscopy, XRD and Raman spectroscopy (5.2). Films were cycled in 1 M KOH (-1.5 - +1V and -0.5 - +0.5V). Changes were observed in voltammograms and in the FTIR spectra as reported elsewhere (5.4, 5.5). The chromaticity coordinates of r.f. sputtered coatings changed after cycling.

5.3 RESULTS OF ANALYSES PERFORMED ON R.F. SPUTTERED NiO

The cyclogram of nickel oxide deposited using r.f. sputtering changed with respect to the number of cycles in 1 M KOH. Specifically, the magnitudes of the anodic and cathodic peaks altered upon cycling (see figures 5.1 and 5.2), Also, an anodic peak was identified at 420 mV (see figure 5.3) as was found for anodically and colloidally deposited coatings. Modifications in cyclograms were accompanied by changes in the infra-red properties of these coatings. This indicated that gradually the material was being transformed into ß-$Ni(OH)_2$ (5.4, 5.5). The free O-H stretch at 3647 cm^{-1} gradually became sharper as the sample was cycled (see figure 5.4). After 12 hours cycling, a well defined OH peak was detected at 3647 cm-1 (5.5). However, even after only one hour an OH peak could be resolved (see figure 5.3). A clear change in the chromaticity of 'grey' sputtered NiO coatings was observed when they were cycled in 1M KOH (see table 5.1). The FTIR spectra of the reduced and oxidised forms of sputtered nickel oxide were very similar to those of anodic and colloidally deposited nickel hydroxide (compare figures 3.19, 4.9 and 5.4). Specifically, after oxidation the OH peak reduced in height.

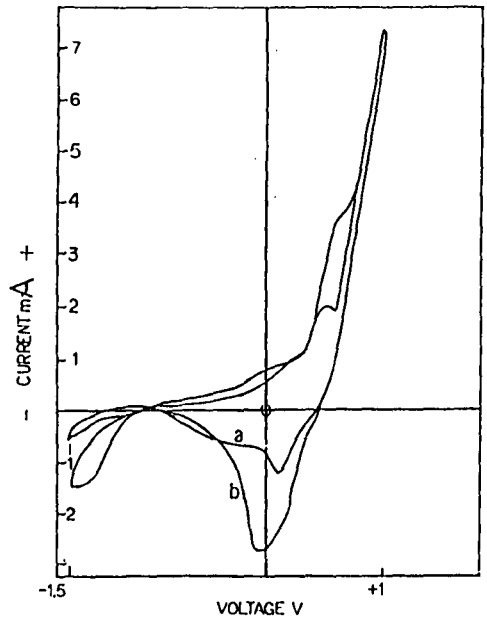

Figure 5.1 Cyclic voltammograms (-1.5V - +1.0V) of a sputtered NiO coating as a function of cycling time in 1M KOH: (a) for 1 hour; and, (b) for 12 hours.

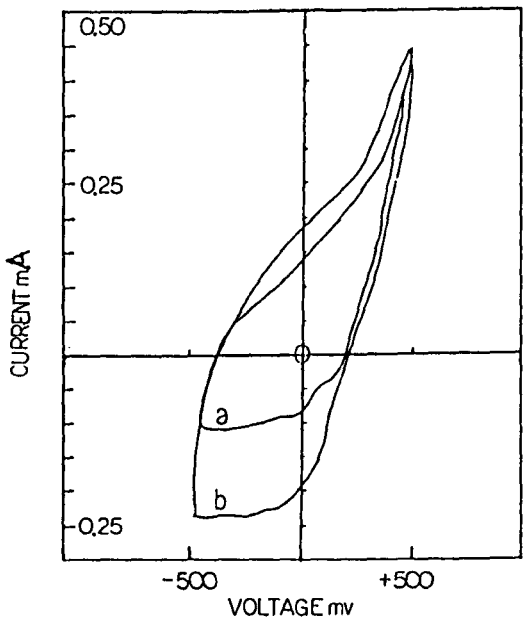

Figure 5.2 Cyclic voltammograms (-0.5V - +0.5V) of a sputtered NiO coating as a function of cycling time in 1M KOH: (a) for 1 hour; and, (b) for 12 hours.

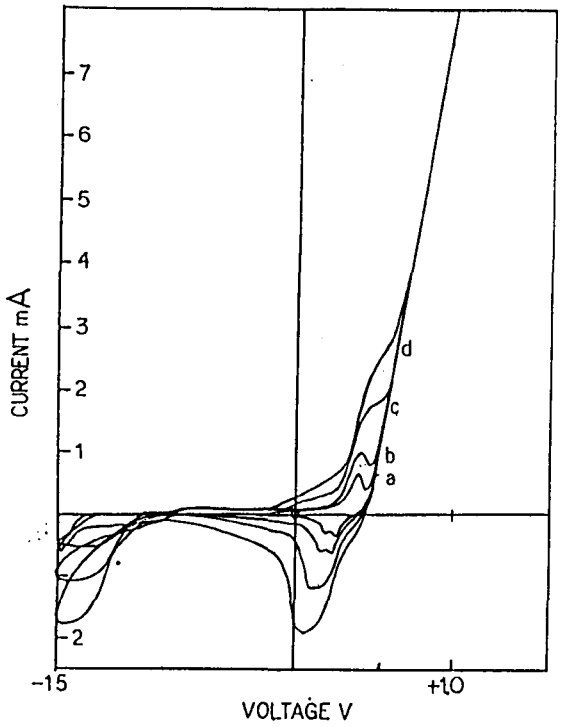

Figure 5.3 Cyclic voltammograms of a sputtered NiO coating: (a) $1mVs^{-1}$; (b) $2\ mVs^{-1}$; (c) $5\ mVs^{-1}$; and, (d) $10\ mVs^{-1}$.

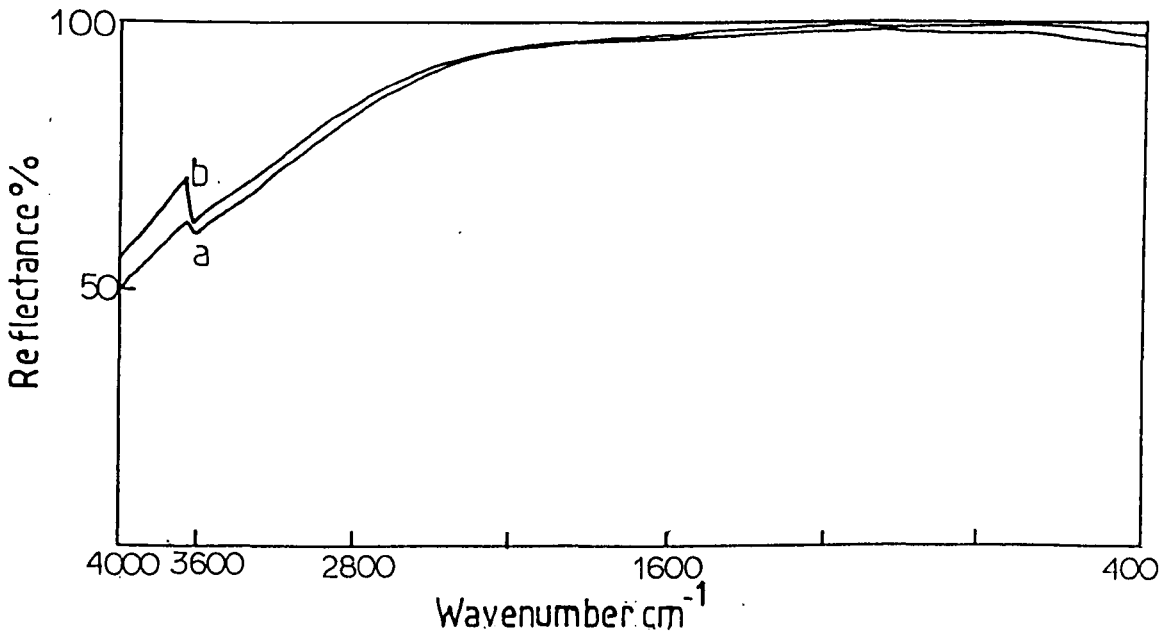

Figure 5.4 Infra-red reflectance of a sputtered coating (high pressure, 6.00×10^{-2} T and low r.f. power, 100W) as a function of cycling time: (a) for 1 hour; and, (b) for 12 hours.

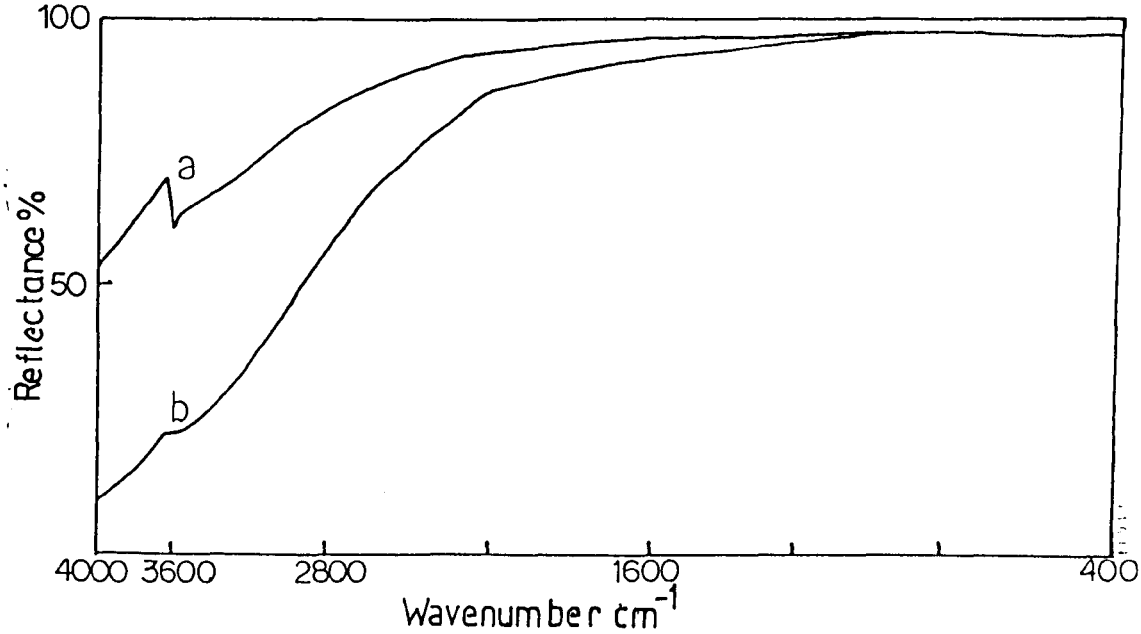

Figure 5.5 Infra-red reflectance as a function of colouration voltage: (a) -1.5 V; and, (b) +1 V.

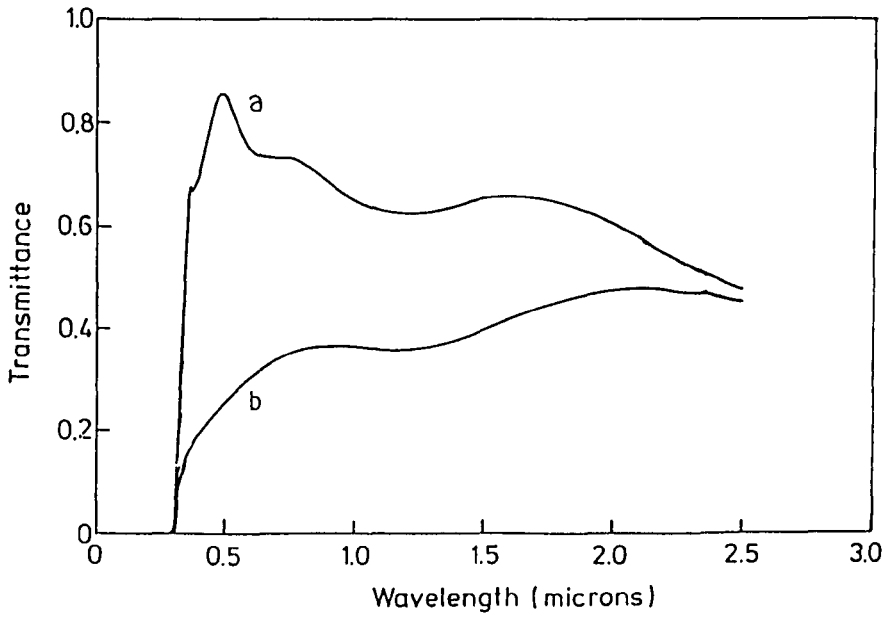

Figure 5.6 Ultraviolet/visible/near-infra-red transmittance as a function of wavelength: (a) in the bleached state; and, (b) in the coloured state.

XRD analyses revealed that the coatings were amorphous in the as-deposited, cycled, coloured and bleached states. Unfortunately, this form of NiO was not Raman active so no peaks were detected. The colouration efficiency was 31 cm^2 C^{-1}, this was measured after 1 hour cycling in 1 M KOH. The Ultraviolet /visible/near-infra-red spectra of sputtered NiO (figure 5.5) were very similar to that reported elsewhere (5.4).

Table 5.1 Chromaticity coordinates x, y and z, for r.f. sputtered film (500 A in the as-deposited, bleached and coloured states (uncorrected for substrate influence).

NiO condition	x	y	z
As-deposited	0.32	0.33	0.35
Bleached	0.30	0.31	0.39
Coloured (after 1 hour cycling)	0.32	0.33	0.35
Coloured (after 12 hours cycling)	0.37	0.33	0.30

5.4 SUMMARY OF R.F. SPUTTERED NICKEL OXIDE ANALYSES

Various analyses were performed on sputtered NiO coatings. These were FTIR, cyclic voltammetry, chromaticity measurements, XRD, Raman and colouration efficiency and ultraviolet/visible/near-infra-red spectrophotometry. It can be deduced from these results that there is a change in the chemical composition of r.f. sputtered NiO during cycling in 1 M KOH, as reported elsewhere (5.4, 5.5). Unfortunately, infra-red measurements could not be supported by the appropriate Raman activity. As was the case in colloidal and anodic electrodeposition, nothing was detected using XRD, indicating that r.f. sputtered coatings had a low degree of crystallinity.

5.5 REFERENCES

5.1 Hutchins, M.G. and McMeeking G.D., Orel Z.C., Optical Materials Technology for Energy Efficiency and Solar Energy Conversion XI: Chromogenics for Smart Windows **1728** 1992 66.

5.2 Hutchins, M.G. and McMeeking, G.D., Xingfang, H., Optical Materials for Solar Energy Efficiency and Solar Energy Conversion SPIE IX. **1272** 1990 139.

5.3 McEwen, R.S., Journal of Physical Chemistry **75** 12 1971 1782.

5.4 Connel, R.S., Corrigan, D.A., and Powell, B.R., Solar Energy Materials and Solar Cells **25** 1992 301.

5.5 Lynam, N.R. and Habibi, H.R., Optical Materials Technology for Energy Efficiency and Solar Energy Conversion SPIE VII. **1016** 1988 63.

CHAPTER 6

ELECTROCHROMIC DEVICES CONTAINING NICKEL OXIDE AND NICKEL HYDROXIDE ELECTRODES

6.1 INTRODUCTION

Solid state electrochromic window (ECW) technology is being intensively researched by leading glass companies such as Asahi Glass (6.1, 6.11). These systems may reduce heating and cooling costs (6.2). This is a major selling point of double glazing and other advanced glazing products. However, other characteristics of ECW technology could be more appealing to potential customers such as privacy, shading (from glare), protection of furnishings from photochemical processes, and novelty value. In order for ECW devices to become products rather than just a research interest, it will be necessary to solve fundamental materials problems, such as, fracturing of component coatings, chemical and physical incompatibility of coatings, degradation of optical response and fatigue reactions.

The major goal of research on electrochromic materials, such as, nickel oxide and tungsten trioxide, is the fabrication of all-solid state devices (6.3). However, these materials are unstable to electrochemical cycling (6.5). During electrochemical oxidation and reduction NiO and WO_3 undergo film dissolution and delamination (6.5). This leads to a reduction in electrochromic activity (6.5). It is likely that the modes of degradation in solid state devices are similar to those observed in coatings of NiO and WO_3. Nickel oxide is a ceramic material and as such exhibits good mechanical properties under compression but poor mechanical properties under tension (low fracture strength) (6.4).

Fracturing of NiO, which leads to delamination from the transparent conductor, is reported in the literature (6.5). Stress due to ion insertion also occurs in tungsten trioxide, but can be reduced by using comparatively small cations such as Li^+ (6.6). Delamination of electrodes must lead to poorer transfer of charge between electrochromic materials and conductive substrates (6.5).

It is evident from the spectra of solid state devices that the majority use electrolytes that contain water (6.5). Water contains the ions necessary for the colouration of WO_3 and NiO (H^+ and OH^- respectively). Hence other modes of degradation may be the loss of water from the electrolyte by absorption into sealant compounds. Another may be removal of water from the electrochromic materials by the electrolyte.

The devices constructed in this study were rudimentary, but exhibited reversible electrochromism. They consisted of combinations of electrochromic materials and electrolytes. The best devices were capable of being cycled about 100 times (between the fully coloured and bleached states) before the coating ceased to exhibit reversible electrochromism. All devices constructed in this study failed in the coloured state. The mode of failure appeared to be due to fracture and delamination of the electrochromic materials. This chapter describes the experimental details for the construction of electrochromic devices that contained $Ni(OH)_2$, NiO, MnO, and organic polymeric electrolyte coatings.

6.2 EXPERIMENTAL

6.2.1 Electrochromic coating preparation

Nickel hydroxide and nickel oxide coatings were deposited using the techniques described in Chapters 3 and 5. The active electrochromic area used in all devices was 50 x 50 mm^2. As described in the literature, counter electrode materials such as MnO were prepared using anodic deposition (6.7). Deposition of MnO was achieved by cycling ITO coated glass substrates between the potentials of -500 mV to +800 mV at 20 mVs^{-1} in solutions containing 0.1 M $MnSO_4$ and 0.1 M NH_4OH. The thickness of the coating was dependent on the number of electrochemical cycles. It was difficult to prepare homogenous electrodes of MnO using the technique reported in the literature (6.11), because coatings fractured during cleaning (with distilled water after deposition). More stable coatings were deposited from solutions containing a detergent (polyoxyethylene sorbitan monolaurate). Even using the modified technique, coatings of MnO were prone to failure after a few cycles (usually a maximum of 20 cycles in 1 M KOH). R.f. sputtered coatings were prepared using the optimised parameters discussed in Chapter 5. Anodically-deposited coatings were produced from solutions that contained 0.024 M of $NiSO_4$ and 0.072 M of NH_4OH with 40% by mass of polyoxyethylene sorbitan monolaurate. The scanning rate used on the potentiostat was 20 mVs^{-1} and the deposition potentials were -500 mV and +1500 mV. The deposition time was 1 hour.

Devices containing colloidally produced material were not fabricated, because colloidally deposited coatings exhibited low durability.

6.2.2 Electrolyte preparation

There are two types of solid state electrolytes: inorganic and organic. The focus of attention in the field of inorganic electrolytes is Ta_2O_5 (6.8). This material can be made by a variety of deposition processes (6.8). The most widely studied polymeric electrolyte is polyethylene oxide (6.9). Polymeric electrolytes can be prepared by using several techniques. These involve solvent casting or polymerisation of the monomer by the application of heat or ultraviolet radiation. Solvent casting was chosen in this study because it was the simplest technique.

Polymeric electrolytes were prepared from solutions containing various polymers and ionic species. These included gelatin, polyvinyl alcohol, polyvinyl acetate and amberlite resin (an ion exchange resin used in chromatography). These polymers were host materials which have the ability to retain water and ionic species such as tertiary amines and quaternary aromatic amines. Amines were chosen because of the high pH that such bases exhibit in solution (up to pH 12). An electrolyte with a high pH is suitable for NiO because NiOOH is stable in alkaline media (6.5). Also from the literature OH^- may be involved in the colouration mechanism (6.5). Acidic electrolytes are not suitable for $Ni(OH)_2$ and NiO, because both are soluble in these solutions. To achieve a high pH with alkyl amines, molecules with longer chain lengths are required because the +I effect increases with chain length (6.10). An increasing +I, has the effect of pushing out the electron density of the lone pair on the nitrogen atom of the amine group, making the amine more basic (6.10). However, increasing the length of the alkyl chain also makes the amine more insoluble (in H_2O). Primary and secondary alkyl amines were not investigated because of the long chain lengths that are required to achieve the same pH as tertiary

and aromatic quaternary amines. This leads to the selection of tertiary alkyl and aromatic amines. Unfortunately quaternary ammonium hydroxides were thermally unstable (< 60 °C). Water soluble polymers such as polyvinylalcohol (average molecular weight 14000) were selected because of the water content of the polymer and the affinity of the polymer for water. Tertiary amine bases were dissolved in solvated (H_2O) polyvinylalcohol. The amine increased the pH of the electrolyte. Ion exchange media, commonly used in chromatography was used as an electrolyte. The form of this material (coloured amberlite spheres of diameter 0.05 mm), was not suitable for optical transparency. Chromatography resins such as amberlite are insoluble in most solvents, so it was not possible to solvent-cast a coating of amberlite. However, further research should be conducted on ion exchange media such as amberlite resins. This is because such media are highly suitable for the transfer of ions in ECW devices.

The solid state electrolytes used in this study were, polyvinylalcohol, gelatin, and amines such as triethylamine and trimethylbenzylamine. Gelatin exhibited the worst cyclic stability, this may have been due to NiOOH (coloured state) oxidising the alcohol groups in the gelatin to carboxylate groups. The alcohol group in polyvinylalcohol is in a secondary alcohol environment so oxidation does not proceed to the carboxylate group. This means that the alcohol group can only feasibly be oxidised to that of a carbonyl group. It is also possible that a photochemical process occurs in gelatin electrolytes leading to the degradation of devices.

Polyvinylalcohol coatings containing amines, were made by dissolving polyvinylalcohol in distilled water. This was achieved by heating to 60°C whilst magnetically stirring a mixture of 10g of polyvinylalcohol in 100 cm^3 of

distilled water. Once the polyvinylalcohol had dissolved it was allowed to cool to room temperature before the amine (triethylamine 0.25 moles) was added and then magnetically stirred. The electrolyte layer was formed by transferring some of the polymer/amine mixture by pipette (previously warmed to prevent solidification of the mixture in the pipette) to the surface of a nickel oxide or nickel hydroxide coating. A spacer consisting of a 60 μm polytetrafluoroethylene (PTFE) tape was used to separate the NiO based coating from the counter electrode that was either MnO coated ITO or ITO. Once the NiO based coating was covered (apart from the ITO connecting terminal) with the polymer/amine mixture, the counter electrode was placed in contact with the polymer/amine electrolyte. Once the electrolyte had set rigid (usually 30 minutes) the device was electrochemically switched between the transparent and coloured states using a stabilised Farnel power supply. Colouration and bleaching times were two minutes. The colouration potential was +1.50 V and the bleaching potential was -1.00 V with all devices (damage occurs to the ITO above these potentials). The ultraviolet/visible/near-infra-red properties were measured using a Beckman 5270 spectrophotometer. The infra-red properties of these devices could not be measured due to the reflecting properties of the transparent conductors.

6.2.3 Device construction

Four types of devices were constructed. These contained:

i) ITO/anodically deposited $Ni(OH)_2$/PVA:$(C_2H_5)_3N$/ITO,

ii) ITO/R.f.sputtered NiO/PVA:$(C_2H_5)_3N$/ITO,

iii) ITO/R.f.sputtered NiO/PVA:$(C_2H_5)_3N$/MnO/ITO,

iv) ITO/R.f.sputtered NiO/PVA:$C_6H_5N^+(CH_3)_3OH$/ITO.

6.2.3.1 *ITO/Anodically deposited $Ni(OH)_2$ /PVA:$(C_2H_5)_3N$/ITO.*

In this device a sputtered coating was placed in contact with polyvinylalcohol 'doped' with triethylamine. The counter electrode used was ITO coated glass. The layer of electrolyte, determined from the PTFE spacer, was 60 μm thick.

6.2.3.2 *ITO/R.f.sputtered NiO/PVA: $(C_2H_5)_3N$/ITO.*

In this device an anodically deposited $Ni(OH)_2$ coating was placed in contact with polyvinylalcohol 'doped' with triethylamine. The counterelectrode used was ITO. The layer of electrolyte, determined from the PTFE spacer, was 60 μm thick.

6.2.3.3 *ITO/R.f.sputtered/NiO/PVA: $(C_2H_5)_3N$/MnO/ITO.*

In this device a sputtered nickel oxide coating was placed in contact with polyvinylalcohol 'doped' with triethylamine. The counterelectrode used was MnO, deposited on to ITO coated glass. The layer of electrolyte, determined from the PTFE spacer, was 60 μm thick.

6.2.3.4 *ITO/R.f.sputtered NiO/PVA: $C_6H_5N^+(CH_3)_3OH$/ITO*

In this device a r.f. sputtered NiO coating was placed in contact with polyvinylalcohol 'doped' with trimethylbenzylamine. The counterelectrode used

was ITO. The layer of electrolyte, determined from the PTFE spacer, was 60 μm thick.

6.3 RESULTS

6.3.1 Solar and visible optical properties.

The solar and visible transmittance for each device was measured in the bleached and coloured states for the first electrochemical cycle. The values are shown in table 6.1. The coloured solar transmittance was measured after the device had been coloured for two minutes at +1.5V and bleached using -1.5V.

Table 6.1 Optical properties of solid state devices

Device Structure	Composition of device	τ_{sc}	τ_{sb}	τ_{vc}	τ_{vb}
i	ITO/Anodically deposited $Ni(OH)_2$/PVA:$(C_2H_5)_3N$/ITO 60 μm thick electrolyte 2000 A thick $Ni(OH)_2$	0.43	0.53	0.53	0.70
ii	ITO/R.f.sputtered NiO/PVA:$(C_2H_5)_3N$/ITO 60 μm thick electrolyte 500 A thick NiO	0.48	0.68	0.51	0.78
iii	ITO/R.f. sputtered NiO/PVA:$(C_2H_5)_3N$/MnO/ITO 60 μm thick electrolyte 300 A thick NiO	0.43	0.53	0.48	0.61
iv	ITO/R.f. sputtered NiO/PVA:$C_6H_5N^+(CH_3)_3OH$/ITO 60 μm thick electrolyte 200 A thick NiO	0.48	0.60	0.50	0.63

Table 6.2 Chromaticity coordinates for solid state devices

Device	X_c	Y_c	Z_c	X_b	Y_b	Z_b
i	0.336	0.346	0.318	0.320	0.334	0.346
ii	0.323	0.337	0.340	0.309	0.323	0.368
iii	0.331	0.340	0.329	0.331	0.340	0.329
iv	0.325	0.335	0.340	0.310	0.322	0.368

6.3.2 Summary of results

All of the solid state devices made in this study exhibited reversible electrochromism. However, the dynamic range of some of the devices was greater than others. The highest bleached solar transmittance obtained was 0.68. This device used ITO as a counter electrode. However, the kinetics of this system were slow. The device that used MnO as a counter electrode exhibited faster kinetics. Although colouration and bleaching (for a 50 x 50 mm^2 device) was faster in devices that contained MnO, the overall dynamic range reduced due to MnO exhibiting a yellow colouration (since MnO is an anodic material) upon bleaching of the NiO. Cell (ii) (table 6.1) exhibited the best dynamic range for solar and visible transmittance Degradation occurred in most of the devices after 100 cycles. However, cell (iv) (table 6.1) showed superior durability. Although this device was cycled considerably more times than other devices (200 times), nonreversible browning of the ITO counter electrode occurred indicating that this type of cell structure is not suitable for advanced glazing applications. The cell shown in (iv) (table 6.1) contained an electrode of r.f. sputtered NiO that was only 200 A thick. To obtain a superior optical density a thicker coating would be necessary. Devices that contained NiO and $Ni(OH)_2$ coatings exhibited similar durabilities. However, the device with the largest dynamic range contained r.f. sputtered NiO.

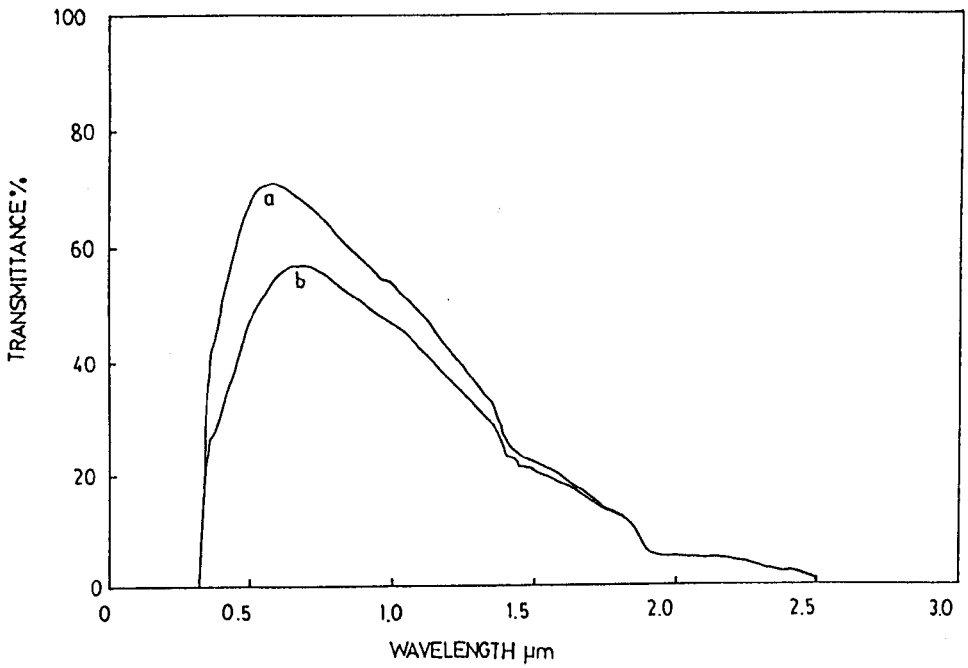

Figure 6.1 (i)ITO/Anodically deposited $Ni(OH)_2$ /PVA:$(C_2H_5)_3N$/ITO.(a) bleached state; and (b) coloured state.

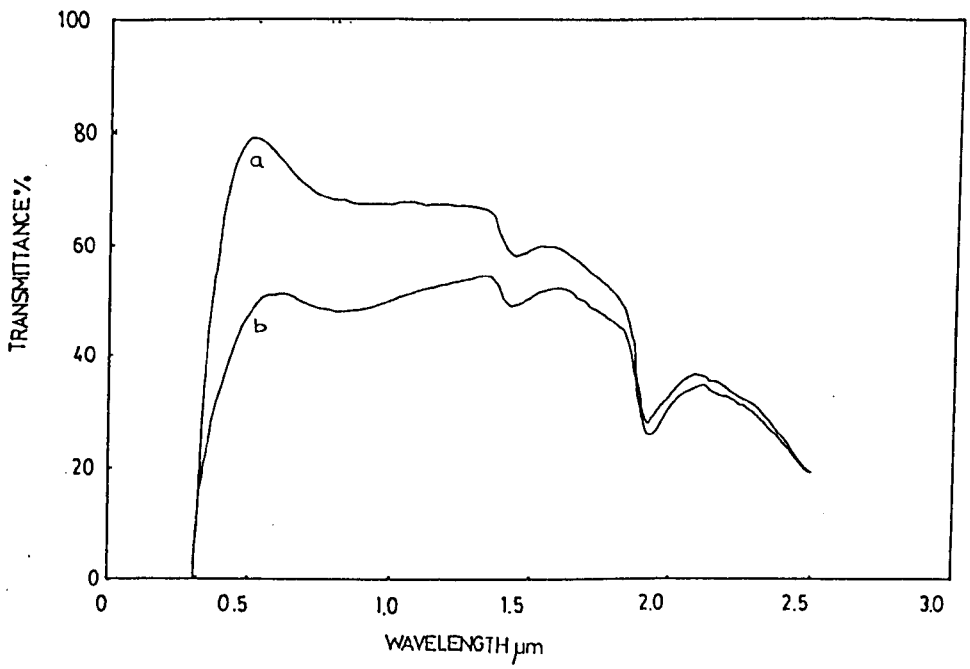

Figure 6.2 (ii) ITO/R.f.sputtered NiO/PVA: $(C_2H_5)_3N$/ITO: (a) bleached state; and, (b) coloured state.

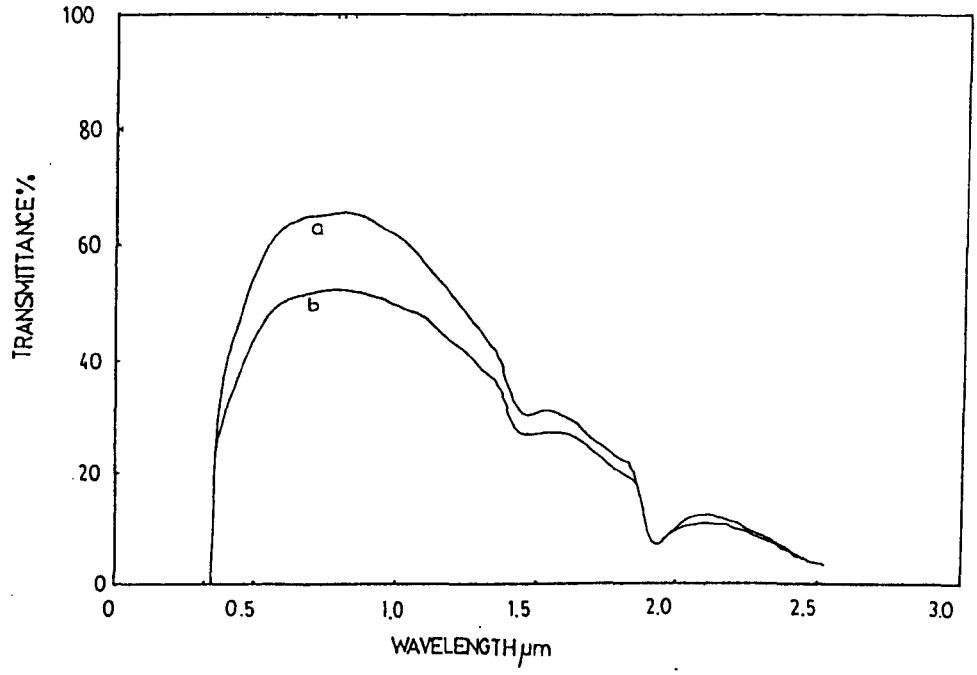

Figure 6.3 (iii) ITO/R.f. sputtered/NiO/PVA:$(C_2H_5)_3N$/MnO/ITO: (a) bleached state; and, (b) coloured state.

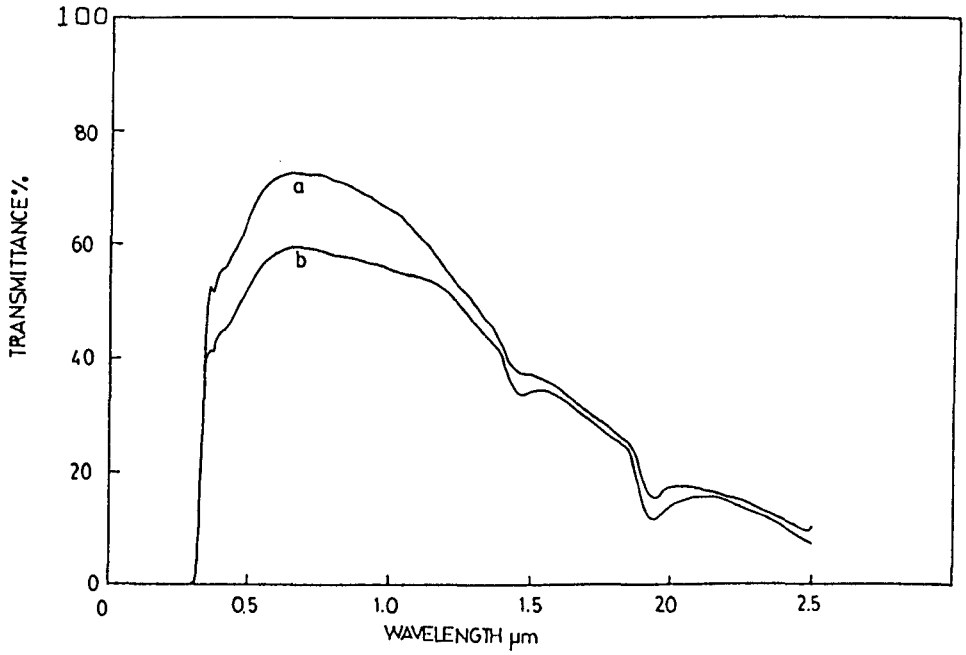

Figure 6.4 (iv)ITO/R.f.Sputtered NiO/PVA:$C_6H_5N^+(CH_3)_3OH$/ITO (a) bleached state; and, (b) coloured state.

6.4 REFERENCES

6.1 Selkowitz, S.E. and Lampert, C.M. (1990), in Lampert, C.M., and Granqvist, C.G. (eds.), Large-Area Chromogenics: Materials and Devices for Transmittance Control (1st Edn.). Bellingham, Washington, U.S.A., SPIE Press IS4 22.

6.2 Reilly, S., Daruish, A. and Selkowitz, S.E., Solar Energy Materials 22 1991 1.

6.3 Deb, S.K., Materials and Optics for Solar Energy Conversion and Advanced Lighting Technology SPIE 692 1986 19.

6.4 Van Vlack, L.H. (1985), Elements of Materials Science and Engineering (5th edn.), Addison-Wesley Reading, Massachusetts, 268.

6.5 Lampert C.M. (1990), in Lampert, C.M., and Granqvist, C.G. (eds.), Large-Area Chromogenics: Materials and Devices for Transmittance Control (1st Edn.). Bellingham, Washington, U.S.A., SPIE Press 414.

6.6 Falaras, P., et.al. (1990), in Lampert, C.M., and Granqvist, C.G. (eds.), Large-Area Chromogenics: Materials and Devices for Transmittance Control (1st Edn.). Bellingham, Washington, U.S.A., SPIE Press IS4 447.

6.7 Lampert, C.M., Ma, Y.P., Pennisi, A., and Simone, F., Electrical and Optical Properties of Electrochromic devices utilizing solid state polymers., Government report., U.S. departments of Energy., Contract no. DE-AC03-76SF00098.

6.8 Troung, V., et.al. (1990), in Lampert, C.M., and Granqvist, C.G. (eds.), Large-Area Chromogenics: Materials and Devices for Transmittance Control (1st Edn.). Bellingham, Washington, U.S.A., SPIE Press IS4 386.

6.9 Nagai, J., et.al. (1990), in Lampert, C.M., and Granqvist, C.G. (eds.), Large-Area Chromogenics: Materials and Devices for Transmittance Control (1st Edn.). Bellingham, Washington, U.S.A., SPIE Press IS4 378.

6.10 Sykes, P., A Guide Book to Mechanism in Organic Chemistry., 2nd Edn., Longmans 1966 496.

6.11 Nagai, J., McMeeking, G.D., Seike, T. and Noutomi, Y., Glazings Today December 1994 33.

CHAPTER 7

DISCUSSION AND CONCLUSIONS

7.1 DISCUSSION

7.1.1 Anodically deposited nickel oxide based coatings

Coatings produced using the deposition solution (0.1 M $NiSO_4$ and 0.1 NH_4OH) reported in the literature exhibited residual colouration, poor uniformity, low cyclic durability (optical and mechanical) and small dynamic range (7.1). Unfortunately there was no ideal concentration range of $NiSO_4$ and NH_4OH from which nickel hydroxide with good electrochromic and mechanical properties could be deposited. The major problem identified in this study was voluminous precipitation of α-$Ni(OH)_2$ during deposition. In this study precipitation was reduced by the addition of a non-ionic surfactant to the deposition solution. and subsequently, nickel hydroxide electrodes with good electrochromic and mechanical properties were produced (7.2, 7.3).

The addition of the detergent prevented agglomerate formation (7.2-7.4). The stabilisation (i.e. the reduction in the rate of agglomeration) of colloidal lyophobic suspensions by the addition of nonionic surfactants can be explained by two theories - the 'mixing mechanism' (7.5, 7.6) and the 'denting mechanism' (7.6-7.9).

7.1.1.1 *Mixing mechanism for the stabilisation of colloidal systems*

In this theory, the repulsive and attractive forces between two colloidal particles with adsorbed layers of detergent molecules are considered as particles are brought together (7.5). When the interparticle distance (the distance between the surfaces of these particles) is less than twice the thickness of the adsorption layer, mixing of the adsorption layers occurs. Repulsion occurs between the two particles if there is a net increase in free energy due to the mixing of the adsorbed layers. However, colloidal particles are attracted to one another by Van de Waal forces. If the repulsive force is greater than the attractive force then the particles are repelled from each another. Colloid stabilisation is the result of many particles repelling each other. This theory is applicable when the concentration of detergent in the adsorbed layer is low.

7.1.1.2 *Denting mechanism for the stabilisation of colloidal systems*

A fundamental requirement of this theory is that there should be a high concentration of detergent in the adsorbed layers. Consequently when colloidal particles approach each other they undergo elastic collisions rather than the mixing of adsorption layers. The stabilisation of colloidal systems in this case is due to many such particles undergoing elastic collisions (7.7-7.9).

7.1.1.3 *Solvent exclusion during close approach of colloidal particles*

An effect that is not taken into account in the denting and mixing mechanisms is the squeezing out of solvent molecules (i.e. molecules other than detergent, for example, water) when particles with adsorbed layers of detergent molecules approach each other (7.5). There is an enthalpy change involved in this process that needs to be considered in both mechanisms.

7.1.1.4 *Application of the denting and mixing mechanisms to the stabilisation of $Ni(OH)_2$ colloids with polyoxyethylene sorbitan monolaurate*

High concentrations of detergent (>10%) were required to stabilise nickel hydroxide colloids. At higher concentrations of detergent, the concentration of detergent molecules adsorbed on to colloid particles increases. Thus the theory which most adequately explains the stabilisation of $Ni(OH)_2$ with polyoxyethylene sorbitan monolaurate is the denting mechanism.

7.1.2 Colloidal precipitation of nickel oxide based coatings

Colloidal deposition of nickel oxide based coatings is reported in the literature (7.3, 7.21, 7.22, 7.43, 7.46). One method involves the dipping of a suitable substrate into a solution containing a nickel salt (for example, nickel sulphate) followed by dipping into potassium hydroxide (7.22). Nickel hydroxide is precipitated when the adsorbed Ni^{2+} comes into contact with an alkaline environment. In order to make thicker layers, the process is repeated until

the desired coating thickness is achieved. Another technique involves dipping a substrate into one solution containing nickel sulphate and potassium hydroxide (7.21). This technique was also used in this study. However, it was found that the rate of film growth and the electrochromic properties of coatings deposited using these technique were poor. The one-step method developed in this study for depositing nickel oxide based coatings not involving firing and/or post deposition cycling, produces films with good electrochromic properties (7.2, 7.3).

7.1.2.1 *Colloidal precipitation and electrophoresis*

Nickel oxide based coatings were deposited without the application of an electric field from solutions containing nickel sulphate and ammonium hydroxide. This implies that deposition by colloidal precipitation occurred during electrodeposition. Deposition of colloidal particles during electrodeposition is known as electrophoresis (7.24). Field-assisted deposition of particles was verified by anodising a substrate. The potential applied was +750mV in a solution containing 0.100 M of $NiSO_4$ and 0.100 M of NH_4OH. After 5 minutes a film 1000 A was produced with a τ_{sc} of 0.30 and a τ_{sb} of 0.75. When a substrate was cathodised in a solution containing the same concentrations of ions and identical ageing time, no deposition occurred. This was a significant experiment because it not only proved that the colloidal particles were negatively charged, it also confirmed that electrophoresis occurred from the deposition solution reported in the literature (7.1) containing 0.100 M $NiSO_4$ and 0.100 M NH_4OH (such deposition also occurs from solutions that contain detergent).

Film growth is dependent on the precipitation of nickel oxide based material.

The addition of detergents to solutions containing $NiSO_4$ and NH_4OH merely slowed down the rate of precipitation. Completely stable solutions are of no practical value for colloidal precipitation. Nevertheless the addition of small quantities (approx. 3%) of nonionic detergents to solutions containing nickel sulphate and ammonium hydroxide facilitated the deposition of uniform films with good electrochromic properties (7.3).

Film growth rate was dependent on the concentration of reactants. Coating deposition rate was the greatest when the rate of precipitation reached a maximum. Although thicker films were deposited when the rate of precipitation increased, the as-deposited films were non-uniform with poor mechanical properties. However, it was possible to achieve a visible transmittance value of 0.03 τ_{vc} in the coloured state (0.22 τ_{sc}). By adjusting the rate of precipitation, coating uniformity was improved. This was achieved by controlling the concentration of reactants and by the introduction of the detergent, polyethylene sorbitan monolaurate.

7.1.3 Nickel oxide based coatings r.f. sputtered at low power (100 W) and high pressures (6 $x10^{-2}$T)

Coatings sputter deposited at high pressures (6 x 10^{-2} T) and low powers (100 W) were analyzed. Coatings deposited under these conditions were examined. The electrochromic properties of these coatings were very different to nickel oxide based electrodes produced using chemical and electrochemical methods. (7.2). The sputter deposited coatings exhibited good durabilities, large dynamic ranges and good cyclic stabilities in the oxidised state (7.10). The durability of films deposited by sputtering was far superior to that of anodically or colloidally deposited coatings when cycled in 1 M KOH (7.36).

7.1.4 Ultraviolet/visible/near-infra-red spectrophotometry of nickel oxide based coatings

7.1.4.1 *Ultraviolet/visible/near-infra-red spectrophotometry of anodically deposited nickel oxide based coatings*

The optical and electrochromic properties of anodically deposited films were dependent upon the stability of the deposition solution. Coatings produced from unstable solutions (0.100 M $NiSO_4$, 0.100 M NH_4OH) exhibited low solar transmittance in the coloured (0.22 τ_{sc}) and bleached (< 0.60 τ_{sb}) states. After optimising the solution concentrations coatings exhibited coloured and bleached solar transmittance of 0.30 and 0.70 respectively. Unfortunately, these films did not show homogeneous optical properties upon colouration: residual colouration occurred in certain areas of the coatings upon bleaching.

Coatings deposited from stable solutions exhibited excellent bleaching characteristics. The solar transmittance of the bleached state was higher than 0.80. The average value for the coloured solar transmittance for the deposition time of 60 minutes was 0.25. The best values for the solar transmittance of the coloured and bleached states were 0.22 and 0.82, respectively. Anti-reflection properties were also noticed for films deposited from stable solutions. Coatings produced from stable and unstable solutions exhibited a brown bronze upon colouration similar to those r.f. sputtered at low pressures and high powers (7.10). For thin films <400 A a grey colouration was observed similar to that of films that had been r.f. sputtered at high pressures and low powers (7.10). This phenomena was also exhibited by coatings produced using colloidal deposition.

7.1.4.2 *Ultraviolet/visible/near-infra-red spectrophotometry of nickel oxide based coatings produced by colloidal deposition*

The ultraviolet/visible/near-infra-red spectra of colloidally deposited coatings and electroplated coatings were very similar in the bleached and coloured states for films of comparable thickness (1000 A). It is also evident that in the bleached state anodically and colloidally deposited coatings absorb less infra-red radiation than r.f. sputtered coatings. Colloidally deposited coatings thicker than 400 A in the coloured state were brown in colour. Coatings thinner than this exhibited grey colouration.

7.1.4.3 *Ultraviolet/visible/near-infra-red spectrophotometry of nickel oxide based coatings produced by r.f. sputtering*

The spectral response of material deposited by r.f. diode sputter deposition was very different to that of coatings produced by either colloidal or anodic deposition, the major differences being that in the oxidised state the observed colour was grey and near-infra-red modulation was possible (7.10). For colloidally and anodically deposited nickel hydroxide the majority of the optical modulation occurs in the visible part of the electromagnetic spectrum. Sputter deposited coatings colour in a neutral manner but have the disadvantage of absorbing radiation uniformly from 300 to 2500 nm. This means that the coating becomes hotter (thermally) in the coloured state than anodically or colloidally deposited nickel hydroxide electrodes when exposed to the solar spectrum.

PAGE
MISSING
IN
ORIGINAL

chromaticity (7.29). Interestingly, this also coincided with an increase in the free OH peak height, optical dynamic range and the area enclosed within cyclograms. This confirms that the grey colouration is not stable to cycling in an aqueous alkaline environment (7.10). However, the transformation from NiO to $Ni(OH)_2$ has been reported previously for both r.f. sputtered (7.29) and evaporated (7.31) coatings.

7.1.5 Fourier transform infra-red spectrophotometry of nickel oxide based coatings

Not all of the infra-red absorbance peaks reported in the literature for nickel hydroxide were identified in this study. Specifically;

(i) Symmetric υ_{OH} at 3580 cm^{-1}

(ii) Deformation δ_{OH} at 553 cm^{-1}

(iii) υNiO at 450 cm^{-1}

(iv) OH libration at 350 cm^{-1}

The symmetric υ_{OH} at 3580 cm^{-1} was probably not detected in the nickel hydroxide stretches in this study due to the resolution of the FTIR instrument. Another reason may be that it was masked by the broad stretch centred at around due to intercalated water or α-$Ni(OH)_2$. The deformation δ_{OH} at 553 cm^{-1} may have been missed due to this process occurring parallel to the surface of the TCO, in which case the absorbance due the deformation δ_{OH} would have been low. υNiO at 450 cm^{-1} for nickel hydroxide was probably not detected due to the higher noise levels incurred in the measurements at these wave numbers (see figures 3.16 - 3.18). Finally the OH libration at 350 cm^{-1} could not have been detected because it was beyond the range of the FTIR used in this study.

7.1.5.1 *Fourier transform spectrophotometry of anodically deposited nickel oxide based coatings*

Results from Fourier transform infra-red spectroscopy show that in the O-H stretch region of the spectra a sharp hydroxy band occurs at 3647 cm^{-1} and a broad band occurs at around 3360 cm^{-1} (7.11, 7.12). Films deposited using different deposition times, show an increasing peak height at 3647 cm^{-1} with respect to increasing film thickness. When coatings were oxidised the hydroxy stretch 3647 cm^{-1} diminished until it disappeared at > + 440 mV. The standard spectra for ß-nickel hydroxide has a sharp band at 3630 cm^{-1} (7.11). This type of band is usually observed in materials that have free OH (7.11, 7.12). The other phase α-nickel hydroxide has a broad band at 3400 cm^{-1} indicating the presence of hydrogen bonded water in the film structure (7.11, 7.12). The sharp band at 3647 cm^{-1} is similar to that reported elsewhere (7.11-7.13). The deposition of a thicker film (3300 A) led to the identification of a band in the coloured state at 564 cm^{-1} and a very broad band in the O-H region (see figure 3.22). The infra-red peak around 580 cm^{-1} is characteristic of both γ and ß-oxyhydroxide (7.11). *It is significant that the LO phonon (at* around 560 cm^{-1}) that is normally observed for nickel oxide coatings was not observed in the bleached state.

7.1.5.2 *Fourier transform spectrophotometry of colloidally deposited nickel oxide based coatings*

Fourier transform infra-red spectrophotometry analysis of the precipitate and coatings produced from solutions containing 0.100 M nickel sulphate and 0.100 M ammonium hydroxide revealed that the precipitate and coatings were in fact

composed of α-nickel hydroxide (7.2). The phase of nickel hydroxide was dependent on deposition conditions and post treatment (7.18). The spectra for the precipitate and a film produced from the same solution were identical. The characteristic stretch at 3400 cm^{-1} corresponding to α-nickel hydroxide was observed in both cases (7.15). As was observed for coloured electroplated films, colloidally precipitated films exhibited a peak at 564 cm^{-1} in the coloured state. Therefore, this study indicates that electroplated and colloidally deposited coatings were very similar and that β- and α-nickel hydroxide were present in the bleached states of anodically and colloidally produced coatings respectively, and γ or β-nickel oxyhydroxide was present in the coloured state. In contrast the characteristic stretch at 3647 cm^{-1} of β-nickel hydroxide was detected in the bleached state for r.f. sputtered films.

7.1.5.3 *Fourier transform spectrophotometry of r.f. sputtered nickel oxide based coatings*

The non-hydrogen bonded O-H stretch at 3647 cm^{-1} (7.2, 7.11, 7.15) was detected in all of the r.f. sputtered films thicker than 300 A, in the bleached state that had been cycled for 1 hour in 1 M KOH. This implies that β-$Ni(OH)_2$ was present in the r.f. sputtered films after cycling in 1M KOH. The O-H stretch was not detected in the as-deposited film but was detected after the films were cycled. This stretch became sharper after 12 hours cycling between -1.500 V and +1.000 V (figure 5.3). It was also observed that this chemical process occurred at lower potentials (-500 mV to +500 mV). The height of the peak at 3647 cm^{-1} became larger as the number of cycles increased (figure 5.3). Another feature of this peak is that it became narrower with cycling. From these facts it can be deduced that the as-deposited material was

gradually converted to ß-$Ni(OH)_2$. Conversion probably occurred by NiO being converted to NiOOH (see equation 7.1). The NiOOH may then be further converted to $Ni(OH)_2$ by gaining a proton from water (see equation 7.2). Water will also be present in coatings due to the material being in contact with an aqueous environment (In this research coatings were in contact with a 1M KOH solution).

$$NiO + OH^- \rightleftharpoons NiOOH + e^- \qquad 7.1$$

$$NiOOH + H_2O + e^- \rightleftharpoons Ni(OH)_2 + OH^- \qquad 7.2$$

$$2OH^- \rightleftharpoons H_2O + 1/2O_2 + 2e^- \qquad 7.3$$

Hydroxide ions that penetrate through the coating and discharge at the ITO surface may react to form water and oxygen (see equation 7.3). This electrochemical process may be the mechanism for the inclusion of H_2O in r.f. sputtered coatings. This process will also occur when the coatings are oxidised in organic electrolytes (because it is extremely difficult to remove the last traces of water from such systems). However, it is likely that the change in colour from grey to brown that occurs upon electrochemically cycling r.f. sputtered NiO in aqueous electrolytes such as KOH (or the dissolution of coatings in $KCl_{(aq)}$) can be delayed by using an organic electrolyte (with a low water content).

The stretch at 564 cm^{-1} corresponding to the nickel oxygen stretch (7.14) or LO phonon of hydrogen bonded linkages (7.35) of α or ß-NiOOH was not detected in the coloured state. However, from the anodic studies it was noticed

that this stretch was only detected in the thicker films (3300 A). The deposition of coatings (at low powers and high pressures) of this thickness was not feasible using the R.F. Polaron coater (20 hour deposition time) available at Oxford Brookes University (as of 1992).

7.1.6 Raman spectroscopy of nickel oxide based coatings

7.1.6.1 *Raman spectroscopy of anodically deposited nickel based coatings*

Raman spectroscopy did not reveal the presence of either α or β-nickel hydroxide in the bleached state. γ-nickel oxyhydroxide was found in the coloured state for coatings deposited from stable solutions. This was unexpected, since some researchers have reported that this phase is electrochemically irreversible (7.15). However, other researchers have confirmed the reversibility of this phase (7.11). Unfortunately, some researchers claim that it is not possible to discriminate between the two phases of the oxyhydroxide using Raman spectroscopy (7.16). The lack of evidence of either α or β nickel hydroxide in the bleached state may be due to nickel hydroxide being a poor Raman diffuser (low Raman activity).

7.1.6.2 *Raman spectrophotometry of colloidally deposited nickel oxide based coatings*

Coatings of nickel hydroxide produced by colloidal precipitation did not exhibit any Raman bands. Coatings of various thicknesses up to 3600 A were examined. However, α- or β-nickel hydroxide was detected in a crystallite on the surface of a colloidally precipitated coating. After colouration the spectra of the

crystallites on the surface had no peaks. Furthermore, the Raman spectra was the same as the coating. Because colloidally deposited coatings are produced by material precipitating from solution, it is likely that the substance present in the bleached state was α and/or β-nickel hydroxide. Using FTIR, an unambiguous O-H stretch corresponding to α-nickel hydroxide was detected. The absence of Raman bands for thicker nickel hydroxide coatings (3600 A) may indicate that this technique was unsuitable for analyzing a material such as α-nickel hydroxide that is a weak Raman diffuser (7.16). Furthermore this result may reveal why some researchers have failed to detect nickel hydroxide in nickel oxide host matrices using Raman Spectroscopy (7.25). Notwithstanding, other researchers (7.26) have identified β-$Ni(OH)_2$ in anodically prepared NiO using S.E.R.S. (Surface Enhanced Raman Spectroscopy).

7.1.6.3 *Raman spectroscopy of r.f. sputtered nickel oxide based coatings*

Raman bands were not detected for r.f. sputtered nickel oxide based coatings in the as-deposited, bleached and coloured states. However, the coatings analysed were only 500 A thick. Therefore, this experiment should be repeated using thicker coatings.

7.1.7 Cyclic voltammetry of nickel oxide based coatings

7.1.7.1 *Reversibility of nickel oxide based electrodes*

The diagnostic tests for determining the reversibility of electrochemical systems were discussed in chapter 2,2.17. During the course of this study the

transfer coefficients α_A and α_C and, n, the number of electrons transferred during electrochemical processes were not evaluated. In order to accurately determine the number of electrons transferred during a particular reaction it is preferable that a coulomb meter be used to measure the charge. Therefore some of the diagnostic tests in referred to in 2.17 cannot be used to determine the reversibility of nickel oxide based electrodes. However, some of the diagnostic tests can be performed to ascertain the reversibility of the nickel oxide electrodes produced in this study, these are;

(i) E_p versus υ

(ii) Presence of reverse peaks

(iii) $|I_p|$ versus $\upsilon^{1/2}$

(iv) ratio of $|I^A_p/I^C_p|$

(v) I^C_p versus $\upsilon^{1/2}$

(vi) Shift of E^C_p

Clearly, the nickel oxide based electrodes examined in this study were not completely reversible because E_p is dependent on υ. However reverse peaks were observed during electrochemical cycling (see figure 3.20). In an irreversible system no reverse peak is observed. However sometimes a fast following chemical reaction can sometimes lead to the absence of a reverse peak, and therefore does not necessarily imply that the process is irreversible. For the coatings produced in this study the ratio of $|I^A_p/I^C_p| \neq 1$, but this does not mean that the system irreversible. $|I_p|$ does increase with $\upsilon^{1/2}$ but is not proportional to $\upsilon^{1/2}$ which would indicate that the nickel oxide based electrodes examined in this study are quasi-reversible. E^C_p also shifts negatively with increasing υ, this would also imply quasi-reversibility. However, a plot of I^C_p is proportional to $\upsilon^{1/2}$. This would imply that the process is irreversible.

However, the data collated in this study was only gathered over two decades of scanning rates. Therefore to have accurately determined whether the nickel oxide based electrodes were electrochemically irreversible, or quasi-reversible, further data should have been collected at other scanning rates (ie 0.1 mV s^{-1}, 100 mVs^{-1} and 1000 mVs^{-1}). The plots of I_p versus υ and I^c_p versus υ may have exhibited some divergence at lower and higher scanning rates from those observed during this experimental. However, based on the negative shift of E^c_p w.r.t. υ, the presence of reverse peaks and that colouration and bleaching are exhibited at slower scanning rates, the coatings may be quasi-reversible.

7.1.7.2 *Cyclic voltammetry of anodically deposited nickel oxide based coatings*

Nickel oxide based electrodes deposited from stable solutions were analyzed using cyclic voltammetry (films deposited from unstable solutions were not mechanically stable to cycling for more than a few cycles). Voltages were measured relative to a saturated calomel electrode (5 M KCl). The curves in figure 3.23 show the oxygen evolution peak and the colouration (anodic) and bleaching (cathodic) peaks (7.12 - 7.14). The maxima of the anodic peak occurred at +420 mV (relative to SCE 1-2 mVs^{-1}). This is the same potential at which the hydroxy stretch started to disappear in the spectral data shown in figure 3.20. It was also noticed that as the scanning rate was increased the anodic peak became smaller until, at 10 mVs^{-1}, the colouration anodic peak was no longer present (figure 3.20). At this scan rate, mass transfer of ions to and from the nickel hydroxide electrode was dominant over electron transfer. Coatings did not exhibit colouration and bleaching at scanning rates faster than 10 mVs^{-1}.

7.1.7.3 *Cyclic voltammetry of nickel oxide based coatings produced by colloidal deposition*

Cyclic voltammetry of colloidally deposited nickel hydroxide was essentially the same as that recorded for anodically deposited nickel hydroxide. The Faradaic anodic peak occurred at +420 mV (relative to SCE at 1-2 mVs^{-1}). Coatings did not exhibit colouration and bleaching at cycling rates faster than 10 mV s^{-1}. This is further evidence for the similarity between anodically and colloidally deposited coatings.

7.1.7.4 *Cyclic voltammetry of r.f. sputtered NiO based coatings*

Cyclic voltammetry of r.f. sputtered coatings revealed an overloop in the cathodic quadrant when coatings were cycled between -1.5V to +1V. This is indicative of deposition, phase change or possibly intercalation of K+ (with hydration sphere). Therefore, coatings were cycled between -500 mv to +500 mv. Using this potential range an overloop was not observed. For coatings cycled between both potential ranges, an increase in the area enclosed within the cyclogram was observed. Some researchers claim that this is due to an increase in the porosity of NiO (7.27). However, the change in the cyclogram coincided with an increase in the height of the free OH peak. Furthermore, as the coating was cycled the optical dynamic range increased. This is reported in the literature for similar coatings (7.10, 7.29). One possible interpretation of this is that NiO is partially converted to the hydroxide when cycled in an alkaline media (7.29, 7.31). An alternative explanation supported by other researchers, is that metal cations are inserted during cycling (7.30). The increase in the dynamic range (*and hence charge stored*) is related to a

greater concentration of metal cations being inserted (7.30). At low cycling rates (1-2 mVs^{-1}) the anodic peak corresponding to colouration occurred at +420 mV. Finally coatings did not exhibit colouration and bleaching at cycling rates faster than 10 mVs^{-1}.

7.1.8 Mechanical properties of nickel oxide based coatings produced by anodic, colloidal and r.f. diode sputter deposition

The mechanical properties of materials anodically deposited from stabilised solutions were superior to those that were deposited from unstable solutions. Nickel hydroxide deposited from unstable solutions generally disintegrated after a few cycles whereas those that were deposited from stable solutions exhibited various degrees of mechanical stability. Some coatings that were deposited from stable solutions were stable for at least 100 cycles (-500 mV to +750 mV at 20 mVs^{-1}) with no visible damage. Failure may have been due to microscopic flaws in the coating or substrate material or may have been due to change in lattice parameter that occurs during the oxidation of nickel hydroxide to nickel oxyhydroxide. The latter may be responsible for the delamination of NiO from the TCO coated glass. In order to improve or at least characterise the mechanical stability of nickel oxide and nickel hydroxide coatings, this mode of film failure should be subject to further research, although this type of failure is inevitable in ceramic materials such as nickel oxide that have low fracture strengths (7.37).

Coatings deposited by colloidal deposition exhibited very poor durability akin to that observed for coatings anodically deposited from unstable solutions, whereas those deposited by r.f. diode sputter deposition exhibited excellent

mechanical durability when cycled in 1M $KOH_{(aq)}$ (> 1000 cycles). The superior mechanical properties of r.f. sputtered NiO may be due to the fact that it is only partially hydrated, and the adhesion of sputter coated films to substrate material such as ITO is usually superior to that of coatings deposited by anodic or colloidal deposition.

7.1.9 XRD of anodic, colloidally and r.f. diode sputter deposited nickel oxide based coatings

The presence of nickel hydroxide, nickel oxyhydroxide or nickel oxide was not detected in coatings produced by anodic, colloidal and r.f. diode sputter deposition. This indicates that all of the coatings produced in this study had a very low degree of crystallinity, i.e. they were amorphous. To improve the degree of crystallinity coatings were also heated (200 - 300 °C). Unfortunately, this had no affect on the crystallinity of the sample. However, in future studies small angle XRD could be used. This method is suitable for analyzing materials with low degrees of crystallinity. An alternative approach may be to improve the crystallinity by hydrothermal treatment (7.18), altering the nature of the deposition solution or TEM studies for r.f. diode sputtered NiO (7.10).

7.1.10 Colouration efficiency of nickel oxide based coatings

7.1.10.1 *Colouration efficiency of anodically deposited nickel oxide based coatings*

The colouration efficiency (C.E.) of coatings produced from unstable solutions was 14 $cm^2\ C^{-1}$. This low value can be attributed to the residual colouration that these coatings exhibited (some coatings would not bleach). For coatings

deposited from optimised unstable solutions the value of C.E increased to 25 cm^2 C^{-1}. The colouration efficiency of anodically deposited nickel oxide based coatings from stable solutions was 29 cm^2 C^{-1}. The average of the literature values for the colouration efficiency (solar) of nickel oxide based coatings is 30 cm^2 C^{-1} (7.18 - 7.20).

7.1.10.2 *Colouration efficiency of colloidally deposited nickel oxide based coatings*

Coatings deposited from unstable solutions exhibited a colouration efficiency of 29 cm^2 C^{-1}. This is similar to that exhibited by coatings deposited by anodic electrodeposition and reported elsewhere for nickel oxide based coatings deposited using a variety of techniques (7.18 - 7-20).

7.1.10.3 *Colouration efficiency of r.f. sputtered NiO based coatings*

The C.E. of r.f. sputtered NiO was 31 cm^2 C^{-1} after cycling for 1 hour in $KOH_{(aq)}$. This was not significantly different to coatings produced by anodic and colloidal precipitation. Whilst colouration efficiency was not measured as a function of cycling time, other researchers report that the dynamic range of these types of coatings increases with respect to the number of cycles in $KOH_{(aq)}$ (7.10, 7.30).

Table 7.1 Optimum optical and colouration efficiency properties of nickel oxide based coatings

Deposition Method	Technique	τ_{sc}	τ_{sb}	τ_{vc}	τ_{vb}	R_{sc}	R_{sb}	R_{vc}	R_{vb}	Coloured Chromaticity			Bleached Chromaticity			C.E. $cm^2\ C^{-1}$	Composition	
										X	Y	Z	X	Y	Z		BL State	Col State
Anodic Electro-deposition	Unstable Solution	0.17	0.50	0.07	0.44	0.15	0.10	0.16	0.06	0.417	0.365	0.219	0.399	0.335	0.325	14	β Ni(OH)$_2$	NiOOH β or γ
	Unstable Solution Optimised	0.26	0.70	0.09	0.66	0.17	0.07	0.16	0.06	0.409	0.361	0.230	0.312	0.326	0.362	25	β Ni(OH)$_2$	NiOOH β or γ
	Stable Solution	0.22	0.82	0.03	0.91	0.04	0.05	0.02	0.03	—	—	—	0.312	0.322	0.367	29	β Ni(OH)$_2$	NiOOH γ
Colloidal Deposition	Unstable Solution	0.48	0.82	0.28	0.92	0.15	0.07	0.18	0.06	0.345	0.329	0.326	0.314	0.320	0.366	29	αNi(OH)$_2$	NiOOH β or γ
RF Diode Sputtering	1 hr cycling 1M KOH	0.30	0.70	—	—	0.24	0.16	—	—	0.320	0.330	0.350	0.300	0.310	0.390	31	NiO&Ni(OH)$_2$ (β)	?

Key: C.E. = Colouration efficiency
BL = Bleached
Col = Coloured

7.1.10.4 *Effect of surface roughness on colouration efficiency*

In this study the surface roughness of coatings was not measured. The surface roughness of coatings may have had an effect on the colouration efficiency (especially since the coatings were deposited using different techniques). The current density due an electrocatalytic process is affected by the real surface area, i.e. the surface roughness (7.64). This is in contrast to electrochemical processes that are dependent on mass transport controlled reactions where the current is independent of surface roughness, provided the surface roughness is smaller than the diffusion layer thickness ($\approx 1 \times 10^{-2}$ cm). The surface roughness of coatings could have been measured using optical interferometry or by stylus profiling.

7.1.11 Solid state devices

All of the solid state devices produced in this study exhibited reversible electrochromism. The major differences in these devices were in chromaticity, the range of optical modulation and kinetics. The only ECW that exhibited a neutral colouration in the coloured state, utilised MnO as a counter electrode. This device also exhibited the fastest kinetics. Typically, colouration and bleaching occurred in less than 10 seconds (for a 50 x 50 mm^2 area). However, the dynamic range of this device was small - only 10% in the solar spectrum and 12% in the visible spectrum (see Table 6.1, device structure (iii) - ITO\R.f.sputtered NiO\PVA:(C_2H_5)N\ITO). This was probably because the r.f. sputtered NiO coating was only 300 A thick. The device with the largest dynamic range is the system represented in (ii) in Table 6.1 (ITO\R.f. sputtered NiO\PVA:$(C_2H_5)_3$N\ITO). However, the kinetics of this system were

slower than that of device (iii). Full colouration and bleaching for this device took 5 minutes. The potentials applied for colouration and bleaching were, +1.00 V and -1.00 V respectively. For all ECW's constructed in this study the kinetics were faster on the first few cycles. With successive cycles the time required for full bleaching and colouration increased for all devices. As previously mentioned the systems characterised in this study were analyzed in the first electrochemical cycle.

Infra-red characterisation of the electrochromic device was not possible (using conventional techniques) due to the presence of the transparent conductors.

7.2 CONCLUSIONS

7.2.1 Chemical identity of the as-deposited coloured and bleached states of anodically and colloidally deposited coatings

The chemical identity of the electroactive centre in as-deposited nickel oxide based coatings is controversial. Furthermore, the compounds present in the as-deposited, bleached and coloured states and the ion(s) responsible for colouration remain the subject of debate (7.25-7.32, 7.47-7.49).

The most important finding of this thesis was that coatings deposited by anodic deposition were predominantly ß-nickel hydroxide, whereas those produced by colloidal deposition contained mainly α-$Ni(OH)_2$. Upon colouration, bands corresponding to ß- or γ-nickel oxyhydroxide were detected using FTIR spectrophotometry for both anodic and colloidally deposited films. Using Raman spectroscopy for coatings anodically deposited from stable solutions the phase

γ-NiOOH was identified. This was evidence for nickel hydroxide being oxidised to nickel oxyhydroxide. Further evidence that the bleached and coloured states of anodically and colloidally deposited coatings were $Ni(OH)_2$ and NiOOH respectively, is the occurrence of the Faradaic anodic peak at +420 mV. This is the same as the literature value for the oxidation of $Ni(OH)_2$ to NiOOH (7.38, 7.41). The ion responsible for colouration was not identified in this study. However, from the data collected, it can be concluded that the mechanisms of colouration for anodically and colloidally deposited coatings are best described by equations 7.4 and 7.5.

$$Ni(OH)_2 + OH^- \rightleftharpoons NiOOH + H_2O + e^- \qquad 7.4$$

$$Ni(OH)_2 \rightleftharpoons NiOOH + H^+ + e^- \qquad 7.5$$

Nickel oxyhydroxide was not detected for r.f. diode sputtered coatings in the coloured state, therefore only the left hand side of equations 7.4 and 7.5 can be applied for these coatings.

7.2.2 Chemical identity of r.f. diode sputtered coatings in the as-deposited, bleached and coloured states

NiO based r.f. diode sputtered NiO exhibited a change in colour of the oxidised state from grey to brown after cycling in alkaline aqueous media (1M KOH). As the colour of the coatings changed, the area enclosed within the cyclogram also increased. Whereas, in the bleached state, the OH peak height at 3647 cm^{-1} increased (7.31) as the number of cycles increased. As the coating was cycled the dynamic range became larger as reported elsewhere (7.29).

One interpretation of the observations made is that electroactive $Ni(OH)_2$ is generated within NiO during cycling (7.29, 7.31). Another is that the production of nickel hydroxide is just a side reaction, the observed electrochromism being due to metal cation intercalation or deintercalation (7.30). The cause of the improved electrochromic properties would be higher concentrations of metal cations stored in the electrode (7.30).

NiO has a cubic structure in which a nickel cation is surrounded octahedrally by 6 oxygen anions (MeO_6). During electrochemical cycling it is conceivable that OH^-, H_2O, M^+ (where, M = H, Li, Na, K, etc.) penetrate the coatings and interact with these octahedral units. Furthermore, it is also possible that some nickel is dissolved into the electrolyte. Hydrogen bonding between water and oxygen atoms of these octahedral species will occur when water is intercalated into the coatings. The formation of hydroxides is also possible due to the interaction of OH^- with central metal cations. Whether ions penetrate from the electrolyte into the film or nickel diffuses into the electrolyte, the coating becomes more porous exposing a greater internal surface area of possible electrochromic sites and/or NiO to the electrolyte. Furthermore, the interfacial capacitance increases as a result of the increased porosity at the electrode/electrolyte interface.

7.2.3 Choice of deposition method for the fabrication of ECW devices

A question raised by this thesis is, which deposition method produces NiO or $Ni(OH)_2$ suitable for electrochromic glazing applications? Clearly all of the coating methods in this study have their advantages and disadvantages.

Colloidal deposition is a relatively inexpensive method of producing large area uniform coatings that exhibit a satisfactory electrochromic response (τ_{sc} .40 τ_{sb} .76). However they are not mechanically stable to electrochemical cycling.

Nickel hydroxide electrodes with superior mechanical durability and larger dynamic ranges can be deposited by anodic electrodeposition. The coatings with the best electrochromic and mechanical properties exhibited dynamic ranges of τ_{sc} .22 and τ_{sb} .82. This is more than adequate for an electrochromic device. The near-infra-red modulation of these coatings is interesting. As previously stated (section 2.8.1), electrochromic coatings heat up when exposed to solar radiation. Whilst approximately 55% of the solar spectrum is in the near infra-red, these coatings do not absorb strongly in this region of the electromagnetic spectrum. Most absorption occurs in the visible part of the spectrum. However, if ECW systems are used in conjunction with other advanced glazings such as heat mirrors, low absorption in the near infra-red may be disadvantageous. It may in fact be desirable to absorb as much of the near infra-red as possible (since a cold heat mirror may be used to reflect the infra-red radiation). This radiation would be re-radiated at thermal wavelengths and then would be reflected by a suitable heat mirror.

The coatings with the best durability were produced using sputter deposition (7.10). R.f. sputtered NiO electrodes also exhibited large modulations in the near infra-red. This type of coating could be used in conjunction with a heat mirror (this heat mirror would not be in direct physical contact with the ECW). The change in optical response (grey to brown) may not occur in an organic electrolyte. This possibility was not researched in this thesis. Although superior dynamic ranges can be achieved with nickel hydroxide

electrodes, they do not at the moment exhibit the excellent durability of r.f. sputtered NiO.

A major disadvantage of r.f. diode sputtered coatings for device applications is the slow deposition rate (about 0.1A s^{-1}). However, the slow rate of deposition gives the superior optical properties and durability of these coatings. The current focus of attention by researchers of electrochromic materials, is evaporated NiO. Some researchers have reported that this material exhibits excellent electrochromic properties, and does not contain the hydroxide (8.28). However, there is evidence for non-hydrogen bonded OH in as-deposited evaporated NiO (7.39). This indicates that this material is a hydrated form of NiO.

7.2.4 Analyses of solid state devices

The solid state devices constructed in this study were rudimentary and exhibited low cyclic stabilities. However, the reversible electrochromism exhibited by these systems showed that nickel oxide based coatings and nickel hydroxide electrodes could be used in solid state devices. The device with the fastest switching kinetics used MnO as a counter electrode. The visible optical modulation was very similar for all of the devices tested in this study. Devices containing r.f. sputtered NiO as the anodic layer exhibited the highest solar transmittance modulation. There was little difference in the durability of devices apart from those that contained MnO. In this case rapid delamination of the MnO occurred. The poor durability of these devices may have been due to the use of a polymeric electrolyte, the reduction of ITO, or some other as yet undetermined process. Clearly the cyclic, thermal and ultraviolet durability of devices containing NiO and nickel hydroxide electrodes is a subject for future research.

7.3 FUTURE WORK

7.3.1 Colouration mechanism(s) of NiO_x and $Ni(OH)_2$

The colouration mechanism of nickel oxide based coatings and nickel hydroxide electrodes is controversial (7.2, 7.10-7.16, 7.25, 7.47-7.50) However, α- and β-nickel hydroxide were detected in the bleached states of colloidally and anodically deposited coatings respectively. There was evidence for either β- or γ-nickel oxyhydroxide in the coloured state of colloidally deposited coatings, whereas for anodically produced coatings from stable solutions only γ-nickel oxyhydroxide was found. For r.f. sputtered films β-$Ni(OH)_2$ was detected in the bleached state after cycling in 1M $KOH_{(aq)}$, but the oxyhdroxide was not detected in the coloured state.

The ion responsible for colouration was not identified for any of the coatings fabricated in this study. From the literature it can be deduced that the most suitable techniques for this task will be impedance (7.49) Q.C.M. (7.39) and nuclear analyses (7.54-7.55). It is necessary to establish if hydroxy ions penetrate and/or protons (or other cations Li^+, Na^+, K^+) are removed from coatings during oxidation (7.49). This is important because if nickel oxide based coatings require OH^- to undergo oxidation, hydrated electrolytes will be required for devices containing such coatings. If this is not the case then non-hydrated electrolytes may be used.

Recent research indicates that the colouration mechanism(s) for NiO in anhydrous environments (7.32, 7.42) may be different to those in aqueous (7.19, 7.29, 7.31). Unfortunately, researchers who claim to use anhydrous systems do not state the water content of the electrolytes used in their studies (7.30, 7.32, 7.42).

7.3.2 Development of anodically deposited nickel hydroxide

Since the electrochromic properties of anodically deposited nickel hydroxide have been optimised in this study, the focus of attention should now be to improve the adhesion and mechanical stability of films deposited using this technique (7.52, 7.53). A quantitative technique of assessing the adhesion of films to substrates is required. Qualitative methods already exist for assessing adhesion such as the 'Sellotape' and finger nail test, but only indicate if the film is good or bad. Working on this basis it would be difficult to detect a trend in improving adhesion with respect to a particular deposition parameter. It has been found in this study that films with poor adhesion tend to disintegrate after a few cycles. An electrochemical and/or weight loss with respect to the number of electrochemical cycles in an electrolyte of known concentration should be performed. This may yield quantitative information about the adhesion of films to substrates. It was noticed during this study that the area enclosed within the cyclogram reduced drastically prior to delamination of coatings. Finally, in situ measurement of film growth during deposition may yield useful information with respect to modifying film properties (7.62).

7.3.3 Development of colloidally deposited nickel hydroxide

Colloidal precipitation from one solution is an extremely attractive method for manufacturing nickel hydroxide electrodes. Unfortunately the mechanical stability of coatings to electrochemical cycling that exhibit good electrochromic responses (τ_{sc} 0.22 - τ_{sb} 0.77) is not as good as r.f. sputtered nickel oxide electrodes. However, this may be improved by the use of a suitable detergent. Uniform coatings of carbon black can be deposited using colloidal precipitation by using the correct detergent (7.40).

The variety of different solution stabilisers that could be used in conjunction with solutions of nickel sulphate and ammonium hydroxide is enormous. In essence, solution stabilisers are added to deposition solutions to produce films that are more uniform than those that are deposited from solutions that do not contain solution stabilisers. The advantage of using stabilisers such as detergents is that they actually effect the way that crystal growth takes place (habit modification) this in turn leads to a reduction in the rate of formation of agglomeration without significantly affecting the deposition rate of films. This is important because another way of reducing the rate of agglomeration would be to simply decrease the concentration of reactants in the solution. This was the first approach of this study but only films with poor electrochromic properties and mechanical adhesion could be made using this technique. This was because although the rate of precipitation was decreased by simply decreasing the concentration of reactants, large agglomerates still formed. Agglomerates that formed on the surface of electrodes (diameter> 1mm) could clearly be seen on the surface of films on removal from the deposition baths. Such agglomerates could also be observed on the walls of the beakers containing the deposition solutions. After washing the films with distilled water, areas of the electrode where agglomerates had been present did not colour as strongly when the coating was switched to the coloured state.

The cationic and anionic detergents used in this study could not be used to stabilise solutions of nickel sulphate and ammonium hydroxide and produce uniform films. However, other researchers in the field of thin film deposition from stabilised colloidal systems have reported that colloidal deposition can be enhanced (with film uniformity) without losing solution stability by the selection of a suitable detergent.

The axioms defining which detergent will enhance colloidal deposition whilst maintaining film uniformity are not stated in the literature. This notwithstanding, it is possible to define some of the qualities that such a detergent should have. Increasing the chain length of the alkyl chain generally improves stabilisation of a colloidal system. However, after a certain chain length is reached there is no advantage in further increasing the chain length (number of carbon atoms in the chain). In fact in some cases this leads to colloid instability due to the increased Van de Waal forces between colloid particles and detergent or interpenetration of the double layer of charge on the colloidal particles by the detergent alkyl chain.

The type of detergent used can also have an effect on the deposition rate and the homogeneity of the deposit. Since colloidal particles are generally charged the stability of the colloid can also be affected by anionic detergents. If the detergent molecule has the same charge as the colloidal particles then the colloid is generally stabilised. The addition of a detergent with an opposite charge destabilises the system and precipitation results. However, at high concentrations, charge reversal on the colloid particles occurs and the colloid becomes stable again.

The deposition of particles on to surfaces depends on the degree of wetting which increases with pH and detergent concentration. So theoretically the rate of deposition could be increased by increasing the pH up to a point. However, increasing the pH too high in some cases leads to the re-dissolving of precipitates. There are, however, other factors to consider. By increasing the pH the physical nature of the precipitates themselves actually change. At low pH values, a solution of nickel sulphate and ammonium hydroxide is usually defined as a sol. A solution containing nickel sulphate and ammonium

hydroxide at higher pH values tends to form precipitates that gel. The gelation of precipitates reduces the rate of film growth because the precipitates crosslink and form a gel. The rate of growth of this gel is faster than the rate of growth of the coating because of the cross linking that occurs between precipitates. At moderate pH values (pH 9) the rate of film growth reaches a maximum. So by increasing the wetting at this point by adding a suitable detergent theoretically the ideal conditions for film growth should be achieved.

To summarise, the interaction of detergent molecules with colloidal particles and substrates is very complex. It is very difficult to predict what effect a particular detergent will have on a particular colloidal system. However, it is likely that the stability of colloidal systems will be dependent on the detergent chain length, charge and interaction with the colloidal particles and substrate.

7.3.4 Development of r.f. sputtered nickel oxide coatings

Coatings deposited using r.f. diode sputtering at high pressures and low powers exhibited different electrochromic properties to those produced using low pressures and higher powers (7.10). Of particular interest was the stability of the coloured state with respect to exposure to air. Coatings produced by colloidal and anodic deposition did not exhibit the same stability as sputter deposited electrodes. Future studies should concentrate on establishing the chemical and physical reasons for the stability of the coloured state. One of the main reasons for the stability of the coloured state may be the density of the film. If the coating is too dense then the formation of water within the structure is unlikely. Consequently nickel oxyhydroxide (a strong

oxidising agent) which forms upon the electrochemical oxidation of nickel oxide (with defects) or the hydroxide will be stable for longer periods of time. The concentration of water in coatings deposited by sputter deposition should be determined. This could be achieved by using FTIR. It is very likely that poor stability of the colour of the oxidised state with respect to electrochemical cycling is due to the formation of water within r.f. sputtered coatings. R.f. sputtered nickel oxide can be electrochemically oxidised and reduced in organic electrolytes such as DMF containing potassium triflouromethyl sulphonate. Solvents such as DMF (dimethylformamide) can have reduced water content (compared with aqueous electrolytes). So coatings could be analyzed in such environments to investigate the hypothesis that the change in the coloured state is due to water formation within the coating. If water is formed in coatings due to cycling in aqueous electrolytes then a solution to the problem may be to analyze r.f. sputtered nickel oxide coatings in non-aqueous electrolytes. The possibility also exists that a device may be fabricated that contains nickel oxide in an anhydrous environment (7.33). Whilst the switching speeds of these devices are very slow (7.34), fast switching speeds are not necessary for the control of solar energy, although for privacy control and product marketing a faster response is desirable. Finally, coatings that are currently deposited using r.f. diode sputtering require some sort of post deposition electrochemical treatment to exhibit electrochromic properties. Therefore, by modifying the deposition conditions it may be possible to deposit r.f. diode sputtered material that does not require electrochemical cycling in 1M $KOH_{(aq)}$.

7.3.5 Development of ECW devices

The number of materials that could be used in ECW devices is enormous (7.56-7.61). However, there are certain materials and chemical properties that

the component coatings should have. The transparent conductor should have a very low sheet resistance, ideally less than 1Ω to improve uniformity of colouration and switching speeds. The electrolyte must contain the ions necessary for colouration and ion mobility should be as high as possible. If organic materials are eventually selected as electrolytes, stability studies will be necessary to analyze solar degradation of the electrolyte and the effect of oxidation and reduction of organic material, due to the direct contact between electrolyte and electrochromic material. The choice of electrolyte will be dependent to a certain extent on the types of electrochromic materials used in the devices. It is highly likely that the electrochromic materials that will be used in future ECW's will be inorganic, because organic electrochromics have thus far proven to be too unstable for device applications.

The optical properties of coatings and devices produced in this study were not measured as function of cycling. Future research should concentrate on the characterisation of optical and electrochemical properties of devices as they are cycled. Thermal durability and photochemical properties should also be examined.

7.4 REFERENCES

7.1 Lampert, C.M., Omstead, T.R. and Yu, P.C., Solar Energy Materials 14 1986 161.

7.2 Hutchins, M.G., McMeeking, G.D. and Orel, Z., Optical Materials Technology for Energy Efficiency and Solar Energy Conversion XI: Chromogenics for Smart Windows **1728** 1992 66.

7.3 Hutchins, M.G. and McMeeking, G.D., Making Electrochromic films Patent No. 90 27 608.0 1990 (European patent no. 91311905.3).

7.4 Shaw, J., (1980) Introduction to Colloid and Surface Chemistry (3rd edn.). London, Butterworths, 183.

7.5 Fischer, E.W., Kolloid-Z. **160** 1958 120.

7.6 Bagchi, P., Journal of Colloid and Interface Science **47** 1 1974 86.

7.7 Bagchi, P., Ph.D. Dissertation, University of Southern California, Los Angeles, California, 1970.

7.8 Hesselink, F.T., Vrij, A., and Overbeek, J.H.G.,Journal of Physical Chemistry **75** 1971 2094.

7.9 Ash, S.G. and Findenegg, G.H., Trans. Faraday Society **67** 1971 2122.

7.10 Hutchins, M.G. McMeeking, G.D. and Xingfang, H., Optical Materials for Solar Energy Efficiency and Solar Energy Conversion IX SPIE. **1272** 1990 139.

7.11 Johnston, C., Graves, P.R., Applied Spectroscopy **44** 1990 105.

7.12 Delichere, P., Joiret, S. and Hugot-le Goff, A., Optical Materials Technology for Energy Efficiency and Solar Energy Conversion SPIE VII **1016** 1988 165.

7.13 Desilvestro, J., Dennis, A. and Weaver, M.J., Journal of physical Chemistry **90** 1986 6408.

7.14 Nazri, G., Corrigan, D.A. and Maheswari, S.P,, Langmuir **5** 1 1989 17.

7.15 Oliva, P., Leonardi, J., and Laurent, J.F., Delmas, C., and Braconnier, J.J., Figlarz, M., and Fievert, F. and de Guibert, A., Journal of Power Sources **8** 1982 229.

7.16 Corodoba, S.I., Hugot-Le-Goff, A., and Joiret, S., Journal of Electrochemical Society **138** 6 1991 1554.

7.17 McEwen, R.S., Journal of Physical Chemistry **75** 12 1971 1782.

7.18 Lampert, C.M., Troung, V., Nagai, J. and Hutchins, M.G. IEA Task X-C, Glazing Materials, Technical Report LBL-29632 1990.

7.19 Seike, T. and Nagai, J., Solar Energy Materials **22** 1991 107.

7.20 Svensson, J.S.E.M. and Granqvist, C.G. (1990), in Lampert, C.M., and Granqvist, C.G. (eds.), Large-Area Chromogenics: Materials and Devices for Transmittance Control (1st Edn.). Bellingham, Washington, U.S.A., SPIE Press **IS4** 285.

7 .21 Macagno, V.A., Vilche, J.R., Arvia, A.J., Journal of Electrochemical Technology **127** 1980 2636.

7.22 Macagno, V.A., Vilche, J.R., Arvia, A.J., Journal of Electrochemical Technology **129** 1980 301.

7.23 Lynam, L.R., Moser, F.H., Hichwa, B.P., Optical Materials Technology for Energy Efficiency and Solar Energy Conversion SPIE VI **823** 1987 130.

7.24 Shaw, J., (1980) Introduction to Colloid and Surface Chemistry (3rd edn.). London, Butterworths, 163.

7.25 Delichere, P., Joiret, S., Hugot le Goff, A., Bange, K. and Hetz, B., Journal of Electrochemical Society **135** 7 1988 1856.

7.26 Melendres, C.A. and Pankuch, M., Journal of Electroanalytical Chemistry **333** 1992 103.

7.27 Agrawal, A., Habibi, H., Agrawal, J.P., Cronin, D.M., Roberts, R.S., Popowich, C. and Lampert, C.M., Thin Solid Films **221** 1992 239

7.28 Hugot le Goff, A., Joiret, A. and Cordoba de Torresi, S., Proceedings of Electrochemical Society **90** 1990 70.

7.29 Connel, R.S., Corrigan, D.A. and Powell, B.R., Solar Energy Materials and Solar Cells **25** 1992 301.

7.30 Xingfang, H., and Xiaofeng, C., Hutchins, M.G., Optical Materials Technology for Energy Efficiency and Solar Energy Conversion XI: Chromogenics for Smart Windows SPIE **1728** 1992 173.

7.31 Lynam, N.R. and Habibi, H.R., Optical Materials Technology for Energy Efficiency and Solar Energy Conversion SPIE VII **1016** 1988 63.

7.33 Passerini, S. and Scrosati, B., Solid State Ionics **53-56** 1992 520.

7.34 Ganson, G., and Hartman, R., Solid state electrolytes for sensors and electrochemistry, conf. proc., Sicily, Italy, July 1992.

7.35 Kober, F.P., Journal of Electrochemical Society:Electrochemical Science **114** 3 1967 214.

7.36 Granqvist, C.G., (1995) Handbook of Inorganic Electrochromic Materials, London, Elsevier, 373.

7.37 Van Vlack, L.H. (1985) Elements of Materials Science and Engineering, (5th edn.) Addison-Wesley, Reading, Massachusetts, 345.

7.38 Nazri, G., Corrigan, D.A. and Maheswari, S.P., Langmuir 5 1 1989 17.

7.39 Nagai, J., Optical Materials Technology for Energy Efficiency and Solar Energy Conversion XI: Chromogenics for Smart Windows **1728** 1992 194.

7.40 Marshall, J.K. and Kitchener, J.A., J. Colloid Interface Science. **22** 342 1966.

7.41 McBreen, J. (1990), Modern Aspects of Electrochemistry, New York and London, Plenum, **21** 29.

7.42 Passerini, S. and Scrosati, B., J.Electrochem. Soc., **141** 1994 889.

7.43 Vazquez, M.V., Avena, M.J. and De Pauli C.P., Electrochimica Acta **40** 7 1995 907.

7.44 Demourges-Guerlou, L. and Delmas C., J. Electrochem. Soc. **141** 3 1994 713.

7.45 Demourges-Guerlou, L. and Delmas C., J. of Power Sources **45** 1993 281.

7.46 Torresi, R.M., Vasquez, M.V., Gorenstein, A. and Cordoba-Torresi, S.I. Thin Solid Films **229** 1993 180.

7.47 Passerini, S. and Scrosati, B., J. Electrochem. Soc. **141** 4 1994 899.

7.48 Granqvist, C.G., (1995) Handbook of Inorganic Electrochromic Materials, London, Elsevier, 339.

7.49 Matupally, S., Strienz, C.C. and Weidner, J.W., J. Electrochem. Soc. **142** 5 1995.

7.50 Arakaki, J., Reyes, R., Horn, M. and Estrada, W., Solar Energy Materials and Solar Cells **37** 1995 33.

7.51 Nishide, T. and Mizukami, F., Thin Solid Films **259** 1995 212.

7.52 Cordoba de Torresi, S.I., Electrochimica Acta **40** 9 1995 1101.

7.53 Chigane, M. and Ishikawa, M., J. Electrochem. Soc. **141** 12 1994 3439.

7.54 Svensson, J.S.E.M. and Granqvist, C.G., Solar Energy Materials **16** 1987 19.

7.55 Corodoba, S.I., Hugot-Le-Goff, A. and Joiret, S., Journal of Electrochemical Society **138** 6 1991 1554.

7.56 Hyodo, K., Electrochimica Acta **39** 2 1994 265.

7.57 Duek, E.A.R, De Paoli, M.A. and Mastragostino, M., Adv. Mater. **5** 9 1993 651.

7.58 Ho, K.C., Rukavina, T.G. and Greenberg, C.B., J. Electrochem. Soc. 141 8 1994 2061.

7.59 Inaba, H., Iwaku, M., Nakase, K., Yasukawa, H., Seo, I. and Oyama, N., Electrochimica Acta 40 2 1995 227.

7.60 Tassi, E.L. and De Paoli, M.A., Electrochimica Acta 39 16 1994 2481.

7.61 Rauh, D.R. and Cogan, S.F., J. Electrochem. Soc. 140 2 1993 378.

7.62 Strienz, C.C., Matupally, S., and Weidner, J.W., J. Electrochem. Soc. 142 4 1995 1085.

7.63 Greef, R., Peat, R., Peter, L.M., Pletcher, D., and Robinson, J., (1990) Instrumental Methods in Electrochemistry, New York, Ellis Horwood Ltd., 231.

APPENDIX 1

EXPERIMENTAL TECHNIQUES FOR THE DEPOSITION AND CHARACTERISATION OF NICKEL OXIDE AND NICKEL HYDROXIDE COATINGS

APPENDIX 1

EXPERIMENTAL TECHNIQUES

DEPOSITION AND CHARACTERISATION OF

NICKEL OXIDE BASED COATINGS

1.1 INTRODUCTION

The coating techniques used in this study were anodic, colloidal and rf sputter deposition. Precise experimental details are discussed in Chapters 3, 4, 5 respectively. However, basic techniques and circuit diagrams are presented in this appendix. Films produced by r.f. diode sputtering were deposited using the optimum conditions previously reported (1.8).

The optical properties of the coatings produced in this study were characterised using ultraviolet/visible/near-infra-red and Fourier transform infra-red (FTIR) spectrophotometry and the electrochemical properties were analyzed using cyclic voltammetry. Cyclic voltammetry was performed using a Princeton 362 scanning potentiostat/galvanostat. Current flowing through the cell was monitored using the current monitor. The potential difference across the cell was measured using the voltage monitor. Voltage and current outputs were connected to a chart recorder (to measure cyclic voltammograms) that was calibrated using a Gould OS300 oscilloscope. Sheet resistance was measured using a four point probe. X-ray diffraction (XRD) analysis was performed using a Phillips apparatus. Raman analysis was executed using a Raman microprobe. Film thickness was determined using a Talysurf Mk5 instrument. All solutions of ammonia were titrated before solution mixing and the indicator used in the titration was methyl red.

1.2 EXPERIMENTAL TECHNIQUES

1.2.1 Use of scanning potentiostat/galvanostat

A scanning potentiostat/galvanostat applies a constant (scanning) voltage in the potentiostat mode or a constant current in the galvanostat mode. Current flows between the working and counter electrode. Flow of current through the reference electrode is avoided (1.1). Various scanning rates can be selected using a triangular waveform. The constant voltage and current modes are controlled using operational amplifiers (see figure 1.1 a and b)

Plate 1.1 Princeton scanning potentiostat/galvanostat 362

1.2.1.1 *Calibration*

Calibration of the scanning potentiostat was achieved by using the procedure detailed in the operating and service manual. The voltage was calibrated using a Gould OS300 oscilloscope (this particular apparatus was a calibrated scope).

1.2.1.2 *Electrochemical oxidation and reduction of coatings*

Oxidation and reduction of coatings was performed using the scanning potentiostat in the 'control E' mode. This was done using the initial potential control without the scanning facility. The current range mode was 10 mA. A circuit diagram is shown in figure 1.1. Unless otherwise stated all coatings were electrochemically oxidised and reduced in 1 M KOH solutions that had previously been degased using nitrogen.

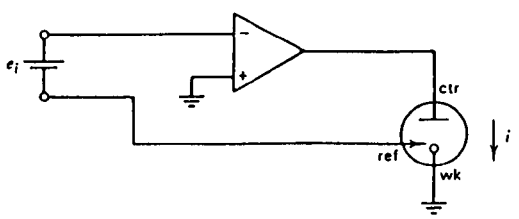

A simple potentiostat

a

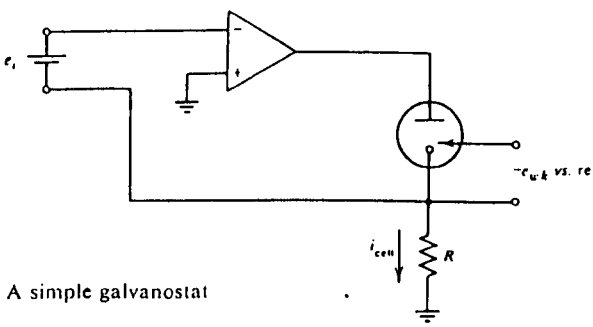

A simple galvanostat

b

Figure 1.1 (a) Circuit diagram of cell and scanning potentiostat
(b) Circuit diagram of cell and galvanostat.

1.2.1.3 *Size of working electrode*

The dimensions of the working electrodes used in this study were usually 50 x 80 mm^2. The active area for electroplating was normally 50 x 50 mm^2. These dimensions were also used to measure the optical properties of the coloured and bleached states. Cyclic voltammetry was performed using smaller dimensions. The working area in this case was 0.5 cm^2. This was because polarisation effects are reduced by having a working electrode smaller than the counter electrode. However, during the course of the experimental, it was found that the same features occurred in the cyclogram at the same voltages no matter what size electrode was used (although the current response was different). The change from NiOx to β-$Ni(OH)_2$ in sputtered material occurred no matter what electrode size was used (the working electrode size was constant throughout the study unless otherwise stated).

1.2.1.4 *Cell dimensions*

The distance between the working electrode and the counter and reference electrodes was 3.0 +/- 0.1 cm (see plate 1.2). There was no difference in the electrochromic properties when the distance between the working, counter and reference electrodes was altered. The distance between the working electrode and the counter and reference electrodes was used in electroplating and during the measurement of electrochromic properties.

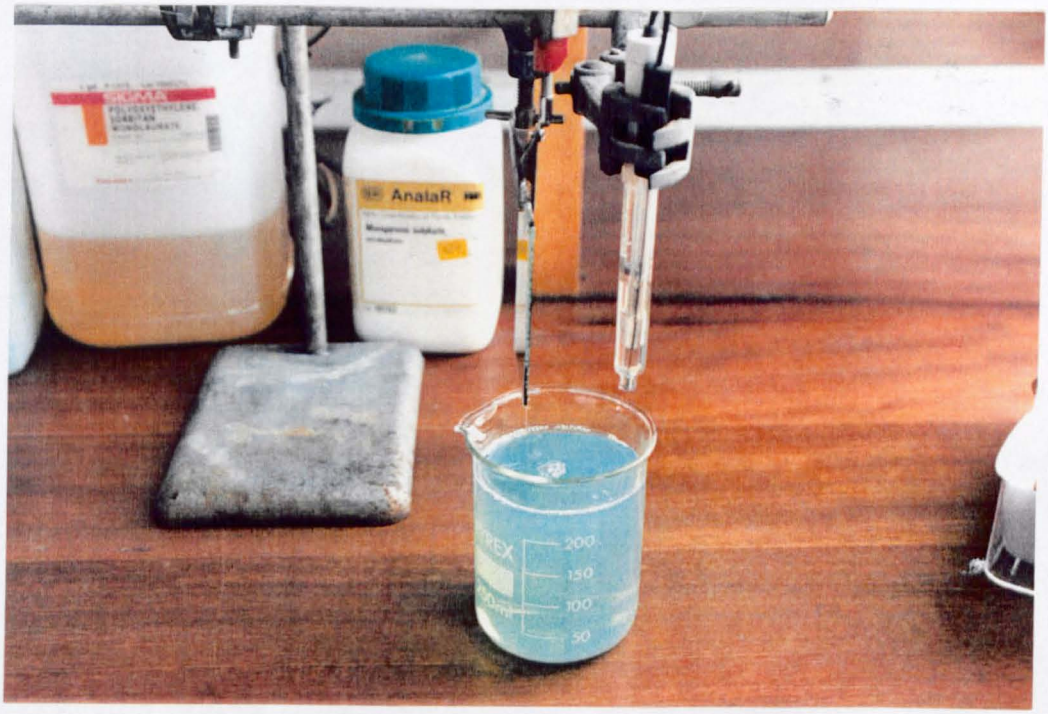

Plate 1.2 Cell dimensions

1.3 pH MEASUREMENTS

The pH of solutions was measured using a pH probe. Before pH measurements were made, dissolved oxygen was removed by purging with N_2. This was not performed in solutions that contained detergent due to foaming. However, before the addition of detergent, oxygen was removed from solutions containing $NiSO_4$ by using N_2.

1.4 SURFACE PROFILOMETRY

The thickness of thin films was evaluated using a Talysurf MK5 apparatus The accuracy of the measurements was +/- 50 A. This method was chosen in preference to weight analysis because weight analysis requires a knowledge of the density of the coatings. Due to the uncertainty in the literature over the identity of material deposited by chemical and physical techniques it was not possible to determine the thickness of coatings with greater accuracy than that obtained with the Talysurf.

1.5 TITRATION OF SOLUTIONS

All solutions of ammonia were titrated before use to determine the precise molarity of these solutions. This was achieved by titrating against a strong acid HCl. The molarity of the acid used was 1M (standard BDH Chemicals). Methyl red was used as an indicator. The indicator became straw coloured at the end point. All solutions of ammonia were kept in volumetric stoppered containers to prevent loss of ammonia due to evaporation.

1.6 ULTRAVIOLET/VISIBLE/NEAR-INFRA-RED SPECTROPHOTOMETRY

All coatings were analyzed using a Beckman 3470 spectrophotometer (see plate 1.3) in the as-deposited, bleached and coloured states. The spectrophotometer was a dual beam instrument. Measurements were performed using an integrating sphere that was coated with barium sulphate ($BaSO_4$). The reference material used was $BaSO_4$. Data was collected from the spectrophotometer using an Apple computer via an A to D converter (analogue to digital converter).

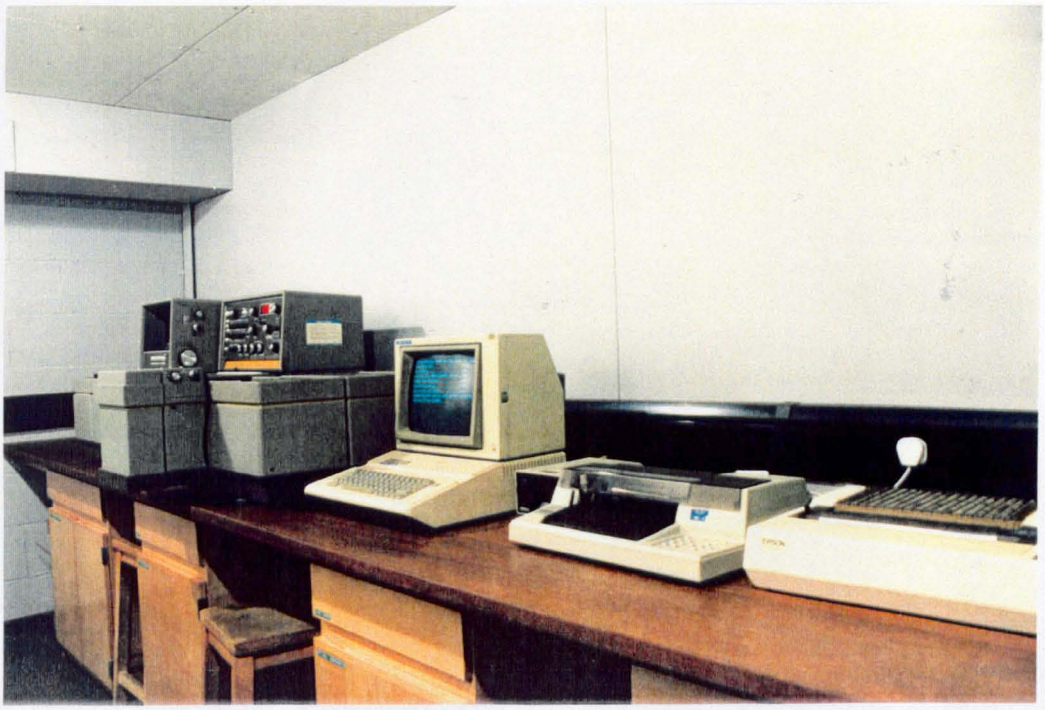

Plate 1.3 Beckman ultraviolet/visible/near-infra-red spectrophotometer 3470

1.6.1 Selected ordinate

A 20 point selected ordinate calculation method for air mass 1.5 was used to determine the solar reflectance and transmittance of coatings (1.2). For solar energy applications, solar weighted transmittance (τ_s), reflectance (R_s) and absorptance (A_s) values are used. For accurate determination of quantities such as τ_s equation 1.1 is used:

$$\tau_s = \frac{\int \tau(\lambda)\, I_s(\lambda)\, d\lambda}{\int I_s(\lambda)\, d\lambda} \qquad 1.1$$

In this equation τ_λ is the spectral transmittance at the particular wavelength (λ). Equations for R_s, A_s are similar to that of equation 1.1.

A more convenient although less accurate method for evaluating quantities such as τ_s is the use of weighted ordinate analysis (see equation 1.2):

$$\tau_s = \frac{\sum \tau\lambda_i I_{si} \Delta\lambda_i}{\sum I_{si} \Delta\lambda_i} \qquad 1.2$$

In this expression i = 1-20 + in equal wavelength intervals, $\Delta_{\lambda i}$ and I_{si} is the corresponding solar intensity *interval.*

Finally, the mathematical technique used in this study to evaluate quantities such as τ_s, was that of selected ordinates. In this method the summation is performed over intervals of equal energy. As with the technique described in equation 1.2, this method is also an approximation. Equation 1.3 is used for this analysis.

$$\tau_s = \frac{1}{20} \sum \tau_{\lambda j} \qquad 1.3$$

where λ_j (μm) is expressed as equal energy intervals.

For the solar spectrum at air mass 1.5, the equal energy units are given in table 1.1 (1.2). Similar expressions can be derived for the visible part of the electromagnetic spectrum (1.2).

This method was used in this study, due to the speed of the calculation. Although more accurate values for τ_s could be determined by using equations

such as 1.1, the time taken to perform such analysis would have been prohibitive.

Table 1.1 Equal energy wavelength intervals (μm) for the solar spectrum at air mass 1.5 (ASTM standard E891)

λ^i	λ(μm)	λ^i	λ(μm)
λ_1	0.3898	λ_{11}	0.7954
λ_2	0.4460	λ_{12}	0.8448
λ_3	0.4833	λ_{13}	0.8967
λ_4	0.5191	λ_{14}	0.9790
λ_5	0.5554	λ_{15}	1.0414
λ_6	0.5962	λ_{16}	1.1444
λ_7	0.6295	λ_{17}	1.2535
λ_8	0.6667	λ_{18}	1.5243
λ_9	0.7070	λ_{19}	1.7001
λ_{10}	0.7505	λ_{20}	2.3220

1.6.2 Optical density

For comparison of electrochromic properties of the films, the change in optical density, d (OD), defined as (see equation 1.4),

$$d\ (OD) = \log_e(\tau_b/\tau_c) \qquad 1.4$$

was used, where τ_b and τ_c are the spectral transmittance of the films in the bleached and coloured states respectively. Chromaticity coordinates and colouration efficiencies were also evaluated from this data.

1.6.3 Chromaticity coordinates (calculation of tristimulus specifications from spectrophotometric data)

A particularly important application of colour mixture theory is the derivation of the colour specification of a stimulus C (see equation 1.5) when the spectral composition (τ_γ) is known (1.4):

$$1.0(C) = r.(R) + g(G) + b(B) \qquad 1.5$$

where, $r = R/(R+G+B)$, $g = G/(R+G+B)$ and $b = B/(R+G+B)$.

It follows from this that $r + g + b = 1$. R, G and B represent the primary colours, red green and blue, respectively. Unfortunately, the terms R, G and B do not by themselves describe scientifically what the precise nature of the colour mix is. It is therefore necessary to use equation 1.6:

$$(C) = x.(X) + y.(Y) + z.(Z) \qquad 1.6$$

where, (X), (Y) and (Z) are a new set of reference stimuli. Expressed algebraically in terms of the C.I.E. system, the tristimulus values X, Y and Z are given by:

$$X = \sum T\lambda.x\lambda \qquad 1.7$$

$$Y = \sum T\lambda . y\lambda \qquad 1.8$$

$$Z = \sum T\lambda . z\lambda \qquad 1.9$$

The unit chromaticity coordinates x, y, z are given by:

$$x = X/(X+Y+Z) \qquad 1.10$$

$$y = Y/(X+Y+Z) \qquad 1.11$$

$$z = Z/(X+Y+Z) \qquad 1.12$$

For exact determination of X, Y and Z the summation process consists of integration of the areas under the three distribution curves. This process is performed after the coordinates have been weighted by the spectral composition of the stimulus. However, the wavelength intervals in tabulated data are sufficiently close together to be equivalent to true integration. As is indicated in equations 1.10 - 1.12, the values for X, Y and Z are a summation of the distribution coefficients for equal energy stimulus for the range of visible spectrum. Consequently, the unit chromaticity coordinates can be evaluated.

1.6.4 Colouration efficiencies

Once the charge extracted was measured and the optical density was calculated, colouration efficiency was determined. Colouration efficiency is a measure of the change in optical density that occurs during charge extraction

(1.2). There are several methods for evaluating colouration efficiency. There is considerable controversy as to whether charge is extracted (or for tungsten oxide injected) per unit area (mc cm^{-2}), per surface density of charge (mc cm^{-2}) or per unit volume should be used (mc cm^{-3}). The method used in this study was $\Delta OD(\tau_{sb\lambda}/\tau_{sc\lambda})/q(cm^{-2})$ so that comparisons could be made with other studies reported in the literature (1.5).

1.7 FOURIER TRANSFORM SPECTROPHOTOMETRY (FTIR)

Infra-red measurements were performed using an IFS25 Bruker FTIR (see plate 1.4). Because the substrate was a heat mirror coated glass substrate, all measurements in this study were carried out in reflectance. Specular reflectance was measured in this study, because all nickel oxide and nickel hydroxide coatings manufactured by sputter, colloidal and anodic deposition exhibited specular reflectance. The diffuse component of the reflected radiation was only 1%. This was within the error of the measurement. Total near normal measurements were performed using a gold integrating sphere. The reference material used was roughened gold. For specular measurements, ITO or Sn:F coated glass was used as reference material. The infra-red source used in this instrument was a Globar. The Globar supplied infra-red radiation to a Michelson Morley interferometer which was used to produce an interferrogram. This interferrogram was then directed via a system of mirrors towards the coating to be analyzed. For total near normal measurements reflected radiation was collected using a gold integrating sphere (for total near normal measurements) and measured using a cadmium mercury telluride detector (cooled to 70K using liquid nitrogen). In the specular mode, the reflected radiation was collected using a parabolic mirror and directed towards a lead sulphide detector (PbS_2). The data was processed using a Dell 486 computer.

The computer was used to perform a Fourier transform on the interferrogram that was measured using one of the detection systems previously described. Prior to the Fourier transform being performed, the sample interferrogram was divided by the reference interferrogram. A Fourier transform was then performed on this interferrogram.

Plate 1.4 Fourier transform spectrophotometer (IFS25 Bruker)

1.8 X-RAY DIFFRACTION

X-ray diffraction studies were performed using a Phillips Pye Unicam X-ray diffraction instrument. For all measurements a copper target (Cu Kα) was used.

This was so that results could be compared with those of studies reported in the literature (1.6).

1.9 RAMAN MICROPROBE ANALYSIS

Spectra were recorded using a Harwell Laser Raman Microprobe (1.7). This used an exciting laser wavelength of 514.5 nm and a laser power of 10 mW, measured at the sample. The beam was focused to a spot diameter of 2 μm. The 180° back-scattered light was collected using a X40 high numerical aperture objective lens. This radiation then passed to a monochromator (spex triplemate) fitted with an intensified 1024 element photodiode array detector (O-SMA, Spectroscopy Instruments GmbH), interfaced to a PDP 11/73 PC (Digital Equipment Corporation).

1.10 SHEET RESISTANCE MEASUREMENTS

Sheet resistance measurements were performed using a four point probe (see plate 1.6 and figure 1.4). These measurements were performed to evaluate the sheet resistance of ITO supplied by Blazers. Attempts were also made to determine the sheet resistance of nickel hydroxide in the as-deposited, bleached and coloured states. In the bleached and as-deposited states, the nickel hydroxide was insulating. However, in the coloured state for anodic and colloidally deposited coatings, the sheet resistance was 4000 Ω. Sheet resistance measurements of sputtered NiO were not performed in this study.

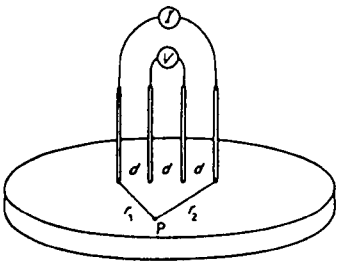

Figure 1.2 Circuit diagram of a four point probe.

1.11 ANODIC ELECTRODEPOSITION OF NICKEL HYDROXIDE COATINGS

A scanning potentiostat (Princeton Applied Research Model 362) was used to electrodeposit coatings anodically (see plate 1.1). Platinum and saturated (5 M KCl) calomel electrodes were used as the counter and reference electrodes respectively. Fluorine or indium doped tin oxide coated glass substrates (with a sheet resistance of 40 Ω) were used as substrate material. Substrate cleaning was very important. Initially substrates were cleaned ultrasonically in a bath containing 10% decon 90 for 20 minutes followed by rinsing. The volume of the electrochemical working solutions used in this study was 250 cm^3. All solutions were magnetically stirred for 4 minutes prior to deposition. Deposition was achieved by setting an initial potential of usually -500 mV and a final potential of +1500 mV. The scan rate was usually 20 mVs^{-1} using a triangular waveform unless otherwise stated. The initial potential that the scan commenced at was normally zero. On occasions when the scanning potentiostat did not start at zero, there was no effect on the electrochromic properties of electrodeposited

coatings. This was proved by depositing two coatings from unstable solutions that had aged identical times using the same deposition parameters on the scanning potentiostat (the deposition time was 5 minutes in both cases). The optical properties were identical even though the scan did not start at same potential (0.00 V, -0.10 V).

1.11.1 Electrodes and cell dimensions

Platinum electrodes of various dimensions were used, however, this did not have any effect on the electroplating experiments. For economic purposes and to provide a systematic basis for this study, a platinum counter electrode of $1cm^2$ was used. Altering the size of the working electrode did have an effect on the colouration properties of coatings. As the area of the working electrode decreased, the colouration increased. However, this did not have any effect on the fundamental problems experienced in this study such as coating fracturing. A luggin probe was not used in this study. IR compensation was performed instead. This was because, placing a luggin probe in front of a coating impaired the uniformity of coatings during electroplating. An irresolvable problem with the electroplating procedure was the formation of $Ni(OH)_2$ on the counter electrode (platinum). This must have modified the resistance of the cell. After each experiment the nickel hydroxide was removed from the platinum electrode by soaking in dilute HCl for 10 minutes. The electrode was then thoroughly washed in distilled H_2O. Conductivity measurements were made to ensure no nickel hydroxide remained on the platinum electrode. The electrochromic properties of freshly prepared coatings were compared with previously deposited films to confirm that no nickel hydroxide remained on the platinum electrode (electrodes prepared using identical deposition parameters). There was no difference in the results that could not be explained in terms of the 1% error in the measurement of optical properties using the Beckman ultraviolet/visible/near-infra-red spectrophotometer.

1.12 COLLOIDAL DEPOSITION OF NICKEL HYDROXIDE COATINGS

The coatings deposited by colloidal deposition involved the simplest experimental procedure. However, meticulous cleaning of the ITO was required to produce good films. Also the order of mixing, solution volumes, precise nature of the wetting of deposition surfaces, type of nickel salt and solution additives used were critical for obtaining coatings with good electrochromic properties. In essence this technique involved a one-step process. The cleaned substrate was lowered into a solution containing the reactants required to produce a coating of nickel hydroxide (see plate 1.7). The thickness of the coating was a function of pH, temperature and solution concentrations. The most difficult property to control during colloidal deposition was coating uniformity. By adding small volumes of detergent, solutions were stabilised for short periods of time (long enough for deposition to occur). Long term stability of solutions was not feasible because the deposition process was dependent on the formation of particles of $Ni(OH)_2$.

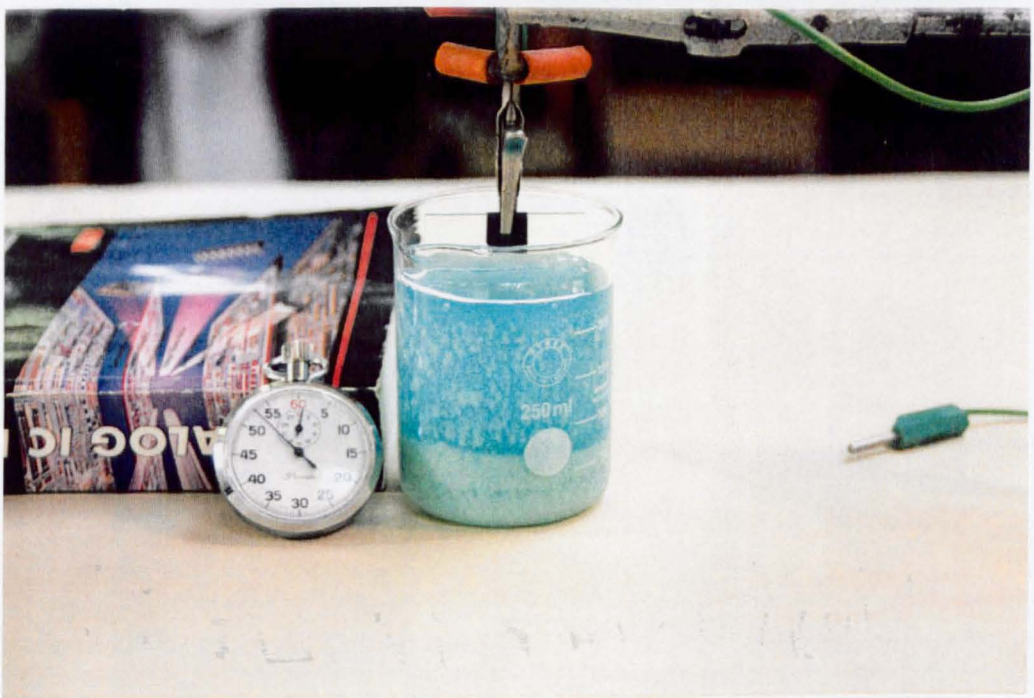

Plate 1.5 Colloidal deposition technique

1.13 REFERENCES

1.1 Greef, R., Peat, R., Peter, L.M., Pletcher, D., and Robinson 1990, Instrumental Methods in Electrochemistry (1st edn.), London, Ellis Horwood.

1.2 Lampert, C.M., Troung, V., Nagai, J. and Hutchins, M.G. IEA Task X-C, Glazing Materials, Technical Report LBL-29632 1990.

1.3 Cogan, S.F., Plante, T.D., McFadden, R.S. and Rauh, D., Optical Materials Technology for Energy Efficiency and Solar Energy Conversion SPIE VI **823** 1987 106.

1.4 Murdoch, J.B. (1985), Illumination Engineering, New York, MacMillian.

1.5 Lampert, C.M. (1990), in Lampert, C.M., and Granqvist, C.G. (eds.), Large-Area Chromogenics: Materials and Devices for Transmittance Control (1st Edn.). Bellingham, Washington, U.S.A., SPIE Press **IS4** 414.

1.6 Svensson, J.S.E.M. and Granqvist, C.G. (1990), in Lampert, C.M., and Granqvist, C.G. (eds.), Large-Area Chromogenics: Materials and Devices for Transmittance Control (1st Edn.). Bellingham, Washington, U.S.A., SPIE Press **IS4** 285.

1.7 Johnston, C. and Graves, P.R., Applied Spectroscopy **44** 1 1990 105

1.8 Hutchins, M.G. and McMeeking, G.D., Xingfang, H., Optical Materials for Solar Energy Efficiency and Solar Energy Conversion SPIE IX **1272** 1990 139.